Dissertation

Spatiotemporal variations of the local stress field and fault asperities at the North Anatolian Fault in NW Turkey analysed based on microseismic recordings.

Michèle Ickrath

Berlin

14th August 2014

The study was funded by the Helmholtz Association within the framework of the Research Program of the Young Investigators Group
'From Microseismicity to Large Earthquakes'

kindly supported by the
GFZ German Research Centre For Geosciences, Potsdam, Germany

Written by Michèle Ickrath

Advisors:

Prof. Dr. Marco Bohnhoff
Helmholtz Centre Potsdam, GFZ German Research Centre for Geosciences
Section 3.2, Geomechanics and Rheology
Telegrafenberg, D-14473 Potsdam, Germany

Prof. Dr. Frederik Tilmann
Helmholtz Centre Potsdam, GFZ German Research Centre for Geosciences
Head of Section 2.4/Seismology
Telegrafenberg, D-14473 Potsdam, Germany

Date of thesis defense : 11th November 2014

Spatiotemporal variations of the local stress field and fault asperities at the North Anatolian Fault in NW Turkey analysed based on microseismic recordings.

DISSERTATION

submitted to the

Institute of Geological Sciences at the

Freie Universität Berlin

to aquire the academic degree of

DOCTOR OF NATURAL SCIENCES

(Dr. rer. nat.)

written by

Dipl.-Geophys. Michèle Ickrath

Berlin, 14th August 2014

GFZ Helmholtz Centre POTSDAM

Freie Universität Berlin

HELMHOLTZ ASSOCIATION

Abstract

Variations of the local stress field might serve as an indicator to characterize the physical status of individual fault segments during the seismic cycle. In this study spatial and temporal variation of the crustal stress field orientations along the North Anatolian Fault Zone (NAFZ) in northwestern Turkey are investigated. The NAFZ is one of the largest currently active strike-slip fault in the world. In 1996 a permanent seismic network, the SApanca BOlu NETwork (SABONET) was deployed to investigate the seismic activity at the Karadere- and Düzce Fault. This region represents the eastern end of a westward migrating earthquake sequence starting in 1939 in eastern Turkey. In 1999 the two most recent major earthquakes, the Izmit- and Düzce events, occurred. In this study a compilation of 939 focal mechanisms and the dataset of more than 10000 well located local earthquakes from the SABONET and German Task Force (GTF) network covering the time period 1997-2001 are processed and analysed. Covering the pre-seismic, inter Izmit-Düzce and post-seismic phase of the Izmit earthquake this dataset provides a fundamental data base to search for systematic stress rotations related to major earthquakes at a major transform fault. Different stress tensor inversion methods were applied using focal mechanism data and first motion polarities as input to study spatiotemporal changes of the stress field orientation along individual fault segments of the 1999 Izmit and Düzce ruptures. Results indicate a stable strike slip regime for the regional stress field prior to the Izmit earthquake and following the two-month Izmit aftershock sequence. In contrast the early aftershock period is dominated by EW-extension below the Akyazi Plain. During the two-month aftershock period significant changes from strike-slip to normal-faulting during the mainshock followed by a systematic back-rotation to the pre-mainshock stress regime is found. This back rotation commences first in the Akyazi Plain hosting a coseismic slip deficit of ≤ 3 m and propagates then further to the east towards the Karadere and Düzce fault where the Düzce M_w7.1 mainshock nucleated 87 days later. The followed detailed analysis of the lateral variations of the stress field within distinct smaller segments along the fault confirms these observations and leads to suggestions regarding the origin of the stress perturbations. Thereby, the stress field evolution of the segments can be followed from the predominantly pre-seismic strike-slip regime in the west, the inter Izmit-Düzce

phase of the dominant E-W extensional regime in the Akyazi plain to the nearly stable post-seismic strike-slip regime along the Düzce and Elmalik faults. These observations and the correlations with co- and postseismic slip confirm the suggestion that shear failure and the associated drop in shear stress during large earthquakes may result in a rotation of the principal stresses. Finally, these observations are used to investigate local depth distribution and kinematics of seismicity along the fault and the determination of possibly locked or creeping parts of a fault. A clear correlation between along-fault variations of the depth-distribution of aftershock activity and cumulative co- and postseismic slip below the seismogenic layer is observed. In addition, local shallow earthquakes below the Düzce fault are analysed and give new insights into the evolution of this part of the rupture. The results from this study reveal that spatiotemporal stress field rotations are a useful indicator for variations of the seismotectonic setting during the seismic cycle.

Zusammenfassung

Variationen des lokalen Spannungsfeldes können als Indikator dienen, um den physikalischen Zustand einzelner Segmente einer Verwerfungszone während des seismischen Zyklus zu charakterisieren. In dieser Studie werden räumliche und zeitliche Veränderungen des Spannungsfeldes der Erdkruste entlang der Nordanatolischen Verwerfungszone (NAFZ) im Nordwesten der Türkei untersucht. Die NAFZ ist eine der größten derzeit aktiven Transformstörungen der Welt. Im Jahr 1996 wurde ein permanentes seismisches Netzwerk, das SApanca BOlu NETzwerk (SABONET) in Betrieb genommen, um die seismische Aktivität entlang der Karadere und Düzce Verwerfung zu untersuchen. Diese Region stellt das östliche Ende einer seit 1939 nach Westen wandernden Erdbeben-Sequenz im Osten der Türkei dar. Zwei starke Erdbeben im August und November des Jahres 1999, das Izmit und Düzce Erdbeben, stellen die jüngsten Erdbeben dieser Sequenz dar. Grundlage dieser Studie bildet ein zusammengestellter Katalog aus 939 Herdflächenlösungen und seismische Daten von mehr als 10000 lokalsierten Erdbeben des *SABO-Netzwerkes* und German Task Force (GTF) Netzwerkes für die Jahre 1997-2001 welche prozessiert und analysiert wurden. Dieser Datensatz bietet eine umfassende Datenbasis für die Zeiträume vor (Pre-seismic), zwischen (Inter Izmit-Düzce) und nach (Post-seismic) den Izmit und Düzce Erdbeben und stellt damit eine einzigartige Möglichkeit dar, systematische raumzeitliche Änderungen des Spannungsfeldes im Zusammenhang mit großen Erdbeben entlang von Verwerfungszonen zu untersuchen. Verschiedene Spannungstensor-Inversionsverfahren basierend auf der Inversion von Herdflächenlösungen und Polaritäten von Ersteinsätzen werden verwendet, um räumliche, sowie zeitliche Veränderungen des Spannungsfeldes entlang einzelner Segmente des 1999 Izmit Bruches zu analysieren. Die Ergebnisse zeigen ein stabiles Blattverschiebungs-Regime für das regionale Spannungsfeld vor dem Izmit Erdbeben und für den Zeitraum nach dem Düzce Erdbeben. Im Gegensatz dazu, ist die Inter Izmit-Düzce Phase geprägt durch Nachbeben mit Abschiebungsmechanismen. Diese werden durch die andauernde Ost-West-Extension in der Akyazi Ebene hervorgerufen. Innerhalb der frühen zweimonatigen Nachbebenfrequenz des Izmitbebens lässt sich zum ersten Mal die signifikante Änderung von dem Blattverschiebungs-Regime zum Abschiebungs-Regime, gefolgt von einer langsamen Rückrotation des Spannungsfeldes in den ursprünglichen Zustand

des Blattverschiebungs-Regime, beobachten. Diese Rückrotation beginnt zunächst in der Akyazi Ebene, welche durch ein Defizit in der Co-seismischen relativen Verschiebung (co-seismic slip) von ≥ 3 m geprägt ist und propagiert dann weiter nach Osten in Richtung der Karadere und Düzce Verwerfungszone. Dort fand die Nukleation des Düzce M_W 7,1 Erdbeben 87 Tage nach dem Izmitbeben statt. Anhand der detaillierten Untersuchung der lateralen Veränderungen des Spannungsfeldes, innerhalb verschiedener kleinerer Segmente entlang der Verwerfung, lassen sich diese Beobachtungen bestätigen und detailierte Aussagen über den Ursprung treffen. Dabei kann die Entwicklung des Spannungsfeldes von dem dominierten Pre-seismischen Blattverschiebungs-Regime im Westen, dem Interseismischen E-W extensionalen Abschiebungs-Regime in der Akyazi Ebene zu dem nahezu stabilen Post-seismischen Blattverschiebungs-Regime entlang der Düzce und Elmalik Verwerfungen verfolgt werden. Diese Beobachtungen und die Korrelationen mit Co- und Postseismischen relativen Verschiebungen bestätigen die Annahme, dass Scherbrüche und der damit verbundene Abbau der Scherspannung bei großen Erdbeben zu einer Drehung der Hauptspannungachsen führen kann. Schließlich werden diese Beobachtungen mit der Tiefenverteilung und der Kinematik der lokalen Seismizität entlang der Verwerfung in Verbindung gebracht, anhand derer blockierte oder kriechende Bereiche der Verwerfung erkannt werden. Dabei kann eine gute Übereinstimmung von Post-seismischen Deformationen in der Tiefe mit oberflächennahen aseismischen Bereichen beobachtet werden. Desweiteren werden lokal auftretende Flachbeben entlang der Düzce Verwerfung analysiert, welche neue Einblicke in die Entwicklung dieses Bereiches der NAFZ geben. Die Ergebnisse dieser Studie zeigen, dass räumliche und zeitliche Rotationen des Spannungsfeldes ein nutzbarer Indikator für Veränderungen der seismotektonischen Bedingungen während des seismischen Zyklus sind.

Contents

List of Figures

List of Tables

List of Abbreviations

Table 0.1.: List of Abbreviations

AP	-	Akyazi Plain
DB	-	Düzce Basin
DF	-	Düzce Fault
FM	-	Focal Mechanism
GFZ	-	German Research Centre for Geosciences
GPS	-	Global Positioning System
GTF	-	German Task Force
InSAR	-	Interferometric Synthetic Aperture Radar
KF	-	Karadere Fault
LSIB	-	Linear Stress Inversion with Bootstrapping
MOTSI	-	Direct Inversion of earthquake first motion
NAFZ	-	North Anatolian Fault Zone
NF	-	Normal-Faulting
PDF	-	Probability Density Function
SABOnet	-	SApanca BOlu NETwork
SAF	-	San Andreas Fault
SATSI	-	Spatial and Temporal Stress Inversion
SS	-	Strike-Slip
STA/LTA	-	Short-time average/ Long-time average
STI	-	Stress Tensor Inversion
TF	-	Thrust-Faulting

Acknowledgments

I would like to express my gratitude to my doctoral advisor Prof. Dr. Marco Bohnhoff for given me the opportunity to carry out this thesis and his support and guidance throughout this study. Besides teaching me a lot about the scientific world i am very grateful for the possibility to attend to international conferences and workshops and to be on-site during the first drilling phase within the GONAF project in NW Turkey.
I would like to sincerely thank Prof. Dr. Frederik Tilmann for taking over the evaluation of my thesis as second supervisor and for the good collaboration during the final phase of the thesis.
A great thanks goes to Prof. Dr. Georg Dresen for helping my understanding the world of rheology and for helpful discussions.
I am very grateful to Dr. Fatih Bulut for his help and guidance for all kinds of seismological and programming problems and also the understanding and guidance during difficult times. I would also like to thank Dr. Tuna Eken for the opportunity to ask questions at all times especially in the early stage of my thesis and to open me the world of awk programming. A very special thanks to Vaclav Vavryčuk for his critical discussion regarding determination of stress field orientations and the great help with the Stress Tensor Inversion method from Angelier (2002).
I would like to acknowledge Jeannot Trampert the editor of the Geophysical Journal International and John Townend for helpful comments for my first paper draft.
A great thanks go the German Task Force for Earthquakes and especially J. Zschau and C. Milkereit for providing the Izmit aftershock waveform data and SABOnet data. Speaking of the huge database a very special thanks goes to Oliver Germer without his passion for handpicking waveform data it would not be possible to handle the amount of data in a proper time.
I am very grateful to Prof. Dr. Kamil Ustaszewski for teaching my the basics of the GOCAD software and his collaboration and support during my supervision of our indian intern Akilesh Goyal.

Special thanks goes to Prof. Dr. Wilfried Jokat my diploma thesis supervisor for helpful advices also after my time at the AWI in Bremerhaven.

A great thanks go to the whole Section 3.2 at the GFZ for their support in any ways and the opportunity to ask questions all the time. I would like to thank all the phd's and postdoc's who made the coffee breaks on the roof, the afterwork beerclubs, the yearly Christmas dinner and get-togethers to a time that i will not forget. I would like to special thank Patricia Martínez-Garzón and Grzegorz Kwiatek for providing the MSATSI Software and for their support and helpful discussions. Special thanks go to Vanessa Helpa, Bita Najdahmadi, Christina Raub, Eva Stierle and Christopher Wollin as great colleagues and friends. I would like to thank Tina for a pleasant working atmosphere over the years, the possibility to ask innumerable questions regarding Matlab programming and all the funny times besides work. I would also give a special thank to Bita for always bringing a smile to my face and a great thanks to Vanessa for her skills as coach to overcome my inner bastard and to find new motivation during the work by chasing me through the woods of the Telegrafenberg. I also would like to thank Nicolas Norberg and Bastian Joachim for giving me a good start for the phd time during my container times.

Besides this, a great thanks go to my friends for their support and understanding especially in the final phase of my thesis. I would like to special thank Johanna Sooß, Andreas Benthin and Thomas Heer for the proofreading. I also like to thank the people from the "Lir-Stammtisch". A great thanks goes to Philipp Berndt for always reminding me to never forget the precisions of mathematics, critical discussion and for his help concerning little dirty tricks of program installations under Linux.
Great thanks goes to Saskia Steinbeck for her support and friendship since the primary school and for her motivation during our "Erfolgsteam-meetings".

Finally the greatest thanks goes to my parents, my brother and my grandparents for their support and understanding all the time and to Christian Feld for his patience and motivation all the time, for the proofreading, for always being there for me and believing in me and support me also during difficult times.

1. Introduction

The North Anatolian Fault Zone (NAFZ) in NW Turkey is one of the most active and best studied strike-slip faults and has produced several destructive (M>7) earthquakes during the last century. Due to its recent sequence of earthquakes the fault zone provides an unique opportunity to study earthquake related processes such as stress accumulation and release during the seismic cycle, earthquake rupture processes and segmentation in space and time. Currently, the Sea of Marmara segment remains as the only section of the NAFZ that has not been activated since 1766 and represents a seismic gap that is in the final state of the seismic cycle with an accumulation of stress that could lead, with a probability of 35-70 %, to a M>7 event in the next 30 years (Parsons, 2004). The most recent earthquakes, the Izmit M_w 7.4 August 1999 and Düzce M_w 7.1 November 1999 ruptured a ∼180 km long segment of the NAFZ in NW Turkey between the Sea of Marmara and the Düzce area both reflecting a right-lateral strike-slip mechanism consistent with the long-term regional stress field.

The principal objectives of the studies presented in this dissertation are to investigate the seismotectonic setting along the rupture zone, and to investigate potential spatiotemporal variations of the local stress field orientation in relation to both mainshocks. In particular, the focus is on the pre-, inter Izmit-Düzce and postseismic phases of the 1999 earthquakes using seismic recordings from available local and regional networks.

1.1. Motivation and Scope

Spatial and temporal variations of the crustal stress field orientation provide information about the evolution of the stress field related to large earthquakes and may serve as an indicator to characterize the physical status of individual fault segments along a fault zone during the seismic cycle. First systematic studies on the recurrence of earthquakes were initiated by the great 1906 San Francisco earthquake on the San Andreas Fault. Amongst others, these studies lead to the postulation of the elastic rebound and a physical understanding of the seismic cycle (Gilbert, 1909; Reid, 1910; Thatcher, 1983; Bürgmann

and Dresen, 2008).

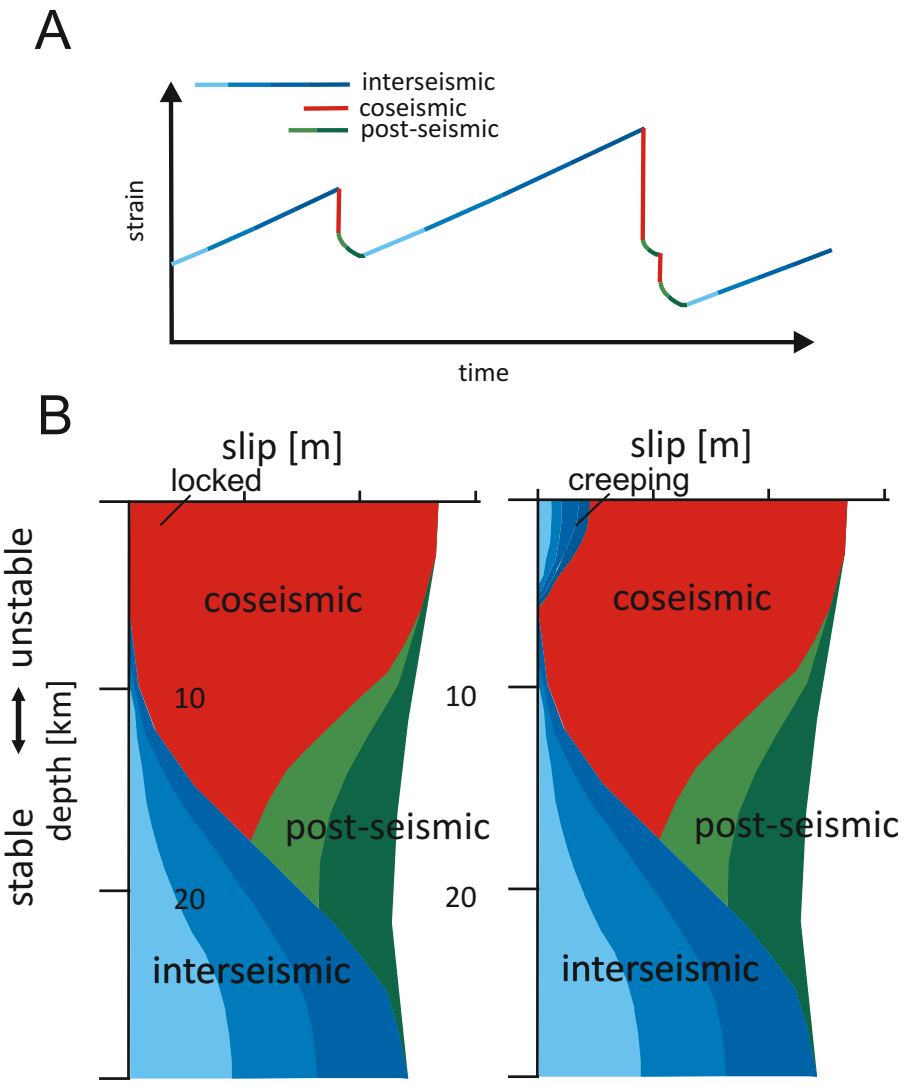

Figure 1.1.: The earthquake cycle and the fault slip versus depth evolution. (A) Sketch illustrating the three main phases of the seismic cycle: inter-seismic, co-seismic and post-seismic and the evolution along the time path (modified after DeMets (2007). (B) Fault slip versus depth for the complete earthquake cycle for a locked (left) and creeping fault (right), respectively. (after Tse and Rice (1986) and Wei (2011)).

Figure 1.1 illustrates the seismic cycle with the three main phases being inter-seismic, co-seismic and post-seismic. The inter-seismic phase refers to the steady accumulation of strain over years between earthquakes that irregularly activate the fault releasing stored energy. The co-seismic phase represents the time during an earthquake and the post-seismic phase starts once rupture terminated and may extend over days, months, or even years after an earthquake (e.g. DeMets (2007)). In terms of crustal deformation the so-

called pre-seismic phase was introduced by Scholz (2002) representing the short-time phase prior to a large earthquake. Zoback (1992) introduced first- and second-order patterns of the stress in the lithosphere and postulated that if the first order regional stress field is well known it is possible to identify local variations in stress field orientation. However, how the local stress field orientation changes during and after a major earthquake has been debated for decades. Apart from the simplified general seismic cycle (Fig. 1.1A), two different models where proposed trying to describe the evolution of the stress field (Hauksson and Jones, 1988) along activated faults in response to a mainshock. The most common one is the stress recovery model first proposed by Michael (1987). It suggests that there is a large stress drop due to an earthquake and that the state of stress rapidly returns back to its pre-earthquake state of stress after the mainshock. In contrast to this, in the stress decay model by Hauksson and Jones (1988), the change of the average post-mainshock stress is of the same magnitude as the co-seismic stress drop along with a general decrease of the average stress which is then followed by a long term stress recovery similar to tectonic reloading (Fig.1.2).

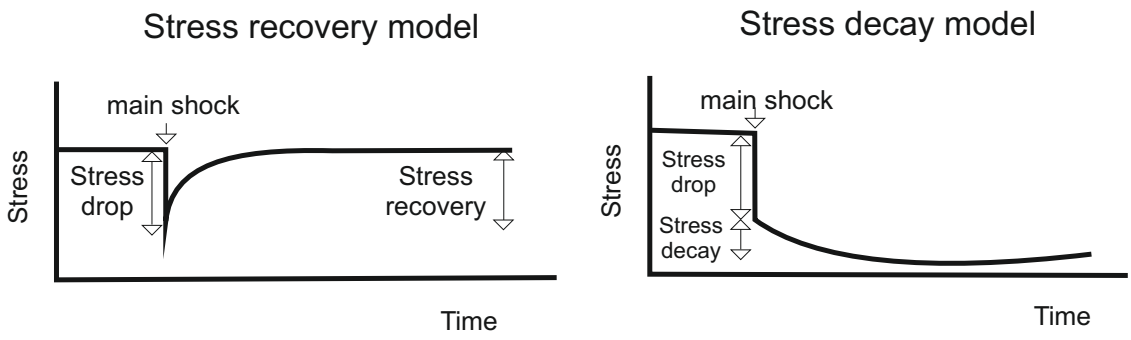

Figure 1.2.: Proposed models for a change in stress field orientation induced by a large earthquake (modified after Hauksson and Jones (1988)). Stress recovery model: The state of stress after the main shock returns rapidly back to the pre-main shock stress state (Michael, 1987). Stress decay model: the average post-main shock stress change is in the same sense as the co-seismic stress drop and stress recovers on the long-term (Hauksson and Jones, 1988).

According to the double-couple force model, the stress drop or release of the tectonic stress and strain in the crust occurs in the shear stress (τ). Whereas, the normal stress (σ) and vertical stress (σ_v) on the fault is assumed to be consistent before and after an

earthquake (see Eq.: 1.1).

$$\begin{aligned} \sigma_v^* &= \sigma_v \\ \tau^* &= \tau - \Delta\tau = \tau(1-\epsilon_0) \\ \sigma^* &= \sigma \end{aligned} \tag{1.1}$$

with $\Delta\tau$ being the co-seismic stress drop and $\epsilon_0 = \Delta\tau/\tau$ is the ratio of the stress drop to the initial shear stress (Kasahara, 1981; Yin and Rogers, 1995). King et al. (1994) and Yin and Rogers (1995) proposed that this change of the state of stress due to large displacements caused by large earthquake rupture can generate large stress changes. These changes from the pre-earthquake background tectonic stress field to the co- and post-earthquake state of stress might then result in a rotation of the local stress field then also activating previously non-favorably oriented fault planes (Fig. 1.3). Yukutake et al. (2007) postulate that stress field rotations caused by static stress changes associated with the mainshock depend on the amplitude of the stresses prior to the mainshock and/or the strength of the fault. Areas with an higher inital stress/fault strength are hence less influenced by stress perturbation whereas areas of lower initial stress/fault strength are possibly dominated by higher local stress field variations from the regional stress. This is the Yukutake hypothesis introduced by Pinar et al. (2010).

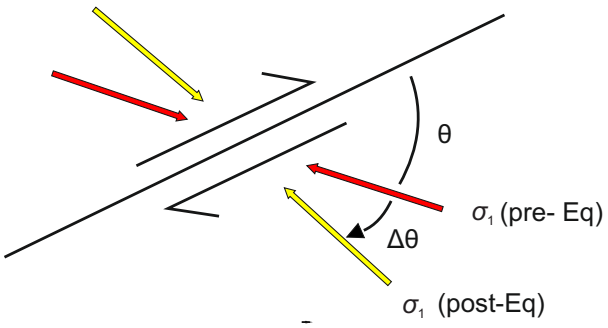

Figure 1.3.: Sketch illustrating the rotation ($\Delta\Theta$) of the maximum principal stress axis (σ_1) acting on a right lateral fault (modified after Hasegawa et al. (2011)).

First studies on the variations of the stress field applying stress inversion to earthquake sequences on major fault ruptures ($M \sim 7$) indicate variations in stress orientation in the order of 10-20° (for example in California the 1983 Coalinga earthquake (Michael, 1987),

the 1986 Oceanside earthquake (Hauksson and Jones, 1988), the 1989 Loma Prieta earthquake (Michael et al., 1990) and the Landers earthquake (Hauksson, 1994)). However, stress field variations are extremely difficult to detect since the accuracy of stress inversion results is limited. Often, the uncertainties in stress field orientation are of the same order of or only slightly less than the amplitude of the expected rotations and should be therefore interpreted with care (Townend and Zoback, 2001). Furthermore, it needs to be considered that focal mechanisms as input parameter themselves have an error of usually 10° or more. Recently, Hasegawa et al. (2011) and Hardebeck (2012) have observed significant rotations of the crustal stress field orientation exceeding 20° in conjunction with the recent $M > 8.7$ earthquakes (Sumatra-Andaman/Indonesia 2004, Maule/Chile 2010, Tohoku-Oki/Japan 2011). These rotations imply a near-complete stress drop during the main shock and were followed by a rapid back rotation of the stress axes within months after the mainshock. These studies would thus support the stress recovery model and confirm the existence of stress rotations indicating that the amplitude of rotation is clearly observable for extremely large earthquakes. While the results for the $M > 8.7$ earthquakes were clearly observable due to large rotation angles no such systematic (back-) rotation has been observed for $M < 8$ earthquakes.

The aim of this study is to investigate such potential spatiotemporal variations of the stress field orientation in conjunction with the 1999 Izmit and Düzce earthquakes at the North Anatolian Fault Zone (NAFZ) and to elaborate on spatiotemporal variations of local stress field variations using high-resolution local seismicity data in general. High-resolution local seismic recordings are used to determine and analyse potential variations of the local stress field orientation with unprecedented detail. Results obtained in this study give new insights for the contribution to the ongoing discussion whether or not local stress field rotations are a useful indicator for the loading status of individual fault segments during the seismic cycle. In addition, the findings are related to distinct seismotectonic features and variations of co-and postseismic slip along M>7 ruptures.

Furthermore, the obtained hypocenter catalogs covering the time period between 1997 and 2001 are used to investigate seismic activity of fault patches along the NAFZ and to identify possible creeping and locked fault patches in relation to postseismic deformation below the seismogenic part of the crust.

1.2. Outline of the thesis

This thesis constitutes seven chapters. Chapter 2 gives an overview of the tectonic setting and geology of the study area followed by a sum-up on the historical seismicity of the region and the segmentation of the fault zone in NW Turkey. In chapter 3 the methodology for deriving information about stress in the earth crust is introduced and different stress tensor inversion algorithms are described. In chapter 4 the data, processing steps, hypocenter location and relocation procedures applied to the Sapanca Bolu seismic network (SABONET) are explained and presented. Results regarding observed stress rotations and its recovery after the Izmit and Düzce earthquakes are discussed in chapter 5 with special focus on the pre-seismic, inter Izmit-Düzce and post-seimic phase of the Izmit and Düzce 1999 earthquake sequence. Chapter 5.2 has recently been published in the Geophysical Journal International as:

M. Ickrath, M. Bohnhoff, F. Bulut and G. Dresen: Stress rotation and recovery in conjunction with the 1999 Izmit M_w 7.4 earthquake, *Geophys. J. Int.*,(2014), 196 (2): 951-956 first published online November 2, 2013.

Chapter 5.3 is in preparation for submission to Geophysical Journal International as: M. Ickrath, M. Bohnhoff, F. Bulut, O. Germer and G. Dresen: Detailed analysis of the spatial and temporal stress field evolution along the Izmit and Düzce ruptures during the seismic cycle.

Chapter 5 also includes a reference to the paper: P. Martínez-Garzón, G. Kwiatek, M. Ickrath and Marco Bohnhoff: MSATSI: A MATLAB© package for stress inversion combining solid classic methodology, a new simplified user-handling and a visualization tool, Seismological Research Letters, (2014), 85, 896-904. This paper is included as Appendix A to this thesis. Chapter 6 is in preparation for submission to Tectonophysics and is focusing on the spatiotemporal distribution of crustal seismicity in conjunction with co- and postseismic slip distribution on the brittle and ductile part of the crust and the occurrence of shallow earthquakes along the Izmit and Düzce ruptures. Finally in chapter 7, the derived results are summarized and a concluding discussion and a short outline about potential future investigations are given.

Data and Resources Seismic waveform recordings used in this study were recorded by the SABONET and GTF seismic networks, which are described in Milkereit et al. (2000) and Baumbach et al. (2003), respectively. These data are proprietary but can be released upon request. The SABOnet in northwestern Turkey is jointly operated by GFZ and the Earthquake Research Department of the General Directorate of Disaster Affairs at Ankara. Figures were generated with the help of Generic Mapping Tools software (Wessel and Smith, 2000) and the MATLAB software program, version R2010b. For the topographic maps the SRTM data set was used which is freely available from the Internet NASA (2005); Farr et al. (2007). Stress Inversion packages LSIB and SATSI can be downloaded from http://earthquake.usgs.gov/research/software/.

2. Seismotectonic Setting of the North Anatolian Fault Zone (NAFZ)

The Eastern Mediterranean region is one of the most seismically and tectonically active areas within Europe and is dominated by the collision of the African and Arabian plates with Eurasia (McKenzie, 1972; Taymaz et al., 1991). Thereby the Arabian and African plates are moving northward relative to Eurasia with a rate of 18 to 25 mm/year and 10 mm/year, respectively (Le Pichon et al., 1999; McClusky et al., 2000). The African plate is subducted below the Eurasian plate along the Hellenic and Cyprus arcs. The Anatolian plate is situated between the converging Eurasian and Arabian plates (Fig. 2.1). Due to the northward migration of the Arabian plate and the collision with the Eurasian plate the Anatolian plate is forced to a west-directed lateral movement and a rotation which is explained by the escape tectonic-model (Ketin, 1948; McKenzie, 1972; Sengör, 1979; Şengör, 1985; Barka, 1996; Yiğitbaş et al., 2004). Caused by the westward propagation the dextral North Anatolian and sinistral East Anatolian Fault Zones were created in eastern Turkey over a time range of 10 Ma in the middle to late Miocene (Flerit et al., 2004). Figure 2.1 illustrates the described main tectonic features in the Eastern Mediterranean region.

The seismically active North Anatolian Fault Zone (NAFZ) in NW Turkey was first recognized as a major strike-slip fault in 1948 by İhsan Ketin (Ketin, 1948; Sengör et al., 2005). It is a nearly east-west trending approximately 1500 km long dextral strike-slip fault which is forming the main part of the boundary between the Eurasian and Anatolian plates (Sengör et al., 2005; Koçyiğit et al., 2001). Extending from the Karliova triple junction ("K" in Fig. 2.1) near Erzican in the east to the Gulf of Saros in the northern Aegean Sea (Koçyiğit et al., 2001) in the west, the fault has formed approximately 11 Ma ago and may have propagated westwards at a rate of 11 cm/year (Sengör et al., 2005). Overall the age of the North Anatolian Fault varies from late Miocene to early Pliocene

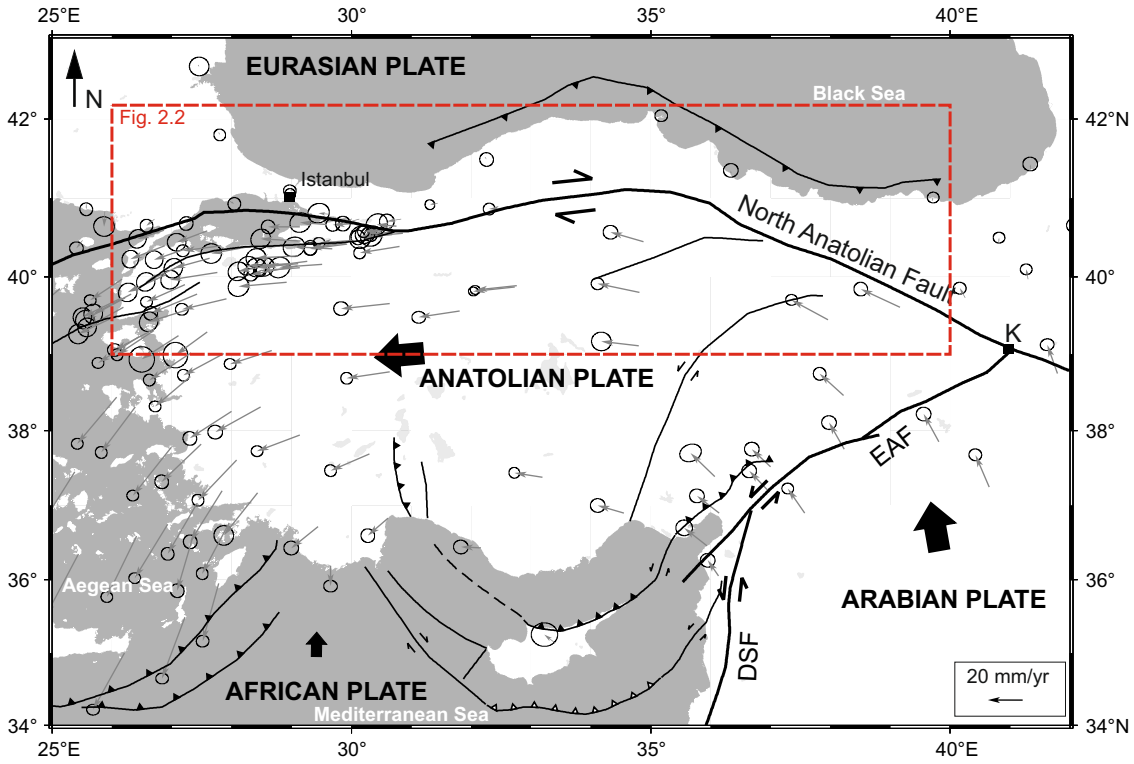

Figure 2.1.: Regional tectonic setting of the Mediterranean Sea and relative motions (grey arrows) (McClusky et al., 2000) between the Anatolian plate and the Eurasian and Arabian plates. EAF- East Anatolian Fault, DSF - Dead Sea Fault. Black arrows indicate general plate movement. Black lines indicate major tectonic plate boundaries. Faults modified after Schildgen et al. (2012). The red dashed box outlines region shown in Figure 2.2.

(13-4 Ma; see e.g., Ketin (1969); Barka and Hancock (1984); Şengör (1985)).

Reilinger et al. (1997, 2006) concluded a present average geodetic slip rate of the Anatolian block relative to Eurasia of the order of 24 ± 1 mm/yr from regional Global Positioning System (GPS) derived velocity field (McClusky et al., 2000) and Armijo et al. (1999) estimated the cumulative geological slip along the fault to 70 to 85 km, which results in a long-term slip-rate of 14 to 17 mm/year. The dextral displacement varies from about 40 km in the east (Barka, 1992), decreasing to the west with 20-30 km near the Sea of Marmara (Barka and Hancock, 1984; Barka, 1992; Sengör et al., 2005).

After the devasting earthquakes Izmit (Kocaeli) August 17, 1999 (Barka, 1999, 2000; Barka et al., 2002; Emre et al., 2003) and Düzce November 12, 1999 (Akyuz et al., 2000; Akyüz et al., 2002) the fault zone became of international interest and the Sea of Marmara and neighboring areas have been intensively investigated by geological and geophysical studies

which are summarized by (Sengör et al., 2005).

2.1. Seismicity along the NAFZ

The NAFZ is in general entirely seismically active. Egeran and Lahn (1944); Lahn (1949); Ketin and Roesli (1953) first recognized the regular occurrence of major earthquakes and their migration from east to west. Ketin (1948) first figured out that all major earthquakes in northern Turkey since 1939 had a EW-striking right-lateral fault character and concluded that they are all caused by a major, active, right-lateral, strike-slip fault. Starting with the 1939 Erzincan earthquake in the east of Turkey a 1000-km section of the North Anatolian fault ruptured in a westward migrating series of nine M>7 events (green segments in Fig. 2.2), producing continuous surface breaks from Erzincan to the eastern Sea of Marmara (Fig. 2.2, e.g.: Ketin (1948, 1969); Ambraseys (1970); Toksöz et al. (1979); Barka and Kadinsky-Cade (1988); Barka et al. (2002); Şaroğlu et al. (1992); Stein et al. (1997); Barka (1996); Lettis et al. (2000)). The time interval between these earthquakes varied from 3 months to 32 yr and the maximum horizontal displacements up to 7.5 m (Barka et al., 2002).

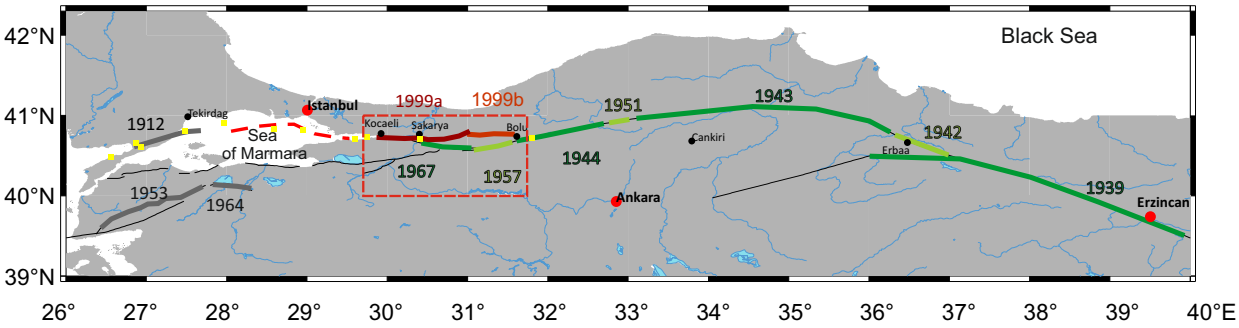

Figure 2.2.: Historical Earthquakes along the North Anatolian Fault Zone (NAFZ) in NW Turkey and the Sea of Marmara. Yellow boxes are historical earthquakes (Ambraseys, 2002), and the simplified fault zone in the Sea of Marmara is modified after Armijo et al. (2005). The green segments indicate the combined 1939-1999 earthquake sequence along the fault zone after Barka (1996); Hubert-Ferrari et al. (2000); Reilinger et al. (2006) and Meghraoui et al. (2012). Red box Fig. 2.3.

The last two major earthquakes on the NAFZ occurred in 1999, the 17 August (M_w 7.4, USGS) Izmit (Kocaeli) and the 12 November 1999 (M_w 7.1, USGS) Düzce earthquakes (1999a/b in Fig. 2.2 and labeled in Fig. 2.3). Fault plane solutions of both earthquakes

Table 2.1.: Source parameters of the Izmit and Düzce earthquakes combined from Milkereit et al. (2000); Tibi et al. (2001); Özalaybey et al. (2002) and Bohnhoff et al. (2006)

	Izmit Earthquake	Düzce Earthquake
Date	August 17, 1999	November 12, 1999
Time	00:01:38.7 UTC	16:57:20.8 UTC
Latitude (°N)	40.75	40.818
Longitude (°E)	29.86	31.198
Depth (km)	17	12.5
Magnitude M_w	7.4	7.1
Seismic Moment $M_0(Nm)$	1.47 x 10^{20}	0.47 x 10^{20}
Strike(°)	270	263
Dip(°)	83	62
Rake(°)	181	184
Rupture velocity (kms^{-1})	4.5 ?	2
Fault area L x W (km^2)	100 x 20	55 x 20
Static stess drop (MPa)	4	2
Average fault slip (m)	2.5	1.6

indicate right-lateral, strike-slip faulting with dominantly east-west striking nodal planes dipping steeply to the north (Örgülü and Aktar, 2001; Tibi et al., 2001; Bohnhoff et al., 2006). Table 2.1 summarizes the source parameters of the Izmit and Düzce earthquakes (Tibi et al., 2001; Bohnhoff et al., 2006).

The Izmit earthquake was the largest and most destructive earthquake in Turkey since the 1939 Erzincan earthquake (Toksöz et al., 1999) and produced fault rupture of 126 km (Lettis et al., 2000) from offshore beneath the eastern Sea of Marmara in the west to the Karadere-Düzce area in the east (Bouchon et al., 2002; Bulut and Aktar, 2007). This segment of the fault was previously identified as a "seismic gap" (Toksöz et al., 1999). Three months later, the Düzce earthquake extended the rupture zone by 40 km to the east (Barka, 1999) and re-ruptured a part of the easternmost already failed segment during the Izmit event (Lettis et al., 2000). The horizontal surface displacements of both events were up to 5.5 m and vertical surface displacements up to 2.4 m locally (Lettis et al., 2000).

Besides the Izmit earthquake the 1912 M_W 7.3 event on the Ganos Fault (Ambraseys, 2002; Altunel et al., 2004; Meghraoui et al., 2012) was the last event at the western end in the broader Marmara region (Fig. 2.2). The Sea of Marmara is located in between a

transition zone where the strike-slip NAFZ is also influenced by the extensional character of the Aegean sea (Sengör, 1979; Şengör, 1985; Yaltırak, 2002) and represents a more than 100 km long seismic gap that did not rupture since 1766 (Toksöz et al., 1979; Stein et al., 1997; Janssen et al., 2009) (red dashed line in Fig. 2.2). Recent studies in this area by Bohnhoff et al. (2013) identified a 30-km-long aseismic fault patch to a depth of 10 km from microseismic recordings of a permanent installed seismic array (PIRES) (Bulut et al., 2009).

King et al. (2001) first modeled the state of stress after the Izmit earthquake. He concluded like Parsons et al. (2000), Hubert-Ferrari et al. (2000) and Le Pichon et al. (2003) that the Izmit and Düzce events have loaded the Marmara segment of the fault and that there a major, M $\geq$ 7 event near Istanbul is expected with 62 $\pm$ 15% probability during the next 30 years and 32 $\pm$ 12% during the next decade (Parsons et al., 2000).

The analysis of historical seismicity along the fault and its regularity is under debate. Sengör et al. (2005) analysed historical seismicity but could not find a similar migration pattern and regular or cyclical behavior of the NAFZ in the last centuries similar to this occurrence of seismic event following the Erzican 1939 earthquake. The history of this earthquake cycle with the most recent Izmit and Düzce earthquakes is summarized by Barka (1996) and Toksöz et al. (1999). Stein et al. (1997) and Lettis et al. (2000) postulate that the NAFZ has undergone several complete cycles of seismic strain accumulation and release over the last thousand years. Ambraseys (1970) observed at least two other similar large earthquake sequences in the last 1000 years along the NAFZ in 1254 to 1784 and 967 to 1050. Sengör et al. (2005) observed two relatively quiescent regions along the fault zone between latitude 36°E and 38°E and between 26°30‘E and 27°30‘E probably caused by great strain energy released during the large earthquakes in 1939 and 1912, respectively in these segments. Fraser et al. (2010) combined all existing studies of paleoearthquakes on the NAFZ and suggested that the NAFZ did not rupture the same fault segments during every seismic cycle. The study revealed that the 20th century earthquake sequence is not typical for the NAFZ but may occur occasionally.

2.2. Segmentation of the Fault Zone

The relationship between fault geometry, seismic activity and clustering of earthquakes is a subject of great interest. Barka and Kadinsky-Cade (1988) describes that the distribution of bends and offsets along a fault plays an important role in controlling the location of large earthquakes and gives an overview of different kinds of geometric pattern and segmentation of a fault.

The NAFZ is defined by a narrow fault valley (Koçyiğit et al., 2001) consisting of numerous discontinuous, a variety of basin types and overlapping fault strand, which often act as barriers to fault rupture and thus divide the fault into specific segments (Fig. 2.4 Lettis et al. (2000)). This segmentation is caused by the Arabian-Eurasian collision in the Miocene (Armijo et al., 1999) which developed a series of *en echelon* and branching fault segments along the fault zone (Lettis et al., 2000).

Stein et al. (1997) postulate that the probability for a future earthquake increases in the region adjacent to a previous occurred large earthquake since the stress drops on the ruptured fault and increases at adjacent sites which brings these areas closer to failure. They interpreted the westward migration of the large earthquakes of the recent seismic cycle at the NAFZ in terms of the Mohr-Coulomb failure model (Coulomb, 1776; Handin, 1969). According to the Mohr-Coulomb failure criterion, if the shear traction on an active fault exceed the critical value τ_c,

$$\tau_c = C + \mu(\sigma_n - p) \tag{2.1}$$

with C is cohesion, μ the fault friction, σ_n the normal traction and p the pore pressure, the fault becomes unstable and an earthquake occurs along this fault. Stein et al. (1997) explain the clustering of the fault with this model of dislocations and explained it by the concentration of the shear stress at the western tip of each broken segments.

In the following, the main tectonic and geological features along the Izmit and Düzce rupture are introduced. Ardel (1965), Neugebauer (1995), Langridge et al. (2002) and Sengör et al. (2005) describe these patterns in more detail.

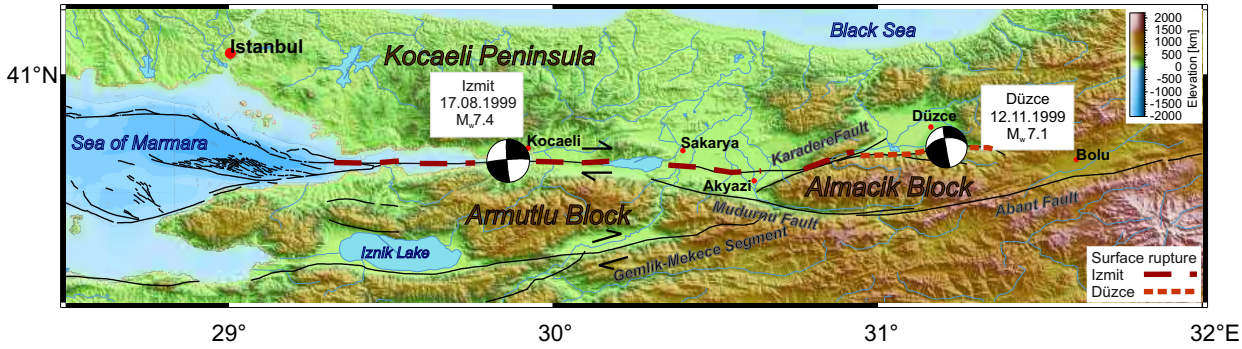

Figure 2.3.: Topographic map of the North Anatolian Fault Zone (NAFZ) with the main tectonic and geological units. Faults are taken from Meghraoui et al. (2012). Fault plane solutions for the Izmit and Düzce events from Tibi et al. (2001).

The geology along the NAFZ reflects the sedimentary and deformation history of northern Turkey caused by the Arabian-Eurasian collision. The bedrock consists of Mesozoic to Eocence aged sequences of mostly lacustrine sediments and volcanic units that were deposited before the collision (Sengör et al., 2005). The NAFZ consists mainly of a single fault strand that splays in two major branches: a northern and southern branch near the Mudurnu valley (Neugebauer, 1995; Karahan et al., 2001) and is segmented by several pull-apart and extensional basins filled with Pliocene and Pleistocene terrestrial sediments. The two branches: the Karadere-Düzce in the north and the Mudurnu in the south (Greber, 1970, 1997) bounding the Almacik block which represents an elevated crustal block with a metamorphic core and local sedimentary and volcanic cover (Fig. 2.3, Sengör et al. (2005)). The Mudurnu fault hosted an M_w 7.1 earthquake in 1967, was not activated during the 1999 Izmit rupture (Ambraseys and Zatopek, 1969) and did not host a single Izmit aftershock (Stierle et al., 2014).

The rupture zones of the Izmit and Düzce earthquake consist of distinct segments of the NAFZ, from west to east: the Yalova, Gölcük, Sapanca, Sakarya, Karadere and Düzce segments (Fig. 2.4, Lettis et al. (2002)). The length of the segments varies from 26 to 36 km and each of it is separated by pull-apart structural basins, releasing en-echelon step-overs of 1-4 km width (Barka et al., 2002) or a gap in the fault trace (Lettis et al., 2002) like the Lake Sapanca stepover basin, Akyazi gap and Eften Lake stepover. These are summarized by Lettis et al. (2002).

Duman et al. (2005) investigated stepovers associated with the Düzce earthquake and

their influence on rupture propagation. Similar to the Izmit rupture the earthquake broke distinct segments, separated by stepovers. Thereby the 40-km-long rupture propagated through 0.8 to 2 km wide stepovers, but was arrested at stepovers wider than 4 km. These observations fit to the general idea of ratios between stepover width and strike-slip displacement collected along strike-slip faults worldwide (Lettis et al., 2002). In the following from west to east the Sapanca, Sakarya, Karadere, Düzce segments and corresponding stepovers will be closer described (Figure 2.4).

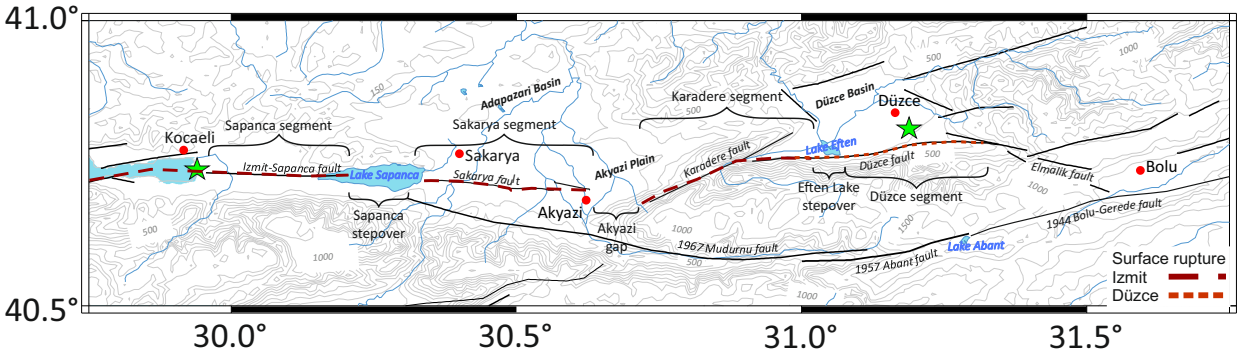

Figure 2.4.: Segmentation along the North Anatolian Fault Zone (NAFZ) associated with the fault ruptures of 17 August 1999 Izmit (Sapanca segment, Sakarya segment and Karadere segment from west to east) and 12 November 1999 Düzce (Düzce segment) earthquakes (green stars). In addition the prominent extensional stepovers are combined from Langridge et al. (2002); Lettis et al. (2002)). Faults are taken from Langridge et al. (2002).
.

2.2.1. The Sapanca Segment

The Sapanca segment hosted the Izmit mainshock epicentre in the west (green star Fig. 2.4). It follows a well-defined preexisting fault trace and crosses broad, alluvial floodplains and bedrock ridges (Lettis et al., 2002). Bohnhoff et al. (2006) investigated focal mechanisms from Izmit aftershocks which indicate predominantly right-lateral strike-slip and a few normal faulting mechanisms. In the east, the segment is connected to the Sakarya segment through the 1- to 2-km-wide right-releasing Lake Sapanca stepover and is forming the junction of the Izmit rupture with the rupture of the M_w 7.1 1967 earthquake at the Mudurnu fault on the southern branch of the NAFZ.

2.2.2. The Sakarya Segment

The Sakarya segment is following the preexisting fault trace by intersecting the broad alluvial Adapazari-Akyazi basin and is separated from the Karadere segment by a 1 to 2 km wide, 6 km long left-restraining gap (Akyazi gap) in the fault near the city of Akyazi (Langridge et al., 2002; Lettis et al., 2002). The segment is dominated by a high aftershock activity with mostly east-west extensional normal faulting mechanism and an abrupt decrease of coseismic displacement of $<$1 m (Bohnhoff et al., 2006).

The Adapazari-Akyazi Basin

The Adapazari-Akyazi basin of Holocene age (Neugebauer, 1995; Karahan et al., 2001) lies east from the triple junction formed by the EW trending Sakarya and NE-trending Karadere fault and the ESE-striking Mudurnu fault (Bohnhoff et al., 2006). In some studies it is considered separately as the Adapazari basin and the Akyazi plain (Ardel, 1965; Greber, 1970, 1997; Ünay et al., 2001). The basin was mainly formed by NW-SE striking normal faulting and oblique NE-SW striking right-lateral faults and is covered with a more than 550 m thick (Bilgin, 1984) sedimentary layer of Upper Pliocene to Lower Pleistocene age interbedded with various tuff layers, indicating concurrent volcanism (Sengör et al., 2005). Inside the basin there is an almost 6-km-long section east of Akyazi - the Akyazi gap (Langridge et al., 2002; Lettis et al., 2002), characterized by no aftershock activity and no recognized coseismic slip (Barka et al., 2002), leading to the conclusion that no strain was released there during the Izmit main shock (Hurd and Bohnhoff, 2012).

2.2.3. The Karadere Segment

This 20 km long segment is the easternmost segment that ruptured during the 17 August 1999 Izmit earthquake and is located near the town of Akyazi. It is separated from the ESE-trending Sakarya segment due to an abrupt change in strike to NNE (N65°E) trend (Dikibaş and Akyüz, 2011) for the Karadere fault. Bulut and Aktar (2007) obtained from relocated Izmit aftershocks that the Karadere fault dips with an angle of 67° to the NNW. The coseismic slip during the Izmit earthquake along the Karadere fault is not uniform and the maximum dextral displacement varies between 2.3 m towards its eastern end (Duman et al., 2003) and 1.5 m in average (Hartleb et al., 2002).

2.2.4. The Düzce Segment

The Düzce segment consists of the Düzce Basin and the Düzce fault, the southern boundary of the basin (Fig. 2.4). The Düzce basin was interpreted by Aydin and Kalafat (2002) as a pull-apart basin filled with approximately 260 m thick clastic fluviatile/lacustrine sediments with an age of upper Pliocene to Holocene sitting on volcanogenic flysch of Eocene age (Sengör et al., 2005; Pucci et al., 2006). The basin has a nearly rhomboidal appearance with irregular eastern and western margins that are bounded by NE-SW mainly right-lateral striking faults and NW-SE striking normal faults (Ardel, 1965).

The Düzce fault separates the older Paleozoic-Eocene formations of the Almacik block from the younger continental deposits of the Düzce basin (Aydin and Kalafat, 2002; Pucci et al., 2007) and splays out from the WSW-ENE trending Karadere fault. The western boundary of the fault represents a major asperity which was activated by the eastern end of the Izmit rupture but did not proceed to rupture until 87 days later (Lettis et al., 2002; Peng and Ben-Zion, 2006; Görgün et al., 2010; Li et al., 2014). According to Lettis et al. (2002) this asperity is formed by the complex right releasing Lake Eften stepover (Fig. 2.4). The Eften lake has migrated 7 km in 2.5 Ma from the central part of the Düzce basin southwestward and represent the present-day Düzce Basin depocentre [1] (Pucci et al., 2006, 2007). The eastern extension of the Düzce fault is not well studied so far and may join the eastern single trace of the NAFZ via some stepovers and the WNW-ESE trending Elmalik fault, where no surface rupture during the Izmit and Düzce earthquake was observed (Fig. 2.4) (Akyüz et al., 2002; Langridge et al., 2002; Pucci et al., 2006).

[1] The site of maximum deposition within a sedimentary basin, where the thickest development of the sedimentary sequence will be found (Allaby and Allaby, 1999).

3. Determining Stress Field Orientation by Stress Tensor Inversion.

3.1. Fundamentals

The stress of the earth's crust is an important parameter in solid earth sciences since all long-term geological processes are driven by forces that generate different types of stresses within the crust (Zoback, 1992; Zang and Stephansson, 2010). Crustal stresses are the direct driving forces of earthquakes and the analysis of spatial and temporal variation of crustal stresses can hence give insights into earthquake mechanics, tectonic loading and earthquake stress interactions. The stress field can be described by three principal stress components: the minimum horizontal stress (S_h), the maximum horizontal stress (S_H) and the vertical stress, S_V.

Crustal stresses can only be measured directly by in situ measurements typically based on drilling boreholes. Since the accuracy is limited and drilling is quite expensive, direct measurements of crustal stresses are rare.

Possibilities to get information about stresses in the crust is to use striations observed on fault planes since they represent the direction of the maximum resolved shear stress on each fault plane (Bott, 1959). The most common method is to use focal mechanisms from earthquakes, since the rupture depends on the stress vector acting on the fault plane. A new approach is to directly invert first-motion polarities from seismological studies (Robinson and McGinty, 2000; Abers and Gephart, 2001).

The state of stress is described by the stress tensor

$$\sigma \equiv \sigma_{ij} \equiv \begin{pmatrix} \sigma_{11} & \sigma_{12} & \sigma_{13} \\ \sigma_{21} & \sigma_{22} & \sigma_{23} \\ \sigma_{31} & \sigma_{32} & \sigma_{33} \end{pmatrix} \tag{3.1}$$

$\sigma \equiv \sigma_{ij}$ that describes the corresponding stress vector for each possible surface plane (A_j) in a volume (V). Because of force equilibrium only six of the nine components of the stress tensor are independent and an essential symmetry $\sigma_{ij} = \sigma_{ji}$ is valid. The three principal stress axes correspond to a stress vector perpendicular to the plane where no shear stress is applied. Figure 3.1 shows the three principal faulting types and the corresponding principal stress axis acting on the fault.

Mostly earthquakes occur on preexisting fault planes under the same state of stress (McKenzie, 1969). Caused by this, the angle between the main principle stress axis σ_1 and the stress tensor that produced the shear stress corresponding to the slip direction is unknown. A variety of observations of fault slip on multiple different oriented fault planes with slip events related to the same stress field are needed to determine possible stress tensors. The best constrained stress tensor is calculated by inversion searching for the global minimum of the total misfit (Plenkers, 2006).

The Stress Tensor Inversion (STI) is a non-linear problem, that can be solved directly using grid-search algorithms (Gephart and Forsyth, 1984; Arnold and Townend, 2007), Monte-Carlo sampling-based optimization methods (?Angelier, 1984) or the Hybrid Global optimization method (Xu, 2004). Due to the high computationally performance of non-linear approaches the problem is often linearized using additional assumptions and a least-square solution (Michael, 1984; Reches, 1987; Hardebeck and Michael, 2006).

Stress inversion algorithms estimate four parameters which define the stress conditions of a region: the orientation of the three principal stresses $\sigma_1, \sigma_2, \sigma_3$ ($\sigma_1 > \sigma_2 > \sigma_3$) and a parameter defining the shape of the deviatoric stress ellipsoid, the stress ratio R ($1 \geq R \geq 0$) (Angelier, 1979) :

$$R = \frac{\sigma_1 - \sigma_2}{\sigma_1 - \sigma_3} \tag{3.2}$$

or ϕ (Carey and Brunier, 1974):

$$\phi = \frac{\sigma_2 - \sigma_3}{\sigma_1 - \sigma_3} \tag{3.3}$$

with

$$R = 1 - \phi \tag{3.4}$$

giving the relative size of the intermediate principal stress with respect to the maximum

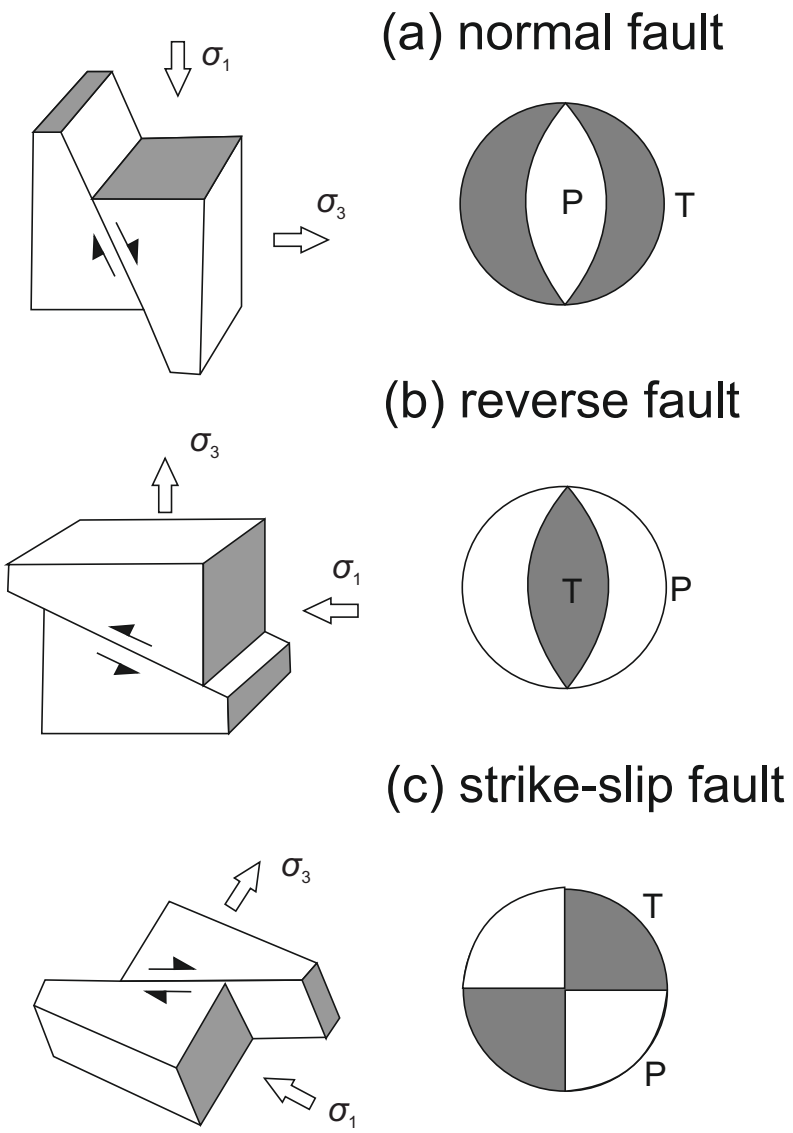

Figure 3.1.: Sketch of the three main faulting types and the corresponding principal stress axis acting on the fault (a-c show the corresponding focal mechanism) modified after *USGS*.

principal stress and minimum principal stress (McKenzie, 1969; Gephart and Forsyth, 1984). The value of R together with the obtained stress tensor gives important insights on the state of stress in the area of interest.

If $R = 1$, σ_2 and σ_3 are nearly equivalent and depending on the stress regime, in a normal faulting ($\sigma_V = \sigma_1$ and $\sigma_{H_{max}} = \sigma_2$) or a strike-slip regime ($\sigma_V = \sigma_2$ and $\sigma_{H_{max}} = \sigma_1$), the stress state is pure normal or transitional to thrust faulting, respectively.

If $R = 0$, σ_2 and σ_1 are nearly equivalent and indicate that the maximum horizontal and vertical stresses are equal ($\sigma_{H_{max}} = \sigma_V$) which implies a stress regime between strike-slip and normal faulting.

In general, values for $R < 0.5$ and $R > 0.5$ indicate a transtensional and transpressional regime, respectively. Bellier and Zoback (1995), Bellier et al. (1997), Ritz and Taboada (1993) and Ghimire et al. (2005) provide detailed discussions on the interpretation of R values.

The different stress inversion methods were extensively discussed in the literature (e.g. Michael (1984); Gephart (1990); Hardebeck and Hauksson (2001b); Townend and Zoback (2001); Abers and Gephart (2001); Plenkers (2006)). All inversion techniques presume two basic assumptions:

(a) that the stress field in the region of interest is homogenous and

(b) slip (s) occurs along the direction of the maximum resolved shear stress (τ) (Wallace-Bott-criterion (preexisting weakness) Wallace (1951); Bott (1959)) :

$$\frac{\vec{\tau}_{max}}{|\vec{\tau}_{max}|} \equiv \frac{\vec{s}}{|\vec{s}|} \tag{3.5}$$

(McKenzie, 1969; Gephart and Forsyth, 1984). The assumption of a homogeneous stress field is widely discussed (e.g.: Michael (1991); Stein et al. (1992); Zoback (1992) and Rivera and Cisternas (1990)) but it is agreed that the stress field is relatively homogeneous when the inversion is restricted to rather small areas because there the long-term background stress field is constant. The standard methods generally provide similar results but differ in the uncertainty assessment (Hardebeck and Hauksson, 2001b; Bohnhoff et al., 2004). Figure 3.2 represents the general procedure of Stress Tensor Inversions.

Techniques which invert earthquake focal mechanisms for deriving stress field orientation (e.g.: Angelier (1984); Michael (1984); Gephart and Forsyth (1984)) are in addition

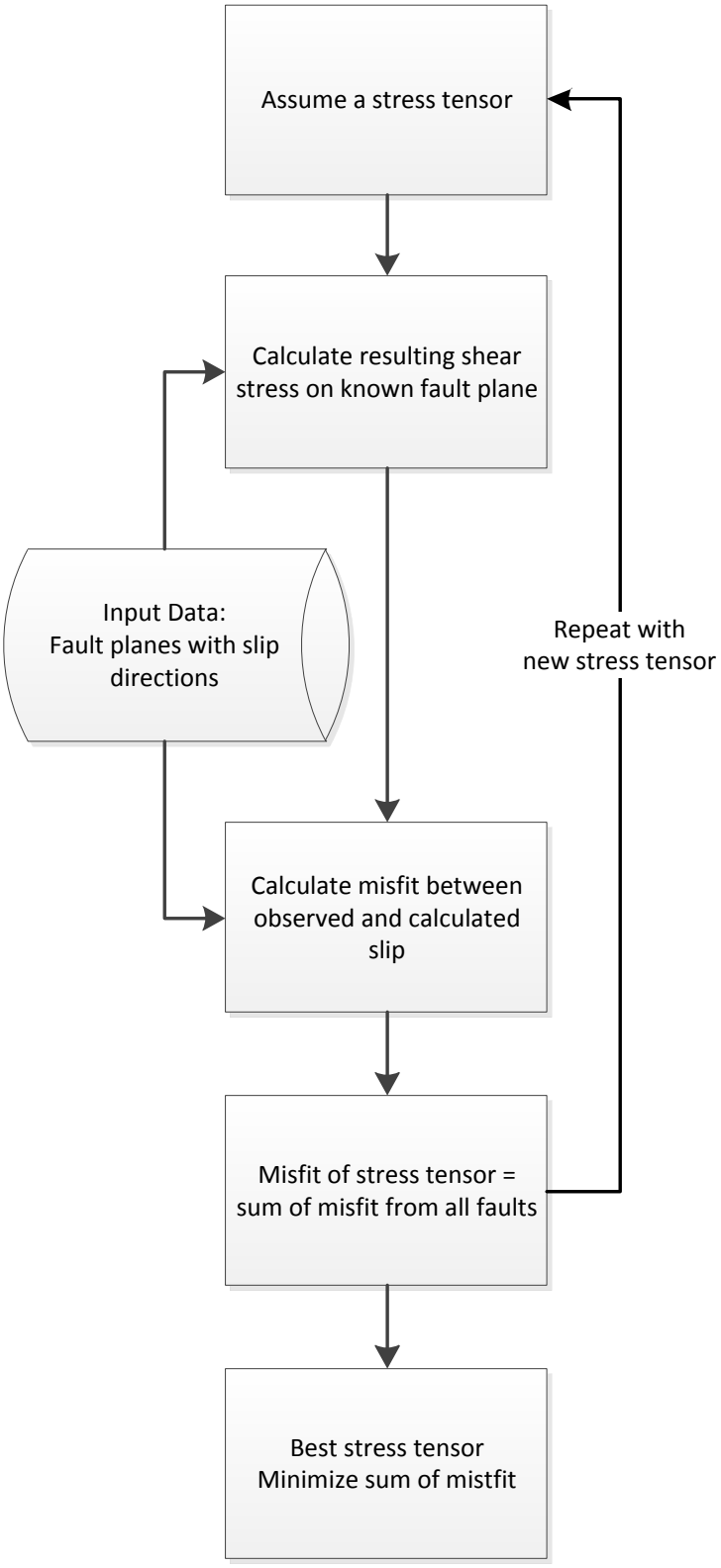

Figure 3.2.: Schematic flowchart for the general procedure of Stress Tensor Inversion (modified after Plenkers (2006))

based on the assumptions that the used focal mechanisms data set should be sufficient diverse (Hardebeck and Hauksson, 2001a) which can be tested by analysing P and T axis distribution. Regarding the general assumption that the stress field is homogeneous, Michael (1991) concluded that an inversion is reliable as far as the average misfit of the focal mechanism to the best fitting stress tensor is less than 35° - 45°. Then the result will correctly represent the uniform part of the stress tensor. There are some restrictions in determining stress from fault plane solutions.
One is the ambiguity of focal mechanisms consisting of two perpendicular nodal planes, the actual fault plane and the auxiliary plane, caused by the symmetry of the double couple force model. There are two possibilities dealing with this, either it is known a priori which nodal plane is the actual fault plane or an algorithm is used that takes the ambiguity into account (Angelier, 2002). Another limitation is that the focal mechanism parameters (strike, dip, rake) often have reasonable large uncertainties in the order of 25° (Hardebeck and Hauksson, 2001a). But it is generally agreed that with a diverse data set consisting of more than 30 focal mechanisms the stress tensor orientation can be determined with much greater accuracy and precision.

Often it is discussed if P- and T-axis may represent the direction of the principal stresses, since the P axis lies within the quadrant of dilatational initial motions and can be described as the axis of max. shortening, whereas the T axis lies within the quadrant of compressional initial motions as the axis of max. lengthening (Fig. 3.1, Barth et al. (2008)). But P- and T-axis differ from the exact direction of the principal stresses since:
(1) earthquakes often occur due to slip on preexisting fault planes with frictional strength far below than the intact rock mass, and
(2) following Byerlee's frictional criteria (Byerlee (1978); Sibson (1994)), even if an earthquake results from the shear failure of intact crust it can lead to a deviation of up to ±20° of the principal stress directions from the P- and T-axes (McKenzie, 1969; Yuichiro and Ghimire, 2011).

In the following Stress Tensor Inversion (STI) methods used in the study will be shortly described and introduced.

3.2. Linear Stress Inversion with Bootstrapping (LSIB) Method.

The unnamed inversion technique proposed by Michael (1984); **?** (source code Slick Package can be downloaded from http://earthquake.usgs.gov/research/software/) was originally designed for slickenside data. Following Hardebeck and Hauksson (2001b) we will refer to this as the Linear Stress Inversion with Bootstrapping (LSIB) method. The method is based on a linear inversion algorithm which uses the orientation of a set of fault planes (strike and dip) and the direction of slip (rake). Given this, the inversion method determines the best-fitting stress tensor by using a least-squares method using Gaussian elimination and minimizing the difference between the predicted shear stress vector on each fault plane and the observed slip direction. To linearize the inversion problem Michael (1984) considered the additional assumption, that the shear stress magnitude $|\vec{\tau}|$ is constant on all fault planes which leads to the adjusted Wallace-Bott-criterion (compare to Eq. 3.5):

$$\vec{\tau}_{max} \equiv \frac{\vec{s}}{|\vec{s}|} \tag{3.6}$$

The bootstrapping procedure for calculating confidence intervals is explained in section 3.5.

3.3. Spatial And Temporal Stress Inversion - SATSI/MSATSI

Additionally, we also use the new developed software package MSATSI based on the Stress Inversion algorithm SATSI (Spatial And Temporal Stress Inversion) (Hardebeck and Michael, 2006) which is a modified version of the slickenside package from Michael (1984, 1987). The inversion is especially designed to study spatial and temporal stress heterogeneity using a damped inversion method that simultaneously inverts for the stress field orientation in subareas while minimizing the difference in stress between adjacent subareas. MSATSI has a user-friendly interface using MATLAB environment with a significant overall performance, stability improvement and comprehensive error handling (Martínez-Garzón et al., 2014). Compared to the Michael code the damped inversion re-

moves possible stress rotation artifacts exhibited by an undamped inversion and resolves true stress rotations more clearly than a moving-window inversion. For a more detailed description of the SATSI/MSATSI software please see the joint manuscript Martínez-Garzón et al. (2014) in Appendix A. The software MSATSI is available to download from: http://www.induced.pl/msatsi and http://www.gfz-potsdam.de/en/research/organizational-units/departments/department-3/geomechanics-and-rheology/projects/software/msatsi/ and the SATSI code is available to download at: http://earthquake.usgs.gov/research/software/SATSI.

3.4. Direct Inversion of Earthquake First Motion - MOTSI

Since inversion schemes using focal mechanism as inputs are depending on the quality of the measurements, clarity of P-wave polarity, number of available seismographs and azimuthal station coverage, misfits may arise due to the errors in determining the fault plane solutions. That is why the approaches for stress inversion algorithms that are directly inverting earthquake first motion data for the stress tensor without assuming that focal mechanism are known, became of special interest.

One approach is the direct inversion of earthquake first motion, called MOTSI (first MOTion Stress Inversion) by Abers and Gephart (2001). It is a nonlinear inversion scheme which is based on the Focal Mechanism Stress Inversion (FMSI) algorithm of Gephart (1990) but calculates the stress tensor from first motions rather than from focal mechanisms. Additional to the Wallace-Bott criteria it is assumed that all motion on a fault within a specific volume of crust are due to the same stress tensor. The inversion uses a grid search technique to estimate the best-fitting stress parameters and the focal mechanism consistent with both the calculated stress and the first motions. The inversion performs two linked grid searches. One outer search is sequentially testing independent stress models. The inner search is calculating a suite of stress consistent focal mechanisms for each stress model over a grid of fault planes for each event. In a last step each stress consistent focal mechanism will be compared to the first motions to find the best fitting solution.

Other approaches of direct first motion inversion are the linearized schemes proposed by Rivera and Cisternas (1990) and nonlinear schemes from Horiuchi et al. (1995) and Robinson and McGinty (2000), which differ in the handling of error assessments.

3.5. Calculation of Confidence Intervals

Since we are in particular looking for small-scale variation of the stress field the calculation of significant confidence intervals is essential. Most statistical analysis assume a Gaussian error distribution but Gephart and Forsyth (1984) showed that this assumption is not the case for fault plane solutions. Hardebeck and Hauksson (2001b) analysed the uncertainties assessment for the two most common STIs from Gephart and Forsyth (1984) and **?**. Both approaches provides accurate estimates of stress orientation but differ in their confidence intervals. Hardebeck and Hauksson (2001b) concluded that the method from Gephart and Forsyth (1984) is preferred for high-quality data sets since the confidence intervals are mostly too large whereas the LSIB method from **?** provides a more appropriate estimate of uncertainty and is recommended for more noisy data sets. Besides the optimized computing time this is another advantage of the LSIB method. The methods from **?** (LSIB) and Hardebeck and Michael (2006)(SATSI) deal with the calculation of confidence intervals by using the statistical tool of bootstrap resampling technique. To simulate a significant repetition of an analysis a number of events is randomly picked from the original data set. Thereby some events can be twice whereas others could be completely absent. Over many resampling repetitions, 2000 times are suggested, the errors will be averaged and will give the true variation of the process. In addition to that, **?** implemented the random selection of one of the two nodal planes of a focal mechanism, if the actual fault plane is not known or is uncertain. Efron and Tibshirani (1986, 1994) give an overview of bootstrap resampling techniques.

The confidence intervals estimations for the MOTSI scheme are done in two steps. First, the error rates for each data subset are calculated. This is based on the unbaised estimation of binominal probabilities, which is here the ratio L_j/N_j, with the number of correctly predicted polarities (L_j) and the total number of picks (N_j). In a second step a score value S_j is determined giving the fit of a focal mechanism to the first motions. The difference between each score value and the maximum score (best fitting stress tensor), which have standard normal distribution with unit variance, builds the basis for the estimation of confidence interval from a probability density function for the four stress parameters (σ_{1-3} and R). For the final result presentation the marginal confidence limits

are calculated for one or two of the four parameters. For detail description please see Abers and Gephart (2001). Balfour et al. (2005) compared three different stress inversion on a dataset from New Zealand and noticed that the MOTSI procedure results mostly in larger confidence regions compared to focal mechanism based stress inversion. They concluded that this is caused by incorporate errors of mispicked first motions and the overall uncertainty in each focal mechanism that are excluded from other algorithms. Hence, the MOTSI procedure gives probably a better indication of the real uncertainties in the stress model given by the original observations.

4. The seismic SApanca-BOlu NETwork (SABONET)

4.1. Network

Within the German-Turkish earthquake research project a permanent seismic network was installed along the northern branch of the North Anatolian fault, east of Istanbul, to detect the seismic activity in the area between the *Sapanca* Lake and the city of *Bolu*. The SApanca-BOlu NETwork (SABONET) covers therefor well the surface ruptures from the Izmit and Düzce earthquakes and the area of aftershock activity. The seismological monitoring between the cities of Adapazari (Sakarya) and Bolu started in 1984. After a technical renewal of the instrumentation in 1996 the data were transferred in real-time and stored at the on-line data analysis center in Adapazari (Sakarya) (Milkereit et al., 2000).

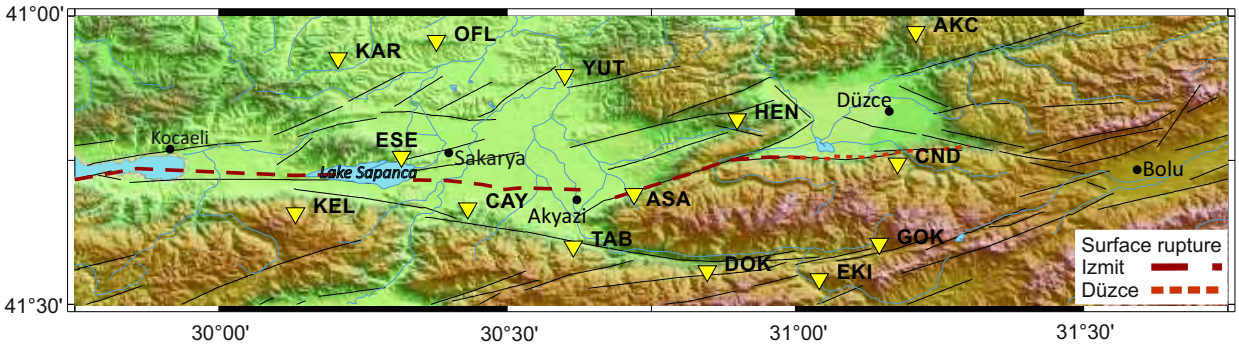

Figure 4.1.: Stationmap of the SApanca-BOlu NETwork (SABONET) in northwestern Turkey. Fault modified after Saroglu (1985). For topography SRTM grid is used.

The complete network, consisting of 15 short period stations, covers an area of about 220 km by 70 km with an average spacing of 20km (Fig. 4.1 and Table 4.1). The stations are equipped with Mark L4-3D 1Hz geophones, 24-bit digitizer with a sampling rate of 100 Hz and global positioning system (GPS) timing (Milkereit et al., 2000; Baumbach

et al., 2003; Bindi et al., 2007). For further station parameters please see Appendix B.2.

Table 4.1.: Station Coordinates and Elevation.

Station ID	Latitude (N)	Longitude (E)	Elevation (m)
AKC	40.9723	31.2089	680
CAY	40.6665	30.4315	291
CND	40.7445	31.1771	950
CIN	40.436	30.3057	1100
DOK	40.5579	30.8467	635
EKI	40.544	31.0412	890
GOK	40.6052	31.1453	228
HEN	40.8214	30.8986	590
KAR	40.927	30.2065	260
KEL	40.6581	30.1328	1150
TAB	40.6006	30.6147	400
YUT	40.8978	30.6001	147
OFL	40.9573	30.3771	350
ASA	40.6915	30.7199	228
ESE	40.7562	30.3167	374

For this study data of a six-year time period between 1997 - 2003 (Appendix: B.3) were available which cover the time span 3 years prior to and after the Izmit and Düzce events. This database which covers the surface ruptures of the Izmit and Düzce earthquakes and the area of aftershock activity represents a fundamental database to determine the local stress field and to search for potential stress rotations related to a major earthquake at a major transform fault.

4.2. Event Database

The real-time data were stored in Nanometrics data format. An event detection technique based on a STA/LTA trigger (short-term-average through long-term-average) was applied to the continuous recordings. For the STA/LTA trigger procedure the signal-to-noise ratio is calculated for two defined time windows that are simultaneously moving along the continuous data. Within the long-term-average (LTA) window, which has a common duration of 60 seconds, the average amplitude of the background noise is calculated. The

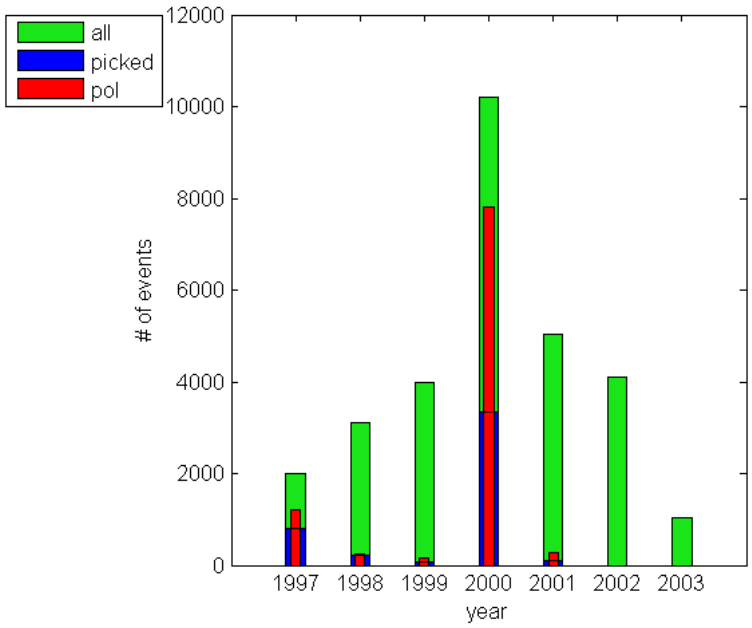

Figure 4.2: Event statistics for the SABONET database for the time period from 1997-2003. Bars represent the triggered events (green), the picked and located events (blue) and the number of picked polarities (red), respectively.

short-term average (STA) window measures the instant amplitude of the seismic signal. Typical lengths of the STA window differ between 0.3 - 0.5 s for local earthquakes and 1-2 s for regional earthquakes (Havskov et al., 2002). In this network a seismic event is defined when the ratio of the STA and LTA window exceeds a given threshold and coherent event times are identified at least at four different stations of the network (Milkereit et al., 2000). For building up the event database the pre-triggered data were converted from Nanometrics to SAC data format (flowchart Appendix B.1). Due to the large false triggering of events caused by the noise conditions and the great number of aftershocks (approximately 40000 aftershocks, 2000 triggers per day one day after Izmit to 100 triggers per day in the beginning of November (Milkereit et al., 2000)) an additional trigger was used. A smaller STA window was used to separate multiple events triggered within one time window and to merge corresponding components that were triggered separately. Figure 4.2 displays a histogram of the triggered (green bar) and located events (blue bar) and the number of picked polarities (red bar) data within the time period of 1997 - 2003. During this time period approximately one third (∼9000 events) of the recorded and pre-triggered seismic signals were real earthquakes.

4.3. Earthquake Location

Within this study data from the SABONET for the years 1997, 1998, 2000 and 2001 were selected and further processed. Caused by the high seismic activity and since P-wave polarities are needed for the stress tensor inversion, an automatic earthquake location procedure was not reliable. All events were manually picked for their P- and S-wave arrival time and first-motion polarity of the P-wave. The total number of processed

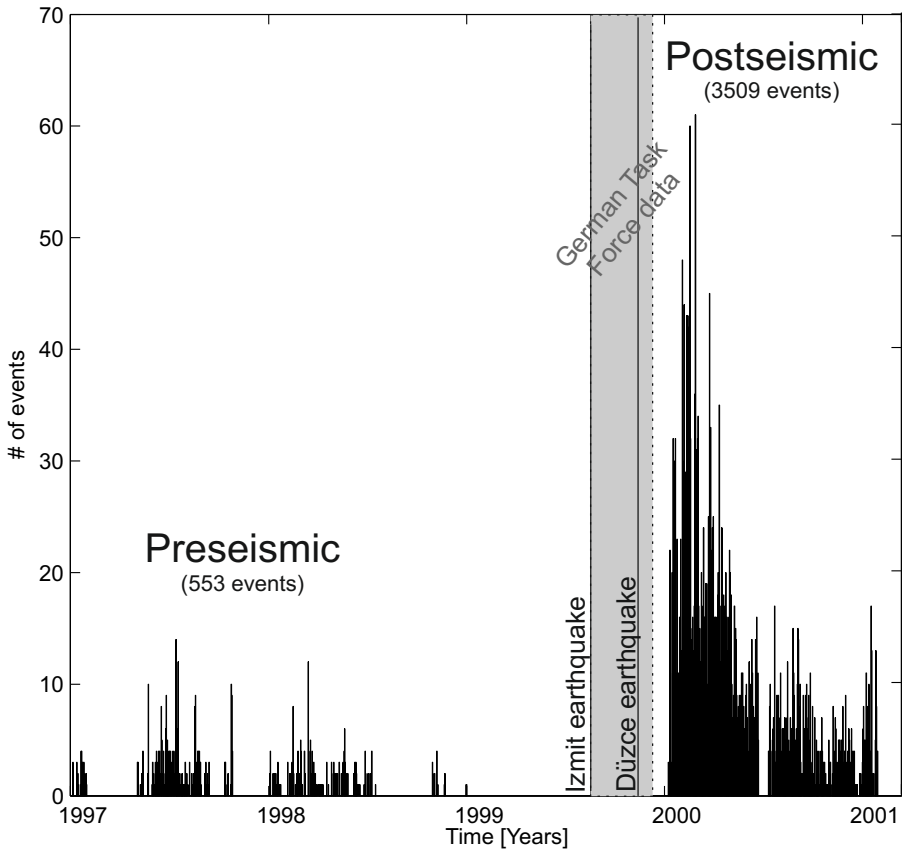

Figure 4.3.: Event-time histogram of the SABONET event database processed within this study for the years 1997, 1998, 2000 and 2001. For the pre and postseismic phase of the Izmit and Düzce earthquakes the number of processed and localized earthquakes is given in brackets. The grey shaded area illustrates the time period of the German Task Force (GTF) Izmit Aftershock catalogue (coseismic phase) that is used additionally in this study.

events is illustrated in the event-time histogram in figure 4.3 for the pre- and post-seismic phase of the Izmit and Düzce earthquakes in 1999.

For the absolute hypocenter determination of the earthquakes the HYPOCENTER

Table 4.2.: 1-D Velocity model after Bulut et al. (2007).

Depths (km)	V_P (km/s)
0.0	2.90
1.0	4.70
7.0	5.30
11.0	6.06
15.0	6.88
35.0	8.06

location program (Lienert et al., 1986; Lienert and Havskov, 1995) based on HYPO71 (Lee and Lahr, 1972) is used. The observed arrival times for P and S waves at different stations are thereby fitted to theoretical calculated arrival times based on a given velocity model and solved for the hypocentral parameters. We used the 1-D velocity model calculated by Bulut et al. (2007) based on the aftershock catalogue of the Izmit 1999 earthquake (see table 4.2).

In total 4062 local events were located based on a total number of 16378 P-picks and 14242 S-picks, this results in 2527 P-picks and 2048 S-picks for the pre-seismic phase and 13851 P-picks and 12194 S-picks for the post-seismic phase. The location errors (rms value, horizontal errors (x,y), depth error, gap) and the histogram for the number of stations and picked P-and S-picks for each event is given in Figure 4.5. The statistically estimated average horizontal and vertical errors are 2.3 and 3.6 km, respectively. The hypocentral depth of the events extends between 5-20 km which correspond to the seismogenic zone of this area and obtained depth distribution in other studies (Fig. 4.4, e.g.: Bohnhoff et al. 2008; Görgün et al. 2009; Aktar et al. 2004; Bulut and Aktar 2007)). A detailed analysis of the distribution of seismicity will follow in Chapter 7.

In addition, magnitudes (M_{coda}) were calculated using the coda length (t_{coda}), which is the total duration in seconds of the earthquake recording from the p-wave onset (t_p) to the end of event where no signal is seen above the noise (t) (Havskov and Ottemoller, 2010). The calculation is based on the equations 4.1 and 4.2:

$$t_{coda} = t - t_p \tag{4.1}$$

$$M_{coda} = alog(t_{coda}) + br + c \tag{4.2}$$

where a, b and c are constants and r is the hypocentral distance (Havskov and Ottemoller, 2010; Lienert and Havskov, 1995). Figure 4.6 illustrates the event-magnitude distribution and the cumulative frequency-magnitude distribution of all events. The geometry of the network allows precise locations of events within the network down to magnitude M = 1 and the overall magnitude threshold of completeness M_c is 2.1 (Fig. 4.6). The location accuracy decreases for events outside the network (Baumbach et al., 2003).

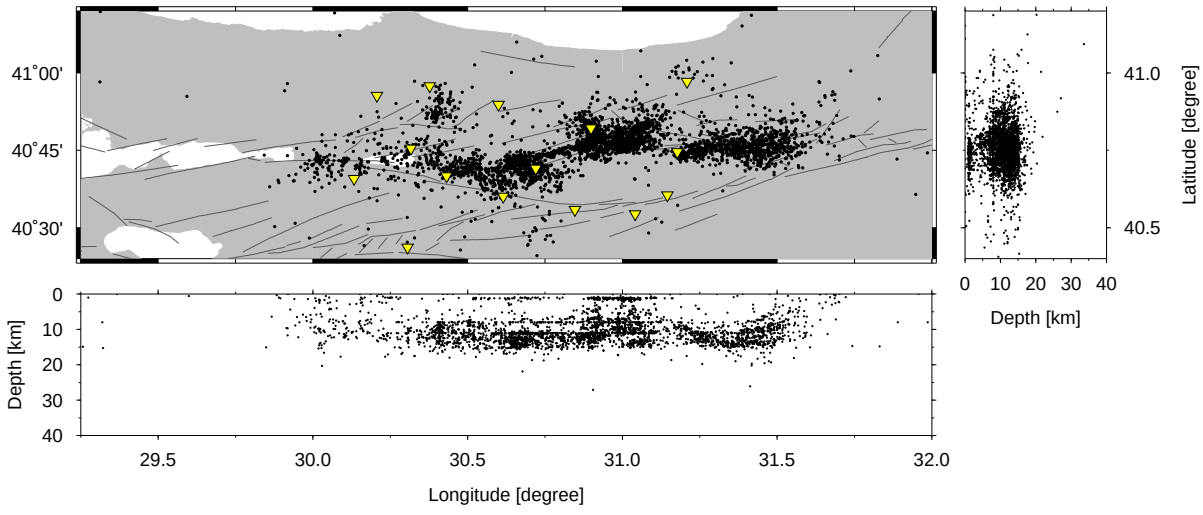

Figure 4.4.: Event catalogue of the 4062 events from the SABONET database for the years 1997,1998, 2000 and 2001. Yellow triangles illustrate the station network introduced in Figure 4.1. Faults are taken from Şaroğlu et al. (1992).

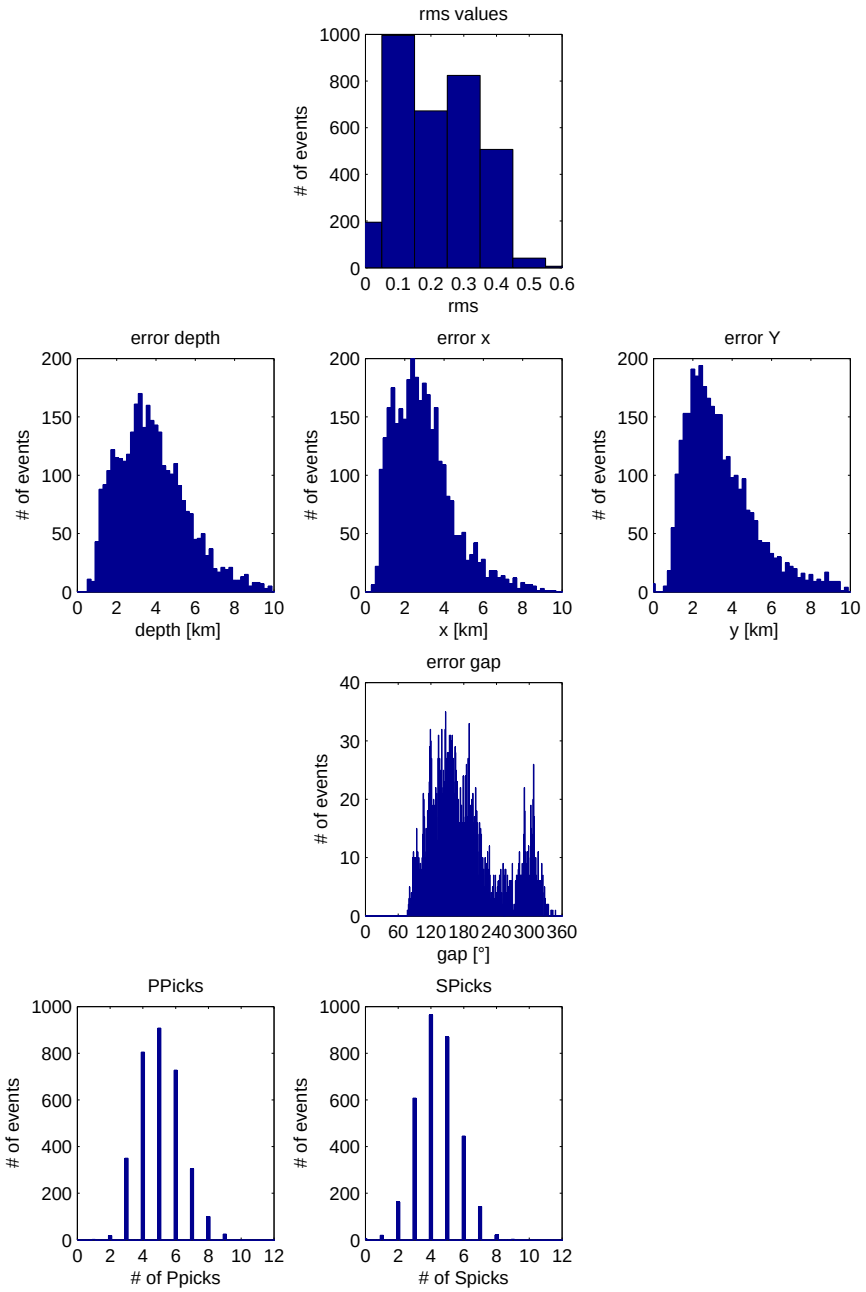

Figure 4.5.: Location errors and statistics for P and S Picks for the obtained hypocenter catalogue of 4062 events.

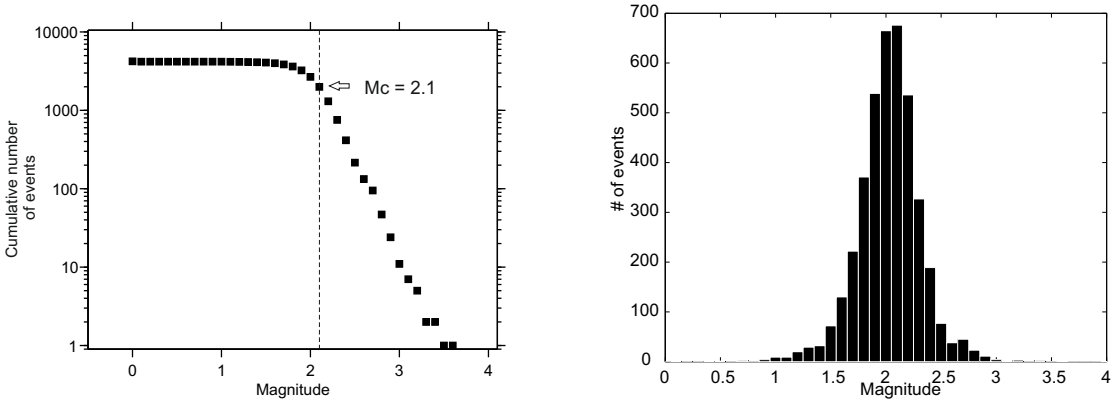

(a) First sub-figure (b) Second sub-figure

Figure 4.6.: Magnitude distribution for the SABONET hypocenter catalogue.(a) Cumulative frequency-magnitude distribution of all events for calculating the magnitude of completeness. (b) Histogram of the number of events for each magnitude bin.

5. Stress Rotation and Recovery in conjunction with the 1999 Izmit and Düzce earthquakes

In this chapter potential spatiotemporal variations of the crustal stress field orientation along the August 1999 Izmit M_w7.4 and November 1999 Düzce M_w7.1 earthquakes in NW Turkey are investigated and related to distinct seismotectonic features and variations of co-seismic slip along the rupture. To achieve this, a significantly enlarged aftershock focal mechanism data base compared to previous studies (Bohnhoff et al., 2006; Bulut et al., 2007) and a newly derived hypocenter catalog from SABONET recordings obtained for a selected time period between 1997 and 2001 (section 4.2) and German Task Force (GTF) network recordings are used. This combined dataset allows to study potential spatial and temporal variations of stress field orientation along distinct rupture segments for the pre- and postseimic phase of the two large earthquakes with unprecedented detail. Furthermore, the occurrence of two $M > 7$ large earthquakes in rapid succession gives the unique opportunity to analyse a short "interseismic phase" between them, i.e. the 87-day long time interval after the Izmit and before the Düzce earthquake. I refer to this phase as the inter Izmit-Düzce phase or two-month aftershock period in the following.

5.1. Previous Stress Field Investigation along the NAFZ

Kiratzi (2002) first performed a stress inversion for NW Turkey using focal mechanisms of the 11 largest earthquakes occurring along the NAFZ east of the Marmara Sea since 1943. The obtained principal stresses for the regional stress field reflect a strike-slip regime with the maximum compressive stress trending N126°E. This is also in accordance with the results of a regional NW-SE $S_{H_{max}}$ orientation striking between 120° and 160° obtained by Heidbach et al. (2008) with the analysis of focal mechanism stress indicators in the World Stress Map. Bohnhoff et al. (2006) first proposed a rotation of the local stresses in NW Turkey following the Izmit mainshock. Together with Görgün et al. (2010) the

authors investigated the local stress field orientation based on aftershock focal mechanisms of the 1999 Izmit earthquake and divided the area in several segments. From separate inversion for the stress field they suggested local variations of $S_{H_{max}}$ along the Izmit rupture and concluded that the Izmit earthquake caused significant stress partitioning along the rupture. Örgülü (2010) studied the stress field of the Marmara Sea region which is mainly governed by a strike-slip regime. Previously, Pinar et al. (2010) investigated the stress field along the Izmit rupture zone by using first-motion polarity data at seven distinct aftershock clusters. For the post-seismic phase they obtained normal-faulting and strike-slip regimes for the Sapanca, Sakarya, and Karadere segments and concluded either low frictional coefficients or fault weakness. However, none of the previous studies allowed to address a potential systematic change of the stress field and thus could not argue on the different stress rotation models proposing long-term stress recovery or short-term decay of a rotation induced by a major earthquake.

5.2. Spatiotemporal variations of the stress field orientation along the Izmit rupture from inversion based on focal mechanisms

The following section has been published in the Geophysical Journal International: M. Ickrath, M. Bohnhoff, F. Bulut and G. Dresen: Stress rotation and recovery in conjunction with the 1999 Izmit M_w 7.4 earthquake,(February, 2014), *Geophys. J. Int.* 196 (2): 951-956, 2014.

Please note that subsection *Introduction* been deleted and subsection 5.2.2 *Method and Data* of the published paper has been shortened since their content has already been introduced in *Chapter* 1 and *Chapter* 3, respectively.

The subsection 5.2.3 *Results and Discussion* is extended now showing in addition to the stress inversion results obtained with the LSIB method (*Chapter* 3.2) also the results obtained using the MSATSI Software package (*Chapter* 3.3) for the publication in Seismological Research Letters: P. Martínez-Garzón, G. Kwiatek, M. Ickrath and M. Bohnhoff: MSATSI: A MATLAB© package for stress inversion combining solid classic methodology, a new simplified user-handling and a visualization tool, 85, 896-904. 2014 (see Appendix

A).

5.2.1. Abstract

Local rotations of the stress field might serve as an indicator to characterize the physical status of individual fault segments during the seismic cycle. In this study we focus on the pre-, two-month aftershock-, and post-seismic phase of the 1999 M_w7.4 Izmit earthquake in northwestern Turkey. Using a compilation of focal mechanism (FM) data we investigate spatiotemporal changes of the stress field orientation and find distinct variations along individual fault segments. Whereas the regional stress field prior to the Izmit earthquake and following the two-month aftershock sequence reflects a stable strike-slip regime, the early aftershock period is dominated by EW-extension below the Akyazi Basin. During the two-month aftershock period we find significant changes from strike-slip to normal-faulting during the mainshock following by a systematic back-rotation to the pre-mainshock stress regime. This back rotation commences first in the Akyazi Plain hosting a co-seismic slip deficit of $\leq$ 3m and propagates then further to the east towards the Karadere and Düzce fault where the Düzce M_w7.1 mainshock nucleated 87 days later. Our results confirm that spatiotemporal stress field rotations are a useful indicator for variations of the seismotectonic setting during the seismic cycle.

5.2.2. Method and Data

There are several stress inversion algorithms which estimate the orientation of the principal stress axes from focal mechanism (FM) data. For detailed descriptions, please see Chapter 3. Here we used the Linear Stress Inversion with Bootstrapping (LSIB) technique proposed by Michael (1984); **?** based on a least-square inversion algorithm, which uses the orientation of a set of fault planes (strike and dip) and the direction of slip (rake) that occurs on these fault planes. Additionally, we use the newly developed software package MSATSI (Martínez-Garzón et al., 2014) based on the Stress Inversion algorithm SATSI (Hardebeck and Michael, 2006), which is a damped inversion method that simultaneously invert for the stress field orientation in subareas while minimizing the difference in stress between adjacent subareas and the nonlinear approach by Angelier (2002). The latter method was used to confirm our findings, the results are briefly summarized in Appendix

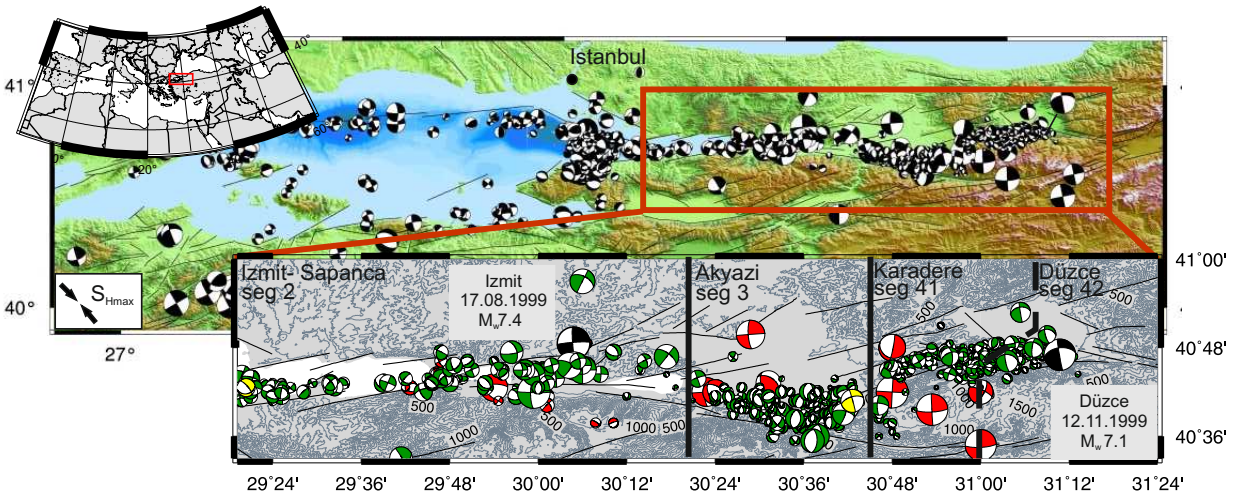

Figure 5.1.: A. Overview map of the focal mechanism (FM) database for the area of investigation at the North Anatolian Fault Zone in NW Turkey (please find the FM database in table 1 in the electronic supplement). The size of the beachballs scales with magnitude. Fault lines are taken from Turkey General Directorate of Mineral Research and Exploration, and Armijo et al. (2002). (Topography: SRTM30 grid, Bathymetry: Armijo et al. (2002), $S_{H_{max}}$: Kiratzi (2002)). Subplot: 656 FM along the Izmit rupture. Beachballs are color-coded with time: prior to Aug 1999, Aug-Nov 1999 and post Nov 1999 in red, green and yellow, respectively. Black beachballs represent the Izmit and Düzce mainshocks. Black vertical lines indicate the segmentation along the Izmit rupture following Bohnhoff et al. (2006). Grey contour lines are isolines of topography.

C. Here, we study the spatiotemporal evolution of the stress field orientation along the Izmit rupture by using a significantly enlarged aftershock focal mechanism data base and additionally post-Izmit events allowing studying detailed temporal stress field variations along distinct rupture segments before, during and following the two-month Izmit aftershock period. We use focal mechanisms of local seismicity from pre-, two-month aftershock- and post-seismic times framing the Izmit event which are recorded by various available local and regional seismic networks. We compiled a set of 939 focal mechanisms of earthquakes along the broader Izmit rupture spanning the time interval 1943-2007 with earthquake magnitudes ranging between 0.8 and 7.4 (Fig. 5.1, 5.2 and 5.3). Individual data sets are compiled from: Bohnhoff et al. (2006), Örgülü (2010), Görgün et al. (2010) and references therein (please find the focal mechanisms database in Appendix E). While the majority of the analysed events are aftershocks from the first two months following the Izmit mainshock (Fig. 5.3b) we also include major regional events since 1943 (56 events) as well as seismicity following the two-month aftershock activity between 2000

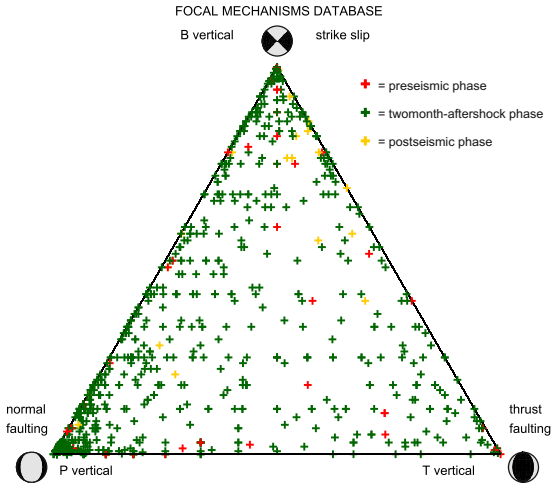

Figure 5.2.: Dipping angle of the P, T, and B axes of all 939 FM of the compiled database for the NAFZ visualized in a ternary scheme after Frohlich (2001) showing individual faulting mechanisms color-coded with time.

and 2007 (19 events). P and T axes of the entire focal mechanisms data set show predominantly vertical but also subhorizontal compressional axes while extensional axes are mostly subhorizontal (Fig. 5.3a). This would reflect a combined strike-slip and normal faulting stress regime.

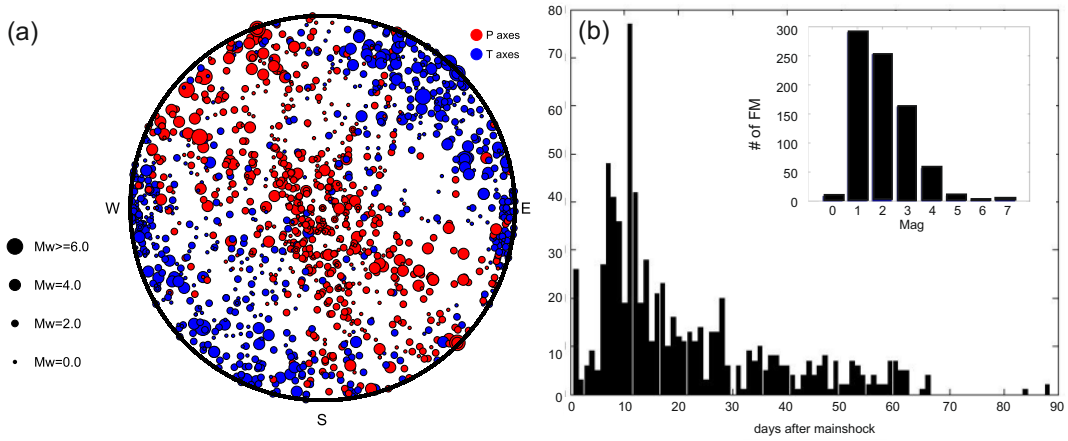

Figure 5.3.: (a) Distribution of P (red) and T (blue) axes for the entire set of 939 focal mechanisms (FM) in polar projection of the lower hemisphere. The size of circles scales with magnitude. (b) Event-time plot for the FM database for the two-month Izmit aftershock period and its magnitude distribution (upper right). Modified after Ickrath et al. (2014)

.

In order to determine potential temporal variations in the stress field we divided the entire data set into a pre-, two-month aftershock-, and post-seismic period and then further subdivided the aftershock period into finer temporal subsets forming moving windows of 70 events with an overlap of 65 events. These subsets were separately inverted for the stress tensor using LSIB and as comparison under same condition as one inversion with 27 grids consisting each of 70 FM with an overlap of 20 FM with the MSATSI Software. Furthermore, within the Izmit aftershock period we also individually analyzed the major rupture segments 2-4 defined by Bohnhoff et al. (2006) (indicated in Fig. 5.1 subplot). Segment 2 (29.3°E-30.4°E) includes the Izmit hypocenter and covers the Izmit-Sapanca area containing 122 FM dominated by a right-lateral strike-slip and minor normal faulting regime. Segment 3 (30.4°E-30.85°E) is located at a triple junction of the EW-striking Izmit-Sapanca fault, the N65°E striking Karadere fault and the ESE-striking Mudurnu fault. It contains 170 FM which mostly indicate an EW-extensional normal faulting regime. Segment 4 (30.85°E-31.3°E) extends along the Karadere Fault and the Düzce Basin containing 318 FM which show a high variety in mechanism from strike-slip to normal faulting. For further analysis we separated this area into segments 41 (Karadere Fault - 115 FM) and 42 (Düzce Basin - 224 FM). To quantify the robustness of each derived stress tensor we also applied a bootstrap technique resampling 2000 times thereby determining the 68% (1 σ) and 95% (2 σ) confidence intervals.

5.2.3. Results and Discussion

Results from both inversion algorithms are in good agreement reflecting for the broader Izmit/Düzce regions a strike-slip regime that remains almost identical during the pre- and post-seismic phases of the Izmit and Düzce 1999 events with a well-resolved N130°E trending sub horizontal maximum principal stress and a relative stress magnitude of ~0.5 (Fig. 5.4 and Fig. 5.5).

In contrast, during the two-month aftershock sequence we observed significant lateral rotations of the trend of σ_{1-3} as well as significant changes for the plunge angle of σ_1 and σ_2 (but not σ_3) indicating temporal changes during the aftershock period. This observation confirms the stress field rotations introduced by the Izmit mainshock that was first observed by Bohnhoff et al. (2006) along the Izmit-Sapanca and Karadere segments

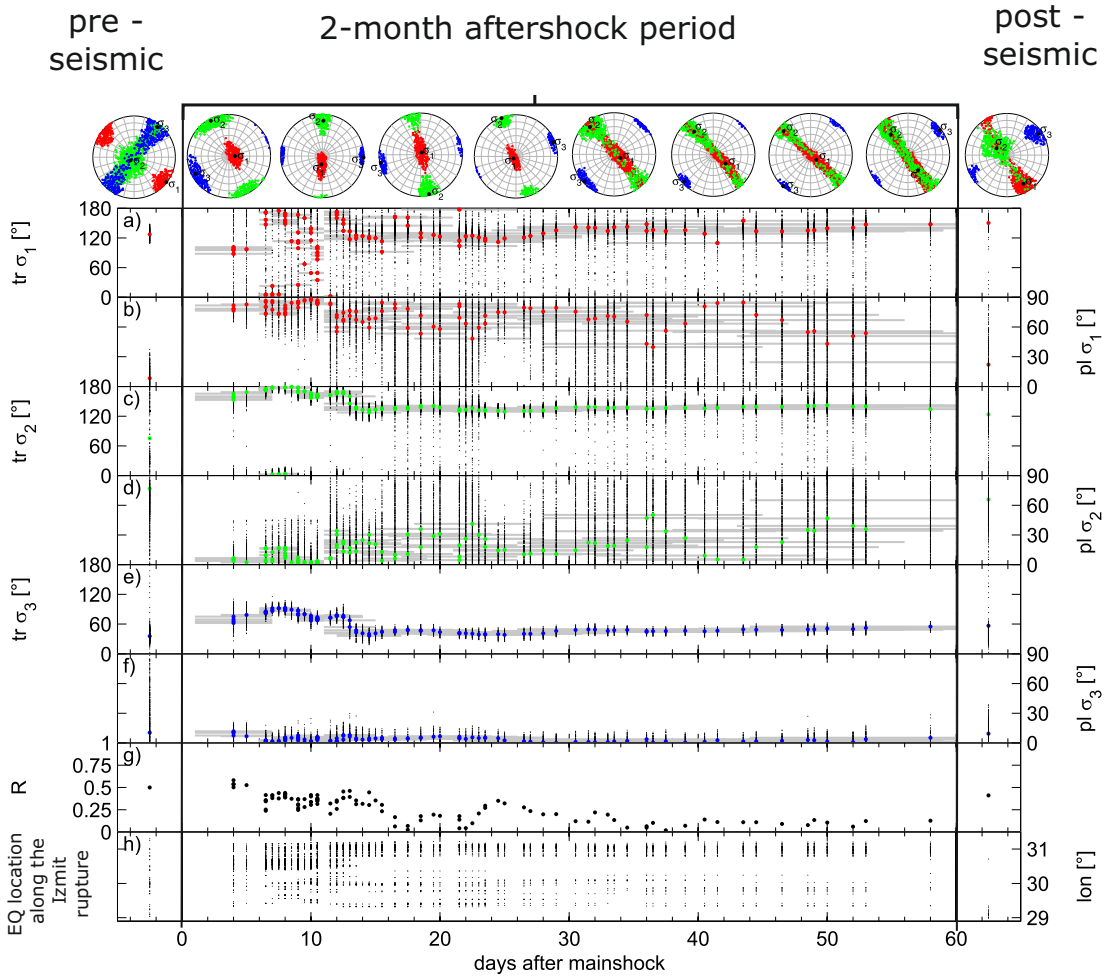

Figure 5.4.: Temporal evolution of the stress field for the pre-, two-month aftershock- and post-seismic phase of the Izmit earthquake. Significant stress tensor results from inversion using the LSIB method for specific time periods are shown in lower-hemisphere projection. Red: maximum compressive stress, σ_1. Green: intermediate principal stress, σ_2. Blue: minimum compressive stress, σ_3. Best solution is indicated by a black dot with 95% uncertainty distribution from bootstrap resampling (colored dots). (a)-(f) Best solutions for the stress tensor from each subset are plotted for the trend and plunge for σ_1 (red), σ_2 (green) and σ_3 (blue) with time. The horizontal grey bars are representing the temporal extent of each particular subset. For each result the 95% confidence limit is plotted vertically. (g) Relative stress magnitude for the best solutions of each subset. (h) Spatial distribution of Izmit aftershocks along the rupture for each stress inversion subset(modified after (Ickrath et al., 2014)).

but with no temporal resolution.

To further investigate the temporal evolution of the stress field orientation and in particular taking into account the resolution capability we plot the plunge and trend for

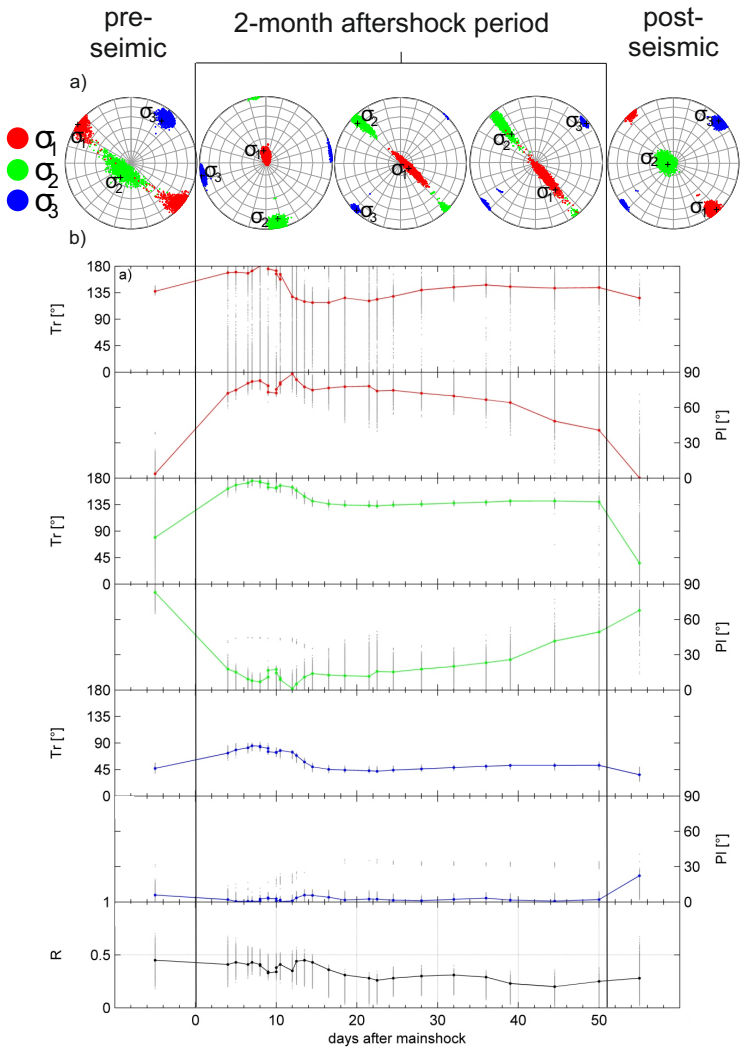

Figure 5.5.: Temporal evolution of the stress field in conjunction with the Izmit earthquake using the MSATSI Software. a) Representative results for specific time periods ('Stereonet'). Black cross: best solution; gray-scaled dots: 95% confidence interval. b) Variation of the stress field orientation over time ('Profile'). Best solutions are plotted separately for the trend and plunge of σ_1 (red), σ_2 (green) and σ_3 (blue). 95% confidence limit is plotted with grey dots (modified after (Martínez-Garzón et al., 2014))

σ_{1-3} as well as their 95% confidence intervals individually with time (Fig. 5.4a-f). Time extend of individual temporal subsets are indicated by horizontal gray lines in Figure 5.4. For the whole aftershock data set we identified an abrupt change in predominant

faulting regime from the pre-seismic strike-slip to a normal faulting regime right after the mainshock. During the two-month aftershock period we then observed a gradual but systematic back rotation with an intermitted transtensional stress field with overlapping confidence intervals of σ_1 and σ_2 and a relative stress magnitude < 0.25. The compiled FM catalog shows that the entire rupture zone and all segments besides the Akyazi Plain are homogeneously sampled by FM for the entire time period (Fig. 5.4h). Towards the end of the two-month aftershock period the stress field seems to return to the pre-seismic state (strike-slip) in agreement with the Michael (1987) stress recovery model.
However, the reduced number of FM and their spatial distribution do not allow to draw concise conclusions in this aspect. During the two-month aftershock period the relative stress magnitude changes from 0.5 to nearly 0, indicating a transtensional stress regime while it returns back to ∼0.4 in accordance with the back-rotation of the stress field towards strike-slip with well-separated confidence regions of the principal stress axes (Fig. 5.4g).
To further investigate the nature of the stress perturbation during the aftershock period we also investigated the temporal evolution of the stress field orientation focusing on the Akyazi Plain and the Karadere-Düzce area at the eastern part of the Izmit rupture (segments 3, 41 and 42; Fig. 5.1 subplot). Below the Akyazi Plain we identified a clear east-west extensional stress field with a vertical maximum principal stress orientation while the Karadere-Düzce area shows a distinctly varying stress field along the N65°E trending Karadere Fault and below the Düzce Basin (Fig. 5.6).

The normal faulting regime below the Akyazi Plain is well-explained by the co-seismic slip deficit of ∼3.5m (Tibi et al., 2001; Barka et al., 2002) introducing a strong EW-trending tensional component in this area. This is also in accordance with the local tectonic setting reflecting an extensional basin structure with reduced topography by ∼500 m compared to the surrounding and thus may be seen as a structure similar to the somewhat larger Sea of Marmara pull-apart basin (Armijo et al., 2002) but in a more juvenile state. East of the Akyazi Plain, along the Karadere Fault we find a remarkable back-rotation from oblique normal faulting towards strike-slip approximately two weeks after the Izmit mainshock (Fig. 5.6 subplot). In contrast, below the Düzce Basin the regime changes approx. 11 days after the mainshock from transtension/strike-slip

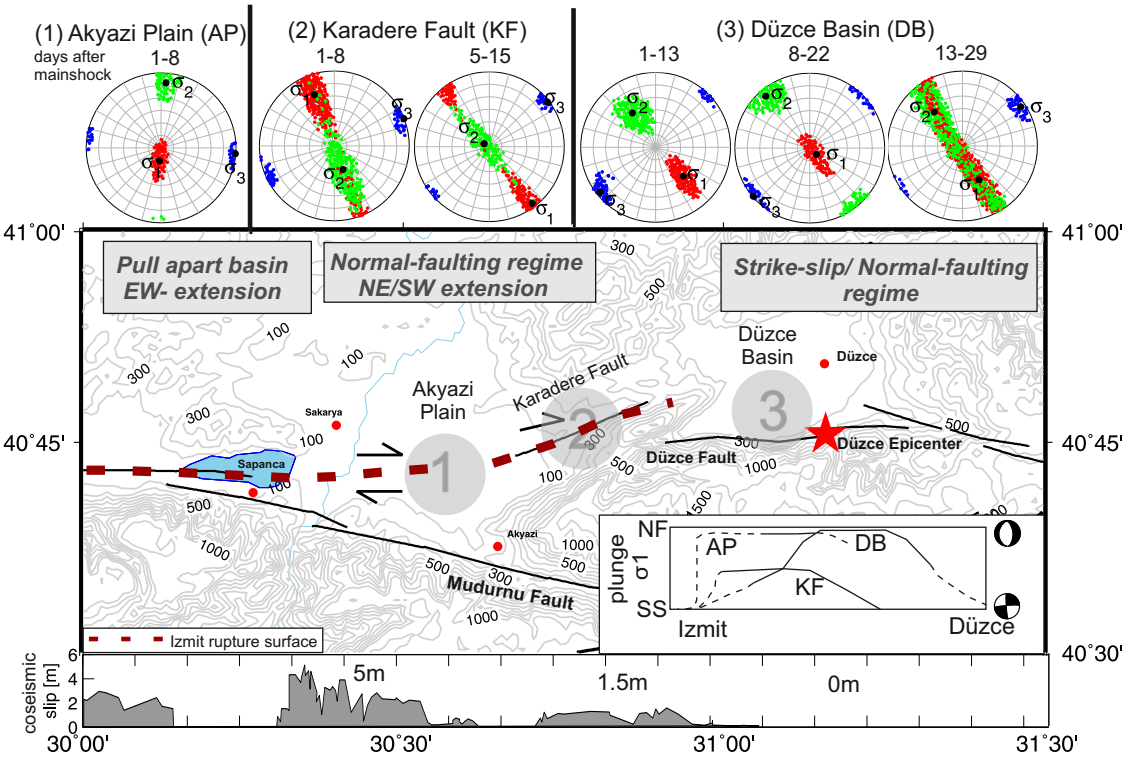

Figure 5.6.: Summary of stress field observations along the Akyazi and Düzce area. Upper part: Stress field orientation for segments 3 (Akyazi Plain-AP), segment 41 (Karadere Fault-KF) and 42 (Düzce Basin-DB) during the two-month aftershock period (days with respect to the Izmit mainshock). Labeling as in Fig. 5.1. Middle part: Summary of observations along the Akyazi and Düzce area. Faults are after Turkey General Directorate of Mineral Research and Exploration. Red dotted lines indicate the simplified surface rupture of the Izmit event (after Barka et al. (2002)). The red star indicates the epicenter of the 1999 Nov11 Düzce mainshock. Grey: Contour lines for topography. Subplot: Sketch of principal results for the stress regime at the individual segments (AP, KF and DB, respectively), showing the temporal change of the plunge of the maximum compressive stress, σ_1 for the pre-, aftershock- and post-seismic phase of the Izmit earthquake and the significant change from SS (strike-slip) to NF (normal-faulting) and backwards in each segment with varying time delays. Lower part: Lateral distribution of co-seismic surface slip along the Izmit rupture after Barka et al. (2002).

towards NE/SW-extensional normal faulting, remaining then constant for at least two weeks and only then starting to rotate back to transtension/strike-slip (Fig. 5.6 subplot). Interestingly, the significant changes in stress field orientation at the Karadere and Dücze segment correlate with an unusual rerise of the seismicity rate ∼20 days after the mainshock (Fig. 5.7). Such a rerise is not observed at the Akyazi Plain where the decay in aftershock activity entirely follows an Omori-decay Utsu (1961) in a stationary normal

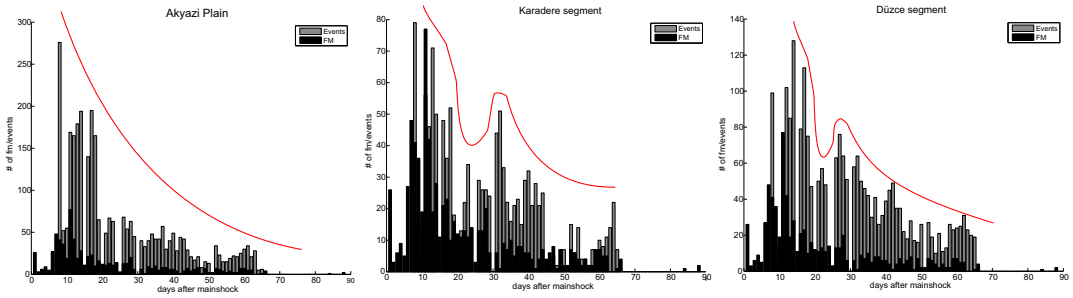

Figure 5.7.: Aftershock activity and focal mechanism distribution for the Akyazi Plain (segment 3), Karadere (segment 41) and Düzce (segment 42) segment.

faulting stress regime (Fig. 5.6). We explain these differences in temporal changes along the individual fault segments by the large variation of right-lateral co-seismic slip along the Izmit rupture. The slip deficit of $\sim$ 3.5m with the highest gradient at the Akyazi Plain results in an immediate normal faulting activity reflected also by a M>5 normal faulting aftershock a few hours following the mainshock (Örgülü and Aktar, 2001; Bulut and Aktar, 2007). Once the slip deficit has been locally adjusted to a certain extent the normal faulting activity vanishes and the tensional regime migrates further to the east where it continues to operate below the Düzce Basin but with a delay of several days (sketch in Fig. 5.6). The Karadere fault in between does not switch to normal faulting since it represents a well-developed steeply NW-dipping strike-slip fault patch confirmed by the observed stress field orientation. The observed local temporal variations of the stress field orientation are significant at the 95% level and in good accordance with the local tectonics along the particular segments of the Izmit rupture. In contrast, GPS-derived surface deformations do not show any significant temporal changes within the time considered here (Bürgmann et al., 2002; Ergintav et al., 2002). This might indicate that the adjustment of the slip deficit mainly occurs at seismogenic depth (8-18 km), but not up to the surface. Our results indicate a migration of the extensional stress regime from the Akyazi Plain that hosted the largest co-seismic slip deficit towards the Düzce Basin at the easternmost tip of the Izmit rupture. Interestingly this was the exact location where the M7.1 Düzce rupture nucleated 87 days after Izmit extending the rupture by another 40 km to the east (Umutlu et al., 2004). Distinct local variations in the crustal stress field potentially reflect activity of a complex fault network varying in space and time. High resolution stress inversion results allow unraveling fault processes at depth related to the

temporal changes of geomechanical parameters.

5.3. Spatiotemporal variations of the stress field orientation along the Izmit-Düzce rupture from inversion based on first motion polarity data

5.3.1. Introduction

Based on the previous study (Chapter 5.2) a substantially enlarged dataset of local seismicity derived from the SABONET network (Chapter 4) for the time span 1997-2001 was used to investigate in greater detail the spatial and temporal evolution of the stress field along the Izmit and Düzce 1999 rupture. While the previous study in Chapter 5.2 focused on the two-month Izmit aftershock period based the inversion of focal mechanisms along the Izmit rupture, the main focus here is including the pre-seismic phase (years 1997/1998), the inter Izmit-Düzce phase and post-seismic phase (years 2000/2001). For the determination of the stress field orientation the direct inversion of first motion polarity data was performed using the (MOTSI) method by Abers and Gephart (2001). The main benefit of the direct inversion of first-motion polarity data is that also areas with unstable focal mechanisms could be studied using all available polarities from pronounced spatial seismicity clusters and inverting them for the stress tensor. With this approach, it is possible to determine the stress field orientation for parts of the Izmit and Düzce ruptures before and after activation for which otherwise no local stress field orientation could be determined since too few or no single-event focal mechanisms at all were available. Thereby and using the Düzce aftershocks new insights into the stress evolution of the easternmost segments of the Izmit and Düzce rupture and the so far poor studied area of the Elmalik fault could be obtained which possibly represents the connection of the rupture zone with the eastern single trace of the NAFZ and the 1944 rupture.

5.3.2. Method and Data

To extend the existing database of local seismicity and better resolve the stress field changes in the Akyazi Plain and Düzce area as described in Chapter 5.2 seismic waveform recordings from the permanent SApanca-BOlu NETwork (SABONET, Milkereit et al. (2000) see Chapter 4) were analysed. SABONET consists of 15 stations covering a six-

year period between 1997-2003 and extending along the entire rupture of the Izmit and Düzce events. SABONET was operated in event triggering mode except for the Izmit aftershock sequence. During this seven year time period ∼ 9000 events were detected of which 4062 could be located for the years 1997-2001 (Chapter 4.2). For the inter Izmit-

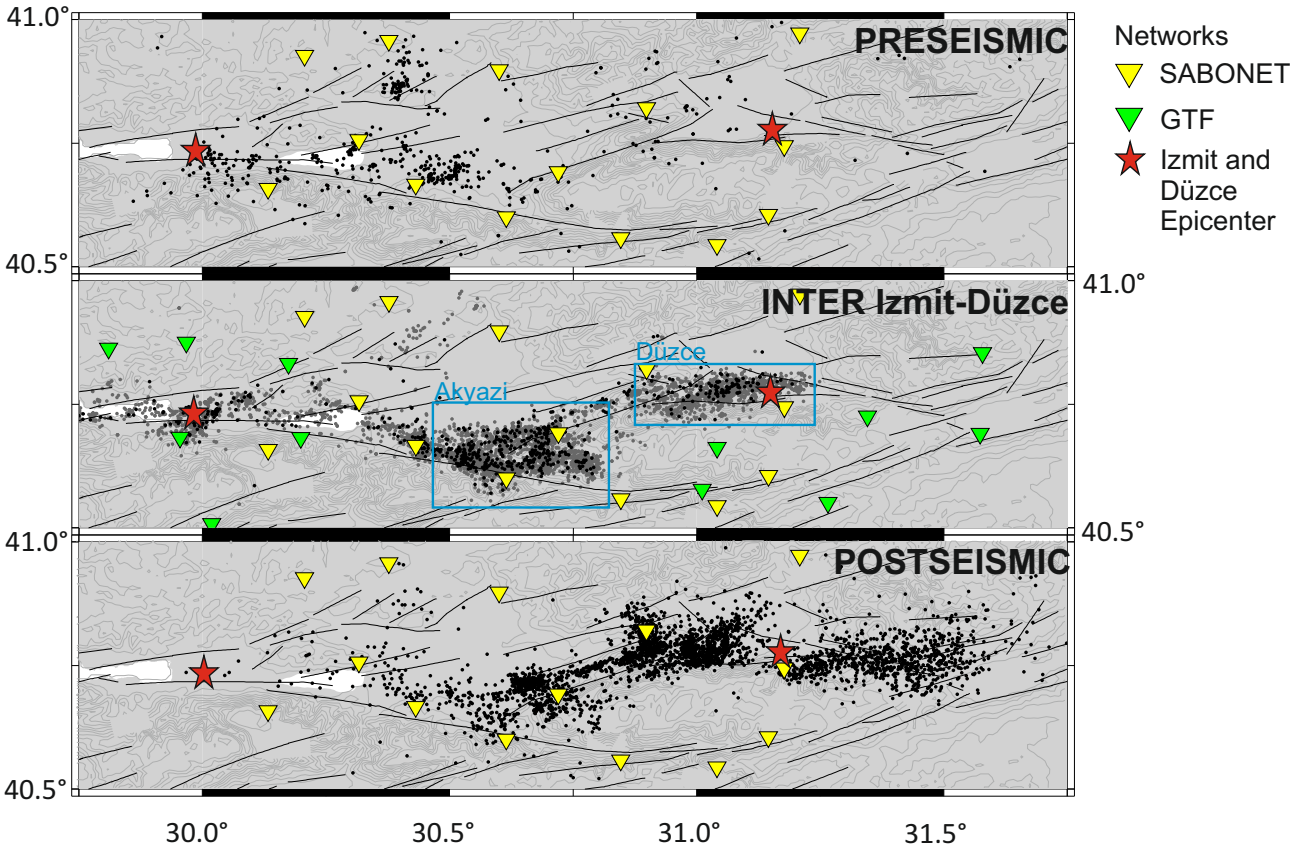

Figure 5.8.: Earthquake hypocenter database for the pre-seismic, inter Izmit-Düzce and post-seismic phase of the joint GTF/SABONET data used for the stress tensor inversion based on first motion polarities. Black circles represent the hypocenter catalog of the 4062 located and processed events from the SABONET in this study (Chapter 4). Grey dots indicate the 692 selected events from the GTF network that were used for a better resolution for the inter Izmit-Düzce phase in the Akyazi and Düzce area (blue boxes).

Düzce phase also data from the temporary German Task Force for earthquakes (GTF) network deployed by the Helmholtz-Centre Potsdam GFZ were considered. This temporary GTF network consisted of 21 short-period stations and was in operation for a period of 60 days between four days after the Izmit earthquake until October 21, 1999 (Grosser et al., 1998; Woith et al., 2000; Baumbach et al., 2003). The GTF network was deployed by invitation from the General Directorate of Disasters Affairs in Ankara and stations

were distributed mainly west of Adapazari to monitor the aftershock activity in the Izmit epicentral region and to increase the coverage of the SABONET (Milkereit et al., 2000; Parolai et al., 2004) towards an average station spacing of 15 km. Waveforms were sampled at 100 samples per second and the aftershock event catalog consists of over 10,000 earthquakes from which 4700 were relocated using the double-difference techniques reaching a relative precision of about 400 m (Bulut et al., 2007).

For this study we focused on the Akyazi and Düzce segment and selected 692 events from the GTF network (see Fig. 5.8 inter Izmit-Düzce phase) for which P-wave polarities were picked in addition to the already processed P- and S-wave arrivals. Figure 5.9 summarizes the location errors and number of P- and S-picks for this data set.

The combined high-quality data set is well suited to investigate local temporal and spatial variations of the stress field and include the less-well covered areas where not enough focal mechanism were available to invert for the stress field (Ickrath et al., 2014). Figure 5.8 illustrates the hypocenter catalog used for this study separated in the pre-seismic, inter Izmit-Düzce, and post-seismic phase in relation to the Izmit and Düzce mainshocks. For the calculation of the stress field orientation the direct inversion of earthquake first motion polarities MOTSI (first MOTion Stress Inversion) procedure from Abers and Gephart (2001) was used which is introduced in Chapter 3.4. One reason for using this method is that the small number of only 15 stations (SABONET) rarely allowed the determination of stable single-event focal mechanism due to the limited coverage of the focal sphere. A second reason is that especially the numerous smaller events where focal mechanism determination is even more difficult are of special interest. And finally, the main advantage of this method is that through using directly first-motion polarities additional uncertainties during the determination of focal mechanisms can be avoided. The advantage of MOTSI is that the entire set of polarity observations are considered, although they would not lead to single-event focal mechanisms. The basic assumption behind this is that smaller earthquakes $M \leq 3$ preferentially occur on faults with orientation clustered along the larger preexisting main fault with the maximum Coulomb failure stress (Robinson and McGinty, 2000). The regional stress tensors varies in space, but Robinson and McGinty (2000) confirm that with a large number of events the average stress tensor can still be well resolved with the direct inversion of first motion polarities.

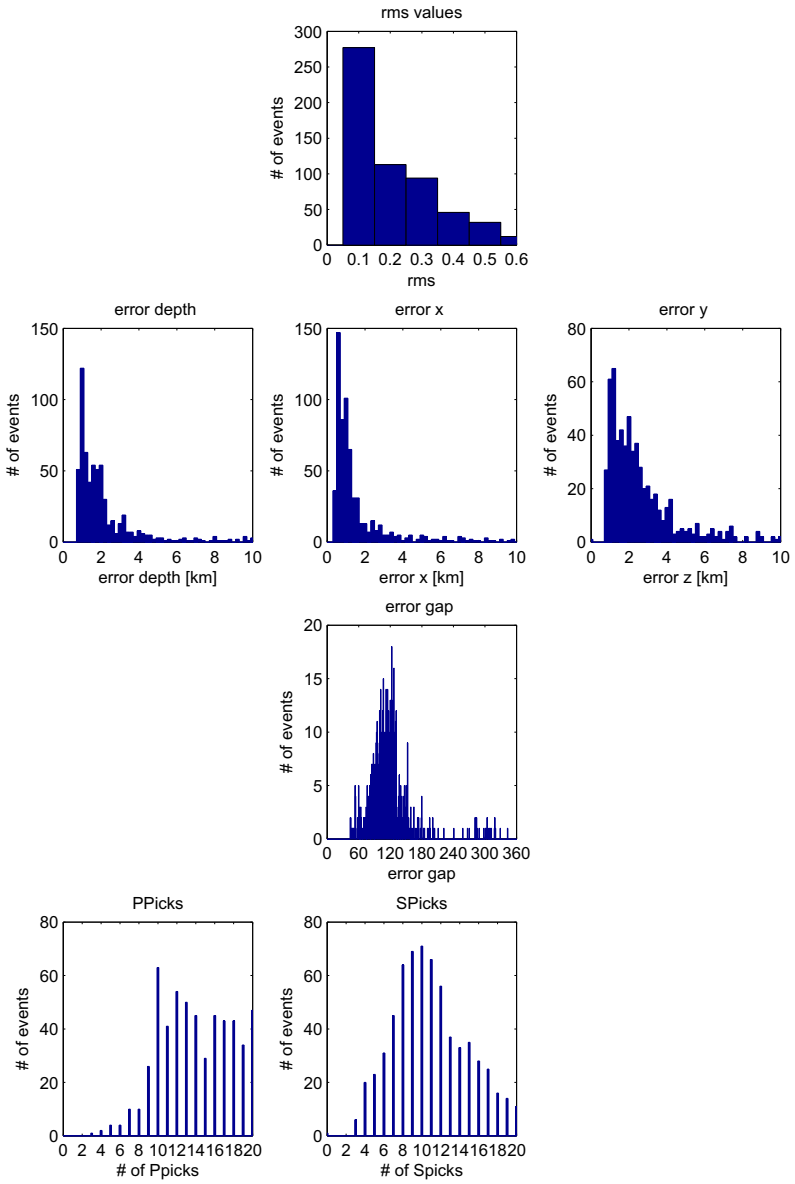

Figure 5.9.: Error Distribution and Pick statistic for the inter Izmit-Düzce phase using selected events from the relocalised earthquake hypocenter catalog from Bulut et al. (2007).

Although Abers and Gephart (2001) suggest to use more than 20 first-motion polarities per event here the idea from Robinson and McGinty (2000) is used which uses the approach for direct inversion of first motion polarity especially for spare networks with a number of first motion polarities smaller than 13 per event. If those events are clustered in space and time, a local homogeneous stress field in the hypocenter area can be assumed. They also compared and confirmed the results to the inversion from focal mechanism data. To confirm results obtained in this study a comparison to the inter Izmit-Düzce phase to the

results of the previous study using focal mechanism as inputs is carried out.

5.3.3. Seismicity clusters

When studying a region for potential spatial and/or temporal stress field variations, a crucial part is to divide the region into subareas (spatial bins) and separately calculate the stress tensor for each subarea. Hardebeck and Hauksson (2000) and Townend and Zoback (2000) discussed the different binning of subareas and the influence on the obtained stress field orientation with regard to the potential to resolve stress changes along along the San Andreas Fault (SAF) system and with distance to the main fault branch. Whereas Hardebeck and Hauksson (2000) use bins perpendicular to the fault, Townend and Zoback (2000) use a subset derived from the recursive gridding method, which results in grids corresponding to the density of data in an area and with that a higher weighting in seismically active areas fulfilling the basic assumption of stress homogeneity. In contrast to Hardebeck and Hauksson (2000), Townend and Zoback (2000) did not find systematic stress rotations and argued that the observation of stress field rotation is caused by the different binning methods. Based on these observations the hypocenter catalog along the Izmit and Düzce ruptures is analysed for spatial seismicity clusters to resolve stress field perturbations on local scale and to relate the results to the segmentation of the fault as described in the previous study by Ickrath et al. (2014) (Fig.5.1). Since this differs from the methods used by Townend and Zoback (2000) and Hardebeck and Hauksson (2000) in using first motion polarities rather than focal mechanism for the STI and the number of seismic events (SAF $\sim$ 50000 events) here the seismicity clusters are analysed based on the polarity distribution and event locations. To avoid potential binning effects only areas that are large enough and time intervals with enough events are inverted to allow a stable detection of the local stress field. For the analysis the entire data set is analysed based on the polarity distribution in space and time. Therefore, in a first step, the quality of the picked polarities was tested with separate plots for up and down polarities for each station of the network for different clusters of data. Besides a quality test another general idea behind this was, that -taking into account a small enough area- the polarities of one station for a specific time window are expected to be either up or down what would indicate a similar faulting mechanism for this segment.

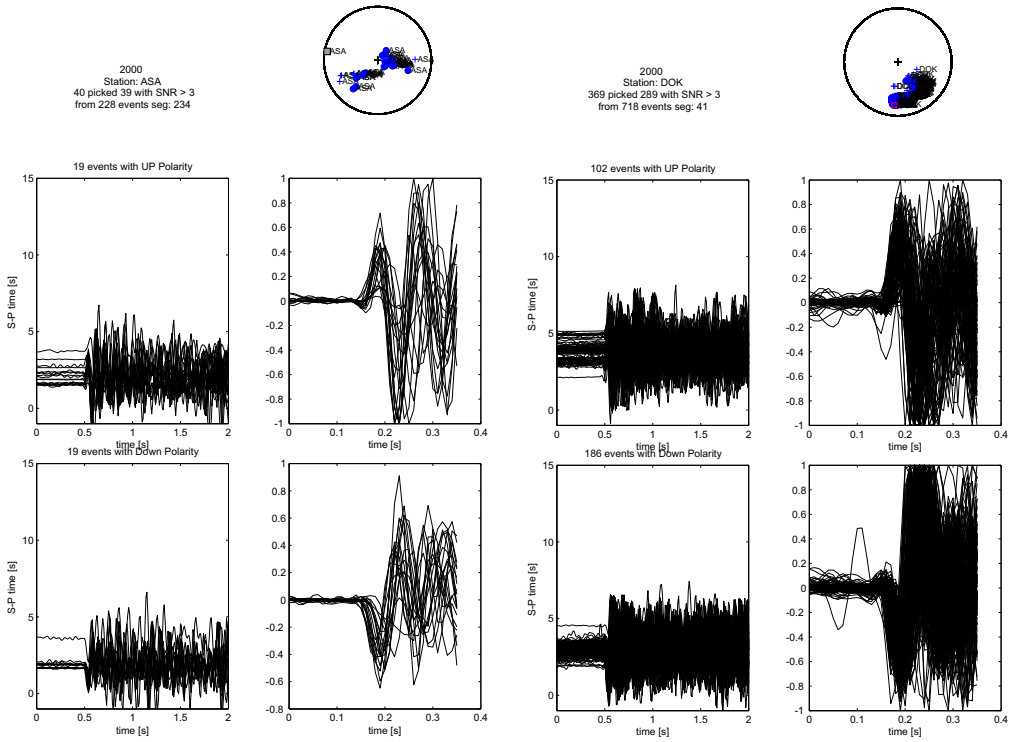

Figure 5.10.: Quality test and first analysis of first motion polarities. For station ASA and DOK from the SABONET the polarities separated for up (upper seismograms) and downs (lower seismograms) are plotted for example segments for the year 2000. In addition to the zoomed first onset plots of the events the S-P time is plotted versus time to give insights into the spatial clustering for the analysed events. Furthermore in the upper part a summary text with the used number of events with a signal to noise ratio (SNR) > 3 and the focal sphere coverage (crosses-up, circles-down) of the events are given.

Figure 5.10 gives two examples for stations ASA and DOK. In addition, the S-P time and the distribution on the focal sphere of the events was plotted to indicate possible spatial clusters. Results showed that the picked first motion polarities have a good quality regarding their positive and negative first-motion polarities. Unfortunately the amount of data was to large that even going in smaller areas there could not be distinguish for specific mechanism out of this first polarity analysis. In the following the first motion polarities again for each station for different time periods was separately plotted in the map view. As example the polarities of stations DOK and YUT are plotted for the pre-seismic year 1997 and post-seismic year 2000 in figure 5.11). The positive and negative first-motion polarities marked by the red crosses and blue circles, respectively lead to a first recognition of areas with possible different faulting mechanisms. Combined with the analysis of the

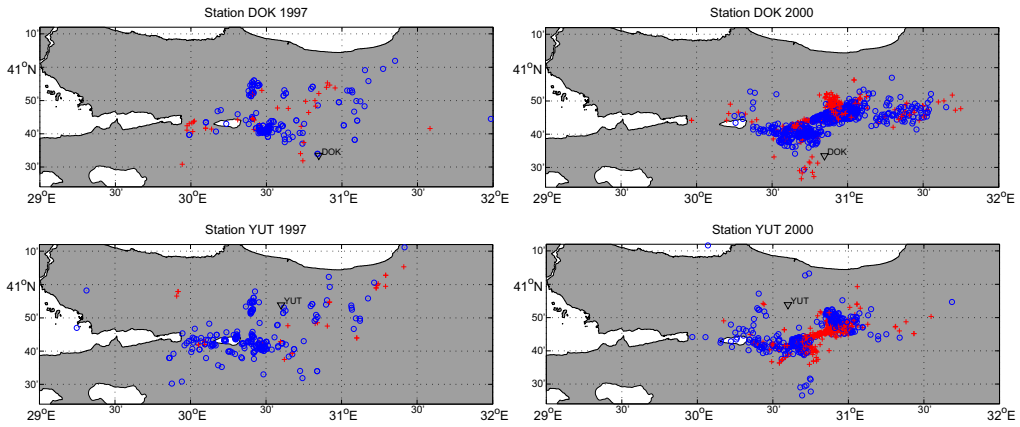

Figure 5.11.: Map view of NW Turkey with the spatial distribution of first motion polarities for station DOK and YUT for the years 1997 (left) and 2000 (right). First motions are shown with red crosses and blue circles for the up and down polarities, respectively.

time dependent distribution of the events shown in figure 5.12 and possible resulting focal mechanisms for the subareas nine seismicity clusters were identified in total which were further studied to resolve the particular stress field during different times (Figures 5.13 and 5.14).

5.3.4. Results and Discussion

In the following the results of stress field orientation obtained by the MOTSI method are described according to the segmentation of the nine seismicity clusters (see Tab. 5.1) from west to east. For the tectonic description for the specific area see also Chapter 2.2. All stress inversion results in Figure 5.13 and 5.14 are plotted in lower hemisphere projection with the best solution for the stress orientation σ_1 and σ_3 being indicated. For all results the marginal confidence limits in location of the stress axis σ_1 and σ_3 are calculated by numerically integrating the probability density function and are color coded from blue (minimum) to red (maximum).

Please note that the color-coding is slightly changing for each stress result depending on how well constrained each stress direction is. All results are also summarized in Appendix D with their corresponding color scale for the probability density function (pdf) and the results obtained within the MOTSI code illustrating the 68% and 95% confidence intervals.

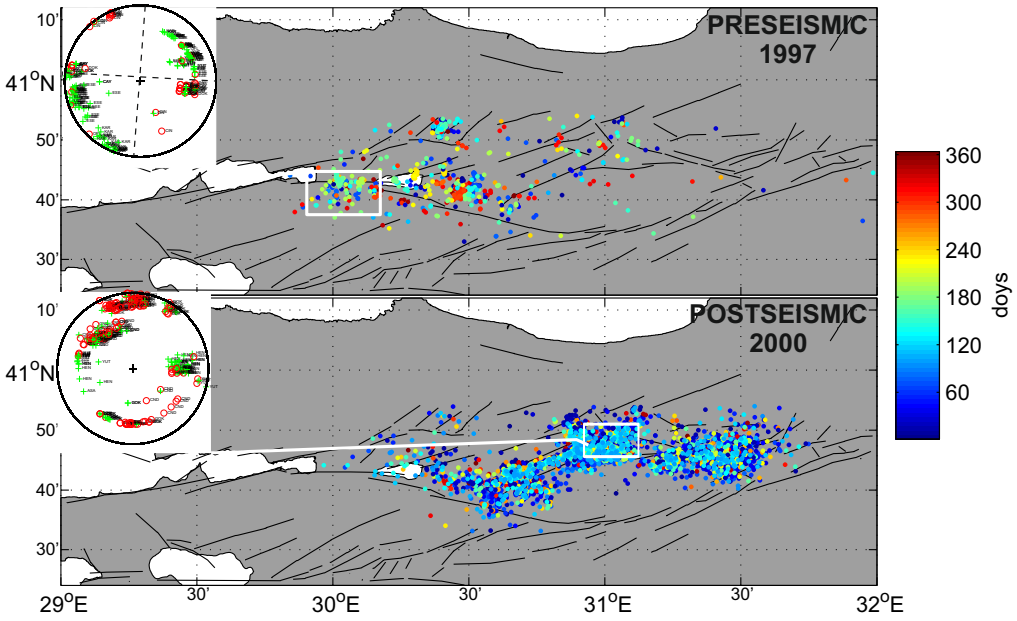

Figure 5.12.: Spatial and temporal distribution of the hypocenter catalog for the pre- and postseismic phase of the Izmit 1999 earthquake and focal sphere coverage of the first motion polarities as example for specific segments. The temporal evolution for each year is indicated by the color bar for the specific days of the year. White boxes mark example segments for which the focal sphere coverage is plotted. For the pre-seismic phase as example a possible strike-slip mechanism for the Izmit-Sapanca area can be assumed (dashed line).

Izmit-Sapanca Fault (segment A)

Segment **A** covers the Izmit-Sapanca fault (Fig.2.4 and section 2.2.1) and includes the Izmit mainshock epicenter. Since the activity here is low for the post-seismic period, stable results for the stress field orientation are obtained only for the pre- and inter Izmit-Düzce phase (Fig. 5.13). Stress inversion results indicate a clear strike slip (SS) regime for the pre-seismic phase with σ_1 trending $\sim$ 125°E in good accordance with the regional stress field. Interestingly, there is a drastic change in the local stress field observed along the Izmit-Sapanca fault during the inter Izmit-Düzce phase. Due to the Izmit mainshock a significant anti-clockwise rotation of the principal stress axis σ_3 of $\sim$ 40° and a clear normal-faulting component (σ_1 vertical, σ_3 subhorizontal trending NS) is introduced. This is the first time a well-constrained stress field orientation could be determined for the time just prior to a major earthquake along the entire NAFZ allowing to compare the pre-seismic setting with the setting immediately after a major rupture.

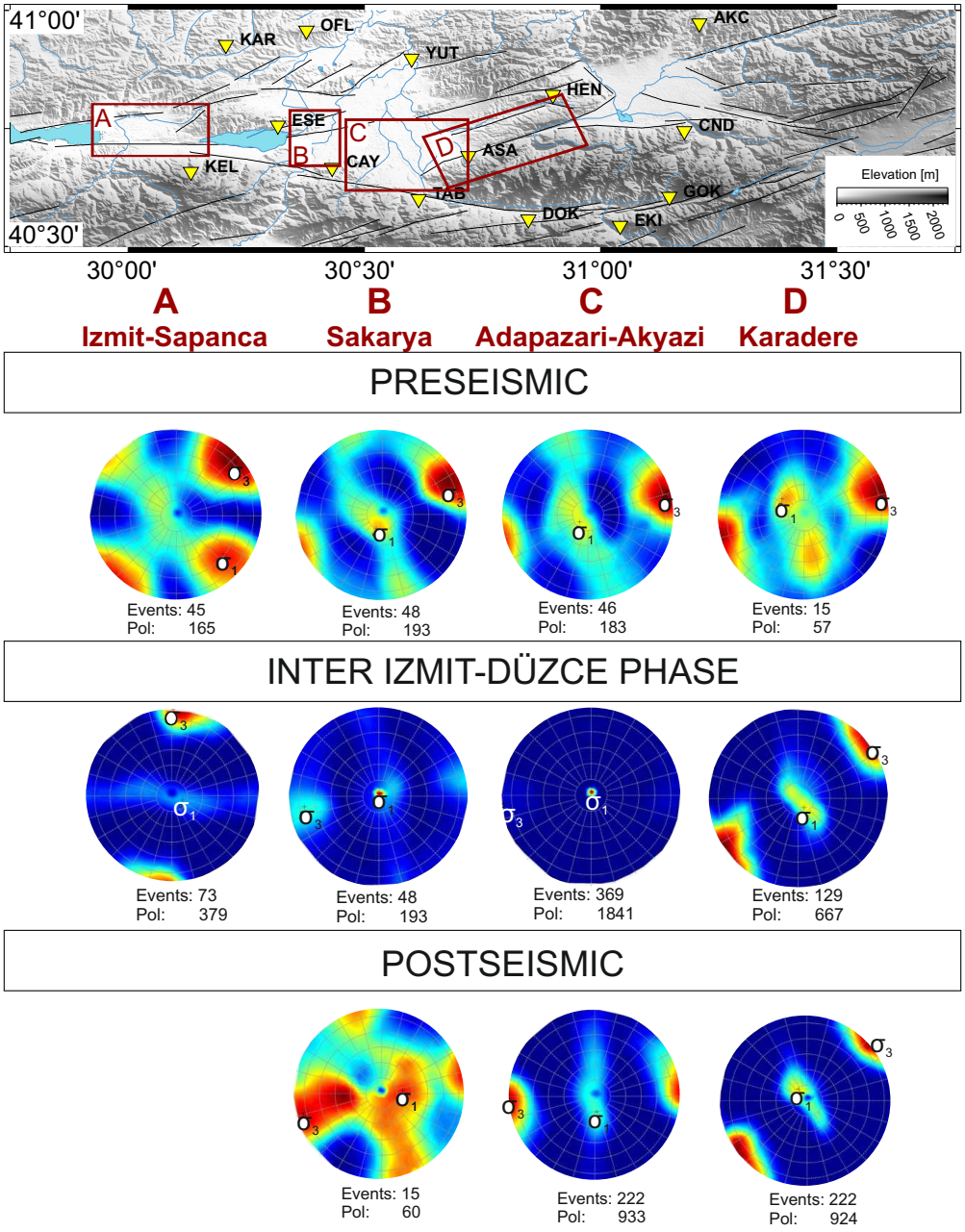

Figure 5.13.: Stress Evolution along the Izmit/Düzce rupture for segments A-D marked with red boxes in the upper map view of the Izmit-Düzce rupture. Fault lines are modified after Saroglu (1985), topography: SRTM30 grid. Stress inversion results are calculated using the MOTSI procedure 3.4 based on first motion polarities. All results are plotted in lower hemisphere projection. The best solution for each of the three stress orientation $\sigma_{1,3}$ is marked with the corresponding σ. For all results the marginal confidence limits for σ_1 and σ_3 are calculated and plotted color coded from blue (minimum) to red (maximum). Green stars indicate Izmit (left) and Düzce (right) mainshocks, respectively.

Pinar et al. (2010) analysed the stress field in distinct Izmit aftershock clusters based on the stress inversion of first motion polartity data using the method of Horiuchi et al. (1995). They observed a similar rotation of 20-25° from the E-W-trending NAFZ to ENE-WSW alignment. Although the coseismic displacement along this part of the Izmit rupture is smaller than on the adjacent Sakarya segment (∼3 m), the rotation can be also explained with the proposed idea of King et al. (1994) that stress rotations occur caused by the large Coulomb failure stress changes due to large displacement on strike-slip faults. In addition, there might also be an impact for the extensional basins further to the east where purely EW-extensional normal faulting aftershocks were observed. The results for the post-seismic phase are poorly resolved due to the decay in seismicity in this area. However, results tend to indicate a back-rotation of σ_3 to its pre-seismic orientation and an again increasing SS component. With this observed pattern the idea of Pinar et al. (2010) can be supported suggesting that the significant rotation in this segment implies a weak crustal patch for the Izmit region.

Sakarya Fault (segment B)

Segment **B** is located east of the Sapanca lake following the main fault trace of the NAFZ along the strike-slip Sakarya fault (Section 2.2.2) and crossing the Adapazari-Akyazi Basin. This segment is considered separately from the following Segment **C**, because of the presumably different setting (SS for the Sakarya fault and NF for the Adapazari-Akyazi Basin) based on the difference in the observed first-motion polarity distribution. This segment appears to be dominated by the extensional Adapazari-Akyazi Basin already prior to the Izmit earthquake. Stress inversion results indicate a dominantly NE-SW extensional normal-faulting regime for the whole time period studied there with a slight strike-slip component during the pre- and post-seismic phase. During the inter Izmit-Düzce phase a clear EW-extensional normal faulting regime is observed. In addition, a clockwise rotation of the σ_3 of $\sim 10°$ is introduced by the Izmit mainshock. The results confirm the observation from Pinar et al. (2010) proposing smaller stress rotations on the Sakarya fault compared to the Akyazi Plain (see also results from the previous study (Chapter 5.2)). A possible explanation for this observation is the higher co-seismic slip together with lower post-seismic slip along this segment compared to the Akyazi plain

(see also Langridge et al. (2002)). In summary, the stress field along the Sakarya fault seems to be dominated by the nearby pull-apart basin to a large extent.

Adapazari-Akyazi Basin (segment C)

Segment **C** extends throughout the Adapazari-Akyazi basin and lies east of the triple junction formed by the east-west trending Sakarya fault, the NE-trending Karadere fault and the ESE-striking Mudurnu fault. The Mudurnu fault was activated in 1967 by a $M > 7$ event and did not show any co-seismic slip or aftershock activity related to the Izmit and Düzce events. It is therefore considered that the Mudurnu fault is still at the early stage of its seismic cycle and no major stress built-up has occurred yet. The Adapazari-Akyazi basin segment is hosting the Akyazi gap which is characterized by very low aftershock activity and no recognized co-seismic slip at the surface (Section 2.2.2). This segment was of special interest for this study, since the FM database used in the previous study was sparse for the time prior to the Izmit event, while a stable stress field could be determined for the complete time period indicating a NF regime with no local or temporal variation (Chapter 5.2). Here, the temporal evolution of the stress field in this segment is investigated in detail. The STI results indicate a significant change from NF/SS regime during the pre-seismic phase to pure normal faulting in the inter Izmit-Düzce phase followed by backrotation to the NF/SS in the post-seismic phase. It thus allows to investigate in more detail how the pull-apart structure was affected by the Izmit rupture. The refined observations do not fully agree with the proposed idea of our previous study, that also in the Adapazari-Akyazi the stress field evolved from the pre-seismic SS-regime to a dominantly NF-regime and then rapidly recovered to the pre-seismic SS regime. Moreover, it shows that the pull-apart structure is general dominated by a normal faulting stress field already during the pre-seismic time and with only minor temporal variations after the mainshock. The minimum principal stress axis σ_3 is nearly stable at a trend of $\sim 85°$ over the whole time period.

These observations are consistent with Hearn et al. (2009) who investigated post-seismic deformation along the Izmit rupture by modeling slip distributions. The authors found evidence for a residual normal-faulting component of NS extension at the Akyazi Plain on a long-term scale. Concluding that coseismic relaxation takes place in effective viscosity

of lower crust and upper mantle, the observed extension is caused by the transfer of background tectonic stress to the upper crust. This is also investigated by Stierle et al. (2014) who obtained stable moment tensors for 17 Izmit aftershocks along the Akyazi Segment that show pure EW-extensional normal faulting mechanisms with significant positive non-DC components. The authors proposed possible tensile fracturing below the Akyazi Plain and they postulated from their observation a substantial fluid motion in the crust in response the accumulated slip deficit thereby reducing the effective normal traction or friction on coseismically stressed normal faults. The study from Greber (1994) who investigated circulations of hot paleo waters would support this suggestion by finding hot mineral spring restricted to extensional structure within the seismically active North Anatolian Fault Zone.

Karadere Fault (segment D)

Segment **D** is the easternmost segment that ruptured during the 17 August 1999 Izmit earthquake and is dominated by an abrupt change in strike of the NAFZ from east-west to north-northeast (N65°E) (Dikibaş and Akyüz, 2011) for the Karadere fault (Section 2.2.3). Iio et al. (2002) found evidence for post-seismic slip or creeping along the segment which is also confirmed by GPS data analysis by Reilinger et al. (2000) and Bürgmann et al. (2002) indicating that the highest coseismic slip occurred below the Karadere Segment. The STI results are nearly consistent along the whole time period indicating a NF regime with a small SS component. This is in accordance with results obtained by Ickrath et al. (2014) but here a different polarity clustering for the southern and northern part of the Karadere fault is found which allows for an in-depth investigation of this segment. Interestingly, both portions of the Karadere fault show significantly different STI results.

The following segments are dominated by aftershocks of the Izmit and Düzce earthquake and do not show significant seismicity during the pre-seismic phase to investigate the stress field separately for each segment. Therefor only results for the inter Izmit-Düzce and post-seismic phase are shown and discussed (Fig. 5.14).

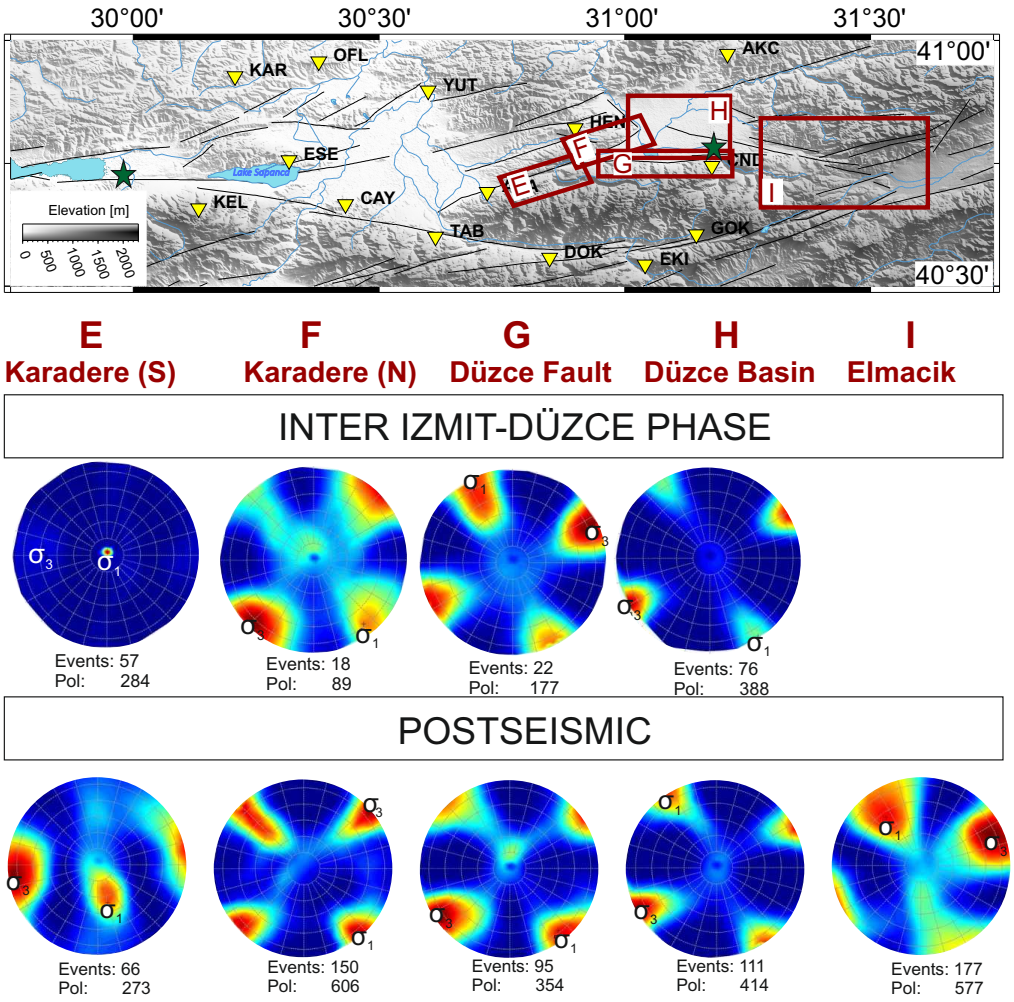

Figure 5.14.: Stress Evolution along the Izmit/Düzce rupture for segments E-I marked with red boxes in the upper map view of the Izmit-Düzce rupture. Stress inversion results are based on first motion polarities and calculated using the MOTSI procedure 3.4. For detailed figure description please see Fig 5.13.

Karadere Fault South (segment E) and Karadere Fault North (segment F)

Whereas the southern Karadere fault (Segment **E**) is showing a clear NF regime for the inter Izmit-Düzce and post-seismic phase the northern Karadere fault (Segment **F**) reflects a clear SS regime. In addition a significant change of the minimum principal stress axis σ_3 from nearly E-W for the southern part to 45° NE-SW in the northern part. This pattern is also observed by Seeber et al. (2000) who found highly diverse focal mechanisms reflecting normal faulting as well as strike-slip mechanisms. Moment tensor solutions from Stierle et al. (2014) also indicate a NF regime at the southern part of

the Karadere fault stressing the influence of the nearby east-west extensional pull-apart basin. Koulakov et al. (2010) investigated distribution of v_p, v_s and attenuation in the crust beneath the fault based on local earthquake tomography. They found evidence for the opening of a pull-apart zone near the western edge of the Almacik block proved by weak and moderate seismicity and low-seismic velocities. That could explain the existence of the normal faulting characteristic along the southern Karadere fault. In contrast, the northern part of the Karadere fault reflects a clear strike-slip regime in accordance with the local morphology and no dominant influence from the Düzce basin to the east is seen.

Düzce Fault (segment G)

Segment **G** inhabits the Düzce Fault which splays out from the WSW-ENE trending Karadere fault and represents a major fault asperity. this part of the fault was seismically activated by the Izmit rupture resulting in considerable aftershock activity. However, the rupture did not proceed further to the east until 87 days later when the Düzce earthquake occurred (Lettis et al., 2002; Peng and Ben-Zion, 2006; Görgün et al., 2010; Li et al., 2014) (Section 2.2.4). The Düzce fault represents a SS fault that is also consistent with the resulting STI results with the maximum principal stress axis σ_1 striking again NW-SE with 135° in good accordance with the regional stress field. The change in fault geometry from the Karadere fault to the Düzce fault was also investigated by Tibi et al. (2001) who analysed focal mechanism of two subevents as part of the Izmit earthquake at the triple junction of the northern Karadere fault and Düzce fault. Both events indicated a E-W trending strike-slip mechanism fault like the Izmit mainshock but have shallow dips (around 60°) than the Izmit mainshock (82°) but similar to that of the Düzce mainshock (62°).

Düzce Basin (segment H)

Segment **H** is dominated by the pull-apart Düzce basin (Section 2.2.4) with a nearly rhomboidal appearance with irregular eastern and western margins that are bounded by NE-SW mainly right-lateral striking faults and NW-SE striking normal faults (Ardel, 1965). As it is seen in the hypocentral distribution for the inter Izmit-Düzce and pre-seismic phase (Fig. 5.8) only the southern part of the Düzce Basin hosts pronounced

seismicity. This was also discussed by Pucci et al. (2006) who pointed out that the northern part of the basin is no longer active. The basin is dominated by one single river stream that flows northward from the Efteni Lake flows and crosses orthogonally the northern Karadere fault. He concluded that only the westernmost part of the Düzce basin is the current "fault related floodplain" (Pucci et al., 2006). This is also supported by the local stress field orientation obtained here. A predominant strike-slip regime with only a small normal-faulting component for the inter Izmit-Düzce phase is observed. These observations confirm that the seismicity in the northern branch of the Düzce basin is dominated by the Düzce fault and that the northern branch is presumably inactive.

Elmalik Fault (segment I)

Segment **I** represents the easternmost extension of the Düzce fault and the rupture zone of the Düzce earthquake. This segment has not been studied in detail previously since no surface slip was observed. The WNW/ESE-trending Elmalik fault connects the Düzce fault with the eastern single trace of the NAFZ (Fig. 2.4) (Akyüz et al., 2002; Langridge et al., 2002; Pucci et al., 2006). With this study the stress field of this area is investigated for the first time and confirm the so far exclusive geological observations of the Elmalik fault. The STI result indicates a SS-regime with a NNW-SSE ($\sim 170°$) striking of σ_1 which would confirm the geological observations and the trend that the fault is probably joining the fault trace of the NAFZ near the city of Bolu.

Table 5.1.: Segments along the Izmit rupture based on the cluster analysis of polarities and resulting preferred faulting mechanism obtained by the MOTSI method within in this study (? - not well resolved, NF- normal faulting, SS - Strike slip).

Segment ID	Area	Stress Inversion results pre-seismic	inter Izmit-Düzce	post-seismic
A	Izmit-Sapanca fault	SS	SS/NF	-
B	Sakarya fault	NF	NF	NF/SS?
C	Adapazari-Akyazi Basin	NF	NF	NF/SS
D	Karadere Fault	NF/SS ?	NF	NF
E	Karadere Fault South	-	NF	NF
F	Karadere Fault North	-	SS	SS
G	Düzce Fault	-	SS	SS
H	Düzce Basin	-	SS	SS
I	Elmalik Fault	-	-	SS

5.4. Summary

In this study the stress field evolution in conjunction with the Izmit and Düzce 1999 mainshock in NW Turkey is investigated. As a first step (see section 5.2) a compilation of focal mechanisms were inverted for the stress tensor and systematic temporal variations of the crustal stress field orientation were observed along distinct segments of the Izmit 1999 rupture focusing the first two month of the the inter Izmit-Düzce phase. A change from the regional long-term strike-slip stress field to EW-extensional normal faulting along two local pull-apart structures (Akyazi Plain and Dücze Basin) was recognized. The observations confirm that shear failure and the associated drop in shear stress during large earthquakes may result in a rotation of the principal stresses acting on the fault along distinct patches and in accordance with lateral variations of co-seismic slip. No variation between the background stress field prior to the 1999 Izmit event and the post-seismic setting following the two-month aftershock period (2000-2007) is observed indicating that the stress field rapidly recovers from a large earthquake as the aftershock rate decreases. In a second step (see section 5.3) a significantly enlarged event database was used to investigate the stress field evolution in greater detail inverting first-motion polarities from local seismicity also before and after the Izmit and Düzce earthquakes. For the determination of stress field orientation the MOTSI procedure was used. This allowed to also cover areas and time

periods for which not sufficient single-event focal mechanisms were available. With the direct comparison of the stress results for the inter Izmit-Düzce phase from the previous study the robustness of results obtained by MOTSI could be tested. As Balfour et al. (2005) figured out by comparison of confidence intervals of focal mechanisms based and first motion based inversions the confidence intervals for the results obtained with MOTSI are often larger but still show significant stress field rotations. Although Robinson and McGinty (2000) suggested that ~ 500 polarity observations are required for a robust result, this study could show that also a smaller number of polarities is sufficient to get stable and reasonable stress inversion results. This is probably also depending on the level of stress heterogeneity and spatial segmentation of the study area. It is therefore suggested to carefully analyse the spatial distribution of polarities before their inversion for the stress tensor. For the analysis of large datasets with events of M $\sim$ 3 the first motion based STI is preferred, since a huge number of smaller events can be taken into account and due to the error assessment the results give a better indication of the real uncertainties. While principal observation of the results obtained from inverting focal mechanisms could be confirmed and refined, the in-depth study from analysing polarities also allowed to see the limits of such studies. Nine distinct segments could be investigated for the first time separately for the pre-, inter Izmit-Düzce and post-seismic phase thus including areas and time intervals for which no sufficient single-event focal mechanisms were available. Figure 5.15 summarizes the results obtained in this study. The Izmit-Sapanca fault (segment A) is displaying for the pre-seismic phase the regional, long-term strike-slip regime. For the inter Izmit-Düzce phase a normal-faulting regime characteristic influenced by the intentional setting in the Adapazari-Akyazi basin where tension is introduced by the 3.5 m coseismic slip deficit can be observed. The Sakarya fault (segment B) is generally dominated by the neighboring pull-apart basin. Thereby a small change from substantially normal-faulting influence in the pre-seismic phase to completely dominated in the inter Izmit-Düzce phase to a slightly start of a backrotation to strike slip in the postseismic phase can be distinguished. Further to the east, the Akyazi plain (segment C) is dominated by the EW-extensional normal faulting regime with the high slip deficit combined with a strike-slip component for the pre-seismic phase. Whereas the southern Karadere fault (segment E) showing a normal-faulting regime is still dominated by the extensional regime

in the Akyazi plain, the northern Karadere fault (segment F) seems to be connected with the Düzce fault reflecting a strike-slip regime. The influence of the normal-faulting regime seems to be concentrated around the Akyazi plain and no influence can be observed further to the east or west. Also the Düzce fault (segment G) indicates a stable strike-slip mechanism and is not influenced by the Düzce pull-apart basin (segment H) which has similar characteristic like the Akyazi plain but no change in the stress regime is observable since no major slip deficit occurred. Finally, the Elmalik fault (segment I) is investigated the first time indicating a strike slip regime. In summary, the stress field evolution of the studied segments along the Izmit and Düzce rupture can be followed from the predominantly pre-seismic strike-slip regime in the west, the inter Izmit-Düzce phase of the dominant E-W extensional regime in the Akyazi plain to the nearly stable post-seismic strike-slip regime along the Düzce and Elmalik faults corresponding to the regional stress field. The different orientation of the stress field in the segments are

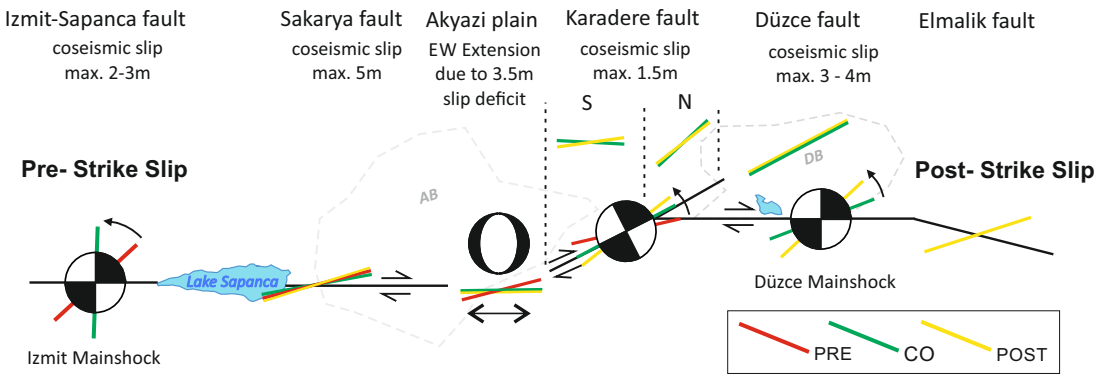

Figure 5.15.: Combined stress inversion results along distinct segment of the Izmit and Düzce rupture based on the inversion from focal mechansim (Section 5.2) and first motion polarities (Section 5.3). Focal mechanism indicate the predominantly regime in the distinct segment. The stress evolution corresponding to the rotation of the minimum principal stress axis (σ_3) along the fault can be followed by the color-coded bars, indicating the pre-, inter Izmit-Düzce and post-seismic state of stress in red, green and yellow, respectively. The regional direction of the maximum principal stress axis (σ_1) is given in the legend for the color coding of the bars. The amount of coseismic slip for each segment is given below the segments names. AB - Adapazari-Akyazi Basin, DB - Düzce Basin.

interpreted with respect to co- and post-seismic displacements observed along the Izmit and Düzce rupture and maintain a good correlation between slip changes and the stress field orientation. These observations can also be used for the analysis of possible creeping

parts of a fault which will be addressed in the following study. Detailed investigation using polarity information for a regional network helps to disclose otherwise undetectable processes.

6. Spatiotemporal variations of aseismic patches along the 1999 Izmit-Düzce rupture zone and their correlation to co- and postseismic deformation.

In this chapter the spatial and temporal distribution and kinematics of local seismicity along the Izmit and Düzce ruptures is studied. A high-resolution microseismicity catalogue including more than 10.000 hypocenters extending along the 1999 Izmit and Düzce rupture zones in northwestern Turkey is generated and analysed. This catalogue extents from prior to the Izmit event to after the Düzce earthquake. The main focus of this study is to relate the spatial and temporal distribution of seismically active and inactive zones to the co- and postseismic deformation within and below the seismogenic layer, respectively. Four large seismically quiet patches are identified along the different NAFZ segments activated during the Izmit and Düzce events showing a systematic spatial shift and a clear relation to the maxima of co- and postseismic deformation.

6.1. Introduction

Studying co -and postseismic deformation is a key for the understanding of rock rheology and the numerous relaxation processes that accompany and follow large earthquakes. While deformation along the surface can be directly measured, the deformation processes at depth can only be derived from inverting observations such as GPS-derived surface deformation or seismic waveforms. The fundamental challenge, however, is that the same postseismic surface deformation pattern can be produced by various models of viscous shear and aseismic slip at depth (Bürgmann and Dresen, 2008).

The investigation of co- and postseismic deformation has largely been improved by advances in geodectic techniques, such as the higher precision of GPS measurements and

Interferometric Synthetic Aperture Radar (InSAR) range change data. For example high-resolution observations of time-dependent surface motions allow deriving improved transient deformation processes at depth (Bürgmann and Dresen, 2008). First studies on the rheology at depth in conjunction with a major strike-slip earthquake were initiated by the great 1906 San Francisco earthquake on the San Andreas Fault. The use of geodetic observations of surface deformation caused by this event firstly lead to the awareness of elastic rebound and the earthquake cycle (e.g. Reid 1910; Thatcher 1983). More recently, studies on the 1992 $M_w = 7.4$ Landers and 1999 $M_w = 7.1$ Hector Mine earthquakes in the Mojave Desert in California display different possible explanations for the postseismic deformations such as deep aseismic afterslip, viscoelastic relaxation in the lower crust, a combination of poroelastic rebound and crustal afterslip or poroelastic rebound and viscoelastic relaxation in the lower crust (see review by Bürgmann and Dresen 2008, and references therein).

Yin and Zhang (1982) established the basic elastoplastic relation of strain softening of fault rocks by decreasing their internal frictional angle and cohesion in laboratory experiments to model earthquake processes and associated afterslip. As introduced earlier, an earthquake occurs when stress reaches a critical value based on the Coulomb criterium (Section: 2.2, Eq.2.1). The ongoing strain softening causes coseismic slip and the stress drop observed during large earthquakes. After stresses are released during an earthquake, the rupture stops and a change from coseismic deformation to interseismic locking is occurring. In laboratory experiments under controlled boundary conditions these processes can be repeatedly observed creating multiple seismic cycles (Luo and Liu, 2010). However, in the field such observations are not frequent since only few large earthquakes are monitored with sufficient precision and recurrence times are usually longer than a century. The analysis of slip caused by an earthquake is based on the Byerlee (1978) law, which describes the minimum shear stress required for the initiation of slip on pre-existing faults. Several models have been proposed to explain the spatial distribution of coseismic slip at depth and in particular its transition from the brittle onto the ductile part at the base of the seismogenic part of the crust in space and time (Fig. 6.11) (Montési, 2004). Whereas Sibson (1986) suggests that brittle frictional sliding is caused by compositional differences of the ductile part of the crust, Tse and Rice (1986) explain the occurrence

of so-called "ductile earthquakes" by the variation of unstable to stable frictional slip on deeply penetrating faults. In general, it is agreed that the depth extent of the seismogenic zone and the transition to ductile behavior depends on four main factors: rock composition, temperature, strain rate, and fluid pressure (Sibson, 1986; Tse and Rice, 1986). Another basic law for investigating slip distribution is the the rate-and-state friction law, introduced by Dieterich (1979). This law was derived from laboratory friction experiments and has been used in numerous studies to model afterslip as well as slow earthquakes, and the occurrence of seismicity in general (Dieterich, 1994; Helmstetter and Shaw, 2009). Depending on the parameters the model is either stable (aseismic slip) or allows slip instabilities (earthquakes) (Helmstetter and Shaw, 2009). It implies that afterslip transfers stresses from sliding to locked parts of the fault, and is thus a potential mechanism for aftershock triggering that is decaying with time following the Omori law (Rice and Gu, 1983; Dieterich, 1994; Segall, 2004). Marone (1998) reviewed studies that used these empirically derived rate- and state-dependent friction laws to explain faulting mechanism in the lower and upper crust.

Still today the considerable uncertainty in determining the hypocentral depth of earthquakes is one reason for the ongoing debate about the nature of earthquakes and the continuation of slip below the brittle part of active fault zones in space and time (Rolandone et al., 2004; Bürgmann and Dresen, 2008). Rolandone et al. (2002) analysed mechanical models of long-term deformation that suggest a wide zone of accommodated slip and ductile flow at the brittle-ductile transition and a change of the deformation mechanisms during the earthquake cycle. Thatcher (1983) and Tse and Rice (1986) suggest that either distributed viscous flow or frictional aseismic faulting could be responsible for deformation process at depth.
Whereas the rheology of the upper crust can be described by linear elastic relations between stress and strain, deformation at larger depths involving higher temperature and pressure consists of both, elastic and viscous behavior. The upper crust rheology can be described by a elastic spring, where stresses are too low to induce brittle fracture of intact rock or frictional sliding of faults (Bürgmann and Dresen, 2008). At larger depths various combinations of viscoelastic stress-strain relations are possible. Often faults are interpreted in terms of velocity weakening and velocity strengthening zones. In the first

case, friction decreases with the sliding velocity which can lead to spontaneous rupture of the fault. The second case allows the existence of aseismic fault slip (Bürgmann and Dresen, 2008) at fault zones. The study of Tse and Rice (1986) suggest that faults become velocity strengthening at mid-crustal temperatures which lead to the assumption that the transition below the seismogenic zone is represented by stable sliding, rather than by distributed ductile flow.

Studies on postseismic deformation reveal that deep rheology is depending on the local lithospheric structure and tectonic setting (Bürgmann and Dresen, 2008). In addition, the duration and spatial extent of the deformation is depending on the size of the earthquake source. The aim of this study is to relate the spatiotemporal distribution of co- and postseismic slip of the 1999 Izmit and Düzce earthquakes, two of the best-studied M>7 strike-slip earthquakes worldwide to the occurrence of crustal seismicity framing both mainshock ruptures in space and time. In total four seismically inactive fault patches and a systematic relation to deformation occurring in the brittle crust during both mainshocks and below the seismogenic layer during postseismic times are found.

6.2. Database

To investigate the spatiotemporal distribution of seismically active and inactive fault patches along the Izmit and Düzce ruptures and their depth-extension as well as their relation to observed afterslip at depth, an accurate hypocenter determination of the local seismicity is crucial as discussed earlier in this thesis. To enlarge the seismicity database for this region and in addition to the hypocenter catalogue presented in Chapter 4 (Figure 4.3 and Figure 6.1, color-coded black) additional events recorded by the SABONET network during the years 1997-1999 were manually picked and located following the same processing scheme as described in section 4.3.

This resulted in absolute hypocenters with lateral and vertical errors of 2.9 and 2.6 km for 67% of the events. To obtain a further improved relative location accurancy of hypocenter distribution the events were relocated following the Double-Difference earthquake relocation method by Waldhauser and Ellsworth (2000). This technique links event-station pairs and minimizes the residuals between observed and theoretical travel-time differences for pairs of earthquakes at each station. Since the ray paths of closely spaced events are

almost identical the effect of unmodeled velocity structure on hypocentral offsets can be suppressed resulting in a considerably improved relative accuracy for studying seismically active structures (Waldhauser and Ellsworth, 2000). Here, the hypoDD approach is not explained in further detail since this has been done in numerous recent studies. For details of the method, the reader is refered to the user manual of the code itself (open source USGS) and a detailed discussion of the method provided by Bulut (2010, dissertation). The final hypocenter catalogue of relocated events obtained from SABONET along the Izmit/Düzce part of the NAFZ for the year 1997 - 1999 consists of 2325 events (Fig. 6.1, color-coded blue) with a relative location accuracy of approximately 500 m. Note that the relocation technique does not allow to improve the absolute precision of the hypocenter cloud. Figure 6.1 illustrates the temporal evolution of seismicity along the Izmit and Düzce ruptures (both striking approximately east-west) and gives an overview on the different earthquake catalogues used in this study. In addition to the SABONET catalogue introduced before the Izmit aftershock catalogue of 4700 relocated events with in internal precision of 400 m (Bulut et al., 2007) (introduced in 5.3.2) is used. From the already obtained SABONET catalogue 4.2 only events with a absolute location error smaller 3 km where used. The complete database for this study consists of 10661 events, hypocenters are plotted for the pre-seismic, inter Izmit Düzce, and post-seismic phase in figures 6.2 - 6.4.

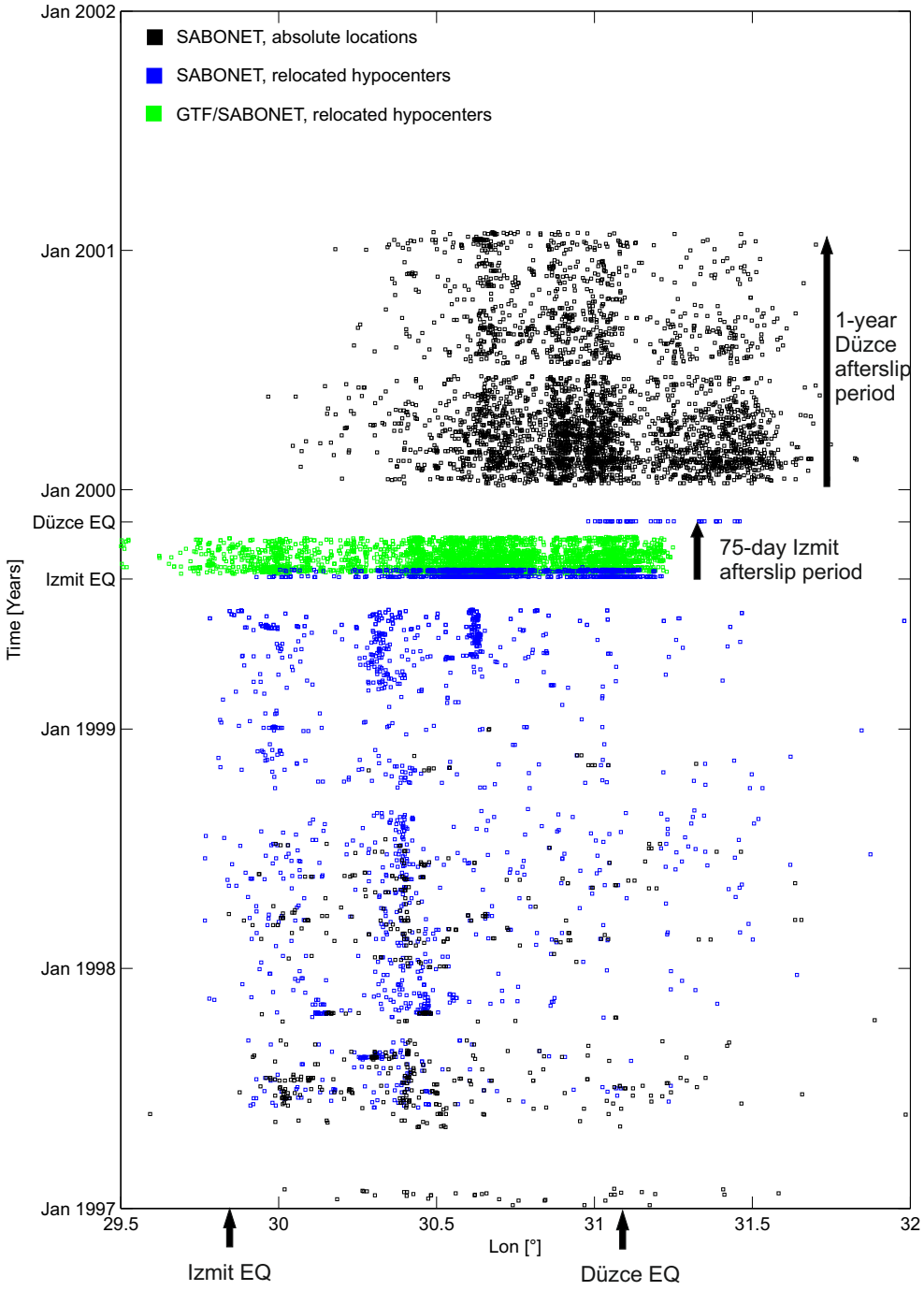

Figure 6.1.: Event-Time Evolution along the Izmit/Düzce rupture. The different data sets contributing to this catalog are color coded in black (SABONET, absolute hypocenters, this study), blue (Sabonet, relocated hypocenters, this study) and green (GTF/SABONET, relocated hypocenters, Bulut et al. 2007).

6.3. Spatial distribution of seismically active and inactive patches along the Izmit and Düzce ruptures

The spatial distribution of seismicity along the two 1999 ruptures shows a clear variation of seismic activity along the fault and with depth. The seismicity catalogue is plotted in map view and as depth section for three time intervals: prior to the Izmit earthquake, inter Izmit-Düzce and post-Düzce, respectively, in figures 6.2 - 6.4. In general, the seismicity is distributed along the entire combined rupture zone forming a ∼20 km wide band of activity. This is consistent with previous studies that investigated the kinematic setting of the seismogenic zone from Izmit aftershocks (Aktar et al., 2004; Bulut et al., 2007; Bohnhoff et al., 2008). In first-order approximation the activity level is increasing from west to east between 29.5°E and 31.5°E along the main rupture. The central part of the seismicity band does not exhibit a narrow vertical plane (the actual fault plane activated during the two mainshocks) which is not an artifact of location precision. This is also in accordance with Bouchon and Karabulut (2008) stating that a substantial portion of the Izmit aftershocks occurs off the main rupture, but not on the activated plane itself. The authors interpret this as an additional constraint for the occurrence of super-shear rupture during the Izmit event. Barka et al. (2002) and Bohnhoff et al. (2008) observed that the seismic activity varies within individual fault segments consistent with the observed coseismic slip distribution and faulting kinematics. While the seismicity along the segments activated during the Izmit earthquake has been discussed earlier (e.g. Özalaybey et al. 2002; Bohnhoff et al. 2006; Bulut et al. 2007), here, an in-depth analysis also for the eastern part including the Akyazi, Karadere and in particular the Düzce segments is provided for the first time.

Pre-Izmit time period: For the pre-Izmit time period considered here (Jan 1997-Aug 1999) the seismicity level is about two events/day and thus considerably lower than after the Izmit and Düzce mainshocks as expected. Most of the seismicity follows the main NAFZ fault branch with pronounced activity along the Izmit-Sapanca segment that also hosted the Izmit hypocenter. In particular the area around the Izmit hypocenter has been recognized as a continuously seismically active patch during the years preceding the 1999 mainshock (Özalaybey et al., 2002; Aktar et al., 2004). Apart from sparse seismicity that

is diffusely distributed throughout the region a pronounced seismicity cluster is observed at 30.4°E/40.9°N (Fig. 6.2). This activity most likely represents quarry blasts which is supported by the distribution of P-wave first-motion polarities (all positive) and from daytime occurrence of the events. Therefore, the seismicity within these dense spatial clusters has been excluded from the depth section in figure 6.2 and from further analysis. The main NAFZ fault branch east of 30.5°E is seismically inactive except for a few individual events that are not clustered in space or time and thus are considered to represent background seismicity.

Inter Izmit-Düzce time period: For the inter Izmit-Dücze time interval (Aug17-Nov11, 1999) a dramatic increase in seismic activity and seismic moment release is observed concentrated on a ∼20km wide band along most of the Izmit rupture (Fig. 6.3). Note that the reduced seismic activity at the westernmost portion of the rupture below the eastern Sea of Marmara is an artifact of the station distribution of the SABONET and GTF networks (see chapter 4). This part of the Izmit aftershock zone is not further analysed here and has been studied e.g. by Özalaybey et al. (2002) and Bulut and Aktar (2007). While the seismicity level is generally high along the fault segments that were activated during the Izmit mainshock there are clear lateral and depth-dependent variations observed in the hypocenter catalogue. In particular it is noted that below the Lake Sapanca region as well as below the Karadere Fault the upper boundary of aftershock activity extends as deep as 10 kilometers (marked A and B in Fig. 6.3) while it is substantially shallower (∼5km) along most parts of the aftershock activity band. This will be discussed later in the text. Towards the eastern end of the Izmit aftershock activity zone there is a sharp termination of seismic activity at 31.2°E. It was exactly on this edge where the Düzce earthquake nucleated 87 days following the Izmit event, on Nov11, 1999 (red star in Fig. 6.3). The Düzce rupture then proagated mainly to the east while a small portion of the easternmost Izmit rupture plane was re-ruptured (Umutlu et al., 2004).

Post-Düzce time period: For the post-Düzce time period (2000-2001), a clear shift in seismic activity towards the east is observed (Fig. 6.4). Most hypocenters are located between 5 and 15 km depth. Starting from the Sapanca segment in the west the density of events is substantially increasing. The highest level of seismic activity can be observed below the Akyazi, Karadere and Düzce segments. Interestingly only about

half of the earthquakes are located along the actual Düzce rupture while the other half follow a similar first-order spatial pattern as during the Izmit aftershock phase (the two months prior to the Düzce event) and primarily occurs on the same activity patches that are highlighted by immediate Izmit aftershocks. Note that most of these patches that still showed pronounced seismicity after the Düzce event had not been re-ruptured by the Düzce event to most extend. The depth-distribution of seismicity shows a clear shift of the post-Izmit/pre-Düzce shallow seismically inactive fault patches (marked as C and D in Fig. 6.4). While the depth-resolution is uniform along most part of the Izmit-Düzce ruptures, the depth resolution for events along the easternmost Elmalik fault is limited in response to the SABONET station distribution with only few stations to the east of the Düzce rupture.

While seismicity throughout the area and time period studied here is generally occurring within the depth interval 5-18 km there is a set of very shallow events located between 30.7°E-31.2°E and close to the activated main fault branch. These events started to occur after the Izmit mainshock and are discussed in detail below (indicated in red in Fig. 6.3 and Fig. 6.4).

Caused by the SABONET station distribution with few stations to the east, the depth determination for the easternmost Elmalik fault is limited. Starting from the Sapanca segment in the west the density of events is substantially increasing. The highest level of seismic activity can be observed below the Akyazi, Karadere and Düzce segments. Different than in previous studies here also Düzce aftershocks are analysed.

Below the junction of the Karadere fault and the Düzce Basin another cluster of high seismicity with hypocenter distributed from really shallow ($<$ 3km) to 15 km depth can be observed. The shallow earthquakes are separately discussed in section 6.4. The high seismic activity at the junction from the Karadere Fault towards the Düzce Basin is well-explained by the repeated activation during both earthquakes. This area is therefore influenced by repeated stress perturbations resulting in numerous and also diffusly distributed aftershocks with no sharp limit in hypocentral depth.

The most striking observation from the here presented seismicity catalogue consisting of more than 10.000 events as shown in figures 6.2-6.4 covering the time interval from prior

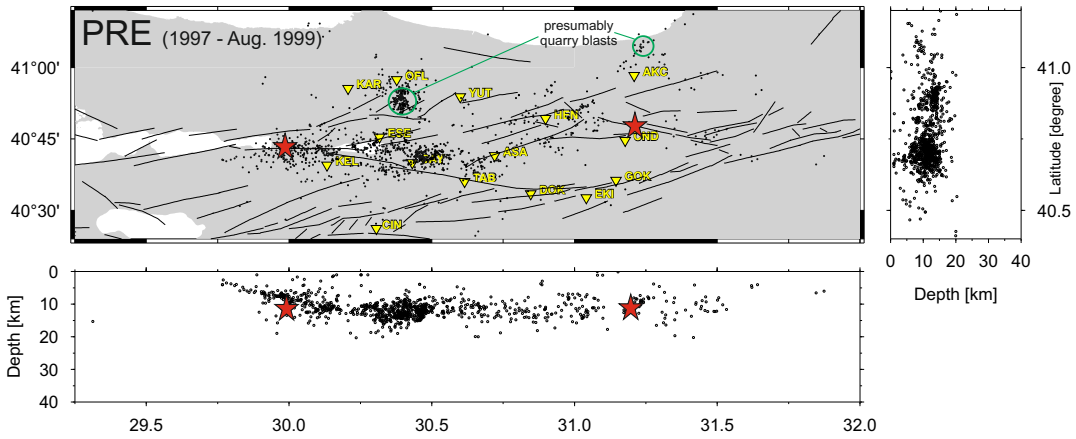

Figure 6.2.: Seismicity distribution along the Izmit/Düzce rupture for the preseismic phase. The red stars show the hypocenters of the Izmit (left) and Düzce (right) earthquakes.

to the Izmit earthquake until after the Düzce earthquake is that four distinct seismically inactive fault patches have been identified along the combined Izmit-Düzce rupture zone. Moreover, these four seismically inactive patches (labeled A-D in Fig.6.3 and Fig.6.4) are not stationary in time but have different locations after the Izmit (before the Düzce) than after the Düzce mainshock. Furthermore, the patches are clearly related to the observed maxima in co- and postseismic deformation within and below the seismogenic layer. The spatial extent of these patches along the fault and with depth heavily depends on the reliability of the depth-precision of the events in the surrounding area. Therefore, the vertical errors are plotted for all those events in Fig.6.5 stressing that the aseismic bahavior of all four patches A-D is well constraint, both laterally and vertically. All four four seismically inactive patches are discussed in detail in the following section.

Patch (A): For the inter Izmit-Düzce phase a nearly 50 km long seismically inactive patch extending down to ∼10 km depth is observed east of the Izmit hypocenter along the Sakarya and Sapanca faults. To either end of this inactive patch of the fault seismicity extends to shallower depths (4-5 km) in the Izmit epicentral region and the Akyazi plain, respectively. To a large extent, the seismically inactive fault patch coincides with the largest maxima of the cumulative 75-day afterslip below the seismogenic layer (Hearn et al. 2009, gray-shaded area A' in Fig. 6.3). In contrast the seismically inactive patch extends only over eastern half of the coseismic high-slip area of the Izmit event while the western portion does show pronounced seismicity.

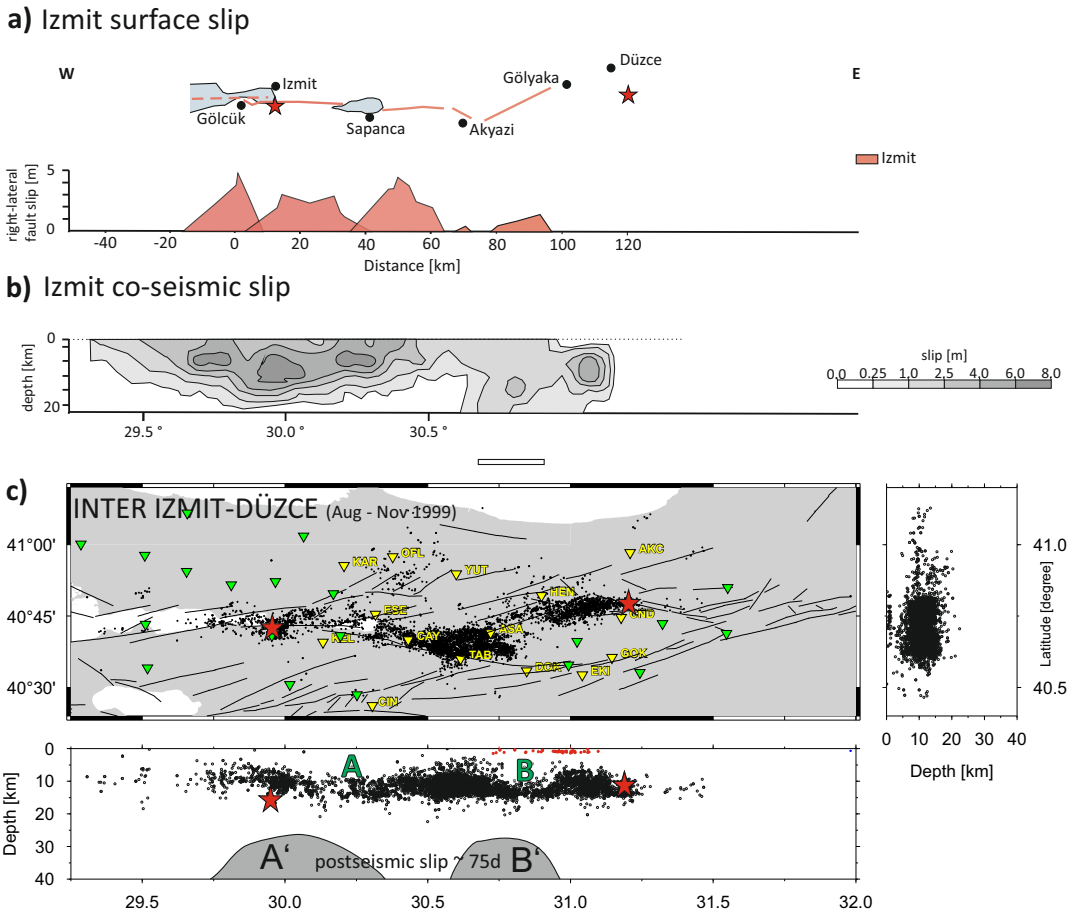

Figure 6.3.: Seismicity and slip distribution along the Izmit/Düzce rupture for the inter Izmit-Düzce phase. a) Surface slip distribution and a sketch of the rupture trace along the Izmit rupture modified after Aydin and Kalafat (2002) in red. b) Izmit coseismic slip distribution modified after Delouis et al. (2002). c) Spatial distribution of local seismicity along the Izmit/Düzce rupture for the inter Izmit-Düzce. Red dots indicate shallow earthquakes which are discussed separately in section 6.4. Grey shaded areas indicate postseismic slip distribution with depth modified after (Hearn et al., 2009). The red stars show the hypocenters of the Izmit (left) and Düzce (right) earthquakes.

Patch (B): For the inter Izmit-Düzce phase a second circle shaped aseismic fault patch is observed extending for ∼10 km along the Karadere fault and down to ∼10 km depth. This zone contains several shallow earthquakes and extends from east of the high-seismicity area in the Akyazi Plain towards the western end of the Düzce basin and fault. Similar to patch A a clear although smaller Izmit postseismic slip maximum was observed below this seismically inactive patch (Hearn et al. 2009, gray-shaded area B' in Fig. 6.3) for the same time period of ∼75 days. Note that the 75-days time interval extends throughout most of the inter Izmit-Düzce time starting right after the Izmit mainshock until 12 days

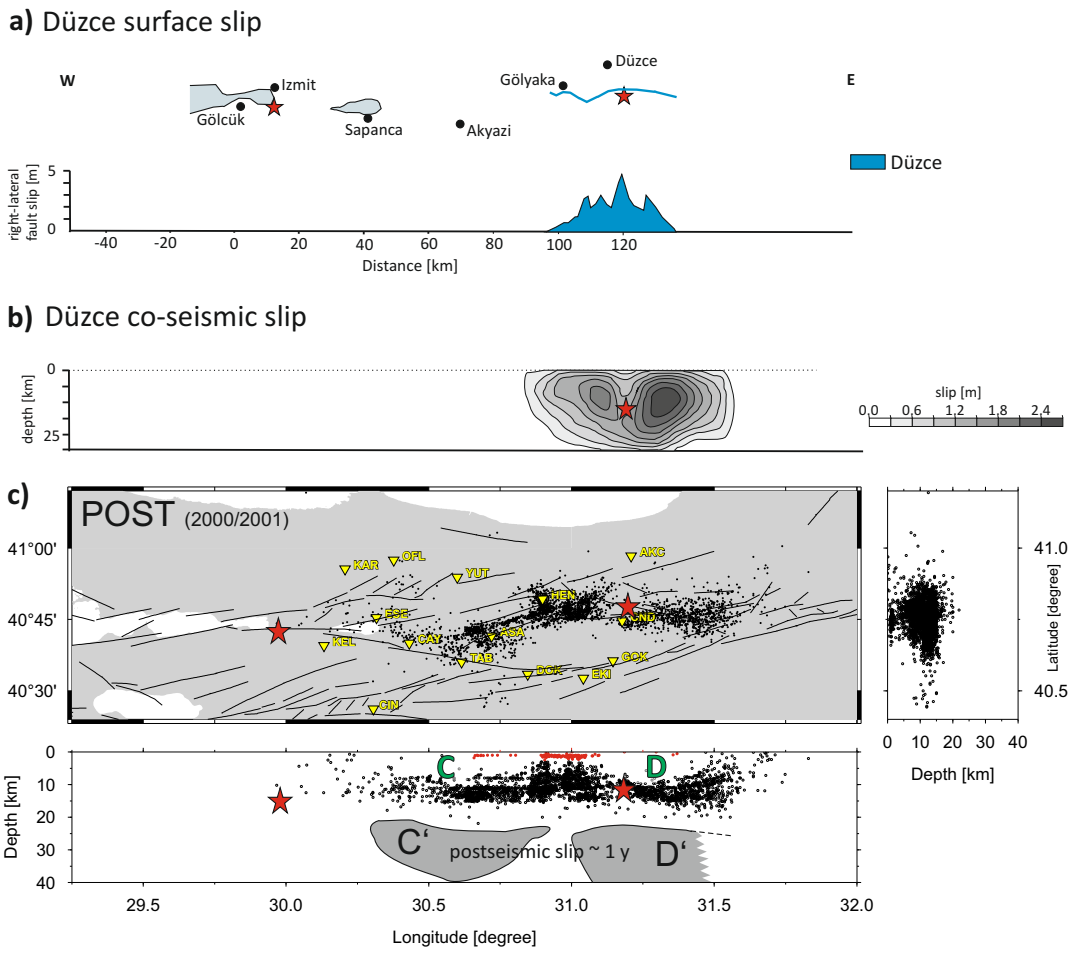

Figure 6.4.: Seismicity and slip distribution along the Izmit/Düzce rupture for the postseismic phase. a) Surface slip distribution and a sketch of the rupture trace along the Izmit/Düzce rupture modified after Aydin and Kalafat (2002) in blue. b) Düzce coseismic slip distribution modified after Umutlu et al. (2004). c) Spatial distribution of local seismicity along the Izmit/Düzce rupture for the postseismic phase. Red dots indicate shallow earthquakes which are discussed separately in section 6.4. Grey shaded areas indicate the postseismic slip distribution with depth modified after (Reilinger et al., 2000). The red stars show the hypocenters of the Izmit (left) and Düzce (right) earthquakes.

prior to the Düzce earthquake. It is note, that patch B is located close to the easternmost portion of notable coseismic slip. However, there is no overlap of both features.

Patch (C): For the postseismic phase a clear spatial shift of the seismically inactive fault patches is observed (Fig. 6.4). Patch C is similar in shape to patch A with regard to along-fault extension and depth. However,it is shifted by 50 km to the east, into an area hosting the overall strongest Izmit aftershock activity below the Akyazi Plain before the Düzce mainshock. As for patches A and B for the 75-days postseismic Izmit time

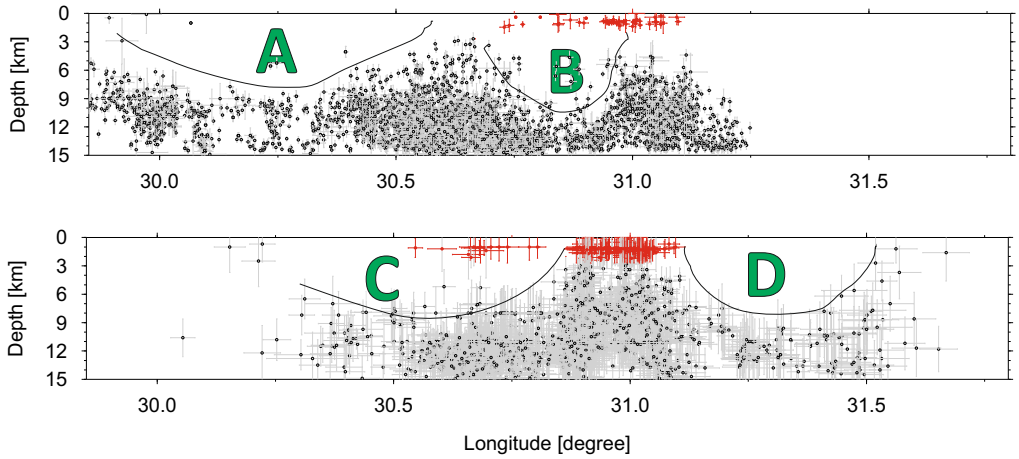

Figure 6.5.: Detailed map of the aseismic patches (A-D) shown in figures 6.3 and 6.4. Grey bars represent the depth and horizontal errors. Red marked events indicate shallow earthquakes that are discussed separately.

there is a clear maximum in postseismic slip (one year time period) below the seismogenic layer with a very similar along-fault extension (Hearn et al. 2009, gray-shaded areas C' and D' in Fig. 6.4). In first-order approximation, C' is complementary to A'. However, the western portion of C' might still include decaying aseismic deformation from A'. No coseismic slip during the Düzce event was observed at the location of patch C.

Patch (D): The seismically inactive patch D is located further to the east below the Düzce Basin and extends 40 km along the main fault branch of the NAFZ activated during the Düzce event. Similar to the other three seismically inactive patches A-C also D extends down to 10 km depth. As all the three previously described patches A-C this seismically inactive brittle fault patch is also mirrored by a maximum in (Düzce-)postseismic deformation below the brittle-ductile transition. Different to the patches A-C this patch coincides with the coseismic slip maximum area of the the Düzce earthquake to a large extent.

6.4. Shallow earthquakes on the Düzce fault

Analysing the variation of hypocentral depth for seismicity along the Izmit and Düzce ruptures a spatially isolated set of 195 shallow (∼3km deep) earthquakes was identified distributed along the junction of the Karadere and Düzce Faults. These events are located within the seismically inactive patches B and C to a large extend. Therefore, their depth-

constraint and internal spatiotemporal and kinematic pattern are of particular relevance. Interestingly, these shallow events (color coded in Fig.6.3, 6.4 and 6.5) only started to occur after the Izmit aftershock and only on the western part of the Düzce fault. Since the hypocentral depth is usually the least well constrained parameter of the hypocentral coordinates the depth distribution of these events is further tested. In general, only events with location errors smaller than 3 km for vertical and horizontal directions were considered throughout this study (Fig. 6.6). For the 195 shallow events, the average rms error is 0.13 and on average 4 P picks and 3 S picks were used. To further test the depth for the 195 'shallow events' their S-P times obtained at the two closest located SABONET stations (HEN and CND, figure 6.7) were analysed and plotted with distance since S-P times are a direct measure of the hypocentral distance from a particular station and thus allow to constrain the depth. The data from stations HEN and DOC show that the events are located at ∼3 to 12 km distance from each station. Calculating the average P-wave velocity for the formation crossed by the P waves of the 195 events on their path towards stations CND and HEN following the equation

$$v_p = (\frac{v_p}{v_s} * (1 - \frac{\frac{1}{v_p - v_s}}{t_s - t_p})) * x \tag{6.1}$$

a value of 3.1 km/s is calculated. This value is very similar to the average v_p of $\sim 3.2 \frac{km}{s}$ derived from the inverse slope of the regression line for the $(T_s - T_p)$ versus hypocentral distance plots in Fig.6.7 and representative for the uppermost kilometers in the area of investigation. This confirms that the 195 events are indeed very shallow and did not occur within the fully seismically inactive patches B and C. In the following these shallow earthquake are further analysed to better understand their nature and role in the local seismotectonic setting.

Figure 6.8 shows the distribution of the shallow earthquakes in the Düzce segment. A clear concentration of earthquakes along the western tip of the Düzce fault can be observed. The instant occurrence of the shallow seismicity after the Izmit earthquake (Fig.6.3) indicates a clear relation to the local coseismic surface slip at this part, close to the eastern termination of the Izmit rupture. Interestingly, the occurrence of these shallow events does not follow an Omori decay after the two mainshocks but shows a strong temporal clustering around March 2000, eight and five months after the Izmit and

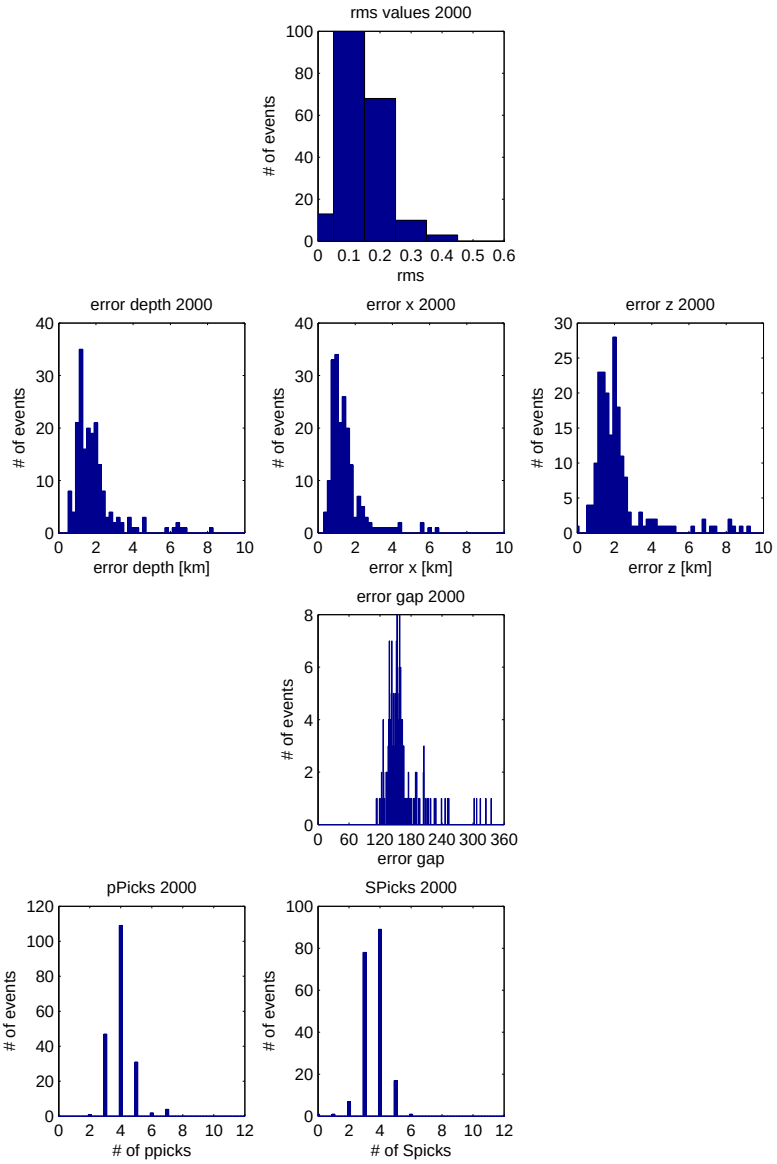

Figure 6.6.: Location errors and statistics for P and S Picks for the shallow earthquakes.

Düzce earthquake, respectively (Fig. 6.9). Furthermore, also the magnitude distribution of these events with time does not give any evidence for a main-shock aftershock sequence, but rather suggest swarm-type behavior.

Inverting the P-wave polarities of the shallow events for the local stress field using the MOTSI approach (see chapter 3.4) allows to derive a clear strike-slip regime for the up-

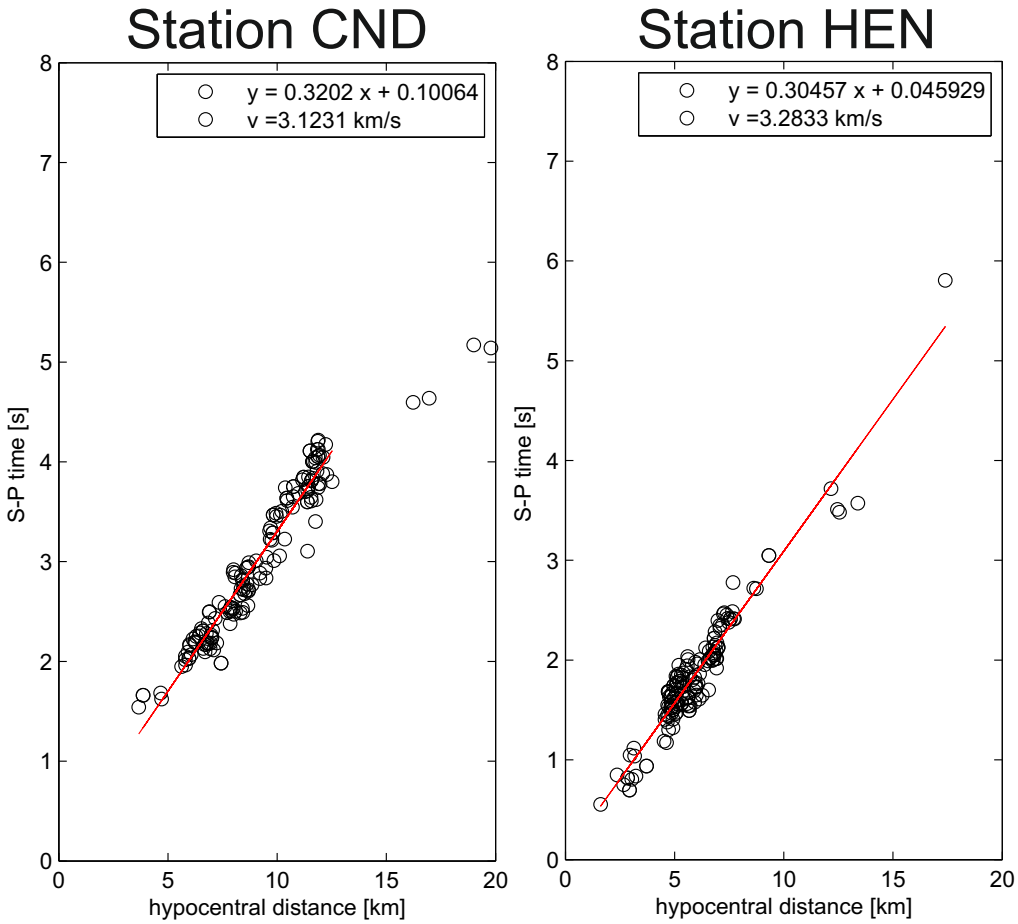

Figure 6.7.: S-P plots for station HEN and CND from the SABONET to reveal the occurrence of shallow earthquakes along the western part of the Düzce fault.

permost kilometers at the junction from the Karadere to the Düzce faults (Fig. 6.8). The obtained orientation for the maximum and minimum principal stresses clearly tends to favor the activation of an east-west-striking vertical fault in a right-lateral sense and is thus in good accordance with the regional stress field.

Studying the postseismic deformation and slip distribution with depth along the Düzce fault Pucci et al. (2006, 2007) observed a separation of the fault along the Eften Lake step-over which is marked by different pattern of slip distribution to its eastern and western part, respectively. The western part show almost no postseismic deformation and a simple linear co-seismically activated fault trace that has probably reactivated an older complex fault system. In contrast, on the eastern part of the fault the co-seismically activated fault

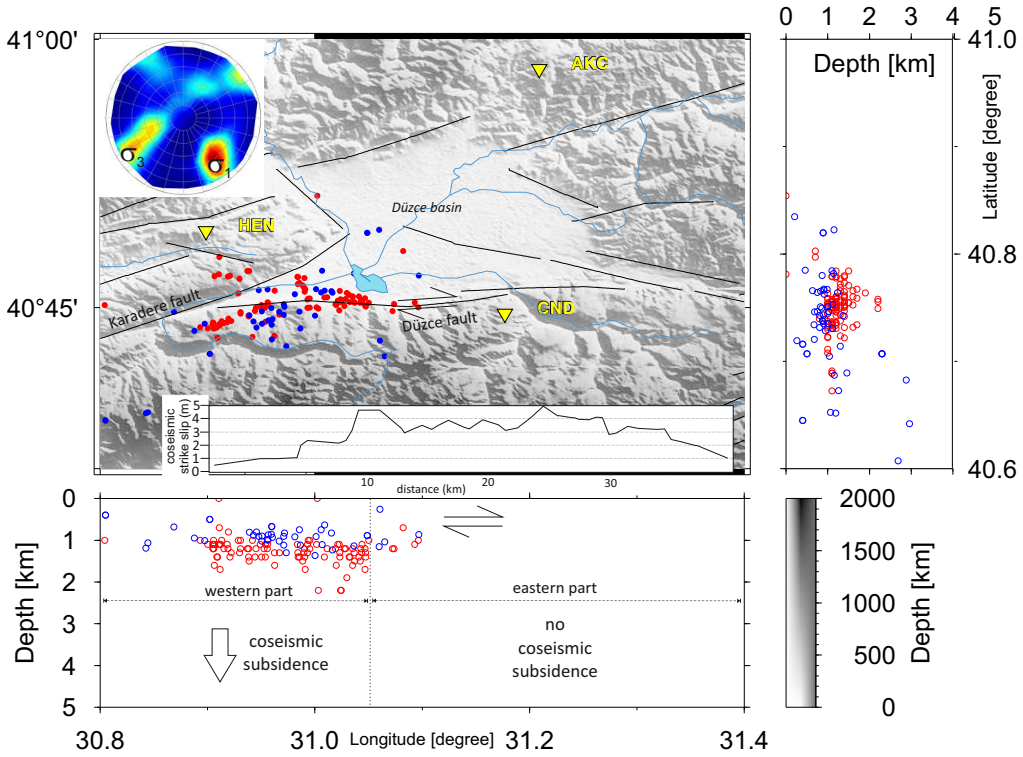

Figure 6.8.: Distribution of shallow earthquake along the eastern Karadere and western Düzce segment in map view (upper part) and depth section (lower part). The color coding indicates events during the years 1999 (blue) and 2000 (red), respectively. Fault lines are taken from Şaroğlu et al. (1992). The coseismic slip of the Düzce event is shown in the inset (modified after Pucci et al. 2006). The arrows indicate the right-lateral strike slip motion of the Düzce fault. The subfigure in the upper left shows the stress inversion results calculated using the MOTSI procedure (see chapter3.4) based on first motion polarities from the shallow events indicating a clear strike-slip regime for the uppermost kilometers. The results are plotted in lower hemisphere projection. The best solution for each of the three stress orientation σ_{1-3} is marked with the corresponding σ. For all results the marginal confidence limits for σ_1 and σ_3 are calculated and plotted color coded from blue (minimum) to red (maxima).

trace crosses this older and complex fault system. The different pattern of the Düzce fault at its eastern and western part is also well reflected by the coseismic slip distribution at depth. Delouis et al. (2002) compared the shallow fault complexities with the slip distribution at depth. The comparison with the surface data by Pucci et al. (2006) shows an abrupt decrease of the slip distribution at depth exactly at the boundary between the western and the eastern part of the Düzce fault. The western part of the fault hosted a slip maximum of 4.5 m at the surface during the Düzce earthquake, but, in contrast is dominated by a low-slip area at depth not exceeding 2 m. In contrast, the eastern part

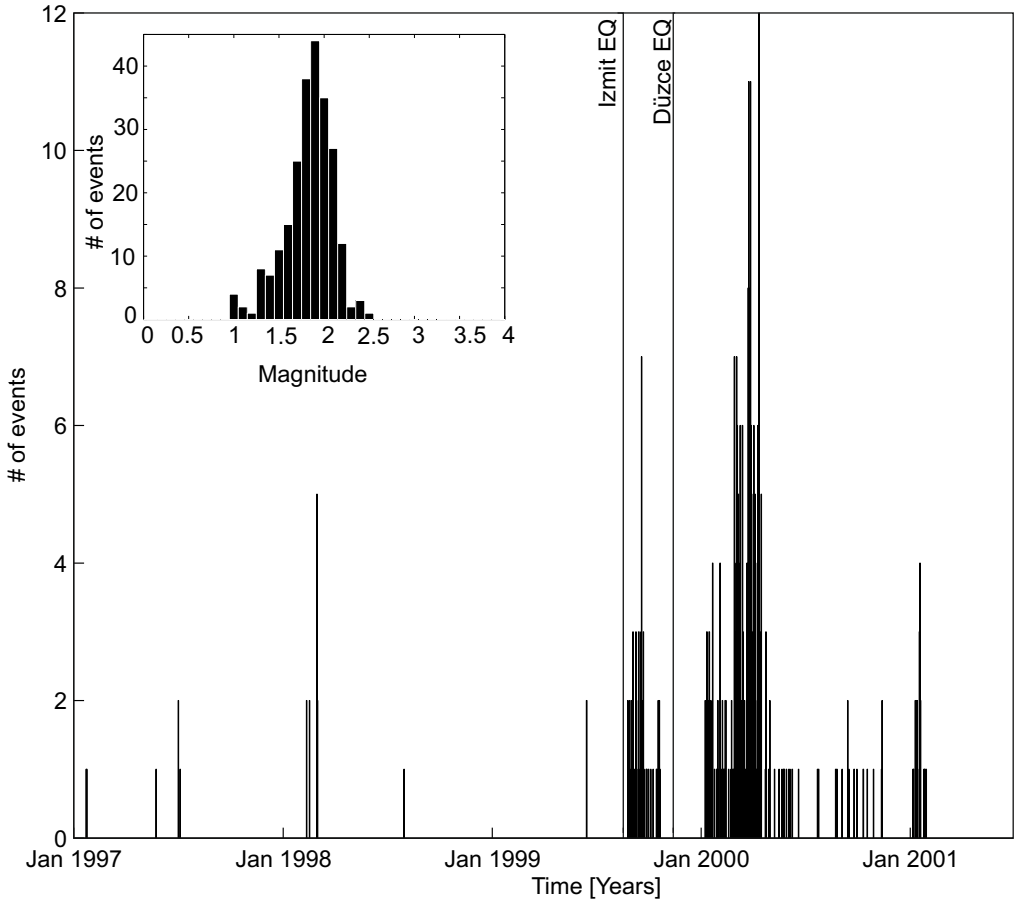

Figure 6.9.: Temporal evolution of the shallow earthquakes for the post-seismic phase which indicate a cluster of earthquakes in the earlier post-seismic phase of 2000.

shows a coseismic slip maxima of up to 5 m. Interestingly, the observed shallow seismicity in this region exactly follows the subdivision of the Düzce fault in that all shallow events tend to occur on the western portion of the Düzce fault while not a single shallow events was located on the eastern portion of the fault. Pucci et al. (2006, 2007) postulate that the eastern and western sections of the Düzce fault may represent different stages of fault-segment evolution with different dynamic properties during and following the mainshock rupture. Thereby the dominant factor of the rupture dynamics below fault discontinuities is assumed to be normal stress rather than shear stress. The western section of the Düzce fault is thereby expected to be under lower normal stress caused by the Karadere-Düzce fault junction and its mechanical interaction and is therefore at an earlier stage of its evolution at the surface. This would also explain the complexities of this side of the fault that has not formed a single fault trace so far. Another fact to consider is the present-day

important subsidence of the southwestern part of the Düzce Basin, which is not entirely fault-related and not an active pull-apart basin as whole. In contrast, the northwestern part of the Düzce basin is shrinking because of the transpressional deformation due to the Karadere fault (Pucci et al., 2006). Sibson 1985; Harris and Day 1993, 1999 studied the phenomenon of rupture arrests of earthquakes. When differences of fluid pressure do not act as a barrier, the lower observed normal stress along the western part of the fault may favor the rupture propagation. However, this would lower the rupture velocity and would lead to a delay of the triggering process for the neighboring fault segment. This could have played a role for the delayed triggering of the shallow events, it might even be a possible explanation for the delayed propagation of the August 17, 1999 Izmit rupture onto the Düzce fault, where the nucleation of the Düzce earthquake on the eastern section on the fault occured only three months later, on November 12, 1999 (Pucci et al., 2006). Pucci et al. (2006) favors different possible explanation for the missing coseismic slip in the western section on the assumption that the regional tectonic loading at the scale of the fault is considered as constant. Possible explanations are: 1) microseismicity; 2) aseismic behaviour, with minor stress storage during the interseismic phase; 3) strain transfer to the eastern asperity as velocity strengthening frictional afterslip (Hearn et al., 2002) during the postseismic phase; 4) partitioning of the slip between the Karadere and western part of the Düzce fault; 5) concurrence of the above hypotheses.
The shallow earthquakes on the western part of the Düzce fault observed in this study would support the first hypothesis of existing microseismicity. The small magnitude shallow earthquakes could have released stresses in the crust after the Izmit earthquake and therefore the coseismic slip is missing on this side of the fault. The Eften Lake step-over thereby formed also a barrier for the shallow earthquake and limit their occurrence on the west side.

6.5. Discussion

The seismicity catalogue presented here consists of >10.000 events extending along the entire combined Izmit-Düzce rupture zone. In total, the Izmit and Düzce mainshock ruptured an almost 200 km long part of the NAFZ in northwestern Turkey extending from the eastern Sea of Marmara in the west to the western end of the 1944 rupture in the

east. This is the first hypocenter catalogue obtained from a local seismic network which allows a reliable hypocenter determination with precision in lateral and vertical directions on the order of 2-3 km and covering the entire time interval from more than two years prior to the Izmit earthquake to 14 months after the Düzce earthquake.
During the two years prior to the two 1999 Izmit and Düzce M>7 mainshocks sparse seismic activity is observed throughout the area with some spatial clustering along distinct parts of the main branch of the NAFZ (Fig.6.2-6.4). The seismicity does not occur on the main NAFZ fault but forms a ∼20 km wide band of activity. Hypocentral depths are mostly between 10 and 18 km, i.e. most of the seismicity is located in the lower half of the seismogenic layer. Following the Izmit and Düzce mainshocks the overall seismicity is drastically increasing as expected. The spatiotemporal distribution of events allows defining several interesting features:

First of all the seismicity forms an approximately 20 km wide band of activity with most events being located along the main fault that was activated during the 1999 M_w 7.4 Izmit and M_w 7.1 Düzce earthquakes but off the principal slip zone (Fig. 6.3 and 6.4). The off-fault location of seismicity, as observed also before the Izmit and after the Düzce events, is in good correspondence with previous observations being limited to the initial two-month Izmit aftershock period (Bulut et al., 2007; Bohnhoff et al., 2008). The seismicity distribution off the fault can be explained by the supershear rupture process introduced by Bouchon and Karabulut (2008). The authors investigated the Izmit rupture as a fault where the rupture speed exceeds the shear wave velocity of the rocks. This lead to the observed off-fault clustering of aftershocks, where secondary faults were activated by a so-called "seismic shock wave" originated by the supershear rupture.

Second, a relatively sharp lower boundary of seismicity throughout the whole study area, i.e. along the entire combined Izmit-Düzce ruptures is observed. This lower boundary is located at ∼18 km depth. While the absolute depth of this lower boundary is subject to the 3 km uncertainty in depth resolution, this boundary is interpreted to reflect the onset of the brittle-ductile transition along this part of the NAFZ. In that respect, it is noted that Rolandone et al. (2004) studied variations in maximum depth of seismicity

during the years following the Landers earthquake in California. Whereas most studies on the brittle-ductile (seismic-aseismic) transition focus on the temperature and lithology differences (e.g. Magistrale 2002) here the authors analysed the evolution of the lower hypocentral depth for aftershocks observing a time-dependent postseismic shallowing on the order of 3 km within a time span of 4 years following the Landers earthquake. Studying

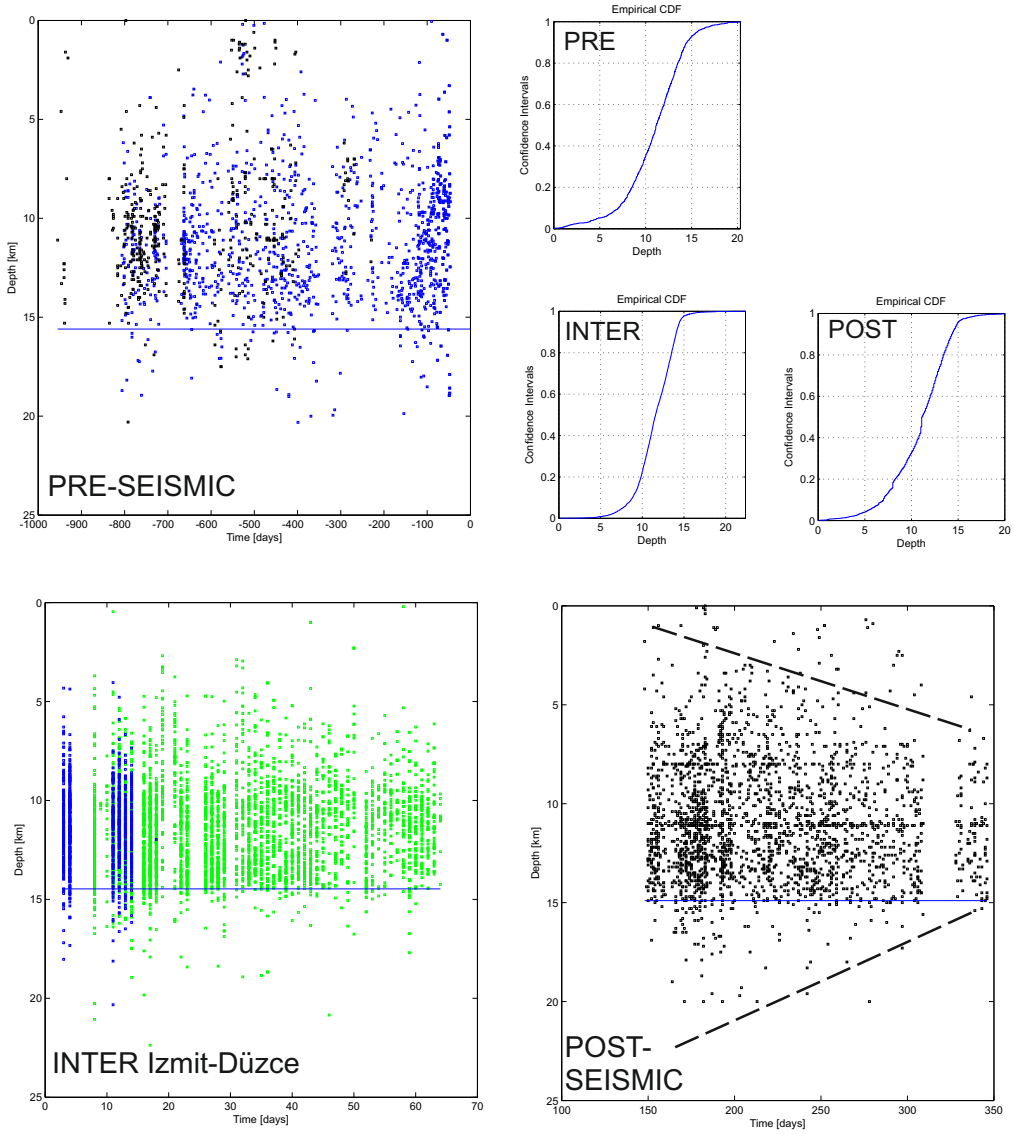

Figure 6.10.: Time-Event evolution with depth for for the preseismic preseismic, inter Izmit-Düzce and postseismic. Catalogues are color coded in black/blue - Sabonet(absolute located/ relative relocated) and green (GTF catalogue). For each time phase the calculated cumulative distribution function for the depth is plotted in the upper right corner. The blue solid line in the figures represents the local maximum depth of earthquakes after Magistrale (2002) which is often used as the seismic-aseismic transition.

the seismicity catalogue for the same effect a small but yet not significant change in the maximum hypcentral depth from the preseismic to inter Izmit-Düzce phase in the order of 1 km (from 15.5 to 14.5 km) and than a deepening during the postseismic phase on the order of 0.5 km is obtained. Since these changes on the order of one kilometer are beyond the depth-resolution capability of the catalogue it cannot be argued for or against a similar effect as observed for the Landers earthquake on the basis of this hypocenter catalogue. It is noted, however, that the limited time period following both mainshocks in this case might not be sufficient to study this effect.

Third, the here presented hypocenter catalogue confirms the clear spatial separation of Izmit aftershock clusters following the segmentation of the rupture in space and time. This segmentation was observed both coseismically in terms of rupture propagation and slip distribution (Tibi et al., 2001; Gülen et al., 2002) as well as from studying aftershock focal mechanisms (Bohnhoff et al., 2006; Ickrath et al., 2014). The most prominent aftershock activity occurs along the Akyazi Plain that represents a pull-apart structure hosting a>3 m slip deficit introduced by lateral variations of coseismic slip along the Izmit rupture (e.g. Barka et al. 2002; Aydin and Kalafat 2002). The slip deficit resulted in systematic spatiotemporal variations of the local kinematic setting in that stress rotations introduced coseismically were recovered within the first weeks following the Izmit mainshock (Bohnhoff et al., 2006; Ickrath et al., 2014). Moreover, significant non-double components in the seismic moment tensor were observed in that area that declined within the first two months following the Izmit mainshock (Stierle et al., 2014). These observations are well explained by a compensation of the coseismically introduced slip deficit through normal-faulting aftershocks until reaching again the preseismic state at seismogenic depths between 5-15 km.

Fourth, and for the first time it is noted that the Düzce mainshock drastically disturbed the Omori-type decline of aftershock activity along the Izmit rupture and basically completely reorganized the spatial occurrence of local seismicity during the time period 2-14 months following the Düzce event considered here (Fig.6.4). The spatial distribution shows a remarkable eastward shift of the seismicity in response to the eastward extension of the rupture introduced by the Düzce mainshock. Similar to the distribution of Izmit af-

tershocks the post-Düzce seismicity shows clear lateral variations in seismic activity along the rupture. In particular, it is noted that the depth distribution of seismicity below the Akyazi plain changed after the Düzce mainshock in that shallow (<10 km) seismicity was 'switched off' while deeper events continued to occur. In contrast, shallower seismicity in between the Akyazi Plain and the Düzce basin including the Karadere fault was 'switched on' by the Düzce mainshock. To this it will be referred later in the text.

The main feature of the here presented hypocenter catalogue is the identification of four seismically inactive fault patches along the Izmit-Düzce rupture extending from down to 10 km depth, i.e. covering the upper portion of the seismogenic layer. These four patches (labeled A-D in Figs. 6.3 and 6.4) extend between 10 and 50 km along the main fault branch activated during the Izmit and Düzce mainshocks, respectively.
The co- and postseismic stress changes due to the Izmit and Düzce earthquake have been studied in kinematic models using the inferred coseismic fault slip for both earthquakes (e.g. Reilinger et al. 2000, Delouis et al. 2002 and Hearn et al. 2009. In Figure 6.3 and 6.4 the distribution of co- and postseismic slip is indicated by the gray shaded areas for 75-days and 1-year time interval following the Izmit earthquake.
The four observed patches show a clear spatiotemporal variation in that two spatially separated doublets of aseismic fault patches were observed during the inter Izmit-Düzce and post-Düzce phase, respectively. Analysing the occurrence of seismically inactive fault patches a clear co-location with the maximum in postseismic deformation below the base of the brittle-ductile transition is found. In the following these four patches in relation to the local seismotectonic setting, and to the coseismic and postseismic slip distributions are discussed.

Patches A-D and local seismotectonic context: The patches A and B are located in areas where the local NAFZ fault branch is characterized by a mostly vertical strike-slip fault, whereas there is a difference in local fault trend (EW in the Sapanca area, N65°E along the Karadere fault). Both patches are separated by the Akyazi Plain as a pull-apart basin. The patches C (Karadere fault at its eastern part) and D (Düzce fault) also include vertical strike-slip faults. However, in contrast to patches A and B they are co-located

with the Akayzi and Düzce pull-apart basins. A possible explanation for a common characteristics of all four patches might be, that the stress drop occurring during the two mainshocks on the principal slip zones relaxed these vertical strike-slip faults (principal slip zones) with the result that they hosted no shallow aftershocks.

Patches A-D and coseismic slip distribution: The Izmit event and to some extent also the Düzce event are among the best studied M>7 earthquakes. This also holds for the along-fault distribution of coseismic slip that has been studied in detail (e.g. Reilinger et al. 2000; Delouis et al. 2002; Umutlu et al. 2004). For the Izmit event with an average right-lateral slip of ∼2.3 m strong variations were observed along the rupture. The main high-slip patch with slip maxima on the order of 6 m was identified along an ∼80 km long segment including the Izmit hypocenter. A second high-slip patch representing the last interval of the rupture was located at the eastern end of the rupture. The Düzce event reflects a rather symmetric slip distribution of up to 2.5 m extending to either side of the hypocenter along a ∼60 km long fault segment. While patch A covers approximately half of the western main high-slip patch of the Izmit earthquake (the other half hosting numerous shallow aftershocks), patch B is located in area of low to intermediate coseismic slip, close to the high-slip patch at the eastern end of the rupture. Patch C is located in an area where almost no coseismic slip occurred during the Düzce event, while patch D covers most of the high-slip area of the Düzce event. In summary no simple systematic relation between coseismic slip maximum and the four patches A-D extending throughout the upper half of the seismogenic layer is observed.

Patches A-D and postseismic slip distribution: Interestingly, the along-fault extension of deep postseismic slip shows a large overlap with the seismically inactive patches below the seismogenic zone at a depth of 30-40 km for the inter Izmit-Düzce time period (75 days) and for the period after the Dücze event (365 days). The slip distribution reveals two aseismic slip maximum each for both time periods indicating a heterogeneous slip distribution along strike similar to the heterogeneous aftershock activity observed in the upper crust. It is conceivable that postseismic slip is accommodated by stable frictional afterslip. However, at elevated temperatures and pressures at greater depth crystal plastic deformation and/or solution precipitation creep may also contribute to postseismic slip.

No first-order postseismic creep was observed at seismogenic depth. Hearn et al. (2002) assumed that the early postseismic phase of the Izmit earthquake is dominated by localized velocity-strengthening afterslip on the downdip extension of the coseismic rupture rather than with distributed viscous flow in the lower crust or upper mantle. However, taking into account the different models of frictional afterslip, kinematic slip inversion and viscous shear zones by Hearn et al. (2009) they assume that the deformation processes on a longer time scale suggest additional contributions of viscous flow in the lower crust and/or upper mantle.

Pucci et al. (2006, 2007) modeled slip distribution at depth obtained by different joint inversions of teleseismic, strong motion, GPS and InSAR data (e.g. Bürgmann et al. 2002; Çakir et al. 2003a). Similar to the observed aseismic patch D in figure 6.4 based on the resulting slip distribution at depth Pucci et al. (2007) observe a single, round-shaped, 10-25 km-wide, 6-8 meters maximum slip asperity located in the eastern part of the Düzce fault. Generally it was concluded that the earliest Izmit postseismic deformation was dominated by afterslip at seismogenic depths followed by an extremely rapid decaying of the postseismic transient component (Bürgmann et al., 2002; Hearn et al., 2002, 2009). In addition, a very fast initial afterslip rate was observed (Ergintav et al., 2009; Çakir et al., 2003b). Following early afterslip in the brittle part of the crust the afterslip was then transferred onto the ductile part of the crust facing a slip deficit increasing with depth due to the average coseismic displacement of 2.3 m throughout the entire brittle part of the crust along the Izmit rupture. Hearn et al. (2009) concluded that the NAFZ along the Izmit rupture has a weak velocity-strengthening rheology. The two inter Izmit-Düzce postseismic slip maximum (A' and B' in Fig. 6.3) extend for about 40-50 km along the fault. While they are clearly spatially separated, they show a clear co-location with the seismically inactive patches A and B in first order approximation taking into account the spatial resolution of the postseismic slip maximum which was estimated as 10 km at best. Iio et al. (2002) found evidence for postseismic slip or creeping along the Karadere segment and installed a dense network to monitor the aftershock activity along this segment. The authors observed that hypocenters are concentrated within a narrow depth range near the bottom of the seismogenic region in accordance with the observation in this study and together with GPS data Reilinger et al. (2000); Bürgmann et al. (2002) concluded that the

highest post-seismic slip during the first three month after the Izmit mainshock occurred beneath the Karadere segment. This afterslip could have concentrate larger stress on this fault segment and could have been the trigger for the 1999 Düzce earthquake.
A similar co-location of the patches is observed comparing the post-Düzce patches C + D (seismically inactive uppermost crust) and C'+ D' (postseismic slip maximum below the brittle-ductile transition), respectively. The pattern of patch A largely overlaps with a large area of aseismic slip around the hypocenter of the 1999 Izmit earthquake which was also observed by Bürgmann et al. (2002). This seems to be in contradiction with the common assumption that afterslip is limited to velocity strengthening zones. Interestingly, it was at this part of the Izmit rupture where an unexpected normal-faulting component and significant back-rotation in the local stress field orientation during the inter Izmit-Düzce phase has been observed (section 5.2 Ickrath et al. 2014), indicating a weak fault for this portion of the fault in accordance with the Yukutake hypothesis (section 1.1). One possible explanation for the similar pattern of patches A and D could be that the aseismic zone has migrated eastwards after the Düzce earthquake in accordance to the eastwards moving slip distribution and seismic activity along the fault rupture.

In order to further investigate the temporal extent of the here observed seismically inactive fault patches A-D, the observations are cross-checked with the long-term hypocenter catalogues derived from the regional Turkish networks of the Kandilli Observatory Earthquake Research Institute (KOERI) and the Directorate of Disaster Affairs (AFAD), respectively. Clearly, the aim of these two nation-wide networks is to detect and locate seismicity throughout the whole of Turkey to identify seismicity-prone zones and to study larger (M>3) earthquakes while the spatial (depth)resolution for smaller (M<3) events is limited by nature due to larger inter-station distances. In both of these catalogues no clear local seismically inactive patches for the uppermost 10 km could be observed along the Izmit and Düzce ruptures due to the limitation in depth resolution and thus does not allow to further constraining on the long-term existence of the seismically inactive fault patches A-D. This, however, again emphasizes the benefit of deploying dense local seismic networks to perform in-depth studies of particular fault segments during the seismic cycle which is beyond the scope of regional networks. Aktar et al. (2004) analysed spatial variation of b-value across the Izmit earthquake rupture and detected three zones

of relatively high b-values which partly coincide with asperities revealed by previous slip inversion studies. Taken into account the resolution the aseismic patches A and C from this study are accompanied by a high b-value ($b \geq 0.8$) zone. This aseismic zone that is assumed to have migrated eastwards is assumed to be a complex fractured zone due to the splitting of the NAFZ in a northern and southern branch along the Karadere and Mudurnu fault, respectively and is representing a weakened fractured zone.

Honkura et al. (2000) found correlations between large variations of the seismic velocity field and electromagnetic induction caused by the interacting of the velocity field with the static magnetic field of the Earth. Honkura et al. (2000), Tank et al. (2005) and Kaya et al. (2009) interpreted observed electrically high resistive zones of the Izmit rupture as indicators of asperity zones which are indicators for high seismic velocity zones. Kaya (2010) investigated thereby the deep crustal structure in NW Turkey along a 250 km northwest southeast profile crossing the Karadere and Mudurnu faults using magnetotelluric and electromagnetic measurements. Combined with gravity data several high conductive zone, correlating with high Bouguer anomaly values, were found along the profile. They correspond to the great Suture zones (Intra-Pontide Suture and Izmir-Ankara Suture) that are crossing the area. These suture zones were formed during plate tectonics starting in the Paleozoic. Continental fragment of the old Gondwana continent were drifting northwards and collided with the Laurasia continent (Robertson and Dixon, 1984; Robertson et al., 2013). In between a collision zone of potential partial melting processes developed. This is seen as the origin of a deep conductive zone (e.g. Gürer 1996 and Bayrak and Nalbant 2001). This is in accordance with the observation of Tank et al. (2005). They analysed two N-S profile of magnetotelluric data along the western part of the NAFZ crossing the epicentral area of the Izmit earthquake and the Adapazari-Akyazi basin, respectively. The results indicate that the hypocenters of the Izmit mainshock and aftershocks are located in a transition between a highly resistive area and a deep conductive zone (up to 50 km). They conclude that earthquakes tend to occur mostly in a high resistivity area underlain by a low resistivity zone. The low resistivity zone or conductive zone can be explained by the presence of fluids (Unsworth et al., 2000). The most favorable model for fluids in this mid-crust depth is the existence of metamorphic fluids generated by partial melting process occurring at a deeper conductor and migrating up-

wards (Tank et al., 2005). Other possible sources would be that fluids are trapped in pore space or a circulation of meteoric water. The high resistivity zone correspond to a high velocity zones with small amount of water, that is also consistent with observations from Nakamura et al. (2002) who investigated the three-dimensional P-wave velocity structure in the region of the Izmit earthquake. Tank et al. (2005) interpreted this high resistivity zone as an asperity characterized by strong coupling at the fault interface. They pointed out that these are zones for the nucleation of an earthquake when the shear stress exceeds the strength of the asperity. A similar asperity was found by Delouis et al. (2002) by waveform modeling of InSAR and teleseismic data. These observations also fit to the assumption of Koulakov et al. (2010) that strong earthquakes often occur along transition zone from high- to low-velocity patterns of a fault. In contrast, weak and moderate seismicity is assumed to be concentrated in low-velocity zones, that are underlay by highly fractured soft rocks that are not able to accumulate strong elastic energy.

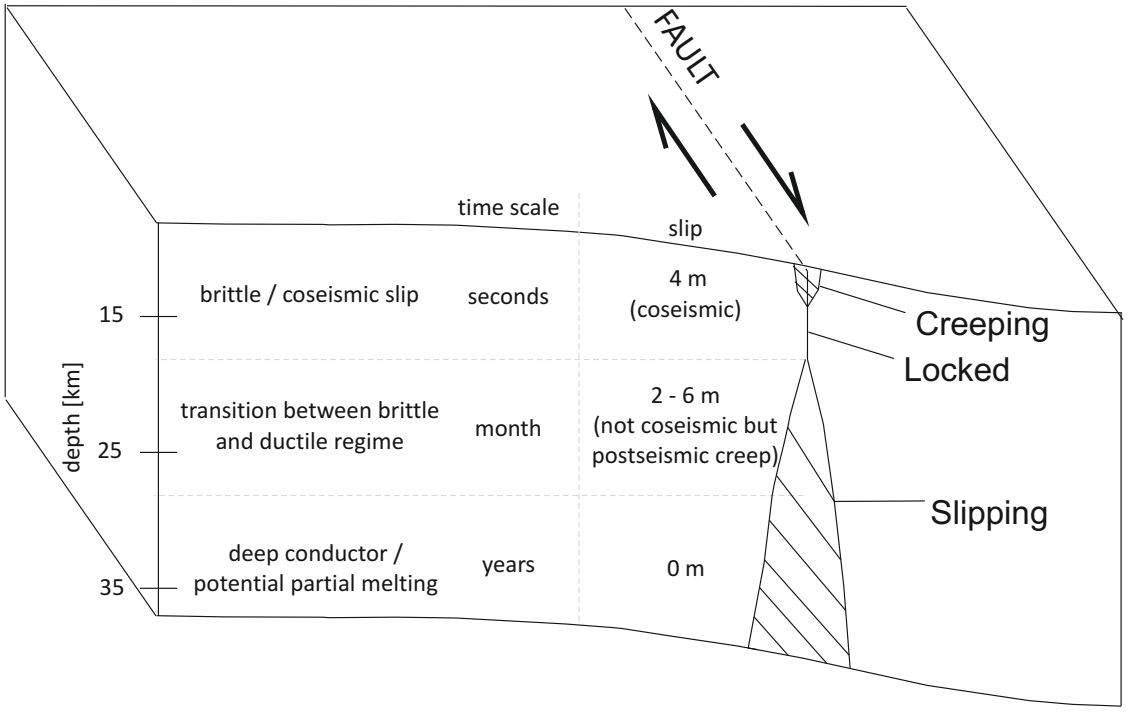

Figure 6.11.: Schematic block model for the lithosphere along the Izmit and Düzce ruptures.

Taken into account the distribution of deformation related to the Izmit and Düzce earthquakes within the crust observed in this study the processes can be systematically subdi-

vided in time and depth range. Thereby the coseismic displacement occurred throughout the entire brittle part of the crust (down to ∼18 km) and the postseismic deformation extends from the base of the seismogenic layer (brittle-ductile transition) down to the base of the crust. This aseismically deforming postseismic deformation is expected to involve crustal fluids and interestingly the maximum of the postseismic deformation are located at the edges of the deep conductor zone and potential partial melting zone in the models of Tank et al. (2005). Ague et al. (1998) investigated these partial melting zones as the reason for postseismic creeping and as a zone of potential seismic hazard since over a long time span these fluid rich region can be a trigger for an earthquake.
Also the different structures of the western and eastern part of the Düzce fault can be explained with different electrical resistivity distribution by Kaya et al. (2009) using magnetotelluric (MT) measurements for the crust and the uppermost mantle in the vicinity of the epicenter of the 1999 Düzce earthquake. Thereby they identified a higher resistive layer on the eastern side of the epicenter and at deeper parts of fault and interpreted it as a zone of high aftershock activity and high rupture velocity. These differences between the western and eastern parts of the Düzce epicenter are in accordance with the observation in this study and with other seismological studies (e.g. Bouchon et al. 2001, Pucci et al. 2006 and Bouchon and Karabulut 2008).

6.6. Summary

The unique sequence of two adjacent M>7 earthquakes occurring on adjacent fault segments allowed to observe within this study a clear spatiotemporal distribution of crustal seismicity in conjunction with co- and postseismic slip distribution on the brittle and ductile part of the crust, respectively. While the mainshocks acted as triggering events for 'switching on and off' particular fault patches in the upper half of the seismogenic layer (uppermost 10 km) there is a clear along-fault relation of these shallow seismically inactive patches with postseismic slip maximum. No such co-location is observed between the patches and maximum of coseismic slip. Incorporating the lateral variations of the local seismotectonic setting along the combined Izmit-Düzce rupture area (strike slip segments and pull-apart basins) it can be concluded that such structural features may be

responsible for along-rupture variations of co- and postseismic deformation in conjunction with strong variations in shallow (<10 km deep) aftershock activity. Analysing the cumulative distribution allows to conclude that those variations are temporal effects only and smoothed out on the long-term.

7. Conclusion and Outlook

The main focus of this study was to investigate potential spatial and temporal variations of the stress field orientation in conjunction with the 1999 Izmit and Düzce earthquakes at the North Anatolian Fault Zone (NAFZ) in NW Turkey. The occurrence of the two $M > 7$ large earthquakes in rapid succession gave thereby the unique opportunity to analyse a short "interseismic phase" between them, i.e. the 87 day long time interval after the Izmit and before the Düzce earthquake.

Therefore in a first step a compilation of focal mechanism (FM) data and high-resolution local seismic recordings covering the inter Izmit-Düzce phase were inverted for the stress tensor. Systematic temporal variations of the local stress field orientation were analysed to find distinct seismotectonic features and variations of co-seismic slip along distinct segments of the Izmit 1999 rupture with unprecedented detail.

In a second step (see section 5.3) a significantly enlarged eventdatabase was used to investigate the stress field evolution in greater detail inverting first-motion polarities from local seismicity also before and after the Izmit and Düzce earthquakes.

In a last step, the obtained hypocenter catalogs from the two 1999 mainshocks between 1997 and 2001 consisting of >10.000 events were used to investigate seismic activity of patches along the NAFZ and to identify possible creeping and locked fault patches in relation to co- and postseismic deformation below the seismogenic part of the crust. Thereby the hypocenter catalogue processed and used here, is the first catalogue obtained from a local seismic network which allows a reliable hypocenter determination with precision in lateral and vertical directions on the order of 2-3 km and covering the entire time interval from more than two years prior to the Izmit earthquake to 14 months after the Düzce earthquake.

Results obtained in this study reveal systematic spatial and temporal variation of the crustal stress field orientation along the Izmit 1999 rupture and especially lead to the awareness of a short-term change in the regional strike-slip stress field towards EW-extensional normal faulting along local pull-apart structures (Akyazi Plain and Dücze

Basin) and a fast recovery to the preseismic regional strike-slip regime. In summary, the stress field evolution of the studied segments along the Izmit and Düzce rupture can be followed from the predominantly preseismic strike-slip regime in the west, the inter Izmit-Düzce phase of the dominant E-W extensional regime in the Akyazi plain to the nearly stable post-seismic strike-slip regime along the Düzce and Elmalik faults corresponding to the regional stress field. The different orientations of the stress field in these segments are interpreted with respect to postseismic displacements observed along the Izmit and Düzce rupture and maintain a good correlation between the postseismic slip and the stress field orientation. Thereby no variation between the background stress field prior to the 1999 Izmit event and the post-seismic setting following the two-month aftershock period (2000-2007) is observed indicating that the stress field rapidly recovers from a large earthquake as the aftershock rate decreases which favors the stress recovery model proposed first by Michael (1987). Smith and Dieterich (2010) hypothesized that possible stress rotations caused by large earthquakes may be artifacts from the binning of different spatial clusters in a heterogeneous stress field. Hardebeck (2010) contradict with the example of the Landers earthquake and also with this study the existence of stress field rotations can be confirmed. The binning is of course crucial and it is off special interest to perform a analysis of seismicity cluster or spatial distribution test before the stress tensor inversion. Within this study all together four different stress inversion algorithms were used which all resolved significant stress rotation caused by the Izmit mainshock on a spatial and temporal scale. Taking this into account, this study could rule out possible doubts regarding the existence of stress field rotations and gives new facts for the contribution to the ongoing discussion whether or not local stress field rotations are a useful indicator for the loading status of individual fault segments during the seismic cycle.
More precisely, it was possible with this study to provide new information about the evolution of the stress field related to large earthquakes and to characterize the physical status of individual fault segments along a fault zone during the seismic cycle. The observations confirm that shear failure and the associated drop in shear stress during large earthquakes results in a rotation of the principal stresses acting on the fault along distinct patches and in accordance with lateral variations of co-seismic slip.

In addition, the unique sequence of two M>7 earthquakes occurring on adjacent fault

segments allowed to observe within this study a clear spatiotemporal distribution of crustal seismicity in conjunction with co- and postseismic slip distribution on the brittle and ductile part of the crust, respectively. While the mainshocks acted as triggering events for 'switching on and off' particular fault patches in the upper half of the seismogenic layer (uppermost 10 km) there is a clear along-fault relation of these shallow seismically inactive patches with postseismic slip maxima. No such co-location is observed between the patches and maxima of coseismic slip. Incorporating the lateral variations of the local seismotectonic setting along the combined Izmit-Düzce rupture area (strike slip segments and pull-apart basins) it can be concluded that such structural features may be responsible for along-rupture variations of co- and postseismic deformation in conjunction with strong variations in shallow (<10 km depth) aftershock activity. The observation of large patches of aseismic slip along the fault are in contradiction with the common assumption that afterslip is limited to velocity strengthening zones. These observation could be also confirm by the stress inversion results from this study for the Izmit Sapanca fault where a unexpected NF-component and significant rotation of the stress field orientation in the coseismic phase has been observed. This would support the assumption that the NAFZ in the Izmit and Düzce area is of a weak velocity strengthening rheology which leads to a possible weak fault in a strong crust. Within the last analysis of the study a detailed analysis of shallow earthquakes along the Düzce rupture zone gives new insights in the depth-evolution of this segment of the fault. Finally, in a last step the observation from this study were started to combined with electromagnetics and magnetotelluric observation to investigate the correlation between high resistivity zones, high velocity zones and the occurrence of earthquake. Thereby potential partial melting zones could be identified as reason for postseismic creeping and as a zone of potential seismic hazard since over a long time span these fluid rich region can be a trigger for an earthquake.

For future work, although this catalogue presented here consists of all together over 10000 mostly relocated events from different datasets for a time period of four year, it is suggested to enlarge this database in a temporal matter. A suggestion for future studies is to investigate for example the depth evolution during the seismic cycle with respect on the rheology of the fault. The time-dependent depth distribution of aftershocks observed by Rolandone et al. (2004) could lead to a better understanding of the brittle and viscous

transitions within the crust. Another idea is to enlarge this study to the western part of the Izmit rupture and investigate especially the stress field in the Eastern Sea of Marmara. Till now the database was to sparse to analyse this area which represents a more than 100 km long seismic gap that did not rupture since 1766 (Toksöz et al., 1979; Stein et al., 1997; Janssen et al., 2009) and which is seen as a possible nucleation for an hazardous M>7 earthquake in the vicinity of the mega-city Istanbul.

To conclude, this study again emphasizes the benefit of deploying dense local seismic networks to perform in-depth studies of particular fault segments during the seismic cycle which is beyond the scope of regional networks. The used procedure in this study of detailed investigation of spatial and temporal evolution of the stress field can also by used for studying other areas like subduction zones. Finally, this study proves that studies of crustal stress and its spatial and temporal variation are crucial for the understanding of earthquake mechanics, tectonic loading, and earthquake stress interactions.

Bibliography

Abers, G. A. and Gephart, J. W. (2001). Direct inversion of earthquake first motions for both the stress tensor and focal mechanisms and application to Southern California. *Journal of Geophysical Research*, 106, 26(B11):523–26,540.

Ague, J., Park, J., and Rye, D. (1998). Regional metamorphic dehydration and seismic hazard. *Geophysical Research Letters*, 25(22):4221–4224.

Aktar, M., Özalaybey, S., Ergin, M., Karabulut, H., Bouin, M.-P., Tapırdamaz, C., Biçmen, F., Yörük, A., and Bouchon, M. (2004). Spatial variation of aftershock activity across the rupture zone of the 17 August 1999 Izmit earthquake, Turkey. *Tectonophysics*, 391(1):325–334.

Akyuz, H., Barka, A., Altunel, E., Hartleb, R., and Sunal, G. (2000). *Field observations and slip distribution of the November 12, 1999 Düzce earthquake (M 7.1)*. The 1999 Izmit and Düzce Earthquakes: Preliminary Results, Istanbul Tech. Univ., Istanbul, Turkey.

Akyüz, H., Hartleb, R., Barka, A., Altunel, E., Sunal, G., Meyer, B., and Armijo, R. (2002). Surface rupture and slip distribution of the 12 November 1999 Düzce earthquake (M 7.1), North Anatolian Fault, Bolu, Turkey. *Bulletin of the Seismological Society of America*, 92(1):61–66.

Allaby, A. and Allaby, M. (1999). "depocentre.". *A Dictionary of Earth Sciences*, Retrieved April 16, 2014 from Encyclopedia.com.

Altunel, E., Meghraoui, M., Akyüz, H. S., and Dikbas, A. (2004). Characteristics of the 1912 co-seismic rupture along the North Anatolian Fault Zone (Turkey) implications for the expected Marmara earthquake. *Terra Nova*, 16(4):198–204.

Ambraseys, N. (1970). Some characteristic features of the Anatolian fault zone. *Tectonophysics*, 9(2):143–165.

Ambraseys, N. (2002). The seismic activity of the Marmara Sea region over the last 2000 years. *Bulletin of the Seismological Society of America*, 92(1):1–18.

Ambraseys, N. N. and Zatopek, A. (1969). The Mudurnu Valley, West Anatolia, Turkey, earthquake of 22 July 1967. *Bulletin of the Seismological Society of America*, 59(2):521–589.

Angelier, J. (1979). Determination of the mean principal directions of stresses for a given fault population. *Tectonophysics*, 56(3-4):T17–T26.

Angelier, J. (1984). Tectonic analysis of fault slip data sets. *Journal of Geophysical Research*, 89(B7):5835–5848.

Angelier, J. (2002). Inversion of earthquake focal mechanisms to obtain the seismotectonic stress IV - a new method free of choice among nodal planes. *Geophysical Journal International*, 150(3):588–609.

Ardel, A. (1965). Anadolu havzalarinin tesekkül ve tekâmülü hakkında düsünceler. *Istanbul Univ. Cograf. Enst. Derg*, 8(15):60–73.

Armijo, R., Meyer, B., Hubert, A., and Barka, A. (1999). Westward propagation of the North Anatolian fault into the northern Aegean: Timing and kinematics. *Geology*, 27(3):267–270.

Armijo, R., Meyer, B., Navarro, S., King, G., and Barka, A. (2002). Asymmetric slip partitioning in the Sea of Marmara pull-apart: a clue to propagation processes of the North Anatolian Fault? *Terra Nova*, 14(2):80–86.

Armijo, R., Pondard, N., Meyer, B., Uçarkus, G., de Lépinay, B. M., Malavieille, J., Dominguez, S., Gustcher, M. A., Schmidt, S., and Beck, C. (2005). Submarine fault scarps in the Sea of Marmara pull-apart (North Anatolian Fault): Implications for seismic hazard in Istanbul. *Geochemistry Geophysics Geosystems*, 6(6):Q06009.

Arnold, R. and Townend, J. (2007). A Bayesian approach to estimating tectonic stress from seismological data. *Geophysical Journal International*, 170(3):1336–1356.

Aydin, A. and Kalafat, D. (2002). Surface ruptures of the 17 August and 12 November 1999 Izmit and Düzce earthquakes in northwestern Anatolia, Turkey: their tectonic and kinematic significance and the associated damage. *Bulletin of the Seismological Society of America*, 92(1):95–106.

Balfour, N., Savage, M., and Townend, J. (2005). Stress and crustal anisotropy in Marlborough, New Zealand: Evidence for low fault strength and structure-controlled anisotropy. *Geophysical Journal International*, 163(3):1073–1086.

Barka, A. (1992). The North Anatolian Fault Zone. In *Annales Tectonicae*, volume 6, pages 164–195.

Barka, A. (1996). Slip distribution along the North Anatolian fault associated with the large earthquakes of the period 1939 to 1967. *Bulletin of the Seismological Society of America*, 86(5):1238.

Barka, A. (1999). The 17 august 1999 Izmit earthquake. *Science*, 285(5435):1858–1859.

Barka, A. (2000). *The 1999 Izmit and Düzce Earthquakes: Preliminary Results*. Istanbul Technical University.

Barka, A., Akyüz, H., Altunel, E., Sunal, G., Cakir, Z., Dikbas, A., Yerli, B., Armijo, R., Meyer, B., de Chabalier, J., Rockwell, T., Dolan, J., Hartleb, R., Dawson, T., Christofferson, S., Tucker, A., Fumal, T., Langridge, R., Stenner, H., Lettis, W., Bachhuber, J., and Page, W. (2002). The Surface Rupture and Slip Distribution of the 17 August 1999 Izmit Earthquake (M7.4), North Anatolian Fault. *Bulletin of the Seismological Society of America*, 92(1):43–60.

Barka, A. and Kadinsky-Cade, K. (1988). Strike-slip fault geometry in Turkey and its influence on earthquake activity. *Tectonics*, 7(3):663–684.

Barka, A. A. and Hancock, P. L. (1984). Neotectonic deformation patterns in the convex-northwards arc of the North Anatolian fault zone. *Geological Society, London, Special Publications*, 17(1):763–774.

Barth, A., Reinecker, J., and Heidbach, O. (2008). Stress derivation from earthquake

focal mechanisms. Technical report, World Stress Map Project (http://www.world-stress-map.org).

Baumbach, M., Bindi, D., Grosser, H., Milkereit, C., Parolai, S., Wang, R., Karakisa, S., Zünbül, S., and Zschau, J. (2003). Calibration of an ML scale in northwestern Turkey from 1999 Izmit aftershocks. *Bulletin of the Seismological Society of America*, 93(5):2289–2295.

Bayrak, M. and Nalbant, S. (2001). Conductive crust imaged in western Turkey by MT. *Geophysical research letters*, 28(18):3521–3524.

Bellier, O., Över, S., Poisson, A., and Andrieux, J. (1997). Recent temporal change in the stress state and modern stress field along the North Anatolian Fault Zone (Turkey). *Geophysical Journal International*, 131(1):61–86.

Bellier, O. and Zoback, M. L. (1995). Recent state of stress change in the Walker Lane zone, western Basin and Range province, United States. *Tectonics*, 14(3):564–593.

Bilgin, T. (1984). Alluvial morphology and geomorphologic development in Quaternary of the Adapazarı Basin and the Sapanca Corridor. *Bull. Univ. Istanbul*, 2572:1–199.

Bindi, D., Parolai, S., Gorgun, E., Grosser, H., Milkereit, C., Bohnhoff, M., and Durukal, E. (2007). ML scale in northwestern Turkey from 1999 Izmit Aftershocks: Updates, journal = Bulletin of the Seismological Society of America. 97(1B):331.

Bohnhoff, M., Baisch, S., and Harjes, H. P. (2004). Fault mechanisms of induced seismicity at the superdeep German Continental Deep Drilling Program (KTB) borehole and their relation to fault structure and stress field. *Journal of Geophysical Research*, 109:B02309.

Bohnhoff, M., Bulut, F., Dresen, G., Malin, P. E., Eken, T., and Aktar, M. (2013). An earthquake gap south of Istanbul. *Nature communications*, 4.

Bohnhoff, M., Bulut, F., Gorgün, E., Milkereit, C., and Dresen, G. (2008). Seismotectonic setting at the North Anatolian Fault Zone after the 1999 Mw= 7.4 Izmit earthquake based on high-resolution aftershock locations. *Advances in Geosciences*, 14:85–92.

Bohnhoff, M., Grosser, H., and Dresen, G. (2006). Strain partitioning and stress rotation at the North Anatolian fault zone from aftershock focal mechanisms of the 1999 Izmit Mw= 7.4 earthquake, journal = Geophysical Journal International. 166(1):373–385.

Bott, M. H. P. (1959). The mechanics of oblique slip faulting. *Geological Magazine*, 96(02):109–117.

Bouchon, M., Bouin, M.-P., Karabulut, H., Toksöz, M. N., Dietrich, M., and Rosakis, A. J. (2001). How fast is rupture during an earthquake? New insights from the 1999 Turkey earthquakes. *Geophysical Research Letters*, 28(14):2723–2726.

Bouchon, M. and Karabulut, H. (2008). The aftershock signature of supershear earthquakes. *Science*, 320(5881):1323–1325.

Bouchon, M., Töksöv, M., Karabulut, H., Bouin, M.-P., Dietrich, M., Aktar, M., and Edie, M. (2002). Space and Time Evolution of Rupture and faulting during the 1999 Izmit (Turkey) Earthquake. *Bulletin of the Seismological Society of America*, 92(1):256–266.

Bürgmann, R., Ergintav, S., Segall, P., Hearn, E., McClusky, S., Reilinger, R., Woith, H., and Zschau, J. (2002). Time-Dependent Distributed Afterslip on and Deep below the Izmit Earthquake Rupture. *Bulletin of the Seismological Society of America*, 92, 1:126–137.

Bulut, F. and Aktar, M. (2007). Accurate relocation of Izmit earthquake (Mw = 7.4, 1999) aftershocks in Çinarcik Basin using double difference method. *Geophysical Research Letters*, 34(10):L10307.

Bulut, F., Bohnhoff, M., Aktar, M., and Dresen, G. (2007). Characterization of aftershock-fault plane orientations of the 1999 Izmit (Turkey) earthquake using high-resolution aftershock locations. *Geophysical Research Letters*, 34(20):L20306.

Bulut, F., Bohnhoff, M., Ellsworth, W., Aktar, M., and Dresen, G. (2009). Microseismicity at the North Anatolian Fault in the Sea of Marmara offshore Istanbul, NW Turkey. *Journal of Geophysical Research*, 114:1–16.

Bürgmann, R. and Dresen, G. (2008). Rheology of the lower crust and upper mantle:

Evidence from rock mechanics, geodesy, and field observations. *Annual Review of Earth and Planetary Sciences*, 36(1):531.

Byerlee, J. (1978). Friction of rocks. *Pure and applied Geophysics*, 116(4-5):615–626.

Çakir, Z., Barka, A. A., De Chabalier, J. B., Armijo, R., and Meyer, B. (2003a). Kinematics of the November 12, 1999 (Mw= 7.2) Düzce earthquake deduced from SAR interferometry. *Turkish Journal of Earth Sciences*, 12(1):105–118.

Çakir, Z., Chabalier, J.-B. d., Armijo, R., Meyer, B., Barka, A., and Peltzer, G. (2003b). Coseismic and early post-seismic slip associated with the 1999 Izmit earthquake (Turkey), from SAR interferometry and tectonic field observations. *Geophysical Journal International*, 155(1):93–110.

Carey, E. and Brunier, B. (1974). Analyse théorique et numérique d'un modèle mécanique élémentaire aplliqué à l'étude d'une population de failles. *C.R. Acad. Sci., Paris*, 179:891–894.

Coulomb, C. (1776). Essai sur une application de maximis et minimis à quelques problèmes de statique, relatifs à l'Architecture. *Mèmoires de Mathématique et de Physique présentés à l'Académie Royale des Sciences, par divers Savans, et lûs dans les Assemblées– Année 1773.*

Delouis, B., Giardini, D., Lundgren, P., and Salichon, J. (2002). Joint inversion of InSAR, GPS, teleseismic, and strong-motion data for the spatial and temporal distribution of earthquake slip: Application to the 1999 Izmit mainshock. *Bulletin of the Seismological Society of America*, 92(1):278–299.

DeMets, C. (2007). Earthquake and the Seismic Cycle. Lecture Material of Mountains and Moving Plates.

Dieterich, J. (1994). A constitutive law for rate of earthquake production and its application to earthquake clustering. *Journal of Geophysical Research: Solid Earth (1978–2012)*, 99(B2):2601–2618.

Dieterich, J. H. (1979). Modeling of rock friction: 1. Experimental results and constitutive

equations. *Journal of Geophysical Research: Solid Earth (1978–2012)*, 84(B5):2161–2168.

Dikibaş, A. and Akyüz, H. S. (2011). Palaeoseismological Investigations on the Karadere Segment, North Anatolian Fault Zone, Turkey. *Turkish Journal of Earth Sciences*, 20(4):395–410.

Duman, T., Awata, Y., Yoshioka, T., Emre, O., Dogan, A., and Ozalp, S. (2003). Detailed maps and inventories of the 1999 Izmit surface rupture. In Emre, Ö., Awate, Y., and Duman, T., editors, *Surface Rupture Associated with the 17 August 1999 Izmit Earthquake*, volume 1, pages 51–55. General Directorate of Mineral Research & Exploration, Special Publications.

Duman, T. Y., Emre, O., Dogan, A., and Ozalp, S. (2005). Step-over and bend structures along the 1999 Düzce earthquake surface rupture, North Anatolian fault, Turkey. *Bulletin of the Seismological Society of America*, 95(4):1250–1262.

Efron, B. and Tibshirani, R. (1986). Bootstrap methods for standard errors, confidence intervals, and other measures of statistical accuracy. *Statistical science*, pages 54–75.

Efron, B. and Tibshirani, R. J. (1994). *An introduction to the bootstrap*, volume 57. CRC press.

Egeran, N. and Lahn, E. (1944). Note sur la carte sismique de la Turquie au 1/2,400,000. *MTA Mecmuasi*, 2:32.

Emre, Ö., Awata, Y., and Duman, T. (2003). Surface rupture associated with the 17 August 1999 Izmit earthquake. *General Directorate of Mineral Research and Exploration, Ankara, Turkey, ISBN*, VII:975–6595.

Ergintav, S., Bürgmann, R., McClusky, S., Çakmak, R., Reilinger, R. E., Lenk, O., Barka, A., and Özener, H. (2002). Postseismic deformation near the Izmit earthquake (17 August 1999, M 7.5) rupture zone. *Bulletin of the Seismological Society of America*, 92:194–207.

Ergintav, S., McClusky, S., Hearn, E., Reilinger, R., Cakmak, R., Herring, T., Ozener, H., Lenk, O., and Tari, E. (2009). Seven years of postseismic deformation following

the 1999, M= 7.4 and M= 7.2, Izmit-Düzce, Turkey earthquake sequence. *Journal of Geophysical Research: Solid Earth (1978–2012)*, 114(B7).

Farr, T. G., Rosen, P. A., Caro, E., Crippen, R., Duren, R., Hensley, S., Kobrick, M., Paller, M., Rodriguez, E., Roth, L., et al. (2007). The shuttle radar topography mission. *Reviews of geophysics*, 45(2).

Flerit, F., Armijo, R., King, G., and Meyer, B. (2004). The mechanical interaction between the propagating North Anatolian Fault and the back-arc extension in the Aegean. *Earth and Planetary Science Letters*, 224(3-4):347–362.

Fraser, J., Vanneste, K., and Hubert-Ferrari, A. (2010). Recent behavior of the North Anatolian Fault: Insights from an integrated paleoseismological data set. *Journal of Geophysical Research: Solid Earth (1978–2012)*, 115(B9).

Frohlich, C. (2001). Display and quantitative assessment of distributions of earthquake focal mechanisms. *Geophysical Journal International*, 144(2):300–308.

Gephart, J. W. (1990). Stress and the direction of slip on fault planes. *Tectonics*, 9(4):845–858.

Gephart, J. W. and Forsyth, D. W. (1984). An improved method for determining the regional stress tensor using earthquake focal mechanism data: application to the San Fernando earthquake sequence. *Journal of Geophysical Research*, 89(B11):9305–9320.

Ghimire, S., Katsumata, K., and Kasahara, M. (2005). Temporal changes in state of stress in the Tokachi Oki area after the 2003 Tokachi Oki Earthquake. *Earth, Planets, and Space*, 57(2):83–91.

Gilbert, G. K. (1909). Earthquake Forecasts Introduction. *Science*, 29(734):121–138.

Greber, E. (1970). Stratigraphic evolution and tectonics in an area of high seismicity: Akyazı/Adapazarı (Pontides, Northwestern Turkey). *Turkish Journal of Earth Sciences*, 5(2):63–79.

Greber, E. (1994). Deep circulation of CO^2-rich paleowaters in a seismically active zone (Kuzuluk/Adapazari, northwestern Turkey). *Geothermics*, 23(2):151–174.

Greber, E. (1997). Stratigraphic evolution and tectonics in an area of high seismicity: Akyazi/Adapazan (Pontides, Northwestern Turkey). In *Active Tectonics of Northwestern Anatolia: The Marmara Poly-Project: a Multidisciplinary Approach by Space-geodesy, Geology, Hydrogeology, Geothermics and Seismology*, page 141. vdf Hochschulverlag AG.

Görgün, E., Bohnhoff, M., Bulut, F., and Dresen, G. (2010). Seismotectonic setting of the Karadere-Düzce branch of the North Anatolian Fault Zone between the 1999 Izmit and Düzce ruptures from analysis of Izmit aftershock focal mechanisms. *Tectonophysics*, 482:170–181.

Görgün, E., Zang, A., Bohnhoff, M., Milkereit, C., and Dresen, G. (2009). Analysis of Izmit aftershocks 25 days before the November 12th 1999 Düzce earthquake, Turkey. *Tectonophysics*, 474(3-4):507–515.

Grosser, H., Baumbach, M. R. G., Berckhemer, H., Baier, B., Karahan, A., Schelle, H., Krüger, F., Paulat, A., Michel, G., Demirtas, R., et al. (1998). The Erzincan (Turkey) earthquake (Ms 6.8) of March 13, 1992 and its aftershock sequence. *pure and applied geophysics*, 152(3):465–505.

Gülen, L., Pinar, A., Kalafat, D., Özel, N., Horasan, G., Yilmazer, M., and Işikara, A. M. (2002). Surface fault breaks, aftershock distribution, and rupture process of the 17 August 1999 Izmit, Turkey, earthquake. *Bulletin of the Seismological Society of America*, 92(1):230–244.

Gürer, A. (1996). Deep conductivity structure of the north Anatolian Fault Zone and the Istanbul and Sakarya Zones along the Gölpazari-Akcaova profile, northwest Anatolia. *International Geology Review*, 38(8):727–736.

Handin, J. (1969). On the Coulomb-Mohr failure criterion, journal = Journal of Geophysical Research. 74(22):5343–5348.

Hardebeck, J. (2012). Coseismic and postseismic stress rotations due to great subduction zone earthquakes. *Geophysical Research Letters*, 39:L21312.

Hardebeck, J. L. (2010). Seismotectonics and Fault Structure of the California Central Coast. *Bulletin of the Seismological Society of America*, 100(3):1031.

Hardebeck, J. L. and Hauksson, E. (2000). The San Andreas Fault in Southern California: A weak fault in a weak crust. In *Proc., 3rd Conf. on Tectonic Problems of the San Andreas Fault System.*

Hardebeck, J. L. and Hauksson, E. (2001a). Crustal stress field in southern California and its implications for fault mechanics. *Journal of Geophysical Research*, 106(B10):21859.

Hardebeck, J. L. and Hauksson, E. (2001b). Stress orientations obtained from earthquake focal mechanisms: what are appropriate uncertainty estimates? *Bulletin of the Seismological Society of America*, 91(2):250.

Hardebeck, J. L. and Michael, A. J. (2006). Damped regional-scale stress inversions: methodology and examples for southern California and the Coalinga aftershock sequence. *Journal of Geophysical Research*, 111(B11):B11310.

Harris, R. A. and Day, S. M. (1993). Dynamics of fault interaction: Parallel strike-slip faults. *Journal of Geophysical Research: Solid Earth (1978–2012)*, 98(B3):4461–4472.

Harris, R. A. and Day, S. M. (1999). Dynamic 3D simulations of earthquakes on en echelon faults. *Geophysical Research Letters*, 26(14):2089–2092.

Hartleb, R. D., Dolan, J. F., Akyüz, H. S., Dawson, T. E., Tucker, A. Z., Yerli, B., Rockwell, T. K., Toraman, E., Çakir, Z., Dikbaş, A., et al. (2002). Surface rupture and slip distribution along the Karadere segment of the 17 August 1999 Izmit and the western section of the 12 November 1999 Düzce, Turkey, earthquakes. *Bulletin of the Seismological Society of America*, 92(1):67–78.

Hasegawa, A., Yoshida, K., and Okada, T. (2011). Nearly complete stress drop in the 2011 Mw 9.0 off the Pacific coast of Tohoku earthquake. *Earth Planets Space*, 63:703–707.

Hauksson, E. (1994). State of stress from focal mechanisms before and after the 1992 Landers earthquake sequence. *Bulletin of the Seismological Society of America*, 84(3):917.

Hauksson, E. and Jones, L. (1988). The July 1986 Oceanside (ML = 5.3) earthquake sequence in the Continental Borderland, Southern California. *Bulletin of the Seismological Society of America*, 78:1885–1906.

Havskov, J. and Ottemoller, L. (2010). *Routine data processing in earthquake seismology*. Springer.

Havskov, J., Ottemöller, L., Trnkoczy, A., and Bormann, P. (2002). Seismic Networks. In *IASPEI: New Manual of Seismological Observatory Practice (NMSOP)*. Bormann, Peter.

Hearn, E., McClusky, S., Ergintav, S., and Reilinger, R. (2009). Izmit earthquake postseismic deformation and dynamics of the North Anatolian Fault Zone. *Journal of Geophysical Research: Solid Earth (1978–2012)*, 114(B8).

Hearn, E. H., Bürgmann, R., and Reilinger, R. E. (2002). Dynamics of Izmit earthquake postseismic deformation and loading of the Düzce earthquake hypocenter. *Bulletin of the Seismological Society of America*, 92(1):172–193.

Heidbach, O., Tingay, M., Barth, A., Reinecker, J., Kurfeß, D., and Müller, B. (2008). The world stress map database release 2008, doi: 10.1594/GFZ. *WSM. Rel2008*.

Helmstetter, A. and Shaw, B. E. (2009). Afterslip and aftershocks in the rate-and-state friction law. *Journal of Geophysical Research: Solid Earth*, 114(B1):B01308–1.

Honkura, Y., Isikara, A., Oshiman, N., Ito, A., Uçer, B., Baris, S., Tunçer, M., Matsushima, M., Pektas, R., Celik, C., et al. (2000). Preliminary results of multidisciplinary observations before, during and after the Kocaeli (Izmit) earthquake in the western part of the North Anatolian Fault Zone. *Earth Planets and Space*, 52(4):293–298.

Horiuchi, S., Rocco, G., and Hasegawa, A. (1995). Discrimination of fault planes from auxiliary planes based on simultaneous determination of stress tensor and a large number of fault plane solutions. *Journal of Geophysical Research: Solid Earth (1978–2012)*, 100(B5):8327–8338.

Hubert-Ferrari, A., Barka, A., Jacques, E., Nalbant, S. S., Meyer, B., Armijo, R., Tapponnier, P., and King, G. C. (2000). Seismic hazard in the Marmara Sea region following the 17 August 1999 Izmit earthquake. *Nature*, 404(6775):269–273.

Hurd, O. and Bohnhoff, M. (2012). Stress-and Structure-Induced Shear-Wave Anisotropy along the 1999 Izmit Rupture, Northwest Turkey. *Bulletin of the Seismological Society of America*, 102(5):2177–2188.

Ickrath, M., Bohnhoff, M., Bulut, F., and Dresen, G. (2014). Stress rotation and recovery in conjunction with the 1999 Izmit Mw 7.4 earthquake. *Geophysical Journal International*, 196(2):951–956.

Iio, Y., Horiuchi, S., Bariş, Ş., Celik, C., Kyomen, J., Üçer, B., Honkura, Y., and Işikara, A. M. (2002). Aftershock distribution in the eastern part of the aftershock region of the 1999 Izmit, Turkey, earthquake. *Bulletin of the Seismological Society of America*, 92(1):411–417.

Janssen, C., Bohnhoff, M., Vapnik, Y., Görgün, E., Bulut, F., Plessen, B., Pohl, D., Aktar, M., Okay, A. I., and Dresen, G. (2009). Tectonic evolution of the Ganos segment of the North Anatolian Fault (NW Turkey). *Journal of Structural Geology*, 31(1):11–28.

Karahan, A., Berckhemer, H., and Baier, B. (2001). Crustal structure at the western end of the North Anatolian Fault Zone from deep seismic sounding. *Annals of Geophysics*, 44(1).

Kasahara, K. (1981). *Earthquake mechanics*, volume 139. Cambridge University Press Cambridge.

Kaya, C. (2010). Deep Crustal Structure of Northwestern part of Turkey. *Tectonophysics*, 489:227–239.

Kaya, T., Tank, S. B., Tunçer, M. K., Rokoityansky, I. I., Tolak, E., Savchenko, T., et al. (2009). Asperity along the North Anatolian Fault imaged by magnetotellurics at Düzce, Turkey. *Earth Planets and Space (EPS)*, 61(7):871.

Ketin, I. (1948). Über die tektonisch-mechanischen Folgerungen aus den grossen anatolischen Erdbeben des letzten Dezenniums. *Geologische Rundschau*, 36(1):77–83.

Ketin, I. (1969). Über die nordanatolische Horizontalverschiebung. *Bull. Min. Res. Explor. Inst. Turkey*, 72:1–28.

Ketin, I. and Roesli, F. (1953). Makroseismische Untersuchungen über das Nordwest Anatolische Beben vom 18 März 1953. *Eelogae Geol. Helvetiae*, 46:187–208.

King, G., Stein, R., and Lin, J. (1994). Static stress changes and the triggering of earthquakes. *Bulletin of the Seismological ...*, 84(3):935–953.

King, G. C., Hubert-Ferrari, A., Nalbant, S. S., Meyer, B., Armijo, R., and Bowman, D. (2001). Coulomb interactions and the 17 August 1999 Izmit, Turkey earthquake. *Comptes Rendus de l'Académie des Sciences-Series IIA-Earth and Planetary Science*, 333(9):557–569.

Kiratzi, A. A. (2002). Stress tensor inversions along the westernmost North Anatolian Fault Zone and its continuation into the North Aegean Sea. *Geophysical Journal International*, 151(2):360–376.

Koçyiğit, A., Yılmaz, A., Adamia, S., and Kuloshvili, S. (2001). Neotectonics of East Anatolian Plateau (Turkey) and Lesser Caucasus: implication for transition from thrusting to strike-slip faulting. *Geodinamica Acta*, 14(1):177–195.

Koulakov, I., Bindi, D., Parolai, S., Grosser, H., and Milkereit, C. (2010). Distribution of seismic velocities and attenuation in the crust beneath the North Anatolian Fault (Turkey) from local earthquake tomography. *Bulletin of the Seismological Society of America*, 100(1):207–224.

Lahn, E. (1949). Seismological investigations in Turkey. *Bulletin of the Seismological Society of America*, 39(2):67–71.

Langridge, R., Stenner, H., Fumal, T., Christofferson, S., Rockwell, T., Hartleb, R., Bachhuber, J., and Barka, A. (2002). Geometry, slip distribution, and kinematics of surface rupture on the Sakarya fault segment during the 17 August 1999 Izmit, Turkey, earthquake. *Bulletin of the Seismological Society of America*, 92(1):107–125.

Le Pichon, X., Chamot-Rooke, N., Rangin, C., and Sengör, A. (2003). The North Anatolian fault in the Sea of Marmara. *Journal of Geophysical Research: Solid Earth (1978–2012)*, 108(B4).

Le Pichon, X., Taymaz, T., and Sengör, A. (1999). The Marmara Fault and the future Istanbul earthquake. In *International conference on the Kocaeli earthquake*, volume 17, pages 41–54.

Lee, W. and Lahr, J. (1972). HYPO-71 a computer program for determining hypocenter, magnitude and first motion pattern of local earthquakes, Open-File Report. *US Geol. Surv., Menlo Park, Calif.*

Lettis, W., Bachhuber, J., Barka, A., Brankman, C., Lettis, W., Somerville, P., and Witter, R. (2000). Geology and Seismicity. *Earthquake Spectra*, 16(S1):1–9.

Lettis, W., Bachhuber, J., Witter, R., Brankman, C., Randolph, C., Barka, A., Page, W., and Kaya, A. (2002). Influence of releasing step-overs on surface fault rupture and fault segmentation: Examples from the 17 August 1999 Izmit earthquake on the North Anatolian fault, Turkey. *Bulletin of the Seismological Society of America*, 92(1):19–42.

Li, Z., Zhang, H., and Peng, Z. (2014). Structure-controlled seismic anisotropy along the Karadere–Düzce branch of the North Anatolian Fault revealed by shear-wave splitting tomography. *Earth and Planetary Science Letters*, 391:319–326.

Lienert, B. R., Berg, E., and Frazer, L. N. (1986). HYPOCENTER: An earthquake location method using centered, scaled, and adaptively damped least squares. *Bulletin of the Seismological Society of America*, 76(3):771–783.

Lienert, B. R. and Havskov, J. (1995). A computer program for locating earthquakes both locally and globally, journal = Seismological Research Letters. 66(5):26–36.

Luo, G. and Liu, M. (2010). Stress evolution and fault interactions before and after the 2008 Great Wenchuan earthquake. *Tectonophysics*, 491(1):127–140.

Magistrale, H. (2002). Relative contributions of crustal temperature and composition to controlling the depth of earthquakes in southern California. *Geophysical research letters*, 29(10):87–1.

Marone, C. (1998). Laboratory-derived friction laws and their application to seismic faulting. *Annual Review of Earth and Planetary Sciences*, 26(1):643–696.

Martínez-Garzón, P., Kwiatek, G., Ickrath, M., and Bohnhoff, M. (2014). MSATSI: A MATLAB Package for Stress Inversion Combining Solid Classic Methodology, a New Simplified User-Handling, and a Visualization Tool. *Seismological Research Letters*, 85(4):896–904.

McClusky, S., Balassanian, S., Barka, A., Demir, C., Ergintav, S., Georgiev, I., Gurkan, O., Hamburger, M., Hurst, K., Kahle, H., et al. (2000). Global Positioning System constraints on plate kinematics and dynamics in the eastern Mediterranean and Caucasus. *Journal of Geophysical Research: Solid Earth (1978–2012)*, 105(B3):5695–5719.

McKenzie, D. (1972). Active tectonics of the Mediterranean region. *Geophysical Journal of the Royal Astronomical Society*, 30(2):109–185.

McKenzie, D. P. (1969). The relation between fault plane solutions for earthquakes and the directions of the principal stresses. *Bulletin of the Seismological Society of America*, 59(2):591–601.

Meghraoui, M., Aksoy, M. E., Akyüz, H. S., Ferry, M., Dikbaş, A., and Altunel, E. (2012). Paleoseismology of the North Anatolian Fault at Güzelköy (Ganos segment, Turkey): Size and recurrence time of earthquake ruptures west of the Sea of Marmara. *Geochemistry, Geophysics, Geosystems*, 13(4).

Michael, A. J. (1984). Determination of stress from slip data: faults and folds, journal = Journal of Geophysical Research. 89:B13, 11 517–11 526.

Michael, A. J. (1987). Stress rotation during the Coalinga aftershock sequence, journal = Journal of Geophysical Research. 92:7963–7979.

Michael, A. J. (1991). Spatial variations in stress within the 1987 Whittier Narrows, California, aftershock sequence: new techniques and results. *Journal of Geophysical Research*, 96(B4):6303–6319.

Michael, A. J., Ellsworth, W., and Oppenheimer, D. H. (1990). Coseismic stress changes

induced by the 1989 Loma Prieta, California earthquake. *Geophysical Research Letters*, 17(9):1441–1444.

Milkereit, C., Zünbül, S., Karakisa, S., Iravul, Y., Zschau, J., Baumbach, M., Grosser, H., Günther, E., Umutlu, N., Kuru, T., et al. (2000). Preliminary aftershock analysis of the Mw= 7.4 Izmit and Mw= 7.1 Düzce earthquake in western Turkey. In Barka, A., editor, *The 1999 Izmit and Düzce Earthquakes: Preliminary Results*, pages 179–187. Istanbul Tech. Univ., Istanbul, Turkey.

Montési, L. G. (2004). Controls of shear zone rheology and tectonic loading on postseismic creep. *Journal of Geophysical Research: Solid Earth (1978–2012)*, 109(B10).

Nakamura, A., Hasegawa, A., Ito, A., Üçer, B., Bariş, Ş., Honkura, Y., Kono, T., Hori, S., Pektaş, R., Komut, T., et al. (2002). P-wave velocity structure of the crust and its relationship to the occurrence of the 1999 Izmit, Turkey, earthquake and aftershocks. *Bulletin of the Seismological Society of America*, 92(1):330–338.

NASA (2005). SRTM data NASA ftp servers.

Neugebauer, J. (1995). Structures and kinematics of the North Anatolian Fault zone, Adapazarı-Bolu region, northwest Turkey. *Tectonophysics*, 243(1):119–134.

Örgülü, G. (2010). Seismicity and source parameters for small-scale earthquakes along the splays of the North Anatolian Fault (NAF) in the Marmara Sea. *Geophysical Journal International*.

Örgülü, G. and Aktar, M. (2001). Regional Moment Tensor Inversion for Strong Aftershocks of the August 17, 1999 Izmit Earthquake (Mw=7.4). *Geophysical Research Letters*, 28(2):371–374.

Özalaybey, S., Ergin, M., Aktar, M., Tapirdamaz, C., Bicman, F., and Yörük, A. (2002). The 1999 Izmit earthquake sequence in Turkey: Seismological and Tectonic Aspects. *Bulletin of the Seismological Society of America*, 92(1):376.

Parolai, S., Bindi, D., Baumbach, M., Grosser, H., Milkereit, C., Karakisa, S., and Zunbul, S. (2004). Comparison of different site response estimation techniques using after-

shocks of the 1999 Izmit earthquake. *Bulletin of the Seismological Society of America*, 94(3):1096.

Parsons, T. (2004). Recalculated probability of M? 7 earthquakes beneath the Sea of Marmara, Turkey. *Journal of Geophysical Research: Solid Earth (1978–2012)*, 109(B5).

Parsons, T., Toda, S., Stein, R. S., Barka, A., and Dieterich, J. H. (2000). Heightened odds of large earthquakes near Istanbul: An interaction-based probability calculation. *Science*, 288(5466):661–665.

Peng, Z. and Ben-Zion, Y. (2006). Temporal changes of shallow seismic velocity around the Karadere-Düzce branch of the north Anatolian fault and strong ground motion. *Pure and Applied Geophysics*, 163(2-3):567–600.

Pinar, A., Ucer, S., Honkura, Y., and Sezgin, N. (2010). Spatial variation of the stress field along the fault rupture zone of the 1999 Izmit earthquake. *Earth Planets ...*, 62(3):237–256.

Plenkers, K. (2006). Quantitative bounds on the resolving power of crustal stress inversions. Master's thesis, University Karlsruhe.

Pucci, S., Pantosti, D., Barchi, M., Palyvos, N., et al. (2006). Evolution and complexity of the seismogenic Düzce fault zone (Turkey) depicted by coseismic ruptures, Plio-Quaternary structural pattern and geomorphology. *Geophysical Research Abstracts*, 8:08339.

Pucci, S., Pantosti, D., Barchi, M. R., and Palyvos, N. (2007). A complex seismogenic shear zone: The Düzce segment of North Anatolian Fault (Turkey). *Earth and Planetary Science Letters*, 262(1-2):185–203.

Reches, Z. (1987). Determination of the tectonic stress tensor from slip along faults that obey the Coulomb yield condition. *Tectonics*, 6:849–861.

Reid, H. (1910). *Permanent displacements of the ground, The California Earthquake of April, 18, 1906.* Report of the State Earthquake Investigation Commission, Washington. Seismic travel and near surface crustal velocity structure bounding the San Andreas Fault zone near Parkfield, California.

Reilinger, R., Ergintav, S., Bürgmann, R., McClusky, S., Lenk, O., Barka, A., Gurkan, O., Hearn, L., Feigl, K., Cakmak, R., et al. (2000). Coseismic and postseismic fault slip for the 17 August 1999, M= 7.5, Izmit, Turkey earthquake. *Science*, 289(5484):1519–1524.

Reilinger, R., McClusky, S., Oral, M., King, R., Toksoz, M., Barka, A., Kinik, I., Lenk, O., and Sanli, I. (1997). Global Positioning System measurements of present-day crustal movements in the Arabia-Africa-Eurasia plate collision zone. *Journal of Geophysical Research: Solid Earth (1978–2012)*, 102(B5):9983–9999.

Reilinger, R., McClusky, S., Vernant, P., Lawrence, S., Ergintav, S., Cakmak, R., Ozener, H., Kadirov, F., Guliev, I., Stepanyan, R., et al. (2006). GPS constraints on continental deformation in the Africa-Arabia-Eurasia continental collision zone and implications for the dynamics of plate interactions. *Journal of Geophysical Research: Solid Earth (1978–2012)*, 111(B5).

Rice, J. R. and Gu, J.-c. (1983). Earthquake aftereffects and triggered seismic phenomena. *pure and applied geophysics*, 121(2):187–219.

Ritz, J. F. and Taboada, A. (1993). Revolution stress ellipsoids in brittle tectonics resulting from an uncritical use of inverse methods. *Bulletin de la Societe Geologique de France*, 164(4):519–531.

Rivera, L. and Cisternas, A. (1990). Stress tensor and fault plane solutions for a population of earthquakes. *Bulletin of the Seismological Society of America*, 80(3):600.

Robertson, A. and Dixon, J. (1984). Introduction: aspects of the geological evolution of the Eastern Mediterranean. *Geological Society, London, Special Publications*, 17(1):1–74.

Robertson, A., Parlak, O., and Ünlügenç, U. C. (2013). Editorial introduction to 'Geological Development of Anatolia and the Easternmost Mediterranean Region'. *Geological Society, London, Special Publications*, 372(1):1–7.

Robinson, R. and McGinty, P. (2000). The enigma of the Arthur's Pass, New Zealand, earthquake 2. The aftershock distribution and its relation to reginal and induced stress fields. *Journal of Geophysical Research*, 105(B7):16,139–16,150.

Rolandone, F., Bürgmann, R., and Nadeau, R. (2004). The evolution of the seismic-aseismic transition during the earthquake cycle: Constraints from the time-dependent depth distribution of aftershocks. *Geophysical Research Letters*, 31(23).

Rolandone, F., Jaupart, C., Mareschal, J., Gariépy, C., Bienfait, G., Carbonne, C., and Lapointe, R. (2002). Surface heat flow, crustal temperatures and mantle heat flow in the Proterozoic Trans-Hudson Orogen, Canadian Shield. *Journal of Geophysical Research: Solid Earth (1978–2012)*, 107(B12):ETG–7.

Saroglu, F. (1985). *Dogu Anadolu nun Neotektonik Dönemde Jeolojik ve Yapısal Evrimi.* PhD thesis, PhD thesis. Istanbul Univ., Fen Bilim. Enst., Istanbul. 240 pp.+ 7 foldouts.

Şaroğlu, F., Emre, Ö., and Kuşçu, İ. (1992). Active fault map of Turkey. *General Directorate of Mineral Research and Exploration, Ankara.*

Schildgen, T., Cosentino, D., Caruso, A., Buchwaldt, R., Yıldırım, C., Bowring, S. A., Rojay, B., Echtler, H., and Strecker, M. (2012). Surface expression of eastern Mediterranean slab dynamics: Neogene topographic and structural evolution of the southwest margin of the Central Anatolian Plateau, Turkey. *Tectonics*, 31(2).

Scholz, C. H. (2002). *The mechanics of earthquakes and faulting.* Cambridge university press.

Seeber, L., Armbruster, J. G., Ozer, N., Aktar, M., Baris, S., Okaya, D., Ben-Zion, Y., Field, E., et al. (2000). The 1999 Earthquake Sequence along the North Anatolia Transform at the juncture between the two main ruptures. *The 1999 Izmit and Duzce Earthquakes: Preliminary Results*, pages 209–223.

Segall, P. (2004). Postseismic Deformation: Different mechanisms in different times and places. In *AGU Fall Meeting Abstracts*, volume 1, page 01.

Sengör, A. (1979). The North Anatolian transform fault: its age, offset and tectonic significance. *Journal of the Geological Society*, 136(3):269–282.

Şengör, A. (1985). Strike-slip faulting and related basin formation in zones of tectonic escape: Turkey as a case study. In Biddle, K. and Christie-Blick, N., editors, *Strike-slip*

Deformation, Basin Formation, and Sedimentation, pages 227–64. Special Publications of SEPM.

Sengör, A., Tüysüz, O., Imren, C., Sakinç, M., Eyidogan, H., Görür, N., Le Pichon, X., and Rangin, C. (2005). The North Anatolian fault: A new look. *Annu. Rev. Earth Planet. Sci.*, 33:37–112.

Sibson, R. H. (1985). Stopping of earthquake ruptures at dilational fault jogs. *Nature*, 316(6025):248–251.

Sibson, R. H. (1986). Earthquakes and rock deformation in crustal fault zones. *Annual Review of Earth and Planetary Sciences*, 14:149.

Sibson, R. H. (1994). An assessment of field evidence for 'Byerlee' friction. *Pure and Applied Geophysics*, 142(3-4):645–662.

Smith, D. E. and Dieterich, J. H. (2010). Aftershock sequences modeled with 3-D stress heterogeneity and rate-state seismicity equations: Implications for crustal stress estimation. *Pure and applied geophysics*, 167(8-9):1067–1085.

Stein, R. S., Barka, A. A., and Dieterich, J. H. (1997). Progressive failure on the North Anatolian fault since 1939 by earthquake stress triggering. *Geophysical Journal International*, 128(3):594–604.

Stein, R. S., King, G. C., and Lin, J. (1992). Change in failure stress on the southern San Andreas fault system caused by the 1992 magnitude= 7.4 Landers earthquake. *Science*, 258(5086):1328–1332.

Stierle, E., Bohnhoff, M., and Vavryčuk, V. (2014). Resolution of non-double-couple components in the seismic moment tensor using regional networks - II : application to aftershocks of the 1999 Mw 7.4 Izmit earthquake. *Geophysical Journal International*, page ggt503.

Tank, S. B., Honkura, Y., Ogawa, Y., Matsushima, M., Oshiman, N., Tunçer, M. K., Çelik, C., Tolak, E., and Işıkara, A. M. (2005). Magnetotelluric imaging of the fault rupture area of the 1999 Izmit (Turkey) earthquake. *Physics of the Earth and Planetary Interiors*, 150(1):213–225.

Taymaz, T., Jackson, J., and McKenzie, D. (1991). Active tectonics of the north and central Aegean Sea. *Geophysical Journal International*, 106(2):433–490.

Thatcher, W. (1983). Nonlinear strain buildup and the earthquake cycle on the San Andreas fault. *Journal of Geophysical Research: Solid Earth (1978–2012)*, 88(B7):5893–5902.

Tibi, R., Bock, G., Xia, Y., Baumbach, M., Grosser, H., Milkereit, C., Karakisa, S., Zünbül, S., Kind, R., and Zschau, J. (2001). Rupture processes of the 1999 August 17 Izmit and November 12 Düzce (Turkey) earthquakes. *Geophysical Journal International*, 144(2):F1–F7.

Toksöz, M., Shakal, A., and Michael, A. (1979). Space-time migration of earthquakes along the North Anatolian fault zone and seismic gaps. In *Earthquake Prediction and Seismicity Patterns*, pages 1258–1270. Springer.

Toksöz, M. N., Reilinger, R., Doll, C., Barka, A., and Yalcin, N. (1999). Izmit (Turkey) earthquake of 17 August 1999: first report. *Seismological Research Letters*, 70(6):669–679.

Townend, J. and Zoback, M. (2000). Focal Mechanism Stress Inversions in Southern California and the strength of the San Andreas Fault. In *Proc., 3rd Conf. on Tectonic Problems of the San Andreas Fault System*.

Townend, J. and Zoback, M. D. (2001). *Implications of earthquake focal mechanisms for the frictional strength of the San Andreas fault system, in The Nature and Significance of Fault Zone Weakening*, volume 186. Geol. Soc. London Spec. Publ.

Tse, S. T. and Rice, J. R. (1986). Crustal earthquake instability in relation to the depth variation of frictional slip properties. *Journal of Geophysical Research: Solid Earth (1978–2012)*, 91(B9):9452–9472.

Umutlu, N., Koketsu, K., and Milkereit, C. (2004). The rupture process during the 1999 Düzce, Turkey, earthquake from joint inversion of teleseismic and strong-motion data. *Tectonophysics*, 391(1-4):315–324.

Ünay, E., Emre, Ö., Erkal, T., and Keçer, M. (2001). The rodent fauna from the Adapazarı pull-apart basin (NW Anatolia): Its bearings on the age of the North Anatolian fault. *Geodinamica Acta*, 14(1):169–175.

Unsworth, M., Bedrosian, P., Eisel, M., Egbert, G., and Siripunvaraporn, W. (2000). Along strike variations in the electrical structure of the San Andreas Fault at Parkfield, California. *Geophysical Research Letters*, 27(18):3021–3024.

Utsu, T. (1961). A statistical study of the occurrence of aftershocks. *Geophysical Magazine*, 30:521–605.

Waldhauser, F. and Ellsworth, W. L. (2000). A double-difference earthquake location algorithm: method and application to the northern Hayward fault, California. *Bulletin of the Seismological Society of America*, 90(6):1353.

Wallace, R. E. (1951). Geometry of shearing stress and relation to faulting. *The Journal of Geology*, pages 118–130.

Wei, M. (2011). *Observations and modeling of shallow fault creep along the San Andreas Fault system*. PhD thesis, University of California, San Diego.

Woith, H., Zschau, J., Yilmaz, R., Karakisa, S., Zünbül, S., Baumbach, M., Grosser, H., Milkereit, C., Lang, D., Raschke, M., et al. (2000). Multidisciplinary investigations of the German Task Force for Earthquakes related to the Izmit earthquake of August 17, 1999 and the Düzce earthquake of November 12, 1999. *The 1999 Izmit and Düzce Earthquakes: Preliminary Results*, pages 233–245.

Xu, P. (2004). Determination of regional stress tensors from fault-slip data. *Geophysical Journal International*, 157(3):1316–1330.

Yaltırak, C. (2002). Tectonic evolution of the Marmara Sea and its surroundings. *Marine Geology*, 190(1):493–529.

Yiğitbaş, E., Elmas, A., Sefunç, A., and Özer, N. (2004). Major neotectonic features of eastern Marmara region, Turkey: development of the Adapazarı–Karasu corridor and its tectonic significance. *Geological Journal*, 39(2):179–198.

Yin, Y. and Zhang, H. (1982). A mathematical-model of strain softening in simulating earthquakes. *Acta Geophysica Sinica*, 25(5):414–423.

Yin, Z. M. and Rogers, G. C. (1995). Rotation of the principal stress directions due to earthquake faulting and its seismological implications. *Bulletin of the Seismological Society of America*, 85(5):1513.

Yuichiro, T. and Ghimire, S. (2011). *Spatio-temporal Changes in Stress Field and Occurrence of the 2003 Tokachi Oki Earthquake in Hokkaido, Northern Japan, New Frontiers in Tectonic Research - General Problems, Sedimentary Basins and Island Arcs*. InTech. ISBN: 978-953-307-595-2.

Yukutake, Y., Iio, Y., Katao, H., and Shibutani, T. (2007). Estimation of the stress field in the region of the 2000 Western Tottori Earthquake: Using numerous aftershock focal mechanisms. *Journal of Geophysical Research: Solid Earth (1978–2012)*, 112(B9).

Zang, A. and Stephansson, O. (2010). *Stress Field of the Earth's Crust*. Dordrecht: Springer Science+ Business Media B.V.

Zoback, M. L. (1992). First-and Second-Order Patterns of Stress in the Lithosphere: The World Stress Map Project. *Journal of Geophysical Research: Solid Earth (1978–2012)*, 97(B8):11703–11728.

EIDESSTATTLICHE ERKLÄRUNG:

Hiermit versichere ich, dass die vorliegende Dissertation mit dem Titel:

Spatiotemporal variations of the local stress field and fault asperities at the North Anatolian Fault in NW Turkey analysed based on microseismic recordings.

von mir selbstständig angefertigt wurde und alle von mir genutzten Quellen und Hilfsmittel angegeben wurden.
Ich erkläre, dass die wörtlichen oder dem Sinne nach anderen Veröffentlichungen entnommenen Stellen von mir kenntlich gemacht wurden.
Die Zeichnungen und Abbildungen in dieser Arbeit sind von mir selbst erstellt worden oder mit einem entsprechenden Quellennachweis versehen.
Diese Arbeit ist in gleicher oder ähnlicher Form noch bei keiner anderen Prüfungsbehörde eingereicht worden.

Berlin, den 14th August 2014

Curriculum Vitae

For reasons of data protection,
the curriculum vitae is not included in the
online version

For reasons of data protection,
the curriculum vitae is not included in the
online version

For reasons of data protection,
the curriculum vitae is not included in the
online version

Publications

04/2014 C. Feld, C. Haberland, B. Schurr, C. Sippl, U. Wetzel, M. Ickrath, U. Abdybachaev and S. Orunbaev, Seismotectonic Study of the Fergana Region (Southern Kyrgyzstan): Distribution and Kinematics of Local Seismicity, submitted to Earth, Planets and Space.

04/2014 W. Jokat and M. Ickrath, Seismic sediment structure of ridges and basins off East Siberia along 81°N, Arctic Ocean, submitted to Geophysical Journal International

04/2014 P. Martínez-Garzón, G. Kwiatek, M. Ickrath and M. Bohnhoff, , (2014), MSATSI: A MATLAB package for stress tensor inversion combining solid classic methodology, a new simplified user-handling and a complete visualization tool, Seismological Research Letters, 85, 896-904.

11/2013 M. Ickrath, M. Bohnhoff, F. Bulut and G. Dresen (2014), Stress rotation and recovery in conjunction with the 1999 Izmit M_w 7.4 earthquake, Geophysical Journal International, 196, 951-956. First published online: November 2, 2013.

10/2013 W. Jokat, M. Ickrath and J. O'Connor (2013), Seismic transect across the Lomonosov and Mendeleev Ridges: Constraints on the geological evolution of the Amerasia Basin, Arctic Ocean, Geophys. Res. Lett., 40.

A. MSATSI: A MATLAB© package for stress inversion

This chapter is published in Seismological Research Letters: P. Martínez-Garzón, G. Kwiatek, M. Ickrath and Marco Bohnhoff: MSATSI: A MATLAB© package for stress inversion combining solid classic methodology, a new simplified user-handling and a visualization tool, 2014, 85, 896-904, http://dx.doi.org/10.1785/0220130189.

For reasons of data protection, the paper is not included in the online version

B. SABOnet

B.1. Conversion from Nanometrics Data Format to SAC

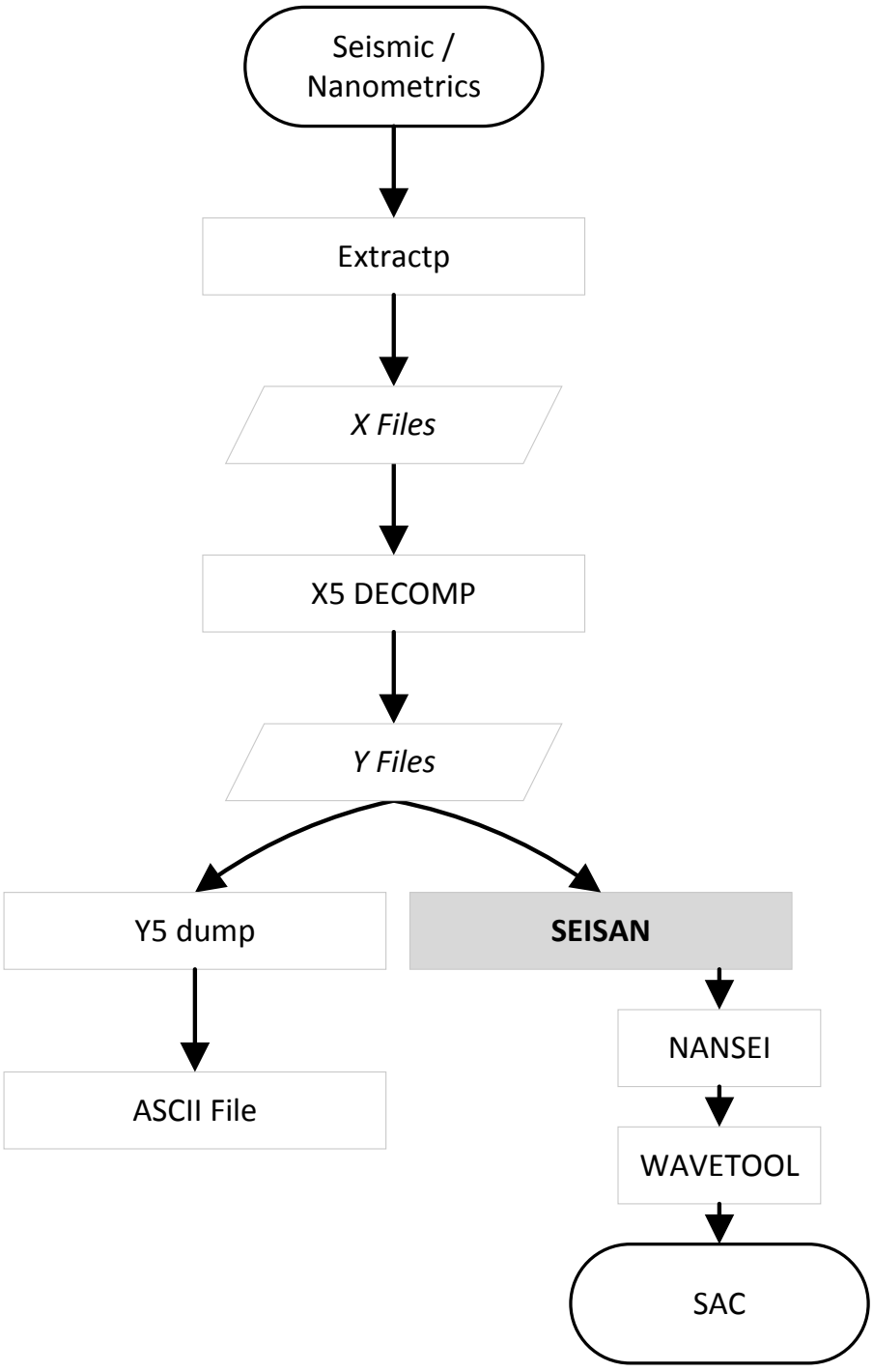

Figure B.1.: Basic Workflow for the Data Conversion from Nanometrics to SAC format used in this study.

B.2. Stationlist

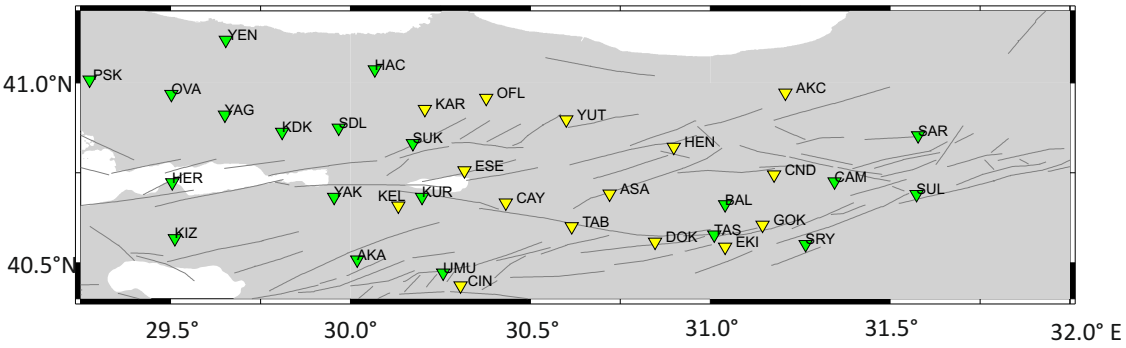

Figure B.2.: Stationmap of SABOnet and German Task Force Stations.

ID	Staton Name	Datalogger	Sensor type	Sensor No.	Lat [°]	Lon [°]	Elevation [m]	Recording period START	used in this study	END		NETWORK
1	PSK	REFTEK	L4-3D	1304	41.0083	29.2747	130	99.08.27	15:10	99.10.21	12:40	GTF
2	OVA	REFTEK	L4-3D	1807	40.9682	29.5021	200	99.08.25	14:00	99.10.20	13.4	GTF
3	YEN	REFTEK	L4-3D	1305	41.1189	29.6532	210	99.08.25	09:30	99.10.20	10:52	GTF
4	YAG	REFTEK	L4-3D	1308	40.9111	29.6510	280	99.08.22	15:00	99.10.19	10:39	GTF
5	KDK	REFTEK	L4-3D	1314	40.8631	29.8100	330	99.08.29	15:25	99.09.07	24:00:00	GTF
6	KDK	REFTEK	L4-3D	1303	40.8631	29.8100	330	99.09.14	11:52	99.10.19	11:34	GTF
7	SDL	REFTEK	L4-3D	1808	40.8750	29.9671	250	99.08.21	15:15	99.10.19	19:10	GTF
8	HAC	REFTEK	L4-3D	1313	41.0369	30.0675	110	99.08.24	17:00	99.10.20	11:34	GTF
9	SUK	REFTEK	L4-3D	1303	40.8319	30.1737	260	99.08.26	15.2	99.09.05	24:00:00	GTF
10	SUK	REFTEK	CMG-40T	4449	40.8319	30.1737	260	99.09.13	10:20	99.10.21	09:13	GTF
11	SAR	REFTEK	L4-3D	1809	40.8535	31.5779	740	99.08.26	13:30	99.10.20	24:00:00	GTF
12	GEM	REFTEK	L4-3D	1311	40.4877	29.0905	10	99.08.23	16:30	99.10.19	24:00:00	GTF
13	HER	REFTEK	L4-3D	1310	40.7232	29.5044	0	99.08.23	13:00	99.10.19	24:00:00	GTF
14	KIZ	REFTEK	L4-3D	1306	40.5673	29.5120	310	99.08.23	07:40	99.10.19	24:00:00	GTF
15	YAK	REFTEK	L4-3D	1314	40.6827	29.9543	280	99.08.27	13:00	99.10.21	08:15	GTF
16	AKA	REFTEK	L4-3D	1307	40.5080	30.0187	790	99.08.21	17:00	99.09.06	13:21	GTF
17	AKA	REFTEK	CMG-40T	4283	40.5080	30.0187	790	99.09.06	14:00	99.10.18	24:00:00	GTF
18	KUR	REFTEK	L4-3D	1309	40.6823	30.1988	220	99.08.27	09:30	99.10.21	11:20	GTF
19	UMU	REFTEK	L4-3D	1300	40.4717	30.2576	240	99.08.21	14:20	99.10.18	24:00:00	GTF
20	TAS	REFTEK	L4-3D	1301	40.5775	31.0112	610	99.08.22	07:00	99.08.31	08:00	GTF
21	TAS	REFTEK	L4-3D	1301	40.5775	31.0112	610	99.09.11	00:00	99.09.12	24:00:00	GTF
22	TAS	REFTEK	L4-3D	1314	40.5775	31.0112	610	99.09.12	00:00	99.09.13	24:00:00	GTF
23	TAS	REFTEK	L4-3D	1303	40.5775	31.0112	610	99.09.13	00:00	99.09.14	24:00:00	GTF
24	BAL	REFTEK	L4-3D	1301	40.6621	31.0411	1340	99.08.31	12:50	99.10.20	24:00:00	GTF
25	SRY	REFTEK	CMG-40T	4455	40.5510	31.2653	870	99.09.10	10:00	99.10.20	24:00:00	GTF
26	CAM	REFTEK	L4-3D	1302	40.7253	31.3452	920	99.08.25	14:00	99.10.20	24:00:00	GTF

27	SUL	REFTEK	L4-3D	1312	40.6902	31.5733	680	99.08.24	13:00	99.09.09	07:28	GTF
28	AKC	NANOME	L4-3D	1000	40.9723	31.2089	680	1996		2003		SABO
29	CAY	NANOME	L4-3D	1001	40.6665	30.4315	291	1996		2003		SABO
30	CND	NANOME	L4-3D	1002	40.7445	31.1771	950	1996		2003		SABO
31	CIN	NANOME	L4-3D	1003	40.4360	30.3057	1100	1996		2003		SABO
32	DOK	NANOME	L4-3D	1004	40.5579	30.8467	635	1996		2003		SABO
33	EKI	NANOME	L4-3D	1005	40.5440	31.0412	890	1996		2003		SABO
34	GOK	NANOME	L4-3D	1006	40.6052	31.1453	228	1996		2003		SABO
35	HEN	NANOME	L4-3D	1007	40.8214	30.8986	590	1996		2003		SABO
36	KAR	NANOME	L4-3D	1008	40.9270	30.2065	260	1996		2003		SABO
37	KEL	NANOME	L4-3D	1009	40.6581	30.1328	1150	1996		2003		SABO
38	TAB	NANOME	L4-3D	1010	40.6006	30.6147	400	1996		2003		SABO
39	YUT	NANOME	L4-3D	1011	40.8978	30.6001	147	1996		2003		SABO
40	OFL	NANOME	L4-3D	1012	40.9573	30.3771	350	1996		2003		SABO
41	ASA	NANOME	L4-3D	1013	40.6915	30.7199	228	1996		2003		SABO
42	ESE	NANOME	L4-3D	1014	40.7562	30.3167	374	1996		2003		SABO

Table B.1.: Station Parameters for the SABOnet and German Task Force (GTF) station networks.

B.3. Station operation times from SABONET

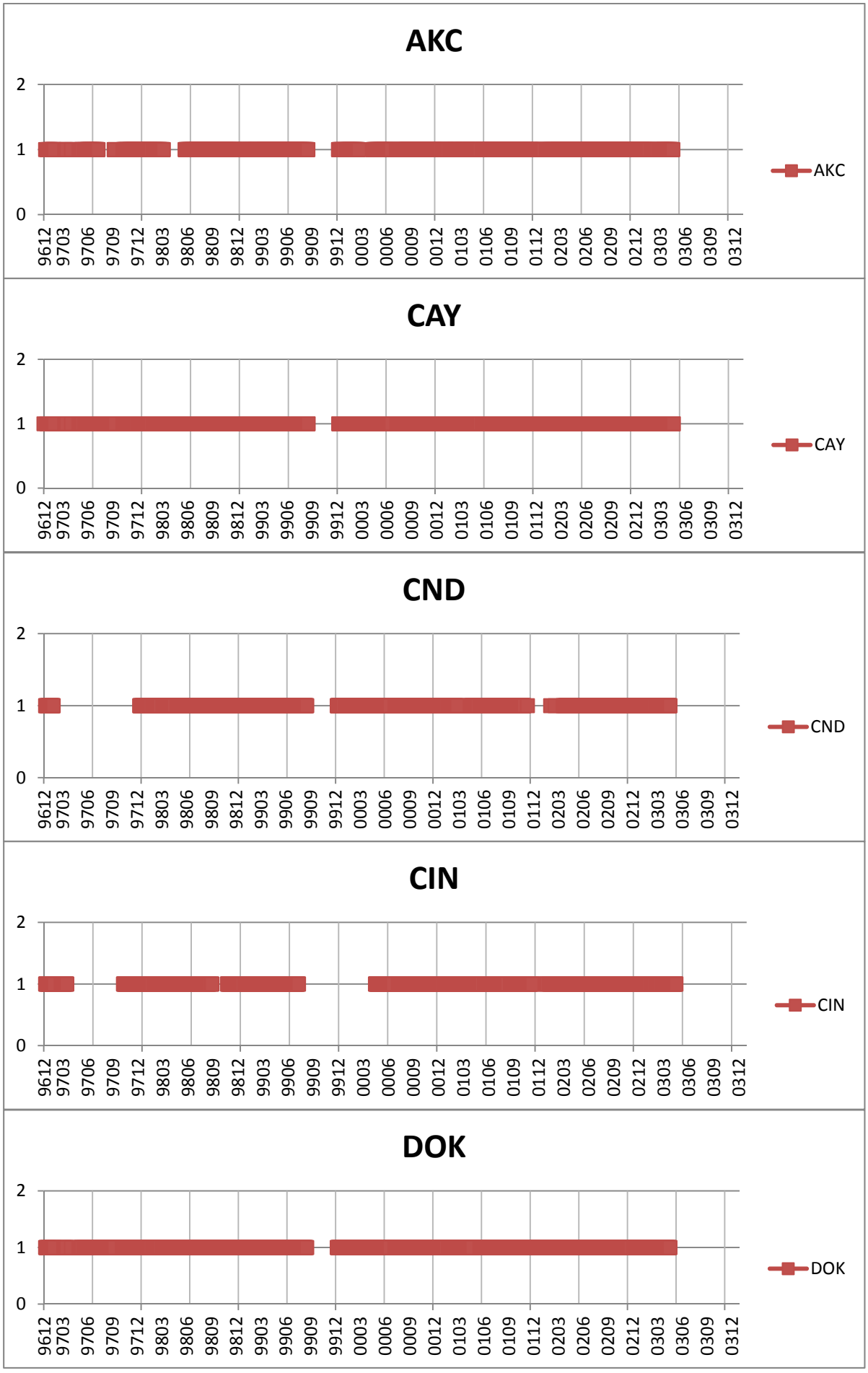
AKC
2
1
0
9612 9703 9706 9709 9712 9803 9806 9809 9812 9903 9906 9909 9912 0003 0006 0009 0012 0103 0106 0109 0112 0203 0206 0209 0212 0303 0306 0309 0312
AKC
CAY
2
1
0
9612 9703 9706 9709 9712 9803 9806 9809 9812 9903 9906 9909 9912 0003 0006 0009 0012 0103 0106 0109 0112 0203 0206 0209 0212 0303 0306 0309 0312
CAY
CND
2
1
0
9612 9703 9706 9709 9712 9803 9806 9809 9812 9903 9906 9909 9912 0003 0006 0009 0012 0103 0106 0109 0112 0203 0206 0209 0212 0303 0306 0309 0312
CND
CIN
2
1
0
9612 9703 9706 9709 9712 9803 9806 9809 9812 9903 9906 9909 9912 0003 0006 0009 0012 0103 0106 0109 0112 0203 0206 0209 0212 0303 0306 0309 0312
CIN
DOK
2
1
0
9612 9703 9706 9709 9712 9803 9806 9809 9812 9903 9906 9909 9912 0003 0006 0009 0012 0103 0106 0109 0112 0203 0206 0209 0212 0303 0306 0309 0312
DOK

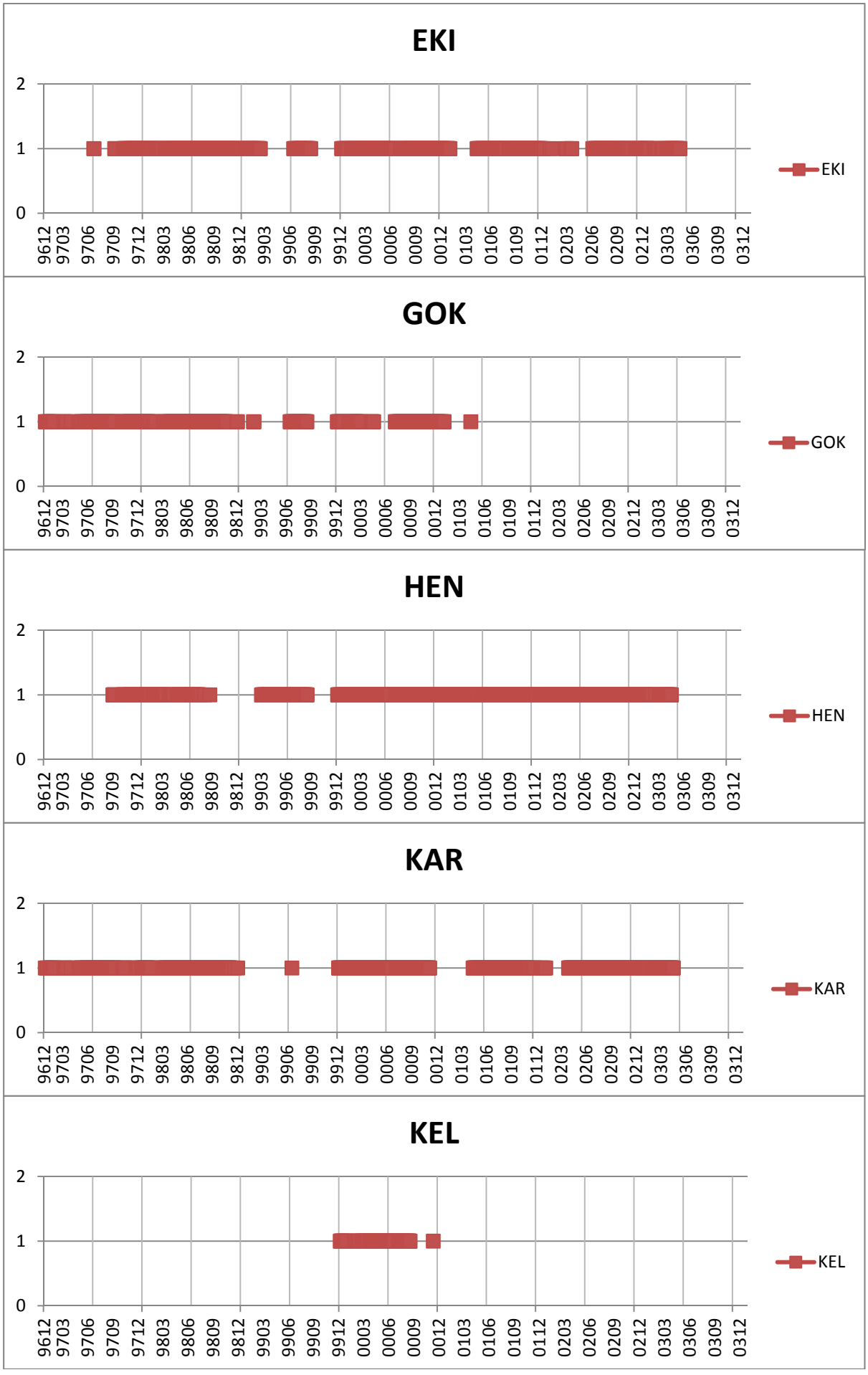
EKI
2
1
0
9612 9703 9706 9709 9712 9803 9806 9809 9812 9903 9906 9909 9912 0003 0006 0009 0012 0103 0106 0109 0112 0203 0206 0209 0212 0303 0306 0309 0312
EKI
GOK
2
1
0
9612 9703 9706 9709 9712 9803 9806 9809 9812 9903 9906 9909 9912 0003 0006 0009 0012 0103 0106 0109 0112 0203 0206 0209 0212 0303 0306 0309 0312
GOK
HEN
2
1
0
9612 9703 9706 9709 9712 9803 9806 9809 9812 9903 9906 9909 9912 0003 0006 0009 0012 0103 0106 0109 0112 0203 0206 0209 0212 0303 0306 0309 0312
HEN
KAR
2
1
0
9612 9703 9706 9709 9712 9803 9806 9809 9812 9903 9906 9909 9912 0003 0006 0009 0012 0103 0106 0109 0112 0203 0206 0209 0212 0303 0306 0309 0312
KAR
KEL
2
1
0
9612 9703 9706 9709 9712 9803 9806 9809 9812 9903 9906 9909 9912 0003 0006 0009 0012 0103 0106 0109 0112 0203 0206 0209 0212 0303 0306 0309 0312
KEL

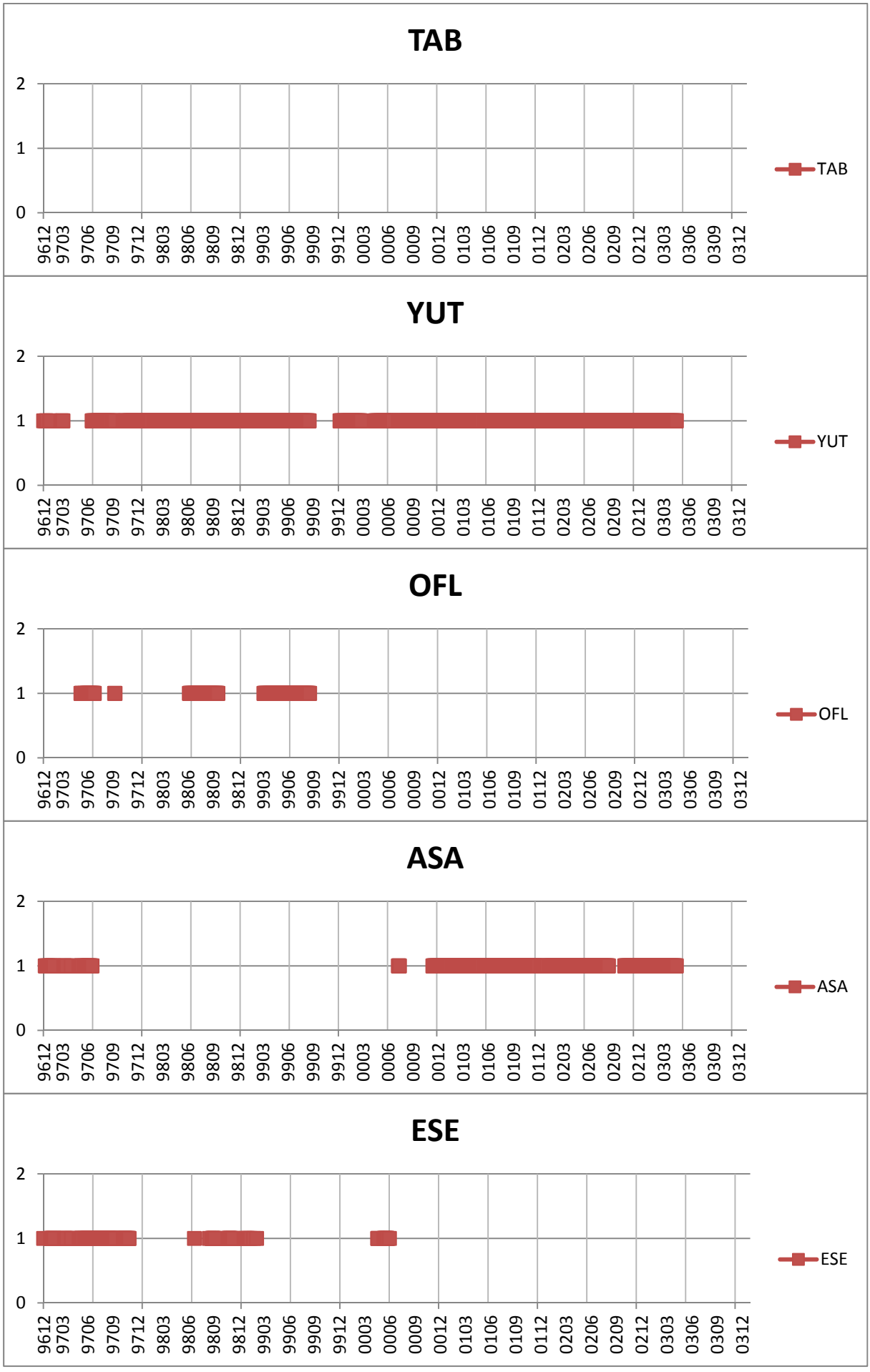
TAB
2
1
0
9612 9703 9706 9709 9712 9803 9806 9809 9812 9903 9906 9909 9912 0003 0006 0009 0012 0103 0106 0109 0112 0203 0206 0209 0212 0303 0306 0309 0312
TAB
YUT
2
1
0
9612 9703 9706 9709 9712 9803 9806 9809 9812 9903 9906 9909 9912 0003 0006 0009 0012 0103 0106 0109 0112 0203 0206 0209 0212 0303 0306 0309 0312
YUT
OFL
2
1
0
9612 9703 9706 9709 9712 9803 9806 9809 9812 9903 9906 9909 9912 0003 0006 0009 0012 0103 0106 0109 0112 0203 0206 0209 0212 0303 0306 0309 0312
OFL
ASA
2
1
0
9612 9703 9706 9709 9712 9803 9806 9809 9812 9903 9906 9909 9912 0003 0006 0009 0012 0103 0106 0109 0112 0203 0206 0209 0212 0303 0306 0309 0312
ASA
ESE
2
1
0
9612 9703 9706 9709 9712 9803 9806 9809 9812 9903 9906 9909 9912 0003 0006 0009 0012 0103 0106 0109 0112 0203 0206 0209 0212 0303 0306 0309 0312
ESE

—

C. Stress Tensor Inversion for the Izmit 1999 earthquake focal mechanism database using STI from Angelier (2002)

Since observed stress field rotation are quite under debate we finally used in addition to the already introduced and performed STI's in this study the nonlinear approach from Angelier (2002) to investigate the stress field evolution for the coseismic phase between the Izmit and Düzce earthquake 1999 based on the focal mechanism database (App. E). This method is a nonlinear inversion using focal mechanism based on the slip shear stress component (SSSC) criterion which assume that the SSSC (the scalar product of the slip $\vec{s}$ and the shear stress $\vec{t}$) is large if $\vec{s}$ is parallel to $\vec{t}$, while it becomes smaller if the vectors differ. Because of the intrinsic properties of the SSSC the inversion needs no choice between the nodal planes of each focal mechanism. The run time is negligible regardless of the size of the data set, because the inverse problem is solved by analytical means so that the numerical aspects are reduced to a minimum (Angelier, 2002). Although the results do not show the clear backrotation of the stress field, they still confirm our previous results in that way that they show the for the pre- and postseismic phase the expected strike-slip regime and for the inter Izmit-Düzce phase the normal faulting mechanism.

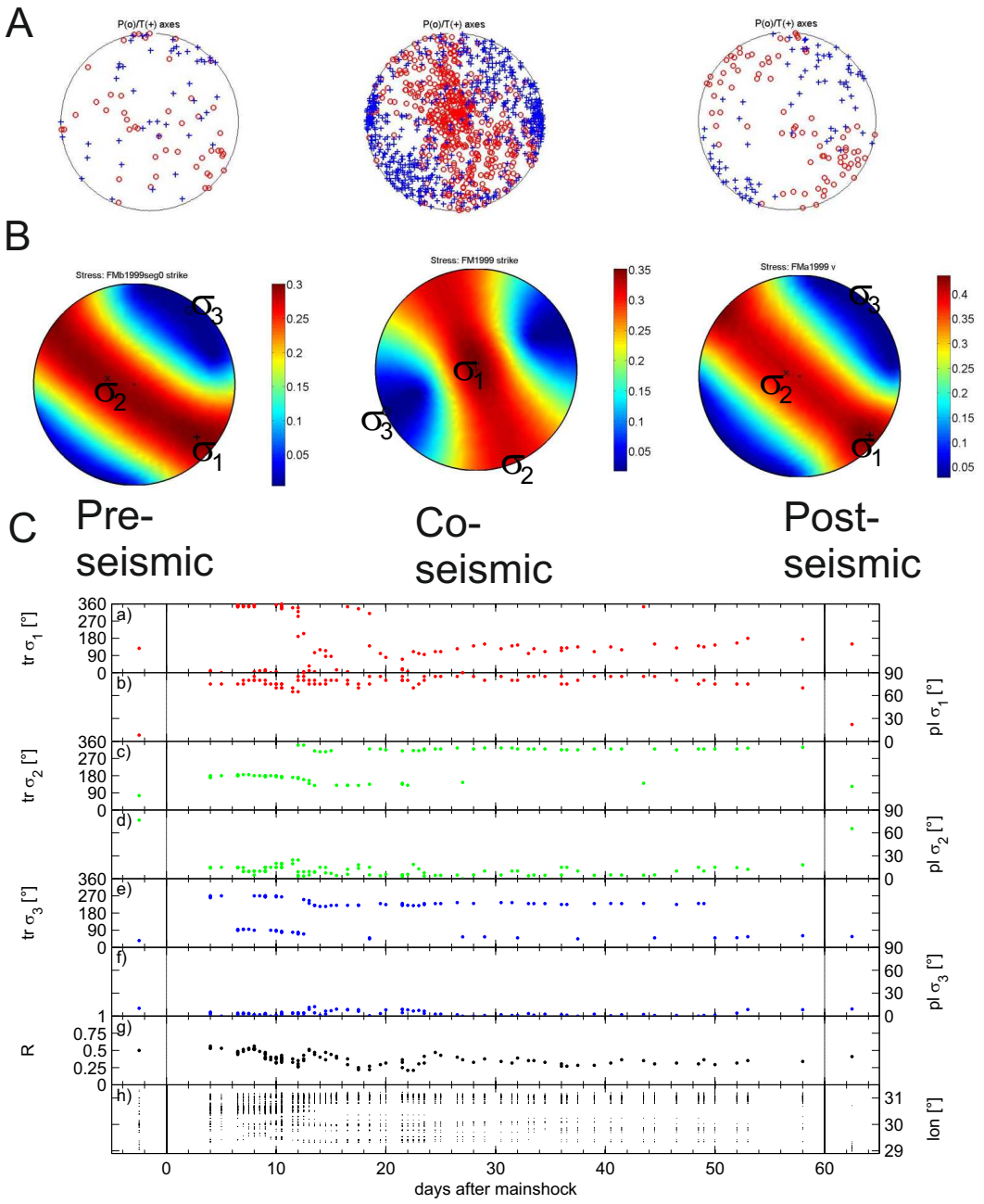

Figure C.1.: Inversion results for the coseismic phase of the Izmit 1999 earthquake using the method of Angelier (Angelier, 2002). The mean value of the slip shear stress component (SSSC) over all input focal mechanisms is shown in color as a function of the σ_1 direction. The optimum σ_1 direction is in the maximum of the SSSC, color-coded in dark-red. The lower-hemisphere equal-area projection is used.

D. STI results obtained with MOTSI

PRESEISMIC

A

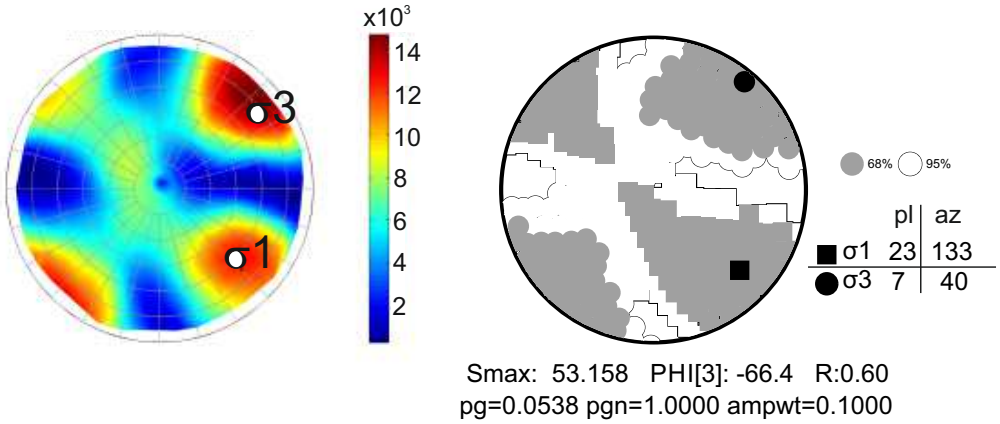

Smax: 53.158 PHI[3]: -66.4 R:0.60
pg=0.0538 pgn=1.0000 ampwt=0.1000

B

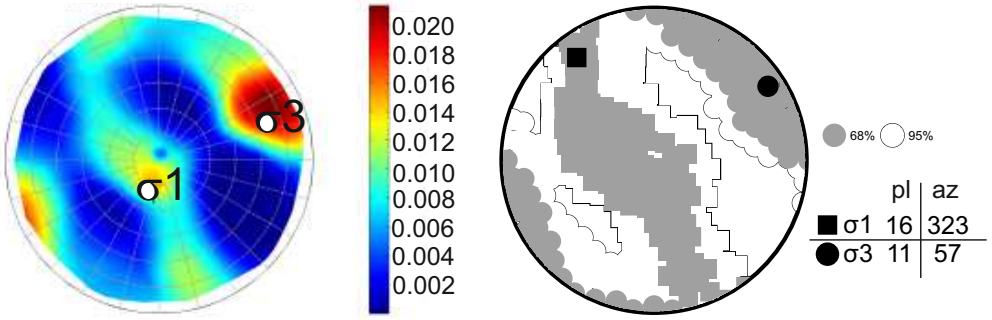

Smax: 56.201 PHI[3]: 73.2 R:0.60
pg=0.0538 pgn=1.0000 ampwt=0.1000

C

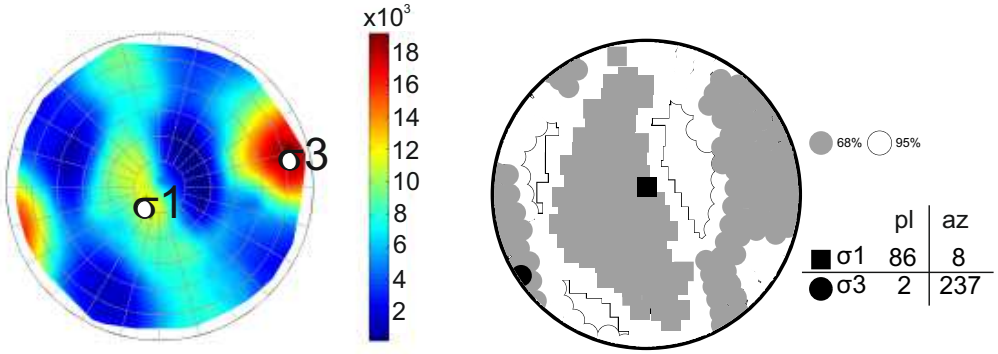

Smax: 54.014 PHI[1]: 2.8 R:0.40
pg=0.0538 pgn=1.0000 ampwt=0.1000

D

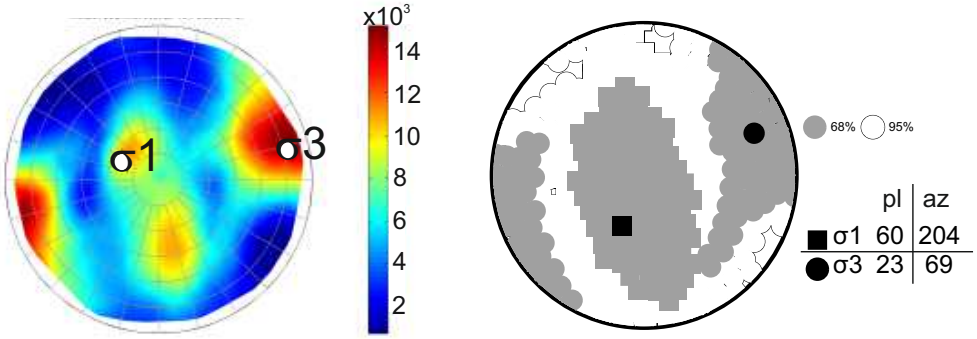

Smax: 32.740 PHI[3]: -20.8 R:0.30
pg=0.0538 pgn=1.0000 ampwt=0.1000

COSEISMIC (A - D)

A

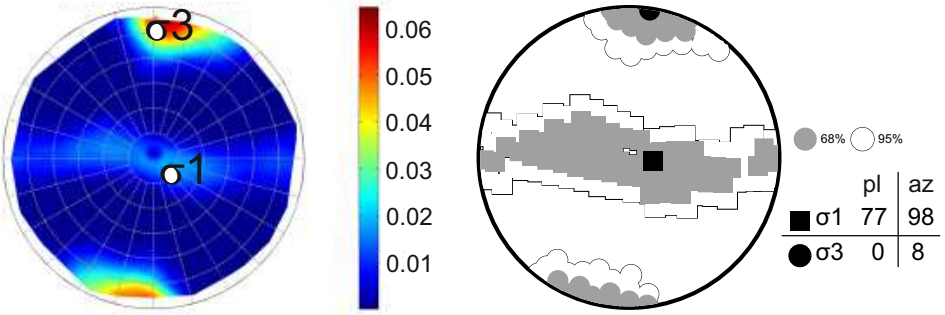

Smax: 97.097 PHI[3]: -13.5 R:0.50
pg=0.0538 pgn=1.0000 ampwt=0.1000

B

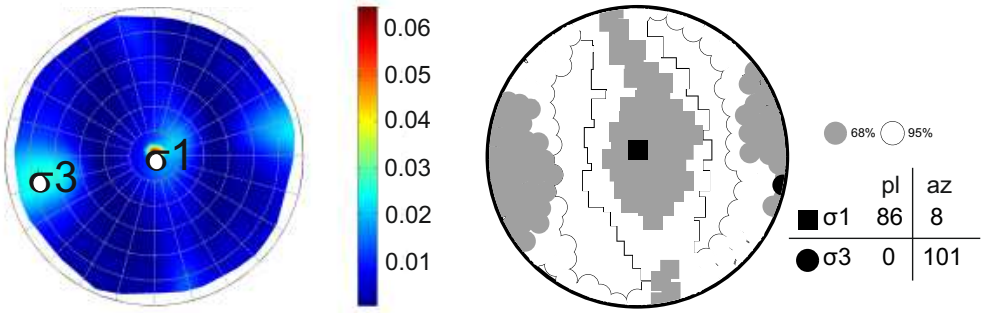

Smax: 92.700 PHI[1]: -40.9 R:0.40
pg=0.0538 pgn=1.0000 ampwt=0.1000

C

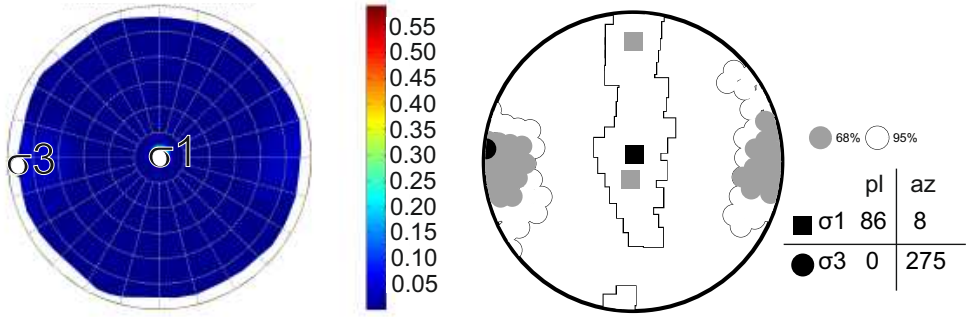

Smax: 197.073 PHI[1]: 40.8 R:0.50
pg=0.0538 pgn=1.0000 ampwt=0.1000

D

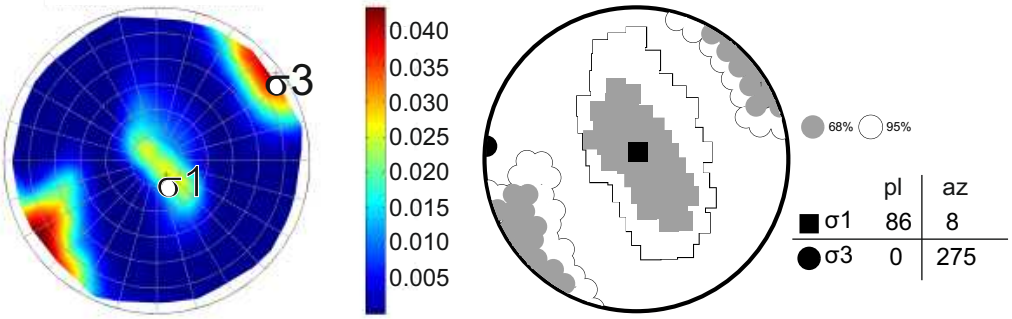

Smax: 136.130 PHI[1]: 40.8 R:0.40
pg=0.0538 pgn=1.0000 ampwt=0.1000

COSEISMIC (E - H)

E

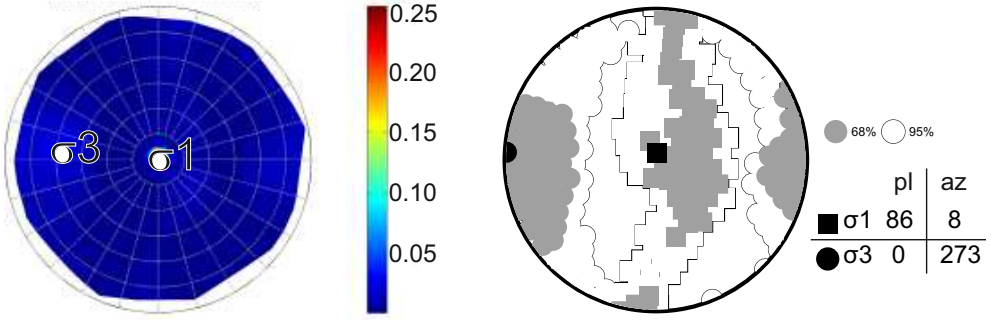

Smax: 97.983 PHI[1]: 26.6 R:0.60
pg=0.0538 pgn=1.0000 ampwt=0.1000

F

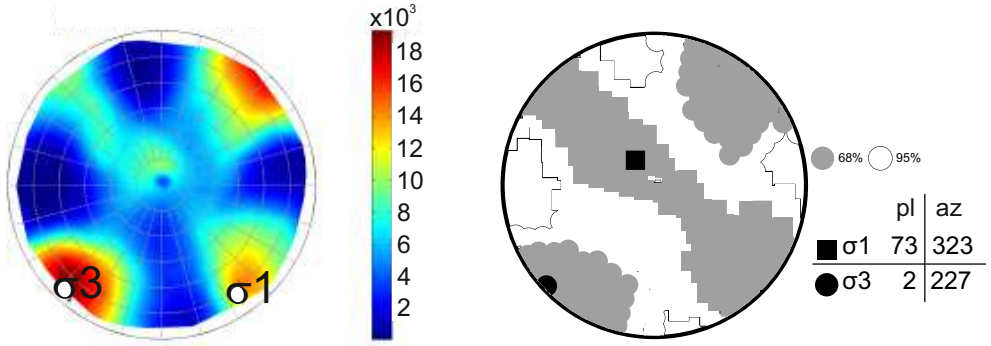

Smax: 45.642 PHI[1]: 84.1 R:0.30
pg=0.0538 pgn=1.0000 ampwt=0.1000

G

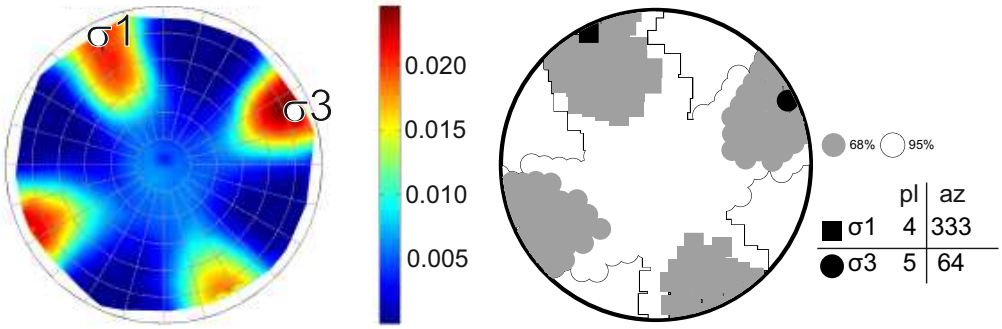

Smax: 53.864 PHI[3]: 85.6 R:0.30
pg=0.0538 pgn=1.0000 ampwt=0.1000

H

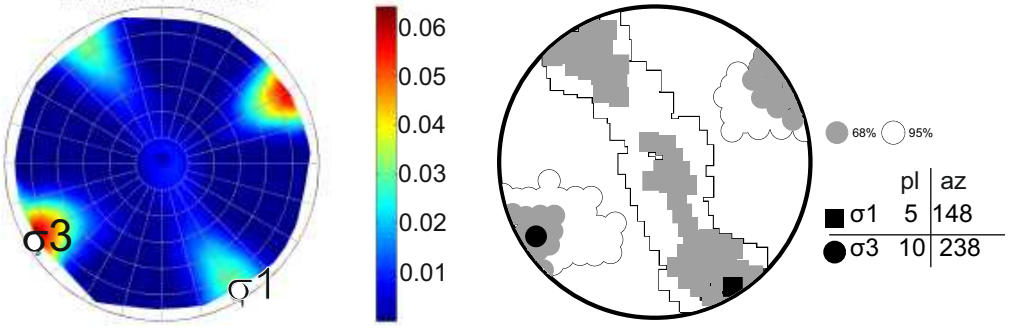

Smax: 95.163 PHI[1]: -80.3 R:0.60
pg=0.0538 pgn=1.0000 ampwt=0.1000

POSTSEISMIC (B - E)

B

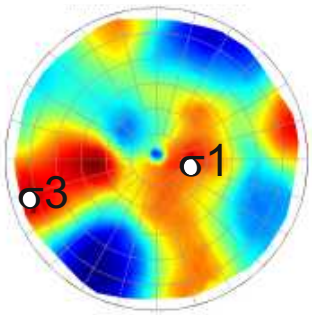

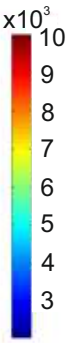

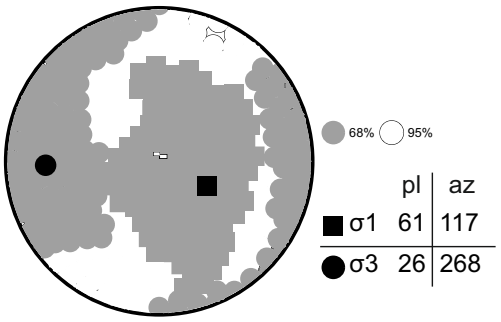

Smax: 31.614 PHI[1]: -25.5 R:0.50
pg=0.0538 pgn=1.0000 ampwt=0.1000

C

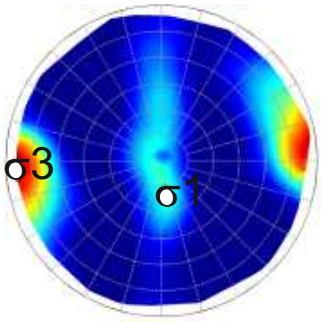

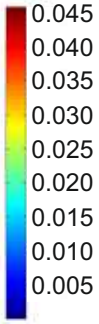

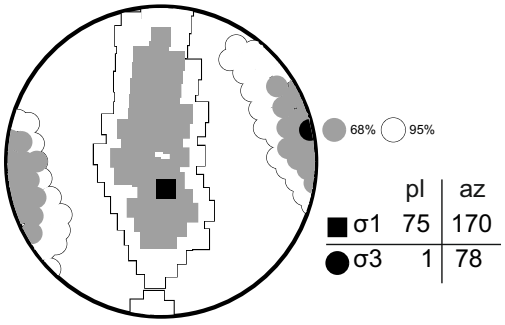

Smax: 121.424 PHI[3]: -14.9 R:0.50
pg=0.0538 pgn=1.0000 ampwt=0.1000

D

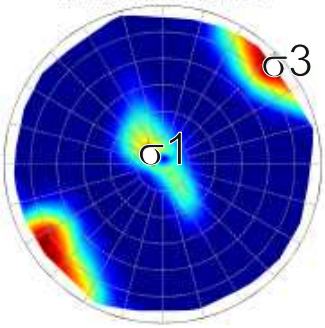

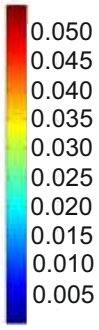

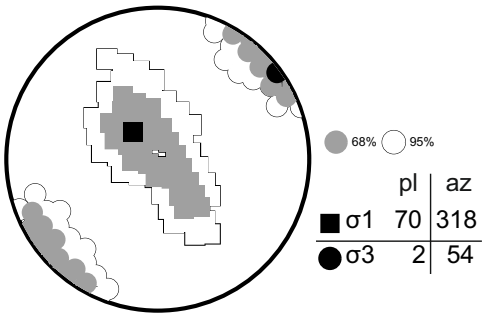

Smax: 120.561 PHI[3]: 19.9 R:0.50
pg=0.0538 pgn=1.0000 ampwt=0.1000

E

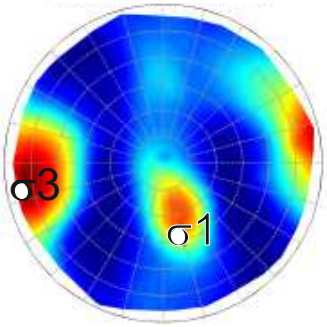

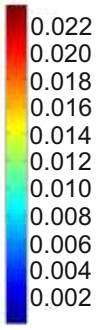

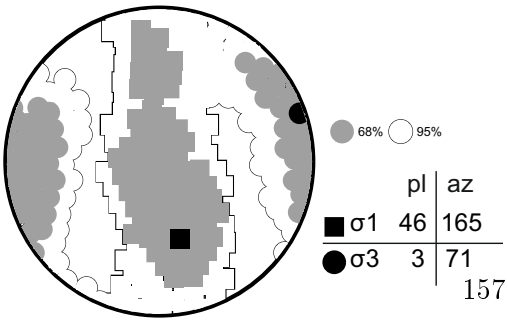

Smax: 67.680 PHI[1]: 85.2 R:0.50
pg=0.0538 pgn=1.0000 ampwt=0.1000

POSTSEISMIC (F - I)

F

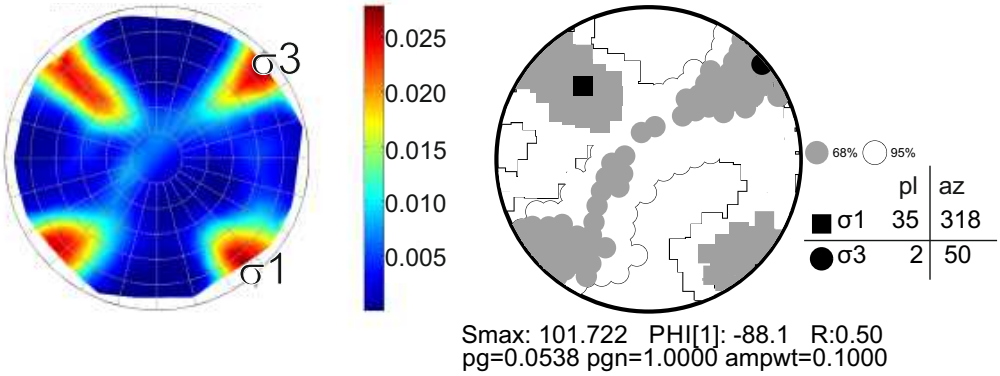

Smax: 101.722 PHI[1]: -88.1 R:0.50
pg=0.0538 pgn=1.0000 ampwt=0.1000

G

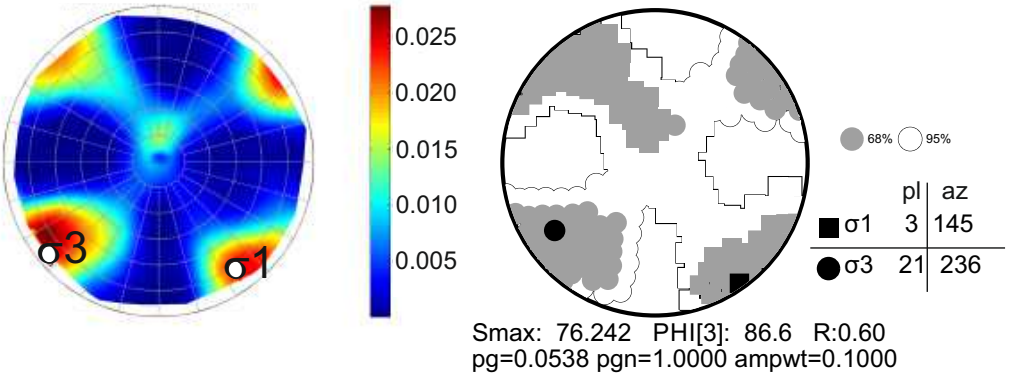

Smax: 76.242 PHI[3]: 86.6 R:0.60
pg=0.0538 pgn=1.0000 ampwt=0.1000

H

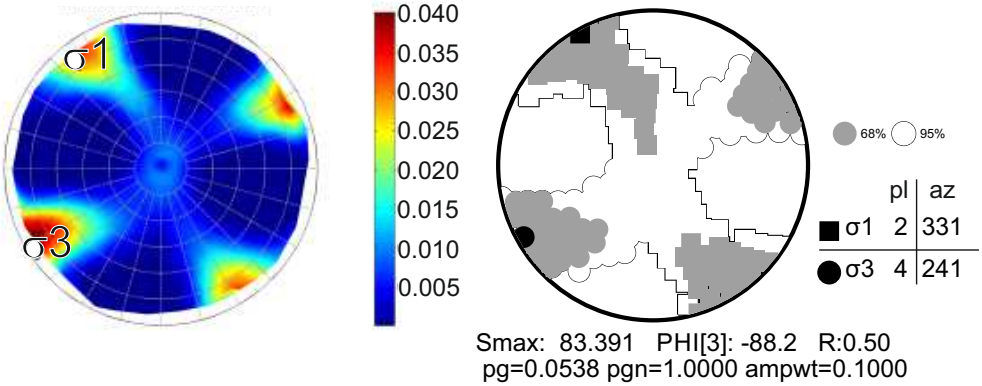

Smax: 83.391 PHI[3]: -88.2 R:0.50
pg=0.0538 pgn=1.0000 ampwt=0.1000

I

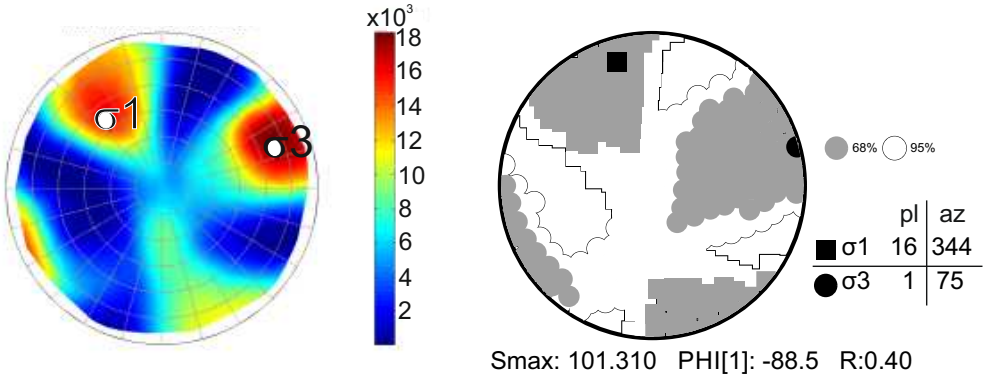

Smax: 101.310 PHI[1]: -88.5 R:0.40
pg=0.0538 pgn=1.0000 ampwt=0.1000

E. Focal Mechanism Database

Year	Month	Day	Hour	Minute	Second	Latitude [°]	Latitude [°]	Depth [km]	Magnitude	Strike	Dip	Rake	Source
1939	12	26	23	57	0	39.8	39.38	0	7.8	200	61	4	Şengör et al., 2005
1942	12	20	14	3	0	40.66	36.35	0	7.1	128	71	-176	Şengör et al., 2005
1943	6	20	15	32	0	40.7	30.38	10	6.5	86	90	166	Kiratzi, 2002, 2002
1943	11	26	22	20	0	40.97	33.22	0	7.3	269	73	173	Şengör et al., 2005
1944	2	1	3	22	0	41.1	33.2	0	7.3	332	77	31	Şengör et al., 2005
1951	8	13	18	33	0	40.86	32.68	0	6.9	348	83	-20	Şengör et al., 2005
1953	3	18	19	6	0	40.02	27.25	7	7.3	60	90	180	Kiratzi, 2002
1953	9	7	3	58	0	40.94	33.13	0	6.1	281	72	-158	Şengör et al., 2005
1956	2	20	0	0	0	39.86	30.49	0	6.5	140	56	-51	Gurbuz et al., 2000
1957	5	26	6	33	0	40.5	31.25	10	7.1	78	90	180	Kiratzi, 2002
1957	5	26	9	36	0	40.6	31.3	10	6	78	90	180	Kiratzi, 2002
1957	5	27	11	1	0	40.7	31	0	5.5	293	74	157	Şengör et al., 2005
1957	7	7	5	58	0	39.21	40.23	0	5.1	237	51	54	Şengör et al., 2005
1963	9	18	16	58	0	40.71	29.09	15	6.4	304	56	-82	Şengör et al., 2005
1964	3	3	0	59	0	40.1	27.5	5	6	60	40	68	Kiratzi, 2002
1964	10	6	14	31	0	40.2	28.2	14	6.9	100	40	-90	Şengör et al., 2005
1965	8	23	14	8	0	40.39	26.12	33	5.9	261	70	-132	Şengör et al., 2005
1967	7	22	16	56	0	40.67	30.69	12	7.1	275	88	-178	Şengör et al., 2005
1967	7	26	18	53	0	39.54	40.38	30	6	194	72	6	Şengör et al., 2005
1967	7	30	1	31	0	40.7	30.4	16	5.6	301	50	-110	Kiratzi, 2002
1969	3	3	0	59	0	40.08	27.5	4	5.7	219	65	45	Şengör et al., 2005
1971	2	23	19	41	0	39.6	27.37	15	5.4	185	72	26	Kiratzi, 2002
1972	4	26	6	30	0	39.5	26.35	26	5.1	150	73	-26	Kiratzi, 2002
1975	3	27	5	15	0	40.34	26.14	15	6.2	68	55	-145	Kiratzi, 2002
1977	10	5	5	34	0	41.02	33.57	8	5.8	76	90	173	Şengör et al., 2005
1979	7	18	0	0	0	39.67	28.66	0	5.2	111	34	-85	Gurbuz et al., 2000
1983	7	5	0	0	0	40.33	27.23	0	6.1	254	49	-173	Gurbuz et al., 2000
1983	7	5	12	1	0	40.32	27.22	10	6.1	254	49	-173	Kiratzi, 2002
1983	10	10	10	17	0	40.23	26.8	11	5.5	70	64	176	Kiratzi, 2002
1983	10	21	20	34	0	40.09	29.33	15	5.4	217	90	180	Kiratzi, 2002
1983	11	18	1	15	0	39.79	39.43	10	5.4	156	21	-102	Şengör et al., 2005
1988	4	24	20	49	0	40.83	28.24	15	5.3	355	70	-11	Kiratzi, 2002
1990	4	20	23	30	0	40.12	40.07	15	5.4	299	90	-180	Şengör et al., 2005
1992	3	13	17	18	0	39.72	39.63	15	6.7	213	85	4	Şengör et al., 2005
1992	3	15	16	16	0	39.53	39.93	15	5.9	61	70	14	Şengör et al., 2005
1995	1	29	4	16	0	39.82	40.64	33	5.2	211	70	1	Şengör et al., 2005
1995	2	8	21	24	0	40.82	27.77	12	4.5	33	42	-137	Pinar et al., 2003
1995	4	13	4	8	0	40.86	27.67	12	5	92	46	-137	Pinar et al., 2003
1995	4	18	5	36	0	40.8	27.84	12	4.5	20	70	133	Pinar et al., 2003
1995	12	5	18	49	0	39.43	40.11	15	5.8	136	70	160	Şengör et al., 2005
1996	1	30	0	0	0	40.75	29.98	0	3	115	55	-30	Ergin et al., 1997
1996	2	6	0	0	0	40.6	29.04	0	2.1	175	70	-20	Ergin et al., 1997
1996	2	8	0	0	0	40.74	29.77	0	2.6	155	65	-10	Ergin et al., 1997
1996	2	8	0	0	0	40.74	29.77	0	3.3	155	70	0	Ergin et al., 1997
1996	2	11	0	0	0	40.69	29.99	0	2.8	175	70	0	Ergin et al., 1997
1996	2	13	0	0	0	40.83	28.89	0	2.9	120	85	-160	Ergin et al., 1997
1996	2	14	0	0	0	40.69	30	0	2.9	115	50	0	Ergin et al., 1997
1996	2	14	0	0	0	40.7	29.98	0	3.5	55	80	-100	Ergin et al., 1997
1996	2	15	0	0	0	40.71	29.99	0	3.1	105	75	110	Ergin et al., 1997
1996	2	16	0	0	0	40.68	29.99	0	3.1	350	40	170	Ergin et al., 1997
1996	2	24	0	0	0	40.7	29.98	0	2.8	140	60	0	Ergin et al., 1997
1996	2	29	0	0	0	40.67	30.02	0	3.2	225	85	150	Ergin et al., 1997
1996	2	29	0	0	0	40.69	30.02	0	3.2	350	70	40	Ergin et al., 1997
1996	3	2	0	0	0	40.61	29.14	0	1.6	65	45	-110	Ergin et al., 1997
1996	3	3	0	0	0	40.72	29.98	0	2.2	100	65	-40	Ergin et al., 1997
1996	3	16	0	0	0	40.77	29.78	0	2.8	155	65	0	Ergin et al., 1997
1996	3	30	0	0	0	40.71	29.71	0	3.3	115	50	-50	Ergin et al., 1997
1996	4	14	8	30	0	40.7	27.2	12	4.6	274	61	-112	Pinar et al., 2003
1996	6	7	0	0	0	40.68	29.91	0	2.1	35	90	0	Ergin et al., 1997
1996	6	10	0	0	0	40.69	29.95	0	2	315	90	180	Ergin et al., 1997
1996	6	25	0	0	0	40.8	29.95	0	2	115	10	-160	Ergin et al., 1997
1996	6	27	0	0	0	40.71	29.7	0	1.9	80	25	170	Ergin et al., 1997
1996	6	27	0	0	0	40.73	29.7	0	2.1	20	70	-90	Ergin et al., 1997
1996	7	1	0	0	0	40.63	30.13	0	2.3	70	25	40	Ergin et al., 1997

1996	7	2	0	0	0	40.71	29.89	0	1.9	355	45	90	Ergin et al., 1997
1996	7	5	0	0	0	40.71	29.88	0	2.2	125	50	110	Ergin et al., 1997
1996	7	8	0	0	0	40.63	30.17	0	2.2	40	15	-120	Ergin et al., 1997
1996	7	15	0	0	0	40.75	30.05	0	2.7	160	25	-90	Ergin et al., 1997
1996	7	16	0	0	0	40.74	30.04	0	2.4	140	55	140	Ergin et al., 1997
1996	7	26	0	0	0	40.77	30.1	0	2.3	40	85	-180	Ergin et al., 1997
1996	7	27	0	0	0	40.81	30.11	0	2.3	85	45	-120	Ergin et al., 1997
1996	7	27	0	0	0	40.87	29.04	0	2.5	290	90	-120	Ergin et al., 1997
1996	8	2	0	0	0	40.72	29.24	0	2.3	45	75	103	Ergin et al., 1997
1996	8	2	0	0	0	40.72	29.26	0	2.2	160	85	-10	Ergin et al., 1997
1996	8	13	0	0	0	40.73	30.02	0	2.7	80	40	80	Ergin et al., 1997
1996	8	14	1	55	0	40.75	35.3	15	5.7	116	70	176	Şengör et al., 2005
1996	8	28	0	0	0	40.73	30	0	3.2	150	65	-90	Ergin et al., 1997
1996	9	2	0	0	0	40.59	29.23	0	2.3	60	15	-90	Ergin et al., 1997
1996	9	3	0	0	0	40.81	30.06	0	2.3	90	45	100	Ergin et al., 1997
1998	4	13	15	14	0	39.18	41.1	15	5.3	272	75	-175	Şengör et al., 2005
1999	4	6	0	8	0	39.4	38.31	15	5.4	326	49	175	Şengör et al., 2005
1999	5	29	22	43	0	40.79	28.71	20	3.1	341	22	72	Pinar et al., 2003
1999	8	17	0	1	0	40.7	29.99	9	7.4	91	87	164	Şengör et al., 2005
1999	8	17	0	1	0	40.81	30.08	11	7.4	266	85	-175	Kiratzi, 2002
1999	8	17	1	31	0	40.75	29.11	11	4.7	202	68	1	Pinar et al., 2003
1999	8	17	1	33	0	40.76	29.11	11	5.2	112	88	170	Pinar et al., 2003
1999	8	17	1	48	0	40.77	29.07	11	4.2	208	82	-27	Pinar et al., 2003
1999	8	17	2	9	0	40.76	29.12	11	3.5	204	76	2	Pinar et al., 2003
1999	8	17	3	14	1.4	40.6	30.63	0	5.5	192	34	-82	Örgülü and Aktar, 2001
1999	8	17	4	14	24.9	40.75	29.12	9	4.6	109	84	144	Örgülü and Aktar, 2001
1999	8	17	5	10	8.8	40.72	30.01	6	4.6	29	80	-173	Örgülü and Aktar, 2001
1999	8	17	5	45	23.6	40.74	30.01	11	4.7	243	45	-163	Örgülü and Aktar, 2001
1999	8	17	5	54	43.5	40.78	29.09	9	4.3	290	74	-167	Örgülü and Aktar, 2001
1999	8	17	6	1	32.5	40.75	29.99	4	4	263	69	147	Örgülü and Aktar, 2001
1999	8	17	6	20	0	40.78	29.03	16	3.1	108	54	-175	Pinar et al., 2003
1999	8	17	6	27	59.2	40.88	31.09	0	4.5	262	46	-178	Örgülü and Aktar, 2001
1999	8	17	9	2	12.8	40.77	31.06	18	4.9	276	39	-159	Örgülü and Aktar, 2001
1999	8	17	9	36	17.4	40.83	31.15	5	4	276	41	-154	Örgülü and Aktar, 2001
1999	8	17	10	46	42.8	40.7	29.74	10	4.1	151	66	151	Örgülü and Aktar, 2001
1999	8	17	11	29	0	40.7	29.47	5	3.1	342	20	25	Pinar et al., 2003
1999	8	17	14	27	0	40.73	29.35	11	3.2	356	49	86	Pinar et al., 2003
1999	8	17	14	31	0	40.44	28.76	17	3.7	248	60	177	Pinar et al., 2003
1999	8	17	18	35	0	40.38	28.71	11	3.8	255	59	-169	Pinar et al., 2003
1999	8	17	20	30	0	40.73	29.35	11	3.9	20	72	17	Pinar et al., 2003
1999	8	17	20	30	42	40.74	29.33	11	4.1	292	65	175	Örgülü and Aktar, 2001
1999	8	18	0	45	0	40.75	29.09	5	3.5	196	66	-18	Pinar et al., 2003
1999	8	18	1	4	25.8	40.66	30.77	6	4	182	39	-77	Örgülü and Aktar, 2001
1999	8	19	3	18	0	40.73	30.03	8.4	3.6	224	64	-124	Özalaybey et al., 2002
1999	8	19	5	11	0	40.71	30.01	7.1	3.6	70	55	-90	Özalaybey et al., 2002
1999	8	19	13	4	13.8	40.64	30.58	9	4.2	195	53	-83	Örgülü and Aktar, 2001
1999	8	19	14	2	0	40.71	29.99	4.7	3.7	85	50	-120	Özalaybey et al., 2002
1999	8	19	14	15	59.3	40.65	29.07	1	4.5	73	72	-125	Örgülü and Aktar, 2001
1999	8	19	14	24	0	40.6	29.1	2	3.8	146	49	-56	Pinar et al., 2003
1999	8	19	15	17	45.1	40.65	29.09	0	4.4	92	60	-110	Örgülü and Aktar, 2001
1999	8	19	15	48	0	40.64	29.15	11	3.7	154	75	-45	Pinar et al., 2003
1999	8	20	0	3	0	40.72	29.8	11.9	3.9	110	71	-60	Özalaybey et al., 2002
1999	8	20	9	28	0	40.59	29.12	5	4.4	105	46	-56	Pinar et al., 2003
1999	8	20	9	28	56.1	40.61	29.08	2	4.2	236	34	-156	Örgülü and Aktar, 2001
1999	8	20	9	34	0	40.62	29.18	8	3.6	114	30	-41	Pinar et al., 2003
1999	8	20	9	48	0	40.75	29.91	6.8	3.5	45	71	168	Özalaybey et al., 2002
1999	8	20	15	59	2.8	40.78	30.93	10	4.1	246	57	150	Örgülü and Aktar, 2001
1999	8	20	20	12	0	40.59	29.05	2	3.9	121	46	-65	Pinar et al., 2003
1999	8	20	20	12	0	40.62	29.06	4.5	3.5	110	70	-60	Özalaybey et al., 2002
1999	8	21	0	40	0	40.76	30.11	10	3.7	65	70	180	Özalaybey et al., 2002
1999	8	21	11	36	0	40.84	28.77	11	3.1	293	58	-143	Pinar et al., 2003
1999	8	21	21	8	0	40.83	28.81	11	3.2	5	72	-40	Pinar et al., 2003
1999	8	21	23	34	0	40.67	29.06	0	4	88	56	-110	Polat et al., 2002
1999	8	22	0	2	3.8	40.66	30.57	9.8	1.1	6	45	-123	Bohnhoff et al., 2006
1999	8	22	0	7	28.6	40.62	30.64	12.2	1.8	72	51	-63	Bohnhoff et al., 2006
1999	8	22	0	25	57.8	40.68	30.35	14.6	1	24	49	17	Bohnhoff et al., 2006

1999	8	22	1	9	32.7	40.71	30.55	6.9	1.2	69	75	-17	Bohnhoff et al., 2006
1999	8	22	1	36	21.4	40.59	30.58	6.3	2.3	39	59	-18	Bohnhoff et al., 2006
1999	8	22	1	43	2.1	40.65	30.55	7.2	2.4	141	51	-121	Bohnhoff et al., 2006
1999	8	22	1	45	12.3	40.73	30.55	22.9	1.3	11	77	77	Bohnhoff et al., 2006
1999	8	22	1	47	0	40.6	29.16	2	4.1	140	23	-77	Pinar et al., 2003
1999	8	22	2	12	45.7	40.65	30.44	7.1	2.4	184	47	-77	Bohnhoff et al., 2006
1999	8	22	2	34	43.5	40.76	30.81	12.3	2.2	159	85	-61	Bohnhoff et al., 2006
1999	8	22	2	44	17.1	40.71	30.42	8.3	2	89	54	-82	Bohnhoff et al., 2006
1999	8	22	2	54	27.5	40.81	31.05	9.5	1.4	9	62	17	Bohnhoff et al., 2006
1999	8	22	3	14	36.2	40.65	30.66	5.7	1.4	1	46	-120	Bohnhoff et al., 2006
1999	8	22	3	17	28.2	40.66	30.67	6.7	2.3	5	47	-117	Bohnhoff et al., 2006
1999	8	22	3	45	30.3	40.68	30.43	11.3	2.1	17	58	-43	Bohnhoff et al., 2006
1999	8	22	3	50	10.3	40.8	31	6.7	2.6	38	67	-160	Bohnhoff et al., 2006
1999	8	22	3	51	12.7	40.67	30.44	9.4	2.9	61	51	-40	Bohnhoff et al., 2006
1999	8	22	4	41	41.1	40.75	29.92	6.7	2.8	20	31	17	Bohnhoff et al., 2006
1999	8	22	4	59	39.3	40.66	30.67	6.2	1.8	185	30	-40	Bohnhoff et al., 2006
1999	8	22	5	49	27.2	40.64	30.61	10.4	2.4	70	51	-77	Bohnhoff et al., 2006
1999	8	22	6	3	47.3	40.62	30.68	12.6	2.3	78	39	83	Bohnhoff et al., 2006
1999	8	22	6	49	51.2	40.7	30.55	8.4	2.8	168	52	-103	Bohnhoff et al., 2006
1999	8	22	8	23	0	40.69	29.42	8	3.6	354	84	-43	Pinar et al., 2003
1999	8	22	8	34	17.9	40.66	30.68	9.2	2.2	1	60	-99	Bohnhoff et al., 2006
1999	8	22	10	30	55.2	40.65	30.59	8.1	1.4	60	54	-99	Bohnhoff et al., 2006
1999	8	22	10	41	19.4	40.66	30.56	8.8	2.1	140	57	-123	Bohnhoff et al., 2006
1999	8	22	12	9	30.7	40.7	30.69	8.9	2.2	21	55	-138	Bohnhoff et al., 2006
1999	8	22	13	36	33.5	40.77	31.01	5	3	20	53	37	Bohnhoff et al., 2006
1999	8	22	14	31	0.4	40.67	30.77	9	4.4	276	72	-165	Örgülü and Aktar, 2001
1999	8	22	15	17	25.9	40.68	30.71	12.4	3.1	26	43	-62	Bohnhoff et al., 2006
1999	8	22	15	29	24.1	40.64	30.69	12.6	1.2	75	69	57	Bohnhoff et al., 2006
1999	8	22	15	57	17.6	40.74	30.98	9.5	2.9	129	38	163	Bohnhoff et al., 2006
1999	8	22	16	30	34.2	40.75	30.98	10.7	2.6	35	65	17	Bohnhoff et al., 2006
1999	8	22	16	36	39.6	40.65	30.56	9.8	1.8	8	47	-123	Bohnhoff et al., 2006
1999	8	22	17	5	17.4	40.67	30.53	10.9	3.5	135	19	-77	Bohnhoff et al., 2006
1999	8	22	17	22	54	40.68	30.7	12	2.6	36	42	-63	Bohnhoff et al., 2006
1999	8	22	17	49	56.5	40.63	30.61	9.8	1.8	24	47	-79	Bohnhoff et al., 2006
1999	8	22	20	34	47	40.81	31.07	12.7	3.3	79	84	-143	Bohnhoff et al., 2006
1999	8	22	20	51	34.7	40.75	30.23	13.8	2.2	36	50	137	Bohnhoff et al., 2006
1999	8	22	22	10	30.9	40.68	30.69	12	2.2	25	40	-77	Bohnhoff et al., 2006
1999	8	22	22	19	43.7	40.65	30.56	9.2	1.8	7	49	-63	Bohnhoff et al., 2006
1999	8	22	22	42	21.9	40.64	30.52	12.1	1.3	320	81	-163	Bohnhoff et al., 2006
1999	8	23	0	4	26.7	40.68	30.4	7.4	2.2	175	68	-97	Bohnhoff et al., 2006
1999	8	23	0	17	36.7	40.65	30.69	10.5	1.6	183	41	-77	Bohnhoff et al., 2006
1999	8	23	0	18	44.8	40.69	30.69	11.6	2.2	27	43	-77	Bohnhoff et al., 2006
1999	8	23	0	21	11.3	40.79	31.15	11.4	2.2	31	58	-40	Bohnhoff et al., 2006
1999	8	23	1	31	1.1	40.66	30.5	10.5	1.7	8	37	-83	Bohnhoff et al., 2006
1999	8	23	1	55	7.5	40.67	30.61	7	3.5	14	45	-82	Bohnhoff et al., 2006
1999	8	23	2	17	52.6	40.67	30.61	6.8	1.6	104	36	-140	Bohnhoff et al., 2006
1999	8	23	2	36	16.3	40.68	30.61	7.4	2.3	16	47	-80	Bohnhoff et al., 2006
1999	8	23	2	45	1.6	40.69	30.46	11.4	2	121	29	-163	Bohnhoff et al., 2006
1999	8	23	2	56	41.3	40.68	30.63	6.6	2.3	20	42	-118	Bohnhoff et al., 2006
1999	8	23	3	21	54	40.75	30.99	8.2	2.3	17	79	17	Bohnhoff et al., 2006
1999	8	23	4	7	38.4	40.67	30.54	11.4	1.9	158	42	-117	Bohnhoff et al., 2006
1999	8	23	4	15	3.6	40.68	30.62	7	2.1	162	49	-122	Bohnhoff et al., 2006
1999	8	23	4	34	35.1	40.68	30.54	10.3	1.3	168	40	-103	Bohnhoff et al., 2006
1999	8	23	4	37	37	40.77	30.85	12.6	1.9	12	73	23	Bohnhoff et al., 2006
1999	8	23	4	40	6.7	40.64	30.55	6.9	2.7	40	78	-20	Bohnhoff et al., 2006
1999	8	23	4	48	50.3	40.7	30.71	11	2.2	131	64	-83	Bohnhoff et al., 2006
1999	8	23	4	50	28.2	40.65	30.69	11.8	2.5	4	58	-123	Bohnhoff et al., 2006
1999	8	23	5	2	45.7	40.68	30.65	10.9	2.1	88	49	-137	Bohnhoff et al., 2006
1999	8	23	5	9	4.5	40.65	30.54	9.9	2.9	34	42	-57	Bohnhoff et al., 2006
1999	8	23	5	36	17.1	40.65	30.52	10.8	2.4	359	52	-122	Bohnhoff et al., 2006
1999	8	23	5	51	49.6	40.78	30.93	11.3	2.8	159	56	-1	Bohnhoff et al., 2006
1999	8	23	6	13	1.6	40.75	30.79	10.1	2.1	13	80	80	Bohnhoff et al., 2006
1999	8	23	6	30	20.6	40.69	30.63	9.1	3	88	59	-77	Bohnhoff et al., 2006
1999	8	23	6	31	18.5	40.64	30.53	10.3	2.3	70	33	-80	Bohnhoff et al., 2006
1999	8	23	7	5	46.1	40.69	30.63	9.5	3.1	19	46	-77	Bohnhoff et al., 2006
1999	8	23	9	18	16.8	40.64	30.65	7.9	3	163	52	-117	Bohnhoff et al., 2006

1999	8	23	9	41	41.5	40.68	30.58	11.6	2.6	170	43	-117	Bohnhoff et al., 2006
1999	8	23	11	5	57.2	40.68	30.58	11.3	2.7	157	47	-117	Bohnhoff et al., 2006
1999	8	23	11	20	47.4	40.79	31.1	4.7	1.8	170	30	38	Bohnhoff et al., 2006
1999	8	23	12	51	15.3	40.65	30.66	6.3	1.3	33	83	-42	Bohnhoff et al., 2006
1999	8	23	12	59	42.4	40.62	30.59	9.1	2.9	156	57	-123	Bohnhoff et al., 2006
1999	8	23	13	16	16.9	40.64	30.77	10.7	2.2	17	48	-63	Bohnhoff et al., 2006
1999	8	23	13	49	54.9	40.64	30.69	10.8	1.9	1	65	-123	Bohnhoff et al., 2006
1999	8	23	13	59	0.7	40.63	30.54	10.2	2.6	26	59	-63	Bohnhoff et al., 2006
1999	8	23	14	9	42.7	40.65	30.57	8.4	2	39	73	-17	Bohnhoff et al., 2006
1999	8	23	14	23	57.2	40.68	30.48	10.9	1.8	171	58	-123	Bohnhoff et al., 2006
1999	8	23	14	30	49.5	40.67	30.69	10.9	1.4	149	89	119	Bohnhoff et al., 2006
1999	8	23	16	0	28.4	40.78	30.44	13.3	2.2	32	72	163	Bohnhoff et al., 2006
1999	8	23	16	32	24.4	40.65	30.65	9.4	2.7	157	55	-123	Bohnhoff et al., 2006
1999	8	23	17	23	42.5	40.66	30.53	10.9	3.6	18	50	-57	Bohnhoff et al., 2006
1999	8	23	18	7	41.8	40.63	30.54	9.6	2.5	34	63	-37	Bohnhoff et al., 2006
1999	8	23	18	31	26.7	40.71	30.5	10.6	2	90	45	-77	Bohnhoff et al., 2006
1999	8	23	19	31	38.3	40.64	30.55	7.7	1.3	61	58	-98	Bohnhoff et al., 2006
1999	8	23	19	36	15.2	40.68	30.67	12.5	3.6	25	42	-57	Bohnhoff et al., 2006
1999	8	23	20	1	0	40.57	28.1	15	3.7	270	67	162	Pinar et al., 2003
1999	8	23	20	35	25.6	40.62	30.59	9.9	3	151	54	-137	Bohnhoff et al., 2006
1999	8	23	20	59	31.6	40.78	31.05	12.4	2.8	96	81	163	Bohnhoff et al., 2006
1999	8	23	21	29	22.5	40.64	30.65	8.8	3.7	159	31	-97	Bohnhoff et al., 2006
1999	8	23	21	44	29.3	40.7	30.67	11.8	2.5	52	54	-38	Bohnhoff et al., 2006
1999	8	23	21	47	3.6	40.68	30.45	12.7	2.5	123	90	163	Bohnhoff et al., 2006
1999	8	23	21	54	0	40.69	29.22	5	3.9	48	56	-168	Pinar et al., 2003
1999	8	23	22	31	2.4	40.68	29.2	6.3	3.4	85	62	162	Bohnhoff et al., 2006
1999	8	23	22	36	0	40.69	29.21	14	3.4	65	36	178	Pinar et al., 2003
1999	8	23	22	36	37.4	40.78	31.16	11.2	1.9	142	21	-163	Bohnhoff et al., 2006
1999	8	23	23	18	54.2	40.63	30.57	10.4	2.6	169	44	-103	Bohnhoff et al., 2006
1999	8	23	23	49	24.5	40.66	30.46	7.3	1.6	23	69	-57	Bohnhoff et al., 2006
1999	8	23	23	55	50.5	40.8	30.89	13	2.4	89	66	77	Bohnhoff et al., 2006
1999	8	24	0	9	18.2	40.67	30.62	8.5	2	71	53	-83	Bohnhoff et al., 2006
1999	8	24	0	14	36.7	40.76	31.02	6.9	1.8	211	54	-37	Görgün et al., 2009
1999	8	24	0	42	55.5	40.69	30.68	9.5	2.7	70	43	-83	Bohnhoff et al., 2006
1999	8	24	1	3	3.6	40.8	30.95	10.8	2.1	8	57	-66	Görgün et al., 2009
1999	8	24	2	13	35	40.77	29.9	13.7	2.1	156	55	-77	Bohnhoff et al., 2006
1999	8	24	2	17	55.6	40.72	29.66	13.7	2.3	51	72	82	Bohnhoff et al., 2006
1999	8	24	2	35	41	40.75	30.81	11.1	1.7	4	79	77	Bohnhoff et al., 2006
1999	8	24	3	43	31.5	40.7	30.43	9.7	2.2	96	25	-42	Bohnhoff et al., 2006
1999	8	24	3	59	29.7	40.78	30.93	10.1	2.3	153	69	-17	Bohnhoff et al., 2006
1999	8	24	4	31	6.8	40.72	29.65	10.4	4.1	118	42	-143	Bohnhoff et al., 2006
1999	8	24	5	30	0	40.72	29.66	7.6	3.7	292	85	-180	Özalaybey et al., 2002
1999	8	24	5	30	31	40.65	30.65	6.9	2.4	41	81	-17	Bohnhoff et al., 2006
1999	8	24	6	42	28.8	40.7	30.68	6.1	3	71	51	162	Bohnhoff et al., 2006
1999	8	24	8	14	0.3	40.7	30.63	11.8	3	12	43	-42	Bohnhoff et al., 2006
1999	8	24	11	9	5.1	40.77	31.05	8	2.1	39	79	-49	Görgün et al., 2009
1999	8	24	11	38	39.7	40.77	31.04	10.2	2.2	45	84	-17	Bohnhoff et al., 2006
1999	8	24	15	3	9.2	40.7	30.62	8.4	2.3	21	55	-123	Bohnhoff et al., 2006
1999	8	24	16	55	33.4	40.69	30.71	12.2	2.5	175	58	-97	Bohnhoff et al., 2006
1999	8	24	18	50	32.3	40.72	30.01	14.2	4.1	57	39	-77	Bohnhoff et al., 2006
1999	8	24	18	58	59	40.72	30.01	13.9	3	107	53	-77	Bohnhoff et al., 2006
1999	8	24	19	1	33.7	40.66	30.47	13.8	1.9	18	36	-138	Bohnhoff et al., 2006
1999	8	24	19	15	14.1	40.72	29.56	4.9	2.7	95	61	63	Bohnhoff et al., 2006
1999	8	24	19	20	33.4	40.64	30.65	6.9	2.7	350	42	-121	Bohnhoff et al., 2006
1999	8	24	20	50	23.8	40.69	30.72	11.7	2.5	159	47	-98	Bohnhoff et al., 2006
1999	8	24	21	13	14.1	40.65	30.65	7	2.7	21	41	-80	Bohnhoff et al., 2006
1999	8	24	21	13	48.6	40.68	30.4	15.3	2.2	175	49	-117	Bohnhoff et al., 2006
1999	8	24	22	48	20.7	40.69	30.67	10.6	3.4	172	52	-117	Bohnhoff et al., 2006
1999	8	24	23	3	55.4	40.68	30.59	6.9	3.1	350	40	-120	Bohnhoff et al., 2006
1999	8	24	23	13	44	40.73	29.83	6.6	2.2	92	47	99	Bohnhoff et al., 2006
1999	8	25	0	6	52.3	40.62	30.64	10.9	1.3	161	55	-123	Bohnhoff et al., 2006
1999	8	25	0	12	27.5	40.63	30.64	6.3	2.5	4	46	-103	Bohnhoff et al., 2006
1999	8	25	0	15	58.2	40.65	30.66	9.3	3.2	17	42	-80	Bohnhoff et al., 2006
1999	8	25	0	36	47	40.64	30.69	6.5	2.2	180	31	137	Bohnhoff et al., 2006
1999	8	25	0	39	18.6	40.64	30.68	7.9	2.2	78	34	-98	Bohnhoff et al., 2006
1999	8	25	0	39	18.6	40.71	30.66	6.9	1	12	50	-103	Bohnhoff et al., 2006

1999	8	25	0	40	14.8	40.6	30.53	12.5	2.8	148	46	-36	Bohnhoff et al., 2006
1999	8	25	0	51	5.8	40.62	30.55	6.8	2.8	172	49	-103	Bohnhoff et al., 2006
1999	8	25	0	51	5.9	40.63	30.57	5.2	1.5	145	30	-83	Bohnhoff et al., 2006
1999	8	25	1	4	19.8	40.72	30.01	10.4	2.5	187	49	146	Bohnhoff et al., 2006
1999	8	25	2	12	18.2	40.63	30.67	11.7	1.6	86	8	-3	Bohnhoff et al., 2006
1999	8	25	2	48	15.3	40.7	30.61	9.9	3.9	15	48	-77	Bohnhoff et al., 2006
1999	8	25	3	6	23.7	40.69	30.62	10.7	2.3	25	48	-63	Bohnhoff et al., 2006
1999	8	25	3	14	26.2	40.64	30.53	11.4	1.8	87	28	-63	Bohnhoff et al., 2006
1999	8	25	3	41	43.4	40.62	30.54	6.9	2.9	43	77	-17	Bohnhoff et al., 2006
1999	8	25	3	44	59.2	40.62	30.54	6.5	3.3	42	76	-17	Bohnhoff et al., 2006
1999	8	25	3	45	47.6	40.62	30.54	5.7	3	42	76	-17	Bohnhoff et al., 2006
1999	8	25	4	5	10.5	40.64	30.53	11.6	2.7	148	52	-143	Bohnhoff et al., 2006
1999	8	25	4	55	17.1	40.75	30.79	13.3	3.7	333	81	42	Bohnhoff et al., 2006
1999	8	25	8	43	25.5	40.63	30.67	11.6	2.6	39	61	-38	Bohnhoff et al., 2006
1999	8	25	9	4	49.6	40.75	29.99	7.5	2.6	5	47	62	Bohnhoff et al., 2006
1999	8	25	10	34	18.7	40.64	30.56	9.3	3.3	150	56	-137	Bohnhoff et al., 2006
1999	8	25	11	18	51.2	40.79	31.16	12.3	2.5	142	72	-163	Bohnhoff et al., 2006
1999	8	25	12	40	13.1	40.66	30.55	8.4	3.5	150	57	-137	Bohnhoff et al., 2006
1999	8	25	15	4	25.8	40.78	30.85	13	2.2	180	87	-23	Bohnhoff et al., 2006
1999	8	25	15	14	9.2	40.79	31.06	12.2	1.9	122	56	-159	Bohnhoff et al., 2006
1999	8	25	15	16	39.4	40.65	30.67	4.2	1.1	141	63	-163	Bohnhoff et al., 2006
1999	8	25	15	46	54.7	40.78	31.03	12.6	2.1	138	50	-137	Bohnhoff et al., 2006
1999	8	25	16	17	8.4	40.67	30.67	8.4	2.3	59	51	-100	Bohnhoff et al., 2006
1999	8	25	18	4	17.9	40.67	30.55	8.4	1.4	148	54	-143	Bohnhoff et al., 2006
1999	8	25	18	44	47.4	40.69	30.4	1	2.6	148	43	-117	Bohnhoff et al., 2006
1999	8	25	19	5	37.2	40.78	31.05	10.4	1.5	28	63	-23	Bohnhoff et al., 2006
1999	8	25	20	56	6.7	40.67	30.63	11.4	1.7	31	69	-82	Bohnhoff et al., 2006
1999	8	25	23	0	48.2	40.65	30.69	10.9	1.8	27	39	-63	Bohnhoff et al., 2006
1999	8	25	23	15	16.9	40.63	30.61	10	2.1	165	53	-123	Bohnhoff et al., 2006
1999	8	26	0	8	29.6	40.79	31.07	10.3	2.2	176	72	-37	Bohnhoff et al., 2006
1999	8	26	1	56	24.8	40.7	30.7	11.8	3	32	39	-63	Bohnhoff et al., 2006
1999	8	26	2	12	27.2	40.79	31.07	12.2	2	100	49	-137	Bohnhoff et al., 2006
1999	8	26	3	24	17	40.71	29.44	11.4	2.4	133	83	-180	Bohnhoff et al., 2006
1999	8	26	4	9	45.6	40.71	29.53	13.5	2	12	83	-19	Bohnhoff et al., 2006
1999	8	26	4	12	32	40.78	31.04	12.4	2.2	48	78	-3	Bohnhoff et al., 2006
1999	8	26	5	3	42.2	40.74	29.13	7.5	2.8	11	88	37	Bohnhoff et al., 2006
1999	8	26	12	9	36.5	40.67	30.49	13.5	2.5	32	38	-58	Bohnhoff et al., 2006
1999	8	26	12	31	23.3	40.69	30.43	11	2.7	342	50	-100	Bohnhoff et al., 2006
1999	8	26	12	38	51.8	40.67	30.45	13.3	3.2	189	54	-62	Bohnhoff et al., 2006
1999	8	26	12	49	46.6	40.65	30.66	11.4	2.7	18	40	-77	Bohnhoff et al., 2006
1999	8	26	13	13	40.8	40.67	30.46	12.7	2.2	186	52	-81	Bohnhoff et al., 2006
1999	8	26	17	17	0.3	40.69	30.49	9.3	3.7	11	56	-83	Bohnhoff et al., 2006
1999	8	26	17	35	6.7	40.63	30.59	11.8	2.8	19	46	-79	Bohnhoff et al., 2006
1999	8	26	17	47	7.8	40.74	30.03	12.5	3.9	67	87	163	Bohnhoff et al., 2006
1999	8	26	17	49	0	40.73	30.04	11.5	3.8	85	90	-178	Özalaybey et al., 2002
1999	8	26	17	49	39	40.79	31.01	9.5	2	155	57	-103	Bohnhoff et al., 2006
1999	8	26	17	53	33.1	40.81	31.13	12.5	1.9	53	81	-17	Bohnhoff et al., 2006
1999	8	26	17	57	0.3	40.79	31.12	8.5	2.7	95	9	157	Bohnhoff et al., 2006
1999	8	26	18	1	24.2	40.81	31.03	8.2	2.6	36	42	117	Bohnhoff et al., 2006
1999	8	26	18	20	29.9	40.66	30.63	11.1	1.6	69	55	-77	Bohnhoff et al., 2006
1999	8	26	18	28	3.7	40.6	30.77	12.2	1.6	224	81	-18	Bohnhoff et al., 2006
1999	8	26	18	43	29.8	40.65	30.52	12.1	1.6	140	65	-159	Bohnhoff et al., 2006
1999	8	26	18	53	53.1	40.75	31	8.3	1.4	133	98	-177	Bohnhoff et al., 2006
1999	8	26	19	0	32.8	40.64	30.67	11.3	1.6	348	35	-99	Bohnhoff et al., 2006
1999	8	26	19	17	19.9	40.71	30.46	10.2	2.3	20	45	-83	Bohnhoff et al., 2006
1999	8	26	19	22	57.2	40.7	30.68	11.2	2.6	28	40	-63	Bohnhoff et al., 2006
1999	8	26	19	29	4.8	40.78	30.86	12.3	1.8	39	59	21	Bohnhoff et al., 2006
1999	8	26	19	33	46.1	40.64	30.62	10.1	1.9	17	46	-77	Bohnhoff et al., 2006
1999	8	26	19	41	45.3	40.64	30.66	9.4	2.3	159	28	-103	Bohnhoff et al., 2006
1999	8	26	19	45	14.9	40.69	30.5	9.3	3	11	56	-83	Bohnhoff et al., 2006
1999	8	26	20	12	25.6	40.66	30.5	11.7	3.6	184	52	-82	Bohnhoff et al., 2006
1999	8	26	20	17	34.3	40.63	30.59	12.1	2.7	3	43	-103	Bohnhoff et al., 2006
1999	8	26	20	22	30.5	40.75	30.12	14.8	1.4	163	57	-77	Bohnhoff et al., 2006
1999	8	26	21	12	1.9	40.7	30.63	9.9	2.2	163	54	-83	Bohnhoff et al., 2006
1999	8	26	21	35	34	40.72	30.71	12.1	1.9	104	49	-117	Bohnhoff et al., 2006
1999	8	26	21	44	45.7	40.74	30.04	11.8	3.2	143	69	-3	Bohnhoff et al., 2006

1999	8	26	21	49	54.5	40.66	30.46	13.6	1.9	189	36	-77	Bohnhoff et al., 2006
1999	8	26	21	53	42.6	40.72	29.49	17.5	2	153	77	163	Bohnhoff et al., 2006
1999	8	26	23	1	7.8	40.7	30.69	12	3	13	38	-143	Bohnhoff et al., 2006
1999	8	26	23	13	22	40.68	30.5	9.5	3.1	121	31	-123	Bohnhoff et al., 2006
1999	8	26	23	39	2.6	40.7	30.57	11.2	2	25	45	-97	Bohnhoff et al., 2006
1999	8	27	0	0	15.1	40.63	30.66	7.7	2.4	170	30	-103	Bohnhoff et al., 2006
1999	8	27	0	25	6	40.63	30.66	6.8	2.2	189	44	-57	Bohnhoff et al., 2006
1999	8	27	0	35	23	40.63	30.59	10.9	0.8	19	48	-77	Bohnhoff et al., 2006
1999	8	27	0	36	55.3	40.73	30.67	11.6	1.6	106	78	-123	Bohnhoff et al., 2006
1999	8	27	0	53	22.6	40.78	30.87	12.1	2	151	75	-85	Görgün et al., 2009
1999	8	27	0	55	6.9	40.67	30.68	6.9	1.3	182	36	-83	Bohnhoff et al., 2006
1999	8	27	1	1	52.4	40.78	31.11	11.1	1.7	84	83	-163	Bohnhoff et al., 2006
1999	8	27	1	7	25.4	40.63	30.66	7.4	2.1	81	31	-98	Bohnhoff et al., 2006
1999	8	27	1	15	6	40.67	30.68	5	1.5	14	47	-63	Bohnhoff et al., 2006
1999	8	27	1	21	6	40.76	30.01	10.1	1.7	135	89	-37	Bohnhoff et al., 2006
1999	8	27	1	52	21.9	40.77	30.09	12.1	1.8	96	66	-38	Bohnhoff et al., 2006
1999	8	27	2	31	1.7	40.77	31.09	12.4	2.1	140	53	-143	Bohnhoff et al., 2006
1999	8	27	2	40	51.3	40.71	30.31	16.5	1.2	81	67	143	Bohnhoff et al., 2006
1999	8	27	2	41	40.8	40.78	31.1	8	2.1	259	62	50	Görgün et al., 2009
1999	8	27	2	52	44.3	40.65	30.53	10.3	1.8	31	47	-77	Bohnhoff et al., 2006
1999	8	27	2	54	42.6	40.79	31.07	13	2.1	130	90	163	Bohnhoff et al., 2006
1999	8	27	3	1	10.3	40.63	30.66	8.9	2.7	171	23	-102	Bohnhoff et al., 2006
1999	8	27	3	1	59.9	40.79	31.09	10.1	2.2	22	56	-77	Görgün et al., 2009
1999	8	27	3	12	33.5	40.76	30.8	12.6	2.8	21	77	77	Bohnhoff et al., 2006
1999	8	27	3	15	20.9	40.71	30.71	9.8	2.3	7	43	-137	Bohnhoff et al., 2006
1999	8	27	3	21	27.8	40.67	30.53	6.9	1.5	189	43	-63	Bohnhoff et al., 2006
1999	8	27	3	31	40.6	40.7	30.83	11.7	1.5	121	89	-180	Bohnhoff et al., 2006
1999	8	27	3	33	54.9	40.66	30.53	12.3	1.9	125	59	-163	Bohnhoff et al., 2006
1999	8	27	3	49	26.3	40.64	30.5	10.1	1.6	10	67	-37	Bohnhoff et al., 2006
1999	8	27	4	13	31.2	40.66	30.68	10.3	2.2	182	42	-77	Bohnhoff et al., 2006
1999	8	27	4	16	55.6	40.66	30.67	9.3	2.6	189	53	-59	Bohnhoff et al., 2006
1999	8	27	4	22	11	40.66	30.51	13.2	1.7	17	61	-63	Bohnhoff et al., 2006
1999	8	27	5	8	5.8	40.69	30.2	14.8	1.8	137	54	-137	Bohnhoff et al., 2006
1999	8	27	5	45	30.1	40.65	30.49	11.6	2.5	142	45	-141	Bohnhoff et al., 2006
1999	8	27	6	9	30.9	40.67	30.52	12.2	1.9	162	70	-137	Bohnhoff et al., 2006
1999	8	27	6	29	38.3	40.78	31	9.9	0.9	316	81	-123	Bohnhoff et al., 2006
1999	8	27	6	41	59.2	40.78	30.98	7.9	1.8	281	90	70	Görgün et al., 2009
1999	8	27	6	59	24.5	40.77	31.02	10.1	3	141	79	-163	Bohnhoff et al., 2006
1999	8	27	7	44	48.6	40.76	30.81	14.5	1.9	143	55	-59	Görgün et al., 2009
1999	8	27	7	53	21.8	40.8	30.92	13.3	2	88	75	80	Görgün et al., 2009
1999	8	27	8	44	56.8	40.78	31.01	10.6	2.6	127	86	-180	Bohnhoff et al., 2006
1999	8	27	8	45	46.3	40.77	31.04	8	3.1	33	65	-55	Görgün et al., 2009
1999	8	27	9	20	16.8	40.76	30.79	12.9	1.7	21	72	79	Bohnhoff et al., 2006
1999	8	27	11	7	19.3	40.78	31.06	12.9	1.9	132	58	-163	Bohnhoff et al., 2006
1999	8	27	12	40	17.1	40.63	30.54	9.6	3.4	41	70	-17	Bohnhoff et al., 2006
1999	8	27	14	39	53	40.77	30.86	15.3	3.1	60	81	-180	Bohnhoff et al., 2006
1999	8	27	14	57	31.1	40.62	30.64	5.4	2	146	81	-162	Bohnhoff et al., 2006
1999	8	27	14	58	20.9	40.78	30.88	12.6	3.2	25	55	30	Görgün et al., 2009
1999	8	27	15	20	26	40.65	30.51	13.4	2	313	81	-176	Bohnhoff et al., 2006
1999	8	27	15	25	59.5	40.74	30.14	16.2	3.6	2	82	3	Bohnhoff et al., 2006
1999	8	27	15	39	40.6	40.69	30.65	11.6	2.1	26	64	-43	Bohnhoff et al., 2006
1999	8	27	16	7	20.6	40.74	29.98	11.1	1.9	46	50	-83	Bohnhoff et al., 2006
1999	8	27	16	10	36.1	40.79	31.19	11.9	2	132	66	-163	Bohnhoff et al., 2006
1999	8	27	16	15	39.1	40.73	29.82	17.2	1.7	78	38	-157	Bohnhoff et al., 2006
1999	8	27	16	56	13.9	40.69	30.52	13	3	78	47	-77	Bohnhoff et al., 2006
1999	8	27	17	20	48	40.73	29.75	7.8	2.5	155	63	18	Bohnhoff et al., 2006
1999	8	27	17	30	55.6	40.68	29.13	16.4	2.1	35	36	57	Bohnhoff et al., 2006
1999	8	27	17	35	0	40.77	29.21	5.7	2.2	135	60	-90	Karabulut et al., 2002
1999	8	27	18	4	14.6	40.78	31.05	10.1	1.8	21	68	-37	Bohnhoff et al., 2006
1999	8	27	18	12	41.2	40.67	30.45	9.1	1.6	70	46	-97	Bohnhoff et al., 2006
1999	8	27	18	15	15.2	40.65	30.6	11.3	2	39	74	-18	Bohnhoff et al., 2006
1999	8	27	18	28	33.6	40.78	31.03	6.9	2.7	169	79	-59	Bohnhoff et al., 2006
1999	8	27	18	56	56.5	40.68	29.16	14.1	2.1	33	64	-83	Bohnhoff et al., 2006
1999	8	27	18	57	45.8	40.77	31.05	6.1	2.8	338	36	-14	Görgün et al., 2009
1999	8	27	19	12	0	40.69	29.18	5.5	2.1	62	87	-49	Karabulut et al., 2002
1999	8	27	19	12	47	40.63	30.52	9	1.7	30	50	-57	Bohnhoff et al., 2006

1999	8	27	19	42	5.9	40.7	30.62	6.6	1	3	48	-123	Bohnhoff et al., 2006
1999	8	27	21	1	30.1	40.72	29.98	11	1.5	118	24	-161	Bohnhoff et al., 2006
1999	8	27	21	3	59.4	40.74	30.29	13.8	1.3	172	67	-57	Bohnhoff et al., 2006
1999	8	27	21	21	29.6	40.78	31.04	12	2.6	9	69	-57	Bohnhoff et al., 2006
1999	8	27	21	39	31.9	40.73	29.98	10.1	1.5	84	59	-99	Bohnhoff et al., 2006
1999	8	27	22	5	56.3	40.71	29.95	8.4	1.6	66	30	-137	Bohnhoff et al., 2006
1999	8	27	23	14	34.9	40.79	31.12	10.2	1.4	185	57	-13	Görgün et al., 2009
1999	8	27	23	38	37.7	40.8	31.18	12.3	1.6	132	63	-163	Bohnhoff et al., 2006
1999	8	27	23	42	52.3	40.74	30.93	13	3	290	83	-166	Bohnhoff et al., 2006
1999	8	28	2	11	3.2	40.77	31.07	9.2	1.8	68	73	-58	Görgün et al., 2009
1999	8	28	2	12	30.7	40.78	31.07	8.8	1.9	17	54	-59	Görgün et al., 2009
1999	8	28	2	17	17.8	40.76	30.94	12.5	2.7	169	30	-80	Görgün et al., 2009
1999	8	28	2	21	10.5	40.79	31.11	10.7	1.9	235	77	38	Görgün et al., 2009
1999	8	28	2	39	0	40.72	29.4	8.5	2.1	160	20	90	Karabulut et al., 2002
1999	8	28	3	3	0.5	40.76	31	7.6	1.4	258	27	67	Görgün et al., 2009
1999	8	28	5	23	0	40.6	29.13	5	3.5	217	77	-161	Pinar et al., 2003
1999	8	28	6	0	59.9	40.78	30.99	5.1	2.1	16	51	-77	Görgün et al., 2009
1999	8	28	8	27	0	40.74	30.04	9.9	3.4	110	80	12	Karabulut et al., 2002
1999	8	28	12	11	0	40.65	29.14	8.6	3.2	30	80	-90	Karabulut et al., 2002
1999	8	28	15	39	31.3	40.77	31.02	8.4	2.1	213	25	35	Görgün et al., 2009
1999	8	28	20	38	23.9	40.8	30.98	11.1	1.6	149	29	-29	Görgün et al., 2009
1999	8	28	23	10	24.6	40.76	30.99	7	2.3	46	35	42	Görgün et al., 2009
1999	8	28	23	57	57.7	40.76	30.99	8.8	2	208	31	17	Görgün et al., 2009
1999	8	29	0	46	46.4	40.79	31.08	14.1	1.5	109	84	-35	Görgün et al., 2009
1999	8	29	1	12	41.3	40.76	30.87	12.6	1.6	207	22	26	Görgün et al., 2009
1999	8	29	2	25	0	40.61	29.15	6.8	2	45	320	-35	Karabulut et al., 2002
1999	8	29	3	8	10.3	40.77	31.02	7.2	1.6	189	30	0	Görgün et al., 2009
1999	8	29	3	32	7.9	40.73	30.82	10.8	1.9	58	38	47	Görgün et al., 2009
1999	8	29	4	4	45	40.75	30.82	12.8	1.6	146	48	-63	Görgün et al., 2009
1999	8	29	4	16	47.8	40.8	31.15	12.5	1.4	77	46	-27	Görgün et al., 2009
1999	8	29	4	42	54.4	40.75	30.82	12	1.9	143	55	-45	Görgün et al., 2009
1999	8	29	4	53	31.5	40.72	30.98	11	1.7	207	22	26	Görgün et al., 2009
1999	8	29	5	10	49.9	40.74	30.81	11.9	1.9	161	85	-70	Görgün et al., 2009
1999	8	29	6	1	9.6	40.75	30.82	12.3	2	132	65	-84	Görgün et al., 2009
1999	8	29	10	15	4.1	40.8	31.12	10	4.3	293	44	-159	Örgülü and Aktar, 2001
1999	8	29	10	24	13.5	40.79	31.1	9.3	3.6	116	40	-58	Görgün et al., 2009
1999	8	29	12	24	0	40.71	29.1	10.5	2.2	91	54	-160	Karabulut et al., 2002
1999	8	29	15	9	4.7	40.8	31.1	11.1	1.9	320	41	-41	Görgün et al., 2009
1999	8	29	18	29	0	40.62	29.02	7.7	3.4	71	307	-68	Karabulut et al., 2002
1999	8	29	20	16	0	40.62	29.08	0	3	96	84	-141	Polat et al., 2002
1999	8	29	20	16	0	40.63	29.02	8.6	3.6	70	158	-23	Karabulut et al., 2002
1999	8	29	20	21	0	40.63	29.02	6.8	2.9	71	327	-68	Karabulut et al., 2002
1999	8	29	20	53	4.2	40.79	31.11	12.4	2.1	138	51	-77	Görgün et al., 2009
1999	8	29	21	4	0	40.64	29.15	11.3	3.4	36	131	-54	Karabulut et al., 2002
1999	8	29	21	12	0	40.62	29.02	7.6	3.3	51	162	-8	Karabulut et al., 2002
1999	8	29	22	37	59.3	40.77	30.88	13.2	1.6	113	14	-45	Görgün et al., 2009
1999	8	29	22	45	9.9	40.79	31.06	9.8	1.8	208	29	29	Görgün et al., 2009
1999	8	29	23	53	20.5	40.79	31.13	9.7	1.9	177	68	-34	Görgün et al., 2009
1999	8	30	0	32	49.7	40.8	31.05	8.3	1.3	111	76	-69	Görgün et al., 2009
1999	8	30	0	43	16.4	40.8	31.05	6.8	2	293	85	-70	Görgün et al., 2009
1999	8	30	0	44	40.9	40.78	30.9	14	1.6	318	32	-36	Görgün et al., 2009
1999	8	30	0	57	3.3	40.81	31.07	9.8	3.1	326	46	-27	Görgün et al., 2009
1999	8	30	1	16	46	40.81	31.1	11.5	1.4	91	62	-67	Görgün et al., 2009
1999	8	30	1	18	47.1	40.79	31.04	10.2	1.8	230	25	-90	Görgün et al., 2009
1999	8	30	1	22	57.5	40.79	31.09	10.9	2.4	9	33	-62	Görgün et al., 2009
1999	8	30	1	38	52	40.81	31.13	12.2	1.3	295	15	-90	Görgün et al., 2009
1999	8	30	2	9	12.7	40.79	31.02	8.9	1.2	285	10	-90	Görgün et al., 2009
1999	8	30	2	11	0.5	40.78	31.06	14	1	305	10	-90	Görgün et al., 2009
1999	8	30	5	18	0	40.77	29.2	10.7	2.2	148	50	-77	Karabulut et al., 2002
1999	8	30	5	28	0	40.66	29.2	9.6	1.9	75	153	-48	Karabulut et al., 2002
1999	8	30	6	43	7.7	40.8	31.19	14.2	1.5	118	77	-59	Görgün et al., 2009
1999	8	30	6	44	0	40.7	29.12	10.4	2.1	93	64	-163	Karabulut et al., 2002
1999	8	30	7	18	0	40.63	29.12	0	3.2	359	66	16	Polat et al., 2002
1999	8	30	7	43	3.2	40.75	30.81	14.2	1.7	145	64	-44	Görgün et al., 2009
1999	8	30	9	0	0	40.49	29.17	0	3	215	54	-156	Polat et al., 2002
1999	8	30	9	39	46.9	40.74	30.99	6.9	2.1	241	52	51	Görgün et al., 2009

1999	8	30	9	53	43	40.75	30.98	12.7	1.7	228	32	49	Görgün et al., 2009
1999	8	30	12	11	6.3	40.79	31.09	13.7	1.8	3	27	-67	Görgün et al., 2009
1999	8	30	15	24	0	40.71	29.32	0	3.3	139	40	-57	Polat et al., 2002
1999	8	30	15	24	0	40.72	29.33	11.9	3.2	93	52	-115	Karabulut et al., 2002
1999	8	30	18	50	1.3	40.75	31	9.1	2	180	64	-24	Görgün et al., 2009
1999	8	30	23	37	15.3	40.78	31.06	14.5	1.5	193	48	-48	Görgün et al., 2009
1999	8	31	8	10	0	40.74	29.99	8.6	4.6	80	70	-143	Özalaybey et al., 2002
1999	8	31	8	10	0	40.74	29.99	8.6	5	80	70	-143	Şengör et al., 2005
1999	8	31	8	10	0	40.79	29.94	15	5.1	82	78	-141	Kiratzi, 2002
1999	8	31	8	10	51.1	40.75	29.97	11	4.6	82	71	-133	Örgülü and Aktar, 2001
1999	8	31	8	33	0	40.74	29.98	10	4.2	60	85	-150	Özalaybey et al., 2002
1999	8	31	8	33	0	40.75	29.97	0	4.5	55	83	163	Polat et al., 2002
1999	8	31	8	33	25.1	40.75	29.97	11	4.2	68	70	-142	Örgülü and Aktar, 2001
1999	8	31	8	44	0	40.78	29.17	13.9	2.2	180	77	-20	Karabulut et al., 2002
1999	8	31	11	6	0	40.68	29.33	0	2.7	271	52	-153	Polat et al., 2002
1999	8	31	22	28	0	40.56	29.13	5	4.2	270	59	-105	Pinar et al., 2003
1999	8	31	22	28	0	40.61	29.08	4.3	4.1	55	141	-75	Karabulut et al., 2002
1999	8	31	22	28	0	40.61	29.08	4.5	4.2	93	66	-123	Özalaybey et al., 2002
1999	8	31	22	28	0	40.62	29.09	0	4	309	57	-103	Polat et al., 2002
1999	8	31	22	28	34.6	40.61	29.08	0	4.2	84	68	-120	Örgülü and Aktar, 2001
1999	8	31	23	12	0	40.61	29.07	6	2.8	53	136	-65	Karabulut et al., 2002
1999	8	31	23	14	0	40.61	29.07	6	3.3	28	133	-43	Karabulut et al., 2002
1999	8	31	23	14	0	40.62	29.09	0	3.3	155	47	-53	Polat et al., 2002
1999	9	1	0	33	39.8	40.8	31.18	15.3	1.4	225	70	79	Görgün et al., 2009
1999	9	1	3	23	0	40.6	29.1	0	3.8	260	79	-178	Polat et al., 2002
1999	9	1	3	23	0	40.6	29.1	5.4	3.6	135	45	-60	Özalaybey et al., 2002
1999	9	1	3	50	58.5	40.63	30.79	14.2	2	69	90	70	Görgün et al., 2009
1999	9	1	4	37	22.4	40.78	30.96	14.9	1.2	312	90	70	Görgün et al., 2009
1999	9	1	5	6	58.5	40.62	30.8	13.5	0.9	216	30	9	Görgün et al., 2009
1999	9	1	5	37	2.6	40.78	31.08	10.6	1.4	163	25	-35	Görgün et al., 2009
1999	9	1	7	2	12.9	40.78	31.07	14.3	4.3	206	71	-24	Görgün et al., 2009
1999	9	1	11	6	0	40.6	29.1	5.7	3	36	319	-66	Karabulut et al., 2002
1999	9	1	16	6	0	40.62	29.15	0	3	134	69	-72	Polat et al., 2002
1999	9	1	19	12	51.2	40.77	31.04	11	1.1	192	25	-11	Görgün et al., 2009
1999	9	1	20	30	14.8	40.77	30.94	12.5	1.9	180	20	-90	Görgün et al., 2009
1999	9	1	21	10	13.6	40.77	31.07	10.8	2.2	330	45	-90	Görgün et al., 2009
1999	9	1	21	42	21.9	40.74	30.91	11.2	1.8	179	30	-9	Görgün et al., 2009
1999	9	1	22	29	10.1	40.78	31.06	11.1	1.1	28	52	-71	Görgün et al., 2009
1999	9	1	23	11	0	40.75	29.97	0	3	339	79	33	Polat et al., 2002
1999	9	2	0	19	0	40.6	29.17	7.6	1.7	56	113	-58	Karabulut et al., 2002
1999	9	2	0	51	48.6	40.8	30.96	11.9	1.7	150	38	47	Görgün et al., 2009
1999	9	2	2	3	14.7	40.77	31.05	11.9	2.8	20	30	0	Görgün et al., 2009
1999	9	2	2	7	0	40.69	29.41	6.1	2.2	122	54	-142	Karabulut et al., 2002
1999	9	2	2	22	50.9	40.74	30.95	9.5	1.5	172	51	-43	Görgün et al., 2009
1999	9	2	2	26	40.5	40.79	31.06	11.1	1.1	177	40	-26	Görgün et al., 2009
1999	9	2	2	56	13.6	40.79	31.05	13.6	1.7	180	30	-90	Görgün et al., 2009
1999	9	2	4	47	15.1	40.8	31.13	11	2.2	23	72	-64	Görgün et al., 2009
1999	9	2	4	55	58.4	40.75	30.97	12.4	1.3	219	40	6	Görgün et al., 2009
1999	9	2	6	44	59.6	40.79	31.07	14.3	1.5	335	50	-90	Görgün et al., 2009
1999	9	2	9	53	0	40.76	29.22	7	2.1	170	50	-90	Karabulut et al., 2002
1999	9	2	10	10	31.3	40.77	31.07	12.8	1.5	350	40	-90	Görgün et al., 2009
1999	9	2	10	50	38.9	40.79	31	13.4	1.5	335	73	58	Görgün et al., 2009
1999	9	2	12	35	45.2	40.77	30.83	10.5	2	337	84	-35	Görgün et al., 2009
1999	9	2	12	36	34.4	40.77	30.96	11.4	1.5	165	85	-65	Görgün et al., 2009
1999	9	2	14	18	43.6	40.81	31.09	10.1	2.3	181	80	-12	Görgün et al., 2009
1999	9	2	16	29	0	40.72	29.76	0	3.4	59	50	-76	Polat et al., 2002
1999	9	2	17	6	30	40.78	31.09	8.8	2.1	359	50	-83	Görgün et al., 2009
1999	9	2	17	8	16.2	40.79	31.04	11.1	1.4	345	50	-90	Görgün et al., 2009
1999	9	2	18	58	17.8	40.77	31.12	15.8	1.3	216	79	-49	Görgün et al., 2009
1999	9	2	19	13	44.3	40.76	31.13	15	1.3	190	55	-90	Görgün et al., 2009
1999	9	2	21	10	11.3	40.76	31.12	11.4	1.5	180	70	-90	Görgün et al., 2009
1999	9	3	0	47	57.4	40.74	31.22	13.3	1.3	9	25	-11	Görgün et al., 2009
1999	9	3	2	38	0	40.72	29.42	14.7	2.1	176	71	-23	Karabulut et al., 2002
1999	9	3	4	0	0	40.72	29.38	6.1	1.9	228	55	77	Karabulut et al., 2002
1999	9	3	4	18	0	40.83	28.74	5	3.2	353	70	19	Pinar et al., 2003
1999	9	3	4	18	0	40.83	28.79	0	3.3	318	48	-82	Polat et al., 2002

1999	9	3	4	18	0	40.83	28.79	10	2.4	99	67	-134	Karabulut et al., 2002
1999	9	3	5	8	40.3	40.76	31.12	12.1	1.7	326	25	-78	Görgün et al., 2009
1999	9	3	10	7	0	40.69	29.21	0	3.5	86	69	-131	Polat et al., 2002
1999	9	3	10	10	0	40.69	29.2	10.1	2.9	162	75	20	Karabulut et al., 2002
1999	9	3	11	21	0	40.61	29.05	0	3.1	115	37	-67	Polat et al., 2002
1999	9	3	12	58	0	40.75	29.21	5.9	1.8	151	41	-74	Karabulut et al., 2002
1999	9	3	16	45	0	40.74	29.78	0	3	52	59	163	Polat et al., 2002
1999	9	3	20	26	0	40.64	29.09	13.2	1.8	50	300	-43	Karabulut et al., 2002
1999	9	3	22	16	0	40.59	29.12	4.3	2.9	57	83	-66	Karabulut et al., 2002
1999	9	3	23	24	0	40.72	29.42	0	1.9	236	74	90	Karabulut et al., 2002
1999	9	4	0	43	0	40.63	29.16	12.7	1.9	31	117	-71	Karabulut et al., 2002
1999	9	4	0	51	0	40.63	29.17	10.7	2.9	80	164	-3	Karabulut et al., 2002
1999	9	4	1	1	0	40.79	30.17	0	3.6	333	48	-53	Polat et al., 2002
1999	9	4	1	34	49.4	40.76	31.04	7.5	2.3	223	48	39	Görgün et al., 2009
1999	9	4	1	37	6.9	40.76	31.04	8.2	2.3	327	22	-63	Görgün et al., 2009
1999	9	4	1	45	0	40.71	29.4	0	3.4	277	87	158	Polat et al., 2002
1999	9	4	1	45	0	40.71	29.42	8	2.8	116	71	156	Karabulut et al., 2002
1999	9	4	6	3	42.1	40.74	30.93	12.7	1.8	348	33	-62	Görgün et al., 2009
1999	9	4	8	20	0	40.64	29.04	9.3	2.1	41	292	-75	Karabulut et al., 2002
1999	9	4	10	30	0	40.73	30.02	11.4	4	53	80	-176	Özalaybey et al., 2002
1999	9	4	10	30	53.7	40.73	30.02	13	4	224	43	153	Örgülü and Aktar, 2001
1999	9	4	14	21	0	40.71	29.32	8.7	1.8	85	74	-147	Karabulut et al., 2002
1999	9	4	15	39	0	40.75	29.96	0	3.2	89	86	-155	Polat et al., 2002
1999	9	4	16	45	0	40.71	29.27	7.2	2	245	54	150	Karabulut et al., 2002
1999	9	4	16	51	0	40.64	29.05	9.2	2.3	64	146	-16	Karabulut et al., 2002
1999	9	4	18	27	0	40.73	30.36	13.3	3.8	250	80	-180	Özalaybey et al., 2002
1999	9	4	20	44	0	40.77	29.23	10.6	2.7	133	64	-123	Karabulut et al., 2002
1999	9	4	20	44	0	40.77	29.24	0	3	277	85	160	Polat et al., 2002
1999	9	4	23	49	0	40.69	29.42	6	2.5	92	50	-123	Karabulut et al., 2002
1999	9	4	23	49	0	40.7	29.39	0	3.2	111	85	-116	Polat et al., 2002
1999	9	5	0	24	0	40.76	29.25	5.9	1.8	134	60	-101	Karabulut et al., 2002
1999	9	5	0	38	0	40.68	29.4	5.9	2.1	183	64	16	Karabulut et al., 2002
1999	9	5	5	29	0	40.59	28.9	0	3.2	106	59	-96	Polat et al., 2002
1999	9	5	5	53	0	40.77	29.22	7.5	2.2	173	61	-72	Karabulut et al., 2002
1999	9	5	12	6	0	40.77	29.18	11.2	1.7	191	64	-16	Karabulut et al., 2002
1999	9	5	14	17	0	40.61	29.04	5.9	3	60	157	-18	Karabulut et al., 2002
1999	9	5	15	38	0	40.63	29.12	0	3	116	68	-92	Polat et al., 2002
1999	9	5	16	43	0	40.63	29.11	10.6	1.9	60	300	-90	Karabulut et al., 2002
1999	9	5	21	3	0	40.76	29.19	4.5	1.9	160	70	-90	Karabulut et al., 2002
1999	9	5	22	45	0	40.45	29.25	0	3	215	71	-120	Polat et al., 2002
1999	9	6	3	0	27	40.77	30.94	12.7	1.9	195	35	-90	Görgün et al., 2009
1999	9	6	6	33	0	40.73	29.78	0	4.1	224	86	-131	Polat et al., 2002
1999	9	6	6	33	0	40.73	29.79	10	3.8	71	41	56	Özalaybey et al., 2002
1999	9	6	6	38	0	40.73	29.79	0	3	338	78	33	Polat et al., 2002
1999	9	6	7	3	0	40.63	29.05	5.7	2.8	36	191	-54	Karabulut et al., 2002
1999	9	6	14	8	0	40.69	29.4	0	3	103	62	-103	Polat et al., 2002
1999	9	6	14	8	0	40.69	29.42	6.1	3.3	160	90	0	Karabulut et al., 2002
1999	9	6	15	57	0	40.6	29.07	0	3.4	135	37	-56	Polat et al., 2002
1999	9	6	20	38	0	40.62	29.03	0	3.3	54	86	160	Polat et al., 2002
1999	9	6	20	38	0	40.62	29.04	5.3	3.3	50	280	-90	Karabulut et al., 2002
1999	9	6	22	57	16.8	40.8	31.11	6.2	2.1	218	66	-74	Görgün et al., 2009
1999	9	7	4	53	16.6	40.79	31.11	10.2	2.3	148	55	-30	Görgün et al., 2009
1999	9	7	6	24	28.4	40.8	30.99	13.4	1.6	188	52	-12	Görgün et al., 2009
1999	9	7	7	59	14.2	40.77	31.07	14.2	1.5	185	60	-90	Görgün et al., 2009
1999	9	7	9	2	29.8	40.77	30.92	14.9	1.3	310	25	-90	Görgün et al., 2009
1999	9	7	16	47	54.8	40.8	31.08	11	1.3	196	85	-80	Görgün et al., 2009
1999	9	7	21	55	54.5	40.79	31.11	10.7	1.3	275	70	-90	Görgün et al., 2009
1999	9	7	22	17	55.8	40.76	31	11.7	1.5	217	40	26	Görgün et al., 2009
1999	9	7	22	56	37.9	40.78	31.11	10.3	1.6	106	25	-78	Görgün et al., 2009
1999	9	7	23	25	0	40.74	29.92	0	2.7	185	32	44	Polat et al., 2002
1999	9	8	1	42	54.6	40.77	31.08	10.8	1.9	28	64	-56	Görgün et al., 2009
1999	9	8	2	42	15.8	40.81	31.04	10.9	2.8	320	30	-90	Görgün et al., 2009
1999	9	8	3	33	0	40.66	29.2	7.9	1.8	74	340	37	Karabulut et al., 2002
1999	9	8	10	15	15.7	40.75	30.99	7.9	2.7	357	32	-36	Görgün et al., 2009
1999	9	8	11	0	0	40.69	29.01	9	1.8	75	166	-33	Karabulut et al., 2002
1999	9	8	11	6	0	40.69	29.01	9.2	2	76	147	-27	Karabulut et al., 2002

1999	9	8	13	23	36	40.77	30.87	14.5	2.2	183	76	-32	Görgün et al., 2009
1999	9	8	15	35	0	40.62	29.11	0	3.2	137	30	-40	Polat et al., 2002
1999	9	8	17	36	39.7	40.74	31	12.2	1.2	358	55	-84	Görgün et al., 2009
1999	9	8	18	36	35.2	40.76	30.84	14	1.4	327	38	-47	Görgün et al., 2009
1999	9	8	20	22	41.9	40.77	31.12	14	1.5	134	42	-51	Görgün et al., 2009
1999	9	8	23	43	0	40.71	29.53	0	3.1	327	73	24	Polat et al., 2002
1999	9	9	1	2	0	40.71	29.54	11.6	3.7	40	90	150	Özalaybey et al., 2002
1999	9	9	1	2	0	40.72	29.53	0	3.3	321	71	14	Polat et al., 2002
1999	9	9	1	2	0	40.72	29.53	11.5	3.8	140	81	-5	Karabulut et al., 2002
1999	9	9	1	32	0	40.69	29.16	7	4	69	80	148	Pinar et al., 2003
1999	9	9	1	32	0	40.7	29.16	0	4.2	339	64	-1	Polat et al., 2002
1999	9	9	1	32	0	40.7	29.16	10	4.6	159	81	-5	Karabulut et al., 2002
1999	9	9	1	32	0	40.7	29.17	9.8	4	72	75	153	Özalaybey et al., 2002
1999	9	9	1	32	8.6	40.7	29.14	6	4	258	66	-174	Örgülü and Aktar, 2001
1999	9	9	1	55	0	40.71	29.18	9.8	2.2	160	86	10	Karabulut et al., 2002
1999	9	9	2	0	0	40.62	29.12	6.8	3.7	89	42	-98	Özalaybey et al., 2002
1999	9	9	3	11	0	40.7	29.15	10	1.9	159	83	-8	Karabulut et al., 2002
1999	9	9	3	24	0	40.71	29.16	9.3	2.1	161	78	-8	Karabulut et al., 2002
1999	9	9	19	18	0	40.72	30.02	0	3.4	338	77	30	Polat et al., 2002
1999	9	9	20	21	0	40.69	29.95	8.8	3.6	82	54	-142	Özalaybey et al., 2002
1999	9	10	11	47	0	40.61	29.15	0	3.1	118	49	-79	Polat et al., 2002
1999	9	11	0	11	57.3	40.8	31.14	14	1.1	36	38	-65	Görgün et al., 2009
1999	9	11	0	22	11.3	40.78	30.94	11.8	1.5	216	22	-26	Görgün et al., 2009
1999	9	11	1	33	29.6	40.79	31.04	12	1.4	193	36	-31	Görgün et al., 2009
1999	9	11	3	12	24.2	40.8	31.14	10.9	1.8	16	45	5	Görgün et al., 2009
1999	9	11	6	25	18.2	40.79	31.11	10.9	1.9	177	80	-28	Görgün et al., 2009
1999	9	11	7	0	19.2	40.79	31.03	10.1	1.2	191	56	78	Görgün et al., 2009
1999	9	11	7	26	0	40.71	29.36	0	3.2	193	38	-4	Polat et al., 2002
1999	9	11	10	11	4.6	40.81	31.12	14.9	1.1	180	35	-90	Görgün et al., 2009
1999	9	11	13	52	16.6	40.8	31.04	10.8	1.5	11	35	-7	Görgün et al., 2009
1999	9	11	14	46	4.3	40.81	31.12	14.3	2	265	25	-90	Görgün et al., 2009
1999	9	11	19	20	57.8	40.76	31.04	13.7	1	206	74	12	Görgün et al., 2009
1999	9	11	20	46	38.9	40.77	31.04	13.8	1.1	5	45	-83	Görgün et al., 2009
1999	9	11	20	50	42.4	40.78	31.14	10.9	2	159	76	-64	Görgün et al., 2009
1999	9	12	0	4	13.4	40.79	31.07	13	1.4	357	35	-81	Görgün et al., 2009
1999	9	12	1	4	51	40.62	30.8	12.4	1.2	325	75	-90	Görgün et al., 2009
1999	9	12	1	18	18.9	40.8	31.17	13	1.4	248	41	-12	Görgün et al., 2009
1999	9	12	2	9	20.1	40.81	31.01	11.1	1.5	116	80	-80	Görgün et al., 2009
1999	9	12	2	30	51.2	40.77	31.04	10.2	1.5	203	52	-71	Görgün et al., 2009
1999	9	12	11	3	38.2	40.79	31.05	10.6	2.2	59	36	54	Görgün et al., 2009
1999	9	12	13	7	49.7	40.8	31.13	10.8	2.2	150	48	-31	Görgün et al., 2009
1999	9	12	14	34	53.8	40.77	31.01	6.8	3.3	351	52	-27	Görgün et al., 2009
1999	9	12	14	38	0	40.71	29.42	0	3	193	38	49	Polat et al., 2002
1999	9	12	14	52	45.5	40.79	31.08	10.6	1.8	181	85	-80	Görgün et al., 2009
1999	9	12	16	12	34.9	40.79	31.08	10.5	1.9	310	35	-90	Görgün et al., 2009
1999	9	12	16	20	0	40.73	29.7	0	3.1	223	80	-135	Polat et al., 2002
1999	9	12	17	46	19.1	40.75	30.95	12.1	1.5	169	59	-60	Görgün et al., 2009
1999	9	12	20	12	15	40.79	30.95	11.4	2.4	327	67	-68	Görgün et al., 2009
1999	9	12	21	37	0	40.71	30	0	2.9	196	49	-72	Polat et al., 2002
1999	9	12	22	31	26	40.75	30.8	10.9	2	138	47	-69	Görgün et al., 2009
1999	9	13	0	28	2.2	40.77	31.01	9.5	1.7	345	50	-90	Görgün et al., 2009
1999	9	13	1	27	0	40.61	29.06	0	3.1	327	57	-45	Polat et al., 2002
1999	9	13	2	53	24.9	40.75	30.82	12.8	1.9	147	51	-43	Görgün et al., 2009
1999	9	13	2	55	14.9	40.79	31.05	12.7	2.1	210	30	9	Görgün et al., 2009
1999	9	13	5	46	50.9	40.79	31.07	10.9	1.7	122	70	-85	Görgün et al., 2009
1999	9	13	11	55	0	40.42	30.24	16	5.7	269	49	180	Kiratzi, 2002
1999	9	13	11	55	0	40.75	30.1	16.7	6.2	90	90	-179	Özalaybey et al., 2002
1999	9	13	11	55	0	40.76	30.07	12	5.8	293	73	164	Şengör et al., 2005
1999	9	13	11	55	29.8	40.76	30.08	14	6.2	293	73	164	Örgülü and Aktar, 2001
1999	9	13	16	22	37.8	40.63	30.8	13.4	2	169	14	-45	Görgün et al., 2009
1999	9	13	19	7	1.9	40.78	31.14	13.8	1.8	14	61	-73	Görgün et al., 2009
1999	9	13	19	42	19	40.77	31.06	12.7	1.4	180	35	-90	Görgün et al., 2009
1999	9	13	20	0	2.4	40.78	31.08	12.2	2.1	255	15	-90	Görgün et al., 2009
1999	9	13	21	0	2.2	40.76	31.03	10.4	1.6	349	47	-69	Görgün et al., 2009
1999	9	13	21	48	40.2	40.76	30.88	9.3	1.3	42	70	-85	Görgün et al., 2009
1999	9	13	22	28	32	40.74	30.94	12	2.2	334	62	-67	Görgün et al., 2009

1999	9	13	22	31	51.9	40.76	31.01	9.4	1.3	310	50	-90	Görgün et al., 2009
1999	9	13	23	31	55.2	40.78	31.06	10.3	2	72	51	-77	Görgün et al., 2009
1999	9	14	2	8	29.3	40.77	31.03	7	2.4	205	21	13	Görgün et al., 2009
1999	9	14	3	12	37.1	40.77	31.09	9.1	1.6	257	38	47	Görgün et al., 2009
1999	9	14	3	25	5.3	40.75	30.84	14.9	2.3	147	51	-43	Görgün et al., 2009
1999	9	14	8	24	49.4	40.75	31.1	11.7	1.5	156	40	-82	Görgün et al., 2009
1999	9	14	20	21	55	40.81	31.08	13.7	1.5	167	87	-35	Görgün et al., 2009
1999	9	14	23	31	36.7	40.79	31.05	12.2	1.2	178	38	-20	Görgün et al., 2009
1999	9	16	0	33	35	40.76	31.05	6.6	2.2	155	46	-27	Görgün et al., 2009
1999	9	16	1	34	23.7	40.79	30.93	12.7	1.7	324	18	-56	Görgün et al., 2009
1999	9	16	15	57	18.1	40.78	31.1	8.4	2.5	185	45	0	Görgün et al., 2009
1999	9	16	20	5	24.7	40.76	30.94	13.1	1.3	200	38	-47	Görgün et al., 2009
1999	9	16	20	12	7.7	40.76	31.05	6.9	2.1	150	38	-20	Görgün et al., 2009
1999	9	16	23	50	34.6	40.71	31	11.8	1.2	358	42	17	Görgün et al., 2009
1999	9	17	1	8	43.1	40.8	30.93	13.4	1.6	233	20	0	Görgün et al., 2009
1999	9	17	19	50	0	40.76	30.1	13.9	4	90	90	-179	Özalaybey et al., 2002
1999	9	17	19	50	0	40.77	30.09	0	3.6	348	71	21	Polat et al., 2002
1999	9	17	19	50	7	40.75	30.08	18	4.5	170	82	-21	Örgülü and Aktar, 2001
1999	9	18	0	26	55.8	40.77	31.07	11	1.5	213	45	-36	Görgün et al., 2009
1999	9	18	0	48	0	40.61	29.16	6	4.3	146	56	-48	Pinar et al., 2003
1999	9	18	0	48	0	40.62	29.16	0	4.1	129	70	-78	Polat et al., 2002
1999	9	18	0	48	0	40.63	29.14	4.6	4.3	144	52	-115	Özalaybey et al., 2002
1999	9	18	2	7	0	40.64	29.08	0	3.1	342	51	-32	Polat et al., 2002
1999	9	18	21	50	3.5	40.77	30.99	10.2	1.8	157	35	-81	Görgün et al., 2009
1999	9	19	3	50	43.1	40.77	30.86	10.6	1.8	315	25	-90	Görgün et al., 2009
1999	9	19	4	25	16.9	40.77	31.08	10.8	2	274	22	63	Görgün et al., 2009
1999	9	19	9	23	7.3	40.75	31	9.8	2	18	50	-23	Görgün et al., 2009
1999	9	19	9	50	20.2	40.74	30.99	9.9	1.6	190	45	-90	Görgün et al., 2009
1999	9	19	11	22	39.5	40.74	30.81	12.3	2.4	150	42	-51	Görgün et al., 2009
1999	9	19	14	19	42.6	40.75	30.81	12.8	2.6	145	44	-60	Görgün et al., 2009
1999	9	19	22	14	49.4	40.77	31.07	13.4	1.4	180	50	-90	Görgün et al., 2009
1999	9	20	9	59	5.2	40.75	30.8	14.1	1.9	163	41	-41	Görgün et al., 2009
1999	9	20	13	41	42	40.75	31.01	9.5	1.9	220	41	41	Görgün et al., 2009
1999	9	20	13	44	27	40.75	31.02	7.1	2.7	11	44	-22	Görgün et al., 2009
1999	9	20	14	14	3.1	40.76	31.08	10.5	2.6	213	63	31	Görgün et al., 2009
1999	9	20	15	4	0	40.64	29.09	0	3	67	86	-178	Polat et al., 2002
1999	9	20	20	36	0	40.67	27.5	0	2.3	285	86	146	Polat et al., 2002
1999	9	20	20	36	0	40.7	27.57	11	3.3	246	51	156	Pinar et al., 2003
1999	9	20	21	1	10.4	40.77	31.06	9.4	2.3	340	55	-90	Görgün et al., 2009
1999	9	20	21	28	0	40.66	27.51	0	5	244	65	-167	Polat et al., 2002
1999	9	20	21	28	0	40.69	27.57	11	4.8	245	40	166	Pinar et al., 2003
1999	9	20	21	44	0	40.7	27.59	5	3.2	211	50	138	Pinar et al., 2003
1999	9	20	22	16	0	40.65	27.51	0	3.2	47	60	38	Polat et al., 2002
1999	9	20	22	16	0	40.71	27.59	11	3.6	238	42	166	Pinar et al., 2003
1999	9	20	23	40	0	40.66	27.52	0	3.4	300	74	165	Polat et al., 2002
1999	9	20	23	40	0	40.72	27.6	5	3.2	209	77	160	Pinar et al., 2003
1999	9	21	1	9	0	40.64	27.49	0	3.5	199	68	-67	Polat et al., 2002
1999	9	21	1	9	0	40.71	27.56	5	3.4	224	75	168	Pinar et al., 2003
1999	9	21	12	46	0	40.7	27.57	11	3.4	208	34	-42	Pinar et al., 2003
1999	9	21	20	34	0	40.72	27.59	11	3.3	273	46	-168	Pinar et al., 2003
1999	9	21	22	9	41.1	40.8	31.12	9.4	2.1	30	59	-60	Görgün et al., 2009
1999	9	22	1	4	0	40.64	29.06	0	3.1	161	48	-50	Polat et al., 2002
1999	9	22	1	49	0	40.65	29.1	0	3	127	52	-74	Polat et al., 2002
1999	9	22	16	55	15.7	40.79	31.04	7.6	2.5	6	56	-10	Görgün et al., 2009
1999	9	22	17	44	0	40.64	29.18	0	3.1	83	64	-127	Polat et al., 2002
1999	9	22	18	17	1.4	40.8	31.05	9.4	2.3	134	38	-36	Görgün et al., 2009
1999	9	22	19	10	4.1	40.79	30.95	11.1	1.8	342	90	35	Görgün et al., 2009
1999	9	22	21	27	35.3	40.77	31.01	11	1.6	350	55	-90	Görgün et al., 2009
1999	9	22	23	2	0	40.56	27.77	0	3.2	65	88	178	Polat et al., 2002
1999	9	22	23	2	0	40.62	27.82	11	3	89	79	-163	Pinar et al., 2003
1999	9	22	23	12	49.2	40.79	31.06	10.4	1.7	138	55	-84	Görgün et al., 2009
1999	9	23	3	20	0	40.75	29.8	0	3.1	107	83	-120	Polat et al., 2002
1999	9	23	5	5	0	40.62	29.15	0	3	87	63	-121	Polat et al., 2002
1999	9	23	5	16	0	40.63	29.05	0	3	316	61	-66	Polat et al., 2002
1999	9	23	6	24	0	40.75	29.85	0	3.3	249	86	-178	Polat et al., 2002
1999	9	23	20	24	0	40.63	29.17	0	3.4	137	30	-41	Polat et al., 2002

1999	9	23	21	33	28.3	40.77	31.04	6.8	2	157	48	-63	Görgün et al., 2009
1999	9	23	22	28	29.9	40.77	31.04	7	1.5	213	35	42	Görgün et al., 2009
1999	9	23	22	36	49	40.76	31.07	11	1.8	331	14	-45	Görgün et al., 2009
1999	9	24	0	1	0	40.46	29.16	0	3.2	226	67	-155	Polat et al., 2002
1999	9	24	1	40	2.1	40.76	30.97	13.3	2.5	238	38	36	Görgün et al., 2009
1999	9	24	3	26	0	40.62	29.16	0	3.1	258	79	-178	Polat et al., 2002
1999	9	24	13	44	0	40.77	30.24	0	3.2	336	66	5	Polat et al., 2002
1999	9	24	18	28	0	40.67	27.46	0	3.3	40	28	-25	Polat et al., 2002
1999	9	24	18	28	0	40.74	27.54	14	3.1	195	39	135	Pinar et al., 2003
1999	9	24	18	51	18	40.77	31.02	6.9	1.8	172	48	-19	Görgün et al., 2009
1999	9	24	20	10	0	40.75	29.25	0	2.8	336	38	-62	Polat et al., 2002
1999	9	24	20	18	53	40.6	30.81	13.7	1.4	169	14	-45	Görgün et al., 2009
1999	9	25	2	30	50.7	40.79	31.12	9.8	1.7	130	45	-83	Görgün et al., 2009
1999	9	25	8	33	54.6	40.73	31.06	12	2.3	343	32	-49	Görgün et al., 2009
1999	9	25	9	49	0	40.62	29.09	0	2.9	143	41	-54	Polat et al., 2002
1999	9	25	17	5	0	40.61	29.07	0	3.1	322	63	-31	Polat et al., 2002
1999	9	25	18	46	59.8	40.74	30.8	12	1.6	131	31	-71	Görgün et al., 2009
1999	9	26	1	59	58.3	40.77	31.17	13.3	1.7	305	35	-90	Görgün et al., 2009
1999	9	26	12	10	58.4	40.77	31.04	13.1	2.1	153	51	-77	Görgün et al., 2009
1999	9	26	14	58	16	40.78	31.04	10	1.5	16	47	-15	Görgün et al., 2009
1999	9	27	3	0	43.9	40.77	30.94	12.5	1.5	335	65	-90	Görgün et al., 2009
1999	9	27	21	44	0	40.41	29.06	0	3.1	52	59	-111	Polat et al., 2002
1999	9	27	23	48	0	40.37	28.11	0	3.3	297	85	120	Polat et al., 2002
1999	9	28	1	51	13.3	40.74	30.98	9.9	1.6	168	56	-53	Görgün et al., 2009
1999	9	28	7	48	27.1	40.78	30.91	12.1	1.9	135	85	-75	Görgün et al., 2009
1999	9	28	17	58	8.6	40.75	30.82	13	1.6	172	47	-15	Görgün et al., 2009
1999	9	28	18	12	52.1	40.76	30.89	12	2.4	181	80	-12	Görgün et al., 2009
1999	9	29	0	9	0	40.79	29.78	0	3.3	202	39	174	Polat et al., 2002
1999	9	29	0	13	0	40.55	29.69	15	5.2	66	48	-171	Kiratzi, 2002
1999	9	29	0	13	0	40.7	29.34	14	5	244	71	170	Pinar et al., 2003
1999	9	29	0	13	0	40.71	29.3	8	5	85	63	-161	Şengör et al., 2005
1999	9	29	0	13	6	40.72	29.31	8	4.8	85	63	-161	Örgülü and Aktar, 2001
1999	9	29	11	1	0	40.7	29.42	0	3.1	190	83	-51	Polat et al., 2002
1999	9	29	16	9	54.6	40.8	30.93	12.5	2.7	312	77	59	Görgün et al., 2009
1999	9	29	17	36	0	40.72	29.76	0	2.9	310	71	-77	Polat et al., 2002
1999	9	29	18	36	30.6	40.75	31.08	9.9	2.1	180	50	-90	Görgün et al., 2009
1999	9	30	1	12	1.4	40.79	30.96	11	2.1	200	21	14	Görgün et al., 2009
1999	9	30	6	14	3.7	40.76	31.08	10.6	2.4	5	38	-65	Görgün et al., 2009
1999	9	30	7	55	0	40.71	29.88	0	3.5	12	45	-14	Polat et al., 2002
1999	9	30	14	51	33.1	40.8	31.09	11.1	1.7	275	70	-90	Görgün et al., 2009
1999	9	30	18	39	0	40.63	29.19	0	2.7	108	33	-63	Polat et al., 2002
1999	10	1	6	10	0	40.61	29.15	0	3.3	116	34	-63	Polat et al., 2002
1999	10	1	8	12	0	40.72	29.88	0	3.4	317	53	-80	Polat et al., 2002
1999	10	1	15	31	56.8	40.61	30.8	10.4	1.5	185	30	-90	Görgün et al., 2009
1999	10	1	17	4	0	40.69	29.35	0	3.1	85	86	-157	Polat et al., 2002
1999	10	1	18	48	33.8	40.78	31.21	12.3	1.8	201	25	-78	Görgün et al., 2009
1999	10	1	22	14	3.1	40.75	31	10	1.1	260	32	49	Görgün et al., 2009
1999	10	2	4	23	39.2	40.78	31.08	9.6	2	190	85	-85	Görgün et al., 2009
1999	10	2	5	48	8.4	40.77	31.07	12.5	1.5	180	25	-90	Görgün et al., 2009
1999	10	2	11	28	0	40.76	27.51	8	3	272	75	170	Pinar et al., 2003
1999	10	2	12	38	44.7	40.76	30.98	7.2	2.6	346	36	-73	Görgün et al., 2009
1999	10	2	12	50	16.8	40.76	30.99	7.3	2.6	219	52	71	Görgün et al., 2009
1999	10	2	19	27	22.6	40.75	30.98	9.9	2.1	349	32	-71	Görgün et al., 2009
1999	10	2	22	6	4.2	40.75	30.98	7.7	1.6	339	50	-83	Görgün et al., 2009
1999	10	2	23	18	0	40.35	28.43	0	2.9	228	89	-143	Polat et al., 2002
1999	10	3	10	23	48.2	40.77	30.93	12.5	1.6	200	22	-26	Görgün et al., 2009
1999	10	3	16	19	0	40.77	29.84	0	3	55	57	-113	Polat et al., 2002
1999	10	3	22	35	0	40.7	29.35	0	3.1	219	62	-149	Polat et al., 2002
1999	10	4	0	40	45.2	40.8	30.99	10.9	1.6	199	30	9	Görgün et al., 2009
1999	10	4	5	53	15.5	40.77	30.89	12.5	2.1	160	87	-40	Görgün et al., 2009
1999	10	4	16	59	25.2	40.74	30.8	12.3	1.6	35	35	42	Görgün et al., 2009
1999	10	4	17	59	22.2	40.77	30.87	13.7	1.5	351	32	-36	Görgün et al., 2009
1999	10	4	18	3	57.9	40.85	30.91	9.5	1.6	320	45	-90	Görgün et al., 2009
1999	10	5	4	10	0	40.76	29.81	0	3.7	52	57	-29	Polat et al., 2002
1999	10	5	6	42	0	40.76	29.22	0	3.1	91	34	-69	Polat et al., 2002
1999	10	5	12	26	0	40.63	29.17	0	3.1	191	37	42	Polat et al., 2002

1999	10	6	6	59	0	40.72	27.6	14	3.2	208	46	139	Pinar et al., 2003
1999	10	6	14	16	0	40.43	28.7	0	3.2	257	59	-164	Polat et al., 2002
1999	10	6	18	35	0	40.63	29.08	0	3.2	271	71	-172	Polat et al., 2002
1999	10	6	23	22	0	40.63	29.08	0	2.9	329	50	-57	Polat et al., 2002
1999	10	7	0	55	0	40.71	27.59	8	3	214	74	142	Pinar et al., 2003
1999	10	7	2	29	20.5	40.66	30.85	13.8	1.2	224	35	7	Görgün et al., 2009
1999	10	7	11	13	0	41.06	29.34	0	3	193	38	101	Polat et al., 2002
1999	10	7	12	7	42.4	40.79	31.17	12.4	1.4	265	40	-90	Görgün et al., 2009
1999	10	7	12	41	0	40.63	29.08	0	3.2	175	57	-50	Polat et al., 2002
1999	10	7	20	15	31.5	40.81	31.16	14.1	1.3	249	40	-6	Görgün et al., 2009
1999	10	7	20	40	41.8	40.79	31.12	13.9	1.6	8	55	-45	Görgün et al., 2009
1999	10	8	1	46	55.8	40.79	31.04	9.9	1.8	220	48	19	Görgün et al., 2009
1999	10	8	8	58	9.5	40.75	30.95	7.8	1.7	161	33	-24	Görgün et al., 2009
1999	10	8	9	20	0	40.73	29.04	0	3.3	266	49	-155	Polat et al., 2002
1999	10	8	13	44	13.2	40.75	30.8	15	1.7	52	76	21	Görgün et al., 2009
1999	10	8	17	43	0	40.76	30.03	0	3.4	255	89	174	Polat et al., 2002
1999	10	8	20	59	55.9	40.78	31.03	10.7	1.6	346	72	64	Görgün et al., 2009
1999	10	9	5	23	0	40.77	29.23	0	2.8	52	59	-51	Polat et al., 2002
1999	10	9	11	31	30.1	40.78	31.02	6.2	2.2	229	36	54	Görgün et al., 2009
1999	10	9	23	17	26.2	40.77	30.88	10.9	2.5	170	42	-31	Görgün et al., 2009
1999	10	10	0	54	15.5	40.77	31.06	8.5	2.4	57	14	45	Görgün et al., 2009
1999	10	10	20	52	32.2	40.77	31.04	4.6	1.6	109	57	-66	Görgün et al., 2009
1999	10	11	0	40	40.9	40.73	30.96	9.9	2.5	224	42	31	Görgün et al., 2009
1999	10	11	5	0	2.7	40.79	31.13	5	2.8	128	57	-40	Görgün et al., 2009
1999	10	11	5	4	0.8	40.79	31.16	6.1	1.6	165	48	-19	Görgün et al., 2009
1999	10	12	23	6	20.3	40.79	30.9	12.4	1.5	54	36	54	Görgün et al., 2009
1999	10	13	1	0	27.7	40.79	31.04	2.4	2.1	111	45	-45	Görgün et al., 2009
1999	10	13	18	17	41.3	40.75	31.03	7.5	1.3	213	75	-48	Görgün et al., 2009
1999	10	14	0	13	1	40.75	30.98	7.9	1.5	235	52	51	Görgün et al., 2009
1999	10	14	3	21	30.1	40.75	30.98	7.8	1.2	18	44	22	Görgün et al., 2009
1999	10	14	4	52	23.3	40.78	31.07	8.9	1.6	350	50	-90	Görgün et al., 2009
1999	10	14	5	25	23.2	40.73	30.95	10.7	1.9	138	55	-84	Görgün et al., 2009
1999	10	14	6	56	26.1	40.77	31.07	10.5	2	10	82	-50	Görgün et al., 2009
1999	10	14	16	55	22.1	40.78	30.88	12.8	1.7	153	74	-37	Görgün et al., 2009
1999	10	14	23	35	45.4	40.78	31.06	8.1	2.2	315	35	-90	Görgün et al., 2009
1999	10	15	1	37	14.6	40.78	30.96	10.8	2.2	357	79	-11	Görgün et al., 2009
1999	10	15	2	7	51.1	40.71	30.9	14.9	1	53	55	-84	Görgün et al., 2009
1999	10	15	3	22	21.5	40.79	31.01	6.8	1.4	211	11	-63	Görgün et al., 2009
1999	10	15	5	38	44.5	40.78	31.05	7.5	1.9	212	16	18	Görgün et al., 2009
1999	10	15	15	30	19.5	40.79	30.92	13	3.5	217	33	24	Görgün et al., 2009
1999	10	15	16	50	29.8	40.79	30.92	12.5	1.9	219	29	29	Görgün et al., 2009
1999	10	15	21	32	12.6	40.78	30.88	10.7	1.9	180	40	6	Görgün et al., 2009
1999	10	16	2	44	23.4	40.76	31.06	11.1	1.1	330	40	-90	Görgün et al., 2009
1999	10	16	3	22	23.5	40.78	30.94	11.7	1.6	190	5	0	Görgün et al., 2009
1999	10	16	3	57	16.7	40.81	31.04	11	2.1	175	25	-11	Görgün et al., 2009
1999	10	16	4	36	54.6	40.79	31.04	11.4	1.5	359	50	-83	Görgün et al., 2009
1999	10	16	18	14	52.7	40.78	30.87	12.1	1.4	330	25	-11	Görgün et al., 2009
1999	10	17	3	47	55.9	40.76	31.06	11.1	1.4	200	30	0	Görgün et al., 2009
1999	10	17	4	22	19.5	40.79	31.13	9.5	1.4	13	51	-43	Görgün et al., 2009
1999	10	17	5	10	46	40.76	30.83	14.2	1.5	327	35	-42	Görgün et al., 2009
1999	10	17	7	54	3.4	40.79	31.02	7.6	1.5	205	40	26	Görgün et al., 2009
1999	10	17	19	22	37.1	40.81	30.93	14.9	1.6	226	16	-18	Görgün et al., 2009
1999	10	20	23	8	21.7	40.8	29.02	7	4.8	293	86	-151	Örgülü and Aktar, 2001
1999	10	20	23	25	0	40.8	29.04	0	3	123	25	-33	Polat et al., 2002
1999	10	21	7	33	0	40.37	28.11	0	3.7	52	59	21	Polat et al., 2002
1999	10	21	8	20	0	40.35	28.58	0	3.1	183	33	17	Polat et al., 2002
1999	10	22	6	43	0	40.37	28.11	0	3.4	92	78	-137	Polat et al., 2002
1999	11	7	16	54	42.2	40.65	30.69	7	5	282	64	166	Örgülü and Aktar, 2001
1999	11	11	14	41	0	40.78	30.29	20	5.5	307	66	179	Şengör et al., 2005
1999	11	11	14	41	0	40.95	30.1	13	5.6	297	55	-179	Kiratzi, 2002
1999	11	11	14	41	25.1	40.78	30.29	22	5	307	66	179	Örgülü and Aktar, 2001
1999	11	12	16	57	0	40.93	31.25	12	7.1	262	53	-177	Kiratzi, 2002
1999	11	16	0	29	0	40.61	27.06	5	3.4	79	79	172	Pinar et al., 2003
1999	11	17	19	14	0	40.83	27.97	11	3.4	276	82	132	Pinar et al., 2003
1999	12	3	8	20	0	40.71	27.58	5	3.8	237	22	-139	Pinar et al., 2003
1999	12	20	22	35	0	40.79	27.48	11	3.6	99	65	-96	Pinar et al., 2003

1999	12	29	12	26	0	40.83	28.58	14	3.4	98	27	132	Pinar et al., 2003
2000	0	0	0	0	0	40.59	29.01	9.3	2	190	65	-40	Sato et al., 2004
2000	0	0	0	0	0	40.63	29.09	6.5	2	240	50	-120	Sato et al., 2004
2000	0	0	0	0	0	40.72	29.02	5.3	2	120	40	-65	Sato et al., 2004
2000	0	0	0	0	0	40.76	28.03	5.4	2	70	90	-180	Sato et al., 2004
2000	0	0	0	0	0	40.76	29.13	9.6	2	0	60	-30	Sato et al., 2004
2000	0	0	0	0	0	40.78	28.86	10.6	2	120	50	-100	Sato et al., 2004
2000	0	0	0	0	0	40.81	27.72	10.1	2	0	80	-10	Sato et al., 2004
2000	0	0	0	0	0	40.82	27.84	11.2	2	70	90	-180	Sato et al., 2004
2000	0	0	0	0	0	40.84	28.67	7.1	2	280	90	170	Sato et al., 2004
2000	1	7	1	48	0	40.79	28.41	5	3.2	283	77	-165	Pinar et al., 2003
2000	1	31	14	38	0	40.71	29.34	8	4.1	76	32	-149	Pinar et al., 2003
2000	2	14	6	56	0	40.9	31.75	4	5.1	260	42	154	Şengör et al., 2005
2000	6	6	2	41	0	40.65	32.92	8	6	2	46	-29	Şengör et al., 2005
2000	7	7	0	15	0	40.84	29.19	5	4.2	142	39	-32	Pinar et al., 2003
2000	8	23	13	41	0	40.68	30.71	18	5.2	253	61	177	Şengör et al., 2005
2001	1	16	3	33	0	40.9	29.14	8	3.7	256	68	-163	Pinar et al., 2003
2001	3	14	20	34	0	40.85	27.64	17	3.7	75	79	147	Pinar et al., 2003
2001	3	24	13	7	0	40.84	28.83	11	3.7	106	87	-160	Pinar et al., 2003
2001	3	24	13	7	0	40.86	28.88	8.5	4	105	78	-170	Özalaybey et al., 2002
2002	5	14	19	32	23.7	40.45	28.72	6	3.3	264	76	-133	Örgülü, 2010
2002	10	1	4	21	36.8	40.83	28.05	11.2	3.3	340	41	-102	Örgülü, 2010
2002	10	9	14	40	20.9	40.72	27.53	7.8	3.2	178	80	-10	Örgülü, 2010
2003	1	27	7	26	0	39.52	39.78	9	6	151	77	-168	Şengör et al., 2005
2003	2	26	6	53	38.3	40.83	27.98	9.2	3.1	260	71	-164	Örgülü, 2010
2003	4	2	17	35	17.7	40.91	28.12	5.3	3.4	6	63	-28	Örgülü, 2010
2003	7	6	22	10	0	40.41	26.1	24	5.7	77	70	180	Şengör et al., 2005
2003	9	24	10	33	12.9	40.77	27.46	6.2	2.8	198	60	6	Örgülü, 2010
2003	10	2	7	50	51.9	40.8	28.14	1.9	3.2	285	71	-164	Örgülü, 2010
2003	11	2	1	24	49.5	40.42	28.55	5.9	3.5	136	70	-11	Örgülü, 2010
2003	11	25	0	29	34.4	40.74	27.37	3.7	3.1	190	44	68	Örgülü, 2010
2003	11	27	1	5	23.8	40.42	28.54	5.9	2.8	153	75	42	Örgülü, 2010
2003	12	14	22	27	47.4	40.82	28.09	10.3	2.8	255	73	-148	Örgülü, 2010
2004	1	16	4	26	20.2	40.83	27.94	3.9	3	315	90	-30	Örgülü, 2010
2004	5	4	1	49	55.9	40.83	28.05	11.1	3.1	318	56	-97	Örgülü, 2010
2004	6	12	10	10	49.6	40.65	27.49	15.6	3	233	80	170	Örgülü, 2010
2004	10	21	22	43	25.1	40.76	27.51	3.7	2.7	244	50	-173	Örgülü, 2010
2004	11	12	23	14	12.7	40.79	27.52	7.1	2.5	94	70	-169	Örgülü, 2010
2004	12	25	3	45	33.4	40.84	27.97	16.2	3.1	58	60	-174	Örgülü, 2010
2005	1	9	15	10	24.8	40.56	28.66	11.2	3	310	90	170	Örgülü, 2010
2005	3	27	9	32	17.4	40.72	27.41	1.7	3.3	295	80	170	Örgülü, 2010
2005	5	22	4	44	14.5	40.43	28.51	2.9	3.1	253	51	-167	Örgülü, 2010
2005	5	23	7	55	0	40.77	27.41	6.1	2.8	60	67	136	Örgülü, 2010
2005	5	24	1	1	0.7	40.31	27.62	7.2	3.2	267	74	-143	Örgülü, 2010
2005	6	26	5	27	48.8	40.35	27.67	6.3	3	75	80	-150	Örgülü, 2010
2005	6	27	2	50	50.6	40.65	27.4	1.1	2.9	256	70	169	Örgülü, 2010
2005	6	27	2	58	16.4	40.66	27.39	2.3	3.5	318	48	-109	Örgülü, 2010
2005	6	27	15	15	0	40.75	27.39	6	2.9	146	67	70	Örgülü, 2010
2005	6	28	5	14	53.4	40.82	28.15	11	3.1	222	56	97	Örgülü, 2010
2005	7	1	9	7	24.5	40.67	27.4	1	2.5	114	72	-154	Örgülü, 2010
2005	7	2	13	29	36.5	40.66	27.39	3.7	3.1	325	41	-102	Örgülü, 2010
2005	7	6	23	26	13.7	40.74	27.39	7.4	2.9	94	80	175	Örgülü, 2010
2005	7	23	2	20	21.6	40.83	28.14	13.2	3.3	256	61	-168	Örgülü, 2010
2005	8	2	6	6	45.4	40.84	28.07	8.8	3.1	266	61	-168	Örgülü, 2010
2005	8	19	8	14	22.8	40.41	28.11	3.1	3.3	250	70	180	Örgülü, 2010
2005	10	6	7	34	32.2	40.52	27.75	12.4	2.9	255	90	180	Örgülü, 2010
2005	10	8	2	15	20.8	40.72	27.43	10	3.2	270	90	175	Örgülü, 2010
2005	11	22	7	3	21.6	40.82	27.96	10.6	3	167	60	-6	Örgülü, 2010
2005	12	5	12	16	52.1	40.39	28.81	10.4	2.8	330	71	164	Örgülü, 2010
2006	2	12	8	8	0	40.62	27.66	13	3.7	249	86	-115	Örgülü, 2010
2006	3	28	13	7	1.3	40.55	28.13	7.8	3.5	333	80	-10	Örgülü, 2010
2006	10	20	18	15	24.7	40.25	27.98	5.9	5	250	90	175	Örgülü, 2010
2006	10	24	14	0	21.5	40.42	28.99	5.7	5	260	57	-123	Örgülü, 2010
2006	12	19	19	15	37.5	40.38	28.32	7.5	4.8	168	80	-10	Örgülü, 2010
2007	-	-	-	-	-	40.7	29.17	7.4	-	209	61	5	Bulut et al., 2009
2007	-	-	-	-	-	40.7	29.23	5.5	-	191	54	21	Bulut et al., 2009

2007	-	-	-	-	-	40.71	29.29	13.8	-	64	74	49	Bulut et al., 2009
2007	-	-	-	-	-	40.73	29.06	10.4	-	196	66	7	Bulut et al., 2009
2007	-	-	-	-	-	40.74	29.06	10.2	-	192	88	5	Bulut et al., 2009
2007	-	-	-	-	-	40.75	29.11	8.2	-	217	74	16	Bulut et al., 2009
2007	-	-	-	-	-	40.76	29.09	8.7	-	190	77	25	Bulut et al., 2009
2007	-	-	-	-	-	40.76	29.2	7.8	-	234	84	15	Bulut et al., 2009
2007	-	-	-	-	-	40.78	29.1	9.5	-	217	49	11	Bulut et al., 2009
2007	-	-	-	-	-	40.79	29.12	10.4	-	200	69	12	Bulut et al., 2009
2007	-	-	-	-	-	40.81	28.99	13.8	-	236	67	26	Bulut et al., 2009
2007	-	-	-	-	-	40.82	28.79	9.9	-	60	57	33	Bulut et al., 2009
2007	-	-	-	-	-	40.85	28.69	7.4	-	239	78	60	Bulut et al., 2009
2007	-	-	-	-	-	40.85	28.81	12.5	-	239	65	44	Bulut et al., 2009
2007	-	-	-	-	-	40.85	28.86	11.4	-	249	83	38	Bulut et al., 2009
2007	-	-	-	-	-	40.86	28.47	6.5	-	184	60	33	Bulut et al., 2009
2007	-	-	-	-	-	40.87	28.68	5.4	-	230	82	62	Bulut et al., 2009
2007	-	-	-	-	-	40.87	28.74	3.7	-	226	80	55	Bulut et al., 2009